BEHAVIOUR OF THREE DIMENSIONAL EXPANDED POLYSTYRENE (EPS) SANDWICHED CONCRETE PANELS UNDER AGGRESSIVE ENVIRONMENT

A thesis

Submitted in fulfilment of the requirement for the award of degree of

DOCTOR OF PHILOSOPHY

IN

CIVIL ENGINEERING

Submitted by

ANIL GARHWAL
Regd. No 951702001

Supervisor(s)

Dr Shruti Sharma
Professor,
Department of Civil Engineering

Dr A. B. Danie Roy
Assistant Professor,
Department of Civil Engineering

DEPARTMENT OF CIVIL ENGINEERING
THAPAR INSTITUTE OF ENGINEERING AND TECHNOLOGY
PATIALA-147004
JULY – 2024

CERTIFICATE

I, Anil Garhwal, hereby declare that the thesis entitled "**Behaviour of Three Dimensional Expanded Polystyrene (EPS) Sandwiched Concrete Panels Under Aggressive Environment**", submitted to Thapar Institute of Engineering and Technology, Patiala in partial fulfilment of the requirement for the award of Degree of Doctor of Philosophy in Civil Engineering is a record of original and independent research work done by me. The thesis has been conducted under the supervision and guidance of **Dr. Shruti Sharma**, Professor, Department of Civil Engineering, Thapar Institute of Engineering and Technology, Patiala and **Dr. A. B. Danie Roy**, Assistant Professor, Department of Civil Engineering, Thapar Institute of Engineering and Technology, Patiala. It has not formed the basis for the award of any degree to any candidate of any university.

(Anil Garhwal)

Registration No. 951702001

This is to certify that the above-mentioned statement made by the candidate is correct to the best of my knowledge.

Dr Shruti Sharma

Professor,
Department of Civil Engineering,
Thapar Institute of Engineering and
Technology (Deemed University),
Patiala, Punjab, India

Dr A. B. Danie Roy

Assistant Professor,
Department of Civil Engineering,
Thapar Institute of Engineering and
Technology (Deemed University),
Patiala, Punjab, India

ACKNOWLEDGEMENTS

I am profoundly grateful to the Almighty for guiding me through this journey. I am grateful to everyone who has supported and guided me throughout my Ph.D. journey. First and foremost, I would like to express my deepest gratitude to my supervisor(s), **Prof. Dr. Shruti Sharma,** Professor, Department of Civil Engineering and **Dr. A. B. Danie Roy,** Assistant Professor, Department of Civil Engineering, for their unwavering support, insightful guidance, and invaluable advice throughout my thesis work. Their methodical approach and cooperation motivated me to work diligently. Their expertise and encouragement have been instrumental in the completion of this thesis.

I would like to extend my deepest gratitude to Dr. Shruti Sharma (HCED), Dr. Prem Pal Bansal (former HCED), and Dr. Naveen Kwatra (former HCED) for providing the lab facilities and fostering an exceptional academic environment. I am profoundly grateful to the doctoral committee members, Dr. Shweta Goyal, Dr. Heaven Singh, and Dr. Rajeev Mehta, for their constructive feedback, time, and effort in reviewing my work, which has significantly enhanced the quality of this research. I am grateful to all teachers in the civil engineering department for their time-to-time support in completing my work. My sincere thanks also go to the entire support staff, especially Mr. Virender Singh, Mr. Ram Sumiran, Mr. Manreet Singh, Mr. Hitesh and all other manpower for their support, invaluable assistance with the experiments.

I express my gratitude to my peers and acquaintances within the Department of Civil Engineering for cultivating an intellectually engaging atmosphere conducive to research. Dr. Ashish Tiwari, Dr. Kamal Anand, Dr. Kirti Vardhan Singla, Dr. Upender Bishnoi, Dr. Gaurav Sharma, Mr. Akshay Sharma and Dr. Nikhil Sharma are to be commended for their support, companionship, and for making this journey more reasonable.

A special note of gratitude goes to my family for their endless love, patience, and encouragement. My beloved parents Sh. Gulab Rai Garhwal and Smt. Bimla, my lifetime mentor Sh. Tara Chand Garhwal (Bade Papa), my saviour Smt. Birma (Bade Mummy), my confidant, Sh. Jagdish Garhwal (Baba ji), and Smt. Kalo (Maa) for their time-to-time support. My steadfast brother, Dr. Sunil Garhwal, who has always enlightened me with solutions throughout this journey. My uplifting sisters Dr. Sunita, Rekha and Aruna who constantly refreshed my life and filled me with hope. My brothers-in-law Dr. Ajay Laura, Sh. Yogesh Siwach and Sh. Navdeep Nehra, for their motivating words. My parent-in-laws, Sh. Ram

Chander, and Smt. Sunita whose encouraging words and timely support made this work possible.

I owe special thanks to my toddler son, Bhavyansh, for constantly relieving my stress with his innocence and mischievous activities. I express my deepest appreciation to my wife, Dr. Priyanka, whose faithful support and unwavering patience were indispensable to the successful completion of this work.

Finally, I wish to express my thanks to all those who worked behind the scenes, contributing quietly to this research.

(Anil Garhwal)

ABSTRACT

The rising need for housing in developing countries has led to a demand for rapid construction materials and techniques. Additionally, the desire for better living comfort and low energy consumption has driven a shift from traditional masonry construction to rapid construction methods that offer advantages such as insulation, lightweight properties, and acoustic insulation. One such extensively used material is Expanded Polystyrene (EPS) Sandwiched Concrete Panels, known for their rapid construction capabilities, cost-effectiveness, insulating properties, and lightweight load-bearing capacity. This study aims to evaluate the flexural performance of these panels under aggressive environmental conditions, including chloride exposure, acid exposure, sulfate exposure, and elevated temperatures. Additionally, the study employs Acoustic Emission (AE) non-destructive testing to monitor the panels.

The EPS panels used in this study have dimensions of 1000 × 600 × 130 mm (Length × Width × Thickness), with welded wire mesh of size 50 × 50 mm serving as wythe reinforcement and truss-shaped shear connectors. In the first phase of this study, chloride exposure, which results in corrosion, is simulated using an impressed current technique for accelerated corrosion. The panels were corroded to different levels by varying the days of exposure of 5-, 10-, 15- and 20-days, the panels were then tested under a monotonically increasing flexural loading. The failure mode and behavior of the corrosion-damaged panels were investigated regarding flexural strength, stiffness, ductility, and composite action. The investigation showed decreases of 6.98%, 13.93%, 20.62%, and 60.45% in the ultimate flexural load-carrying capacity after 5, 10, 15, and 20 days of accelerated corrosion, respectively. The ductility, evaluated using the Ductility Factor (DF), showed a decrease of up to 85.01% in highly corroded panels. AE parameters, such as cumulative AE hits, amplitudes, and X-Y event plots, were used to detect faults, reliably indicating damage in the tested panels. The AE hits correlated with the decreasing flexural load-carrying capacity as corrosion increased, and X-Y event plots accurately located faults in all corroded panels.

In the second phase of the study, significant exposure conditions involving acid and sulphate attacks were also established. The aggressive environment of acid attack was created by immersing the EPS panels in sulfuric acid (H_2SO_4) solution at pH=1 for varying 7, 14, 21, and 28 days. Similarly, a sulphate attack was simulated by immersing the panels in sodium sulphate (Na_2SO_4) solution for 90, 180, 270, and 360 days. The panels were tested for residual

flexural strength post-exposure. Acid-exposed panels retained 99%, 82.28%, 74.42%, and 37.25% of the control panel's strength for EPS-A07, 14, 21, and 28 days, respectively. Sulfate-exposed panels retained 91.64%, 88.89%, 77.19%, and 57.28% of their original strength for EPS-S90, 180, 270, and 360 days, respectively. The ductility of acid-exposed panels decreased, while sulfate-exposed panels showed a loss in stiffness after 180 days. AE monitoring during flexural testing revealed correlations between AE parameters (cumulative AE hits, amplitudes, Rise Angle (RA), and Average Frequency (AF)) and the mechanical properties of the panels. RA-AF plots analyzed during different loading stages indicated that shear cracks dominated from the initial loading phase as the panels degraded.

In the third phase of the study, the performance of EPS panels exposed to elevated temperatures was evaluated by subjecting them to 50ºC, 100ºC, 150ºC, and 200ºC using hot plates. Post-exposure, the panels underwent four-point flexural loading tests to assess their mechanical properties. The study found that temperatures above 100ºC significantly affected the panels' yield load, stiffness, ultimate load, and composite action. Detailed analysis of AE parameters—hit counts, amplitudes, average frequency (AF), cumulative signal strength (CSS), and rise angle (RA)—provided precise indications of the panels' degradation. The AE data revealed patterns correlating with thermal exposure levels, identifying critical temperature thresholds compromising panel integrity. These findings underscore the importance of temperature management in applications involving EPS sandwiched concrete panels, offering insights for enhancing their durability and performance in environments subject to elevated temperatures.

This study investigates EPS panels' flexural performance and durability under various environmental exposures—chloride, acid, sulfate, and elevated temperatures. The results indicate significant degradation in mechanical properties with increasing exposure, highlighting the need for careful evaluation and management of these panels in harsh conditions. These insights are crucial for improving the resilience and longevity of EPS panels in construction applications.

Table of Contents

CHAPTER 1 17

INTRODUCTION 17

1.1 GENERAL 17

1.2 EPS SANDWICHED CONCRETE PANELS 18

1.2.1 Expanded polystyrene (EPS) Insulation 19

1.2.2 Concrete wythes 21

1.2.3 Shear connectors 25

1.3 ENVIRONMENTAL EXPOSURE VARIABLES 25

1.3.1 Chloride exposure 26

1.3.2 Acid exposure 28

1.3.3 Sulphate exposure 29

1.3.4 Heat exposure 29

1.4 NON-DESTRUCTIVE EVALUATION TECHNIQUES 31

1.5 ACOUSTIC EMISSION TECHNIQUE 35

1.5.1 Principle of acoustic emission technique 35

1.5.2 Piezoelectric AE sensors 36

1.5.3 AE signal analysis 37

1.6 OBJECTIVES OF THE STUDY 38

1.7 ORGANISATION OF THESIS 39

1.8 CLOSING REMARKS 40

CHAPTER 2 41

LITERATURE REVIEW 41

2.1 GENERAL 41

2.2 EPS SANDWICHED CONCRETE PANELS 41

2.2.1 Flexural behavior of EPS panels 41

2.2.2 Compression behavior of EPS panels 47

2.2.3 Shear Stiffness and composite action 50

2.3 EXPOSURE CONDITIONS 55
2.4 NON-DESTRUCTIVE ACOUSTIC EMISSION TECHNIQUES 62
2.5 SUMMARY OF LITERATURE REVIEW 66
2.6 GAPS IN RESEARCH AREA 67
2.7 CLOSING REMARKS 68
CHAPTER 3 69
EXPERIMENTAL DETAILS AND METHODOLOGY 69
3.1 GENERAL 69
3.2 MATERIALS USED 69
3.2.1 Cement 69
3.2.2 Fine Aggregates 70
3.2.3 Expanded Polystyrene (EPS) insulation 71
3.2.4 Welded wires 72
3.2.5 Mix proportions 72
3.3 CASTING OF PANELS 73
3.4 EPS PANELS AND ENVIRONMENT EXPOSURE 74
3.4.1 Accelerated corrosion 75
3.4.2 Acid and Sulphate Exposure 78
3.4.3 Heat exposure 79
3.5 FLEXURAL TESTING OF EPS PANELS 80
3.6 ACOUSTIC EMISSION MONITORING 82
3.7 CLOSING REMARKS 85
CHAPTER 4 87
EVALUATION OF CORROSION EFFECTS ON FLEXURAL PERFORMANCE OF EPS PANELS 87
4.1 GENERAL 87
4.2 VISUAL OBSERVATIONS 88

4.3 CORRELATION BETWEEN CORROSION CURRENT AND EXPOSURE DURATION IN EPS PANELS 91
4.4 MECHANICAL TESTING PARAMETERS OF CORRODED EPS PANELS ... 93
4.4.1 Load-displacement behaviour 93
4.4.2 Ductility and energy absorption of corroded EPS panels 98
4.5 DEGREE OF COMPOSITE ACTION 99
4.6 PASSIVE ACOUSTIC EMISSION MONITORING 102
4.6.1 Cumulative AE hits & their amplitudes 102
4.6.2 Acoustic Emission (AE) X-Y Event Plots of corroded EPS panels 108
4.7 CLOSING REMARKS 111
CHAPTER 5 112
EVALUATING THE EFFECTS OF AGGRESSIVE ACIDIC AND SULPHATE ENVIRONMENTS ON EPS PANELS 112
5.1 GENERAL 112
5.2 ACID AND SULPHATE EXPOSURE 113
5.2.1 Acid exposure 113
5.2.2 Acid attack impacts cement mix 114
5.2.3 Sulphate attack impact of cement mix 114
5.3 VISUAL OBSERVATIONS OF EXPOSED PANELS 116
5.4 MECHANICAL TESTING OF ACID AND SULPHATE EXPOSED EPS PANELS 118
5.4.1 Load-deflection behaviour of acid exposed EPS panels 118
5.4.2 Ductility and energy absorption of acid exposed EPS panels 123
5.4.3 Load-deflection behaviour of Sulphate Exposed EPS Panels 125
5.4.4 Ductility of the sulphate exposed EPS panels 126
5.4.5 Implications of acid and sulphate exposure 127
5.5 AE MONITORING OF ACID AND SULPHATE EXPOSED EPS PANELS .. 127
5.5.1 Cumulative AE Hits 127

5.5.2 Effect of acid exposure on AE 129
5.5.3 Effects of sulphate exposure on AE 134
5.6 CRACK CLASSIFICATION USING RISE ANGLE AND AVERAGE FREQUENCY 138
5.6.1 RA vs AF of acid exposed EPS panels 140
5.6.2 RA vs AF of sulphate exposed EPS panels 140
5.7 CLOSING REMARKS 149
CHAPTER 6 150
PERFORMANCE OF EPS PANELS UNDER ELEVATED TEMPERATURES 150
6.1 GENERAL 150
6.2 THERMAL BEHAVIOUR OF EPS PANELS 151
6.2.1 Observation of EPS panel at elevated temperature 151
6.2.2 Visual observations of elevated temperature exposed EPS panels 153
6.3 FLEXURAL BEHAVIOUR OF EPS PANELS SUBJECVTED TO ELEVATED TEMPERATURES 155
6.3.1 Load deflection response of control panel 156
6.3.2 Performance of Heat Exposed EPS Panels 156
6.3.3 Stiffness and energy dissipation of heat exposed EPS panels 158
6.4 DEGREE OF COMPOSITE ACTION 159
6.4.1 Evaluation of composite action 159
6.5 PASSIVE ACOUSTIC EMISSION MONITORING FOR DAMAGE DETECTION 161
6.5.1 Impact of heat exposure on AE signature 162
6.6 RISE ANGLE VS AVERAGE FREQUENCY FOR CRACK CLASSIFICATION 165
6.6.1 Understanding RA and AF for crack classification 165
6.6.2 Impact of heat exposure on crack modes 166
6.7 CUMULATIVE AE SIGNAL STRENGTH FOR DAMAGE ASSESSMENT 168

6.7.1 Quantifying damage using AE signal strength 168
6.7.2 AE signal strength analysis of EPS panels 169
6.8 CLOSING REMARKS 173
CHAPTER 7 174
CONCLUSIONS 174
7.1 GENERAL 174
7.2 EVALUATION OF CORROSION EFFECTS ON FLEXURAL PERFORMANCE OF EPS PANELS 174
7.3 EVALUATING THE EFFECTS OF AGGRESSIVE ACIDIC AND SULPHATE ENVIRONMENTS ON EPS PANELS 175
7.4 PERFORMANCE OF EPS PANELS UNDER ELEVATED TEMPERATURES 176
7.5 LIMITATIONS OF THE STUDY 177
7.6 CLOSING REMARKS 178
7.7 PRACTICAL APPLICATION 178
7.8 FUTURE SCOPE OF WORK 178
REFERENCES 180

LIST OF PUBLICATIONS

- Garhwal, Anil, Shruti Sharma, and Danie Roy AB. "Performance of expanded polystyrene (EPS) sandwiched concrete panels subjected to accelerated corrosion." *Structures*. Vol. 43. Elsevier, 2022. (Impact Factor: 3.9) https://doi.org/10.1016/j.istruc.2022.07.020
- Garhwal, Anil, Shruti Sharma, and Danie Roy AB. "Corrosion Effects on Flexural Behavior of EPS Sandwich Concrete Panels: A Study Using Acoustic Emission Technique" *Canadian Journal of Civil Engineering.* Submission ID: cjce-2024-0128. (Impact Factor: 1.5) (**Accepted on:** 2nd September 2024)

COMMUNICATED PAPER

- Garhwal, Anil, Shruti Sharma, and Danie Roy AB. "Mechanical and AE Evaluation of the EPS Panels Exposed to Acid and Sulphate Environments". *Iranian Journal of Science and Technology, Transactions of Civil Engineering.* Submission ID: 396df6e8-3f84-42e7-a945-6cbd5bbccb54. (Impact Factor: 1.7). (**Minor Revisions Submitted:** 3rd September 2024**)**

ABBREVIATIONS

AE	Acoustic Emission
AF	Average Frequency
AET	Acoustic Emission Technique
BCJ	Beam Column Joints
CACC	Calcium Aluminate Cement Concrete
CBRI	Central Building Research Institute
CSS	Cumulative Signal Strength
DF	Ductility Factor
EIS	Electrochemical Impedance Spectroscopy
EPS	Expanded Polystyrene
FEA	Finite Element Analysis
FRP	Fiber Reinforced Polymer
GFRG	Glass Fiber Reinforced Gypsum
ICF	Insulated Concrete Forms
ICSWP	Insulated Concrete Sandwich Wall Panels
IEM	Impact-Echo Method
LVDT	Linear Variable Displacement Transducer
MOI	Moment of Inertia
NDE	Non-destructive evaluation
OPC	Ordinary Portland Cement
PCSP	Precast Concrete Sandwich Panel
PFCSP	Precast Foamed Concrete Sandwich Panels
PET	Polyethylene Terephthalate
PUR	Polyurethane Foam
RA	Rise Angle
RC	Reinforced Concrete
RCSP	Reinforced Concrete Sandwich Panels
SCC	Self-Compacting Concrete
SIPs	Structural Insulated Panels
SRCL	Steel Reinforced Concrete Layers
UGW	Ultrasonic Guided Waves
UPV	Ultrasonic Pulse Velocity
VDCP	Variable Density Concrete Panels
XPS	Extruded Polystyrene

LIST OF FIGURES

FIG. 1.1 SCHEMATIC DIAGRAM OF A TYPICAL EPS SANDWICHED CONCRETE PANEL 19

FIG. 1.2 FLOW CHART OUTLINE - STAGES IN THE PRODUCTION OF EPS 22

FIG. 1.3 VAPORIZATION OF THE POLYSTYRENE BEADS INTO PRE-EXPANDED BEADS 23

FIG. 1.4 STRAIN PROFILES OF FULLY COMPOSITE, NON-COMPOSITE AND PARTIALLY COMPOSITE SANDWICHED PANELS 24

FIG. 1.5 SCHEMATIC ILLUSTRATION OF THE EMBEDDED STEEL CORROSION IN CONCRETE (AHMAD 2003) 27

FIG. 1.6 VOLUME EXPANSION OF THE CORROSION RUST PRODUCED 28

FIG. 1.7 FAILURES IN MATERIALS EXPOSED TO ELEVATED TEMPERATURES AND FIRES (COMFORTECH BUILDING PERFORMANCE SOLUTIONS). 30

FIG. 1.8 SCHEMATIC REPRESENTATION OF THE OPERATION OF THE REBOUND HAMMER (ALYAMAÇ ET AL. 2018B). 32

FIG. 1.9 SCHEMATIC ILLUSTRATION OF AE MONITORING PROCESS (OHTSU AND ONO 1986) 36

FIG. 1.10 VARIOUS AE WAVEFORM PARAMETERS (GROSSE AND OHTSU 2008) 38

FIG. 3.1 COMPARISON OF GRADATION OF SAND 71

FIG. 3.2 SCHEMATIC EPS SANDWICHED CONCRETE PANELS 73

FIG. 3.3 CASTING OF EPS SANDWICHED CONCRETE PANELS 74

FIG. 3.4 CURING OF EPS SANDWICHED CONCRETE PANELS 74

FIG. 3.5 APLAB REGULATED DC POWER SUPPLY 75

FIG. 3.6 CORROSION SET-UP FOR EPS PANELS. 76

FIG. 3.7 SCHEMATIC OF ACID AND SULPHATE EXPOSURE SET-UP 79

FIG. 3.8 SQUARE 400 MM HEATING PLATE USED FOR THE ELEVATED TEMPERATURE SET-UP 80

FIG. 3.9 HEAT EXPOSURE SET-UP OF EPS PANELS. 81

FIG. 3.10 HEAT EXPOSURE VS TIME GRAPH FOR HEAT EXPOSED EPS PANELS 81

FIG. 3.11 FLEXURAL TESTING SET-UP 82

FIG. 3.12 PARAMETERS OF AE WAVEFORM (ALI ET AL. 2019) 83

FIG. 3.13 AE DATA MONITORING SYSTEM EQUIPMENT 84

FIG. 3.14 R6A AE SENSOR DIMENSIONS 84

FIG. 3.15 AE SENSOR'S LOCATION ON EPS PANEL 85

FIG. 4.1 VISUALS OF EPS SANDWICHED CONCRETE PANELS CORRODED TO VARYING LEVELS. 90

FIG. 4.2 INSIDE VIEW OF THE EPS PANEL AFTER CORROSION 91

FIG. 4.3 EXTRICATED EPS AND WIRE MESH AFTER PANEL TESTING 91

FIG. 4.4 VARIATION IN IMPRESSED CURRENT WITH TIME. 92
FIG. 4.5 LOAD DEFLECTION CURVE OF CONTROL EPS PANEL (EPS-00) 94
FIG. 4.6 CRACKS DURING DIFFERENT ZONES OF FLEXURAL TESTING (EPS-00) 95
FIG. 4.7 LOAD-DEFLECTION CURVE OF CORRODED EPS PANELS 97
FIG. 4.8 COMBINED LOAD DEFLECTION CURVES FOR EPS PANELS CORRODED TO DIFFERENT LEVELS. 101
FIG. 4.9 VARIATION IN AE HITS VS TIME IN CONTROL PANEL (EPS-00) 103
FIG. 4.10 VARIATION IN AE HITS VS TIME WITH VARYING CORROSION. 105
FIG. 4.11 AMPLITUDE OF AE HITS WITH TIME IN EPS-00. 106
FIG. 4.12 AMPLITUDE OF AE HITS WITH TIME OF CORRODED EPS PANELS. 108
FIG. 4.13 AE X-Y EVENT PLOTS WITH INCREASING FLEXURAL LOADING – EPS-00 109
FIG. 4.14 AE X-Y EVENT PLOTS FOR CORRODED SPECIMENS 110
FIG. 5.1 VARIATION OF PH IN ACIDIC SOLUTION 113
FIG. 5.2 AGGRESSIVE ACID EXPOSURE EFFECT ON MORTAR 115
FIG. 5.3 AGGRESSIVE SULPHATE ENVIRONMENT EXPOSURE EFFECT ON CONCRETE 116
FIG. 5.4 VISUALS OF EPS PANELS SUBJECTED TO AGGRESSIVE ENVIRONMENTS 117
FIG. 5.5 FAILURES IN ACID EXPOSED EPS PANELS 119
FIG. 5.6 LOAD DEFLECTION PLOTS OF ACID EXPOSED EPS PANELS 121
FIG. 5.7 COMBINED LOAD-DEFLECTION PLOTS OF ACID EXPOSED EPS PANELS. 122
FIG. 5.8 LOAD DEFLECTION PLOTS OF SULPHATE EXPOSED EPS PANELS 125
FIG. 5.9 COMBINED LOAD-DEFLECTION PLOTS OF SULPHATE EXPOSED EPS PANELS 126
FIG. 5.10 AE PLOTS OF CONTROL EPS PANEL (EPS-00) 128
FIG. 5.11 AE PLOTS OF ACID EXPOSED EPS-A07 PANEL 129
FIG. 5.12 AE PLOTS OF ACID EXPOSED EPS-A14 PANEL 130
FIG. 5.13 AE PLOTS OF ACID EXPOSED EPS-A21 PANEL 131
FIG. 5.14 AE PLOTS OF ACID EXPOSED EPS-A28 PANEL 132
FIG. 5.15 AE PLOTS OF SULPHATE EXPOSED EPS-S90 PANEL 133
FIG. 5.16 AE PLOTS OF SULPHATE EXPOSED EPS-S180 PANEL. 134
FIG. 5.17 AE PLOTS OF SULPHATE EXPOSED EPS-S270 PANEL 135
FIG. 5.18 AE PLOTS OF SULPHATE EXPOSED EPS-S360 PANEL 136
FIG. 5.19 RA VS AF PLOT DURING STAGES IN THE CONTROL PANEL (EPS-00) 139
FIG. 5.20 RA VS AF PLOT DURING STAGES-IN THE ACID EXPOSED EPS-A07 141
FIG. 5.21 RA VS AF PLOT DURING STAGES-IN THE ACID EXPOSED EPS-A14 142
FIG. 5.22 RA VS AF PLOT DURING STAGES IN THE ACID EXPOSED EPS-A21 143

FIG. 5.23 RA VS AF PLOT DURING STAGES IN THE ACID EXPOSED EPS-A28 PANEL 144
FIG. 5.24 RA VS AF PLOT DURING STAGES IN THE SULPHATE EXPOSED EPS-S90 PANEL. 145
FIG. 5.25 RA VS AF PLOT DURING STAGES IN THE SULPHATE EXPOSED EPS-S180 PANEL. 146
FIGURE 5.26 RA VS AF PLOT DURING STAGES IN THE SULPHATE EXPOSED EPS-S270 PANEL 147
FIG. 5.27 RA VS AF PLOT DURING STAGES IN THE SULPHATE EXPOSED EPS-S360 PANEL. 148
FIG. 6.1 EXPOSURE OF EPS SKELETON TO ELEVATED TEMPERATURE 152
FIG. 6.2 VISUALS OF FLEXURAL TESTED EPS PANELS EXPOSED TO ELEVATED TEMPERATURES 154
FIG. 6.3 INTERNAL VIEWS OF EPS-H150 155
FIG. 6.4 LOAD DEFLECTION CURVE OF CONTROL EPS SANDWICHED CONCRETE PANELS 156
FIG. 6.5 LOAD-DEFLECTION CURVE OF CONTROL AND TEMPERATURE EXPOSED EPS SANDWICHED CONCRETE PANELS 157
FIG. 6.6 CUMULATIVE HITS-AMPLITUDE VS TIME PLOTS OF CONTROL PANEL 162
FIG. 6.7 CUMULATIVE HITS-AMPLITUDE VS TIME PLOTS HEAT EXPOSED EPS PANELS 164
FIG. 6.8 RISE ANGLE VS AVERAGE FREQUENCY PLOTS OF CONTROL PANEL 166
FIG. 6.9 RISE ANGLE VS AVERAGE FREQUENCY PLOTS OF HEAT EXPOSED EPS PANELS 167
FIG. 6.10 CSS-LOAD VS TIME PLOT OF CONTROL PANEL 169
FIG. 6.11 CSS-LOAD VS TIME PLOT OF HEAT EXPOSED PANELS EPS-H150 & EPS-H200 171

LIST OF TABLES

TABLE 1.1 PHYSICAL PROPERTIES OF EXPANDED POLYSTYRENE (EPS) 23
TABLE 3.1 PHYSICAL PROPERTIES OF CEMENT 69
TABLE 3.2 SIEVE ANALYSIS RESULTS FOR SAND 70
TABLE 3.3 GRADING ZONES OF FINE AGGREGATES (IS 383:2016) 70
TABLE 3.4 PHYSICAL PROPERTIES OF SAND 71
TABLE 3.5 PHYSICAL PROPERTIES OF EXPANDED POLYSTYRENE (EPS) -BY SUPPLIER 72
TABLE 3.6 NOMENCLATURE AND EXPOSURE DETAILS OF EPS PANELS 77
TABLE 4.1 MASS LOSS OF CORRODED EPS PANELS. 93
TABLE 4.2 VARIOUS PARAMETERS UNDER FLEXURAL LOADING 98
TABLE 5.1 MECHANICAL TESTING PARAMETERS OF ACID AND SULPHATE EXPOSED EPS PANELS 123
TABLE 6.1 VARIOUS PARAMETERS UNDER FLEXURAL LOADING 158
TABLE 6.2 STIFFNESS OF THE EPS PANELS AND ENERGY DISSIPATION 158
TABLE 6.3 MOMENT OF INERTIA CALCULATION FOR COMPOSITE AND NON-COMPOSITE EPS PANELS 160
TABLE 6.4 COMPOSITE ACTION OF EPS PANELS 160

CHAPTER 1

INTRODUCTION

1.1 GENERAL

The demand for housing is consistently rising due to ongoing development and population growth. In developing nations like India, with a population exceeding 1.44 billion, and rural-to-urban migration, with the desire for improved living standards has exponentially increased instant need for housing. The demand for housing is difficult to fulfill with snail's pace of conventional construction techniques. Conventional construction methods, such as clay brick masonry, concrete blocks and stone masonry are both labor-intensive and costly. Also, the need for better and low energy consumption housing has increased. This demand has led to a shift towards more efficient and rapid construction techniques. The materials used for rapid construction and effective insulation in cold countries have been increasingly adopted in tropical countries like India. The materials need evaluation for durability according to the climate of use. The various innovative precast materials and building methods used are Insulated Concrete Forms (ICF) (Solomon and Hemalatha 2017), which serve as stay-in-place forms. The use of Glass Fiber Reinforced Gypsum (GFRG) panels and plastic aluminum forms in monolithic concrete construction systems has improved erection and manufacturing processes, facilitating faster construction. Additional methods using pre-cast panels include Variable Density Concrete Panels (VDCP) (Bellamy 2014), Polyurethane panels, and Expanded Polystyrene (EPS) sandwiched concrete panels.

These rapid techniques have their own advantages and disadvantages, Insulated Concrete Forms (ICF) are hollow foam blocks that are stacked to create the shape of the walls, which are then filled with concrete to form a solid structure. The primary advantages of ICFs include excellent thermal and sound insulation, high energy efficiency, strong durability, and resistance to natural disasters. However, they come with higher initial costs, require specialized labor for installation, and repairs often involve reinstalling the insulation with specialized labor. (Solomon and Hemalatha 2017).

Glass Fiber Reinforced Gypsum (GFRG) panels are constructed by combining gypsum with glass fibers, resulting in a strong yet lightweight building material. These panels are advantageous because they are lightweight, easy to handle, quick to install, fire-resistant, and environmentally friendly. On the downside, GFRG panels are typically limited to non-load-

bearing applications and require protective coatings in moisture-prone areas. They can also be fragile during transport and handling, necessitating careful management (Hou et al. 2020).

Plastic aluminum forms are modular formwork systems made from aluminum and plastic, used to shape concrete. These forms are reusable and durable, offering the benefits of being lightweight, which reduces labor costs, and providing high precision and a quality finish. They are also quick to assemble and disassemble. However, the initial investment for plastic aluminum forms is high, and they are susceptible to damage if not handled properly. Regular maintenance is required to ensure their longevity and performance.

Variable Density Concrete Panels (VDCP) are concrete panels with varying densities, which provide tailored strength and insulation properties. The customization of density allows for improved thermal and acoustic insulation, enhanced structural performance, and versatile applications. Despite these advantages, VDCPs have a complex manufacturing process and are more expensive compared to standard panels. Additionally, they have limited availability and require specialized expertise for proper handling and installation (O'Hegarty and Kinnane 2020).

Out of the various materials, EPS sandwiched concrete panels (EPS panels) are increasingly used in the construction industry. The advantage of the light weight and better heat insulation has attracted the tropical countries like India to increasing use of the EPS panels. These panels, as compared to conventional methods, are light in weight, have better insulation, economy, and strength making it preferable over other materials. The panels are effective in resisting the load but are misgauged to be durable. Many factors including chlorides, acid rains, sulphates, carbon dioxide and other aggressive chemicals largely affect the durability of the panels. The impact of various levels of exposure and their corresponding deterioration needs to be evaluated. Additionally, early detection of deterioration is crucial to prevent catastrophic structural failures. Thus, it demands a dependable durability assessment and non-destructive monitoring for the EPS panels used in structures affected by corrosion, acid attack, sulphate attack and heat exposures.

1.2 EPS SANDWICHED CONCRETE PANELS

EPS sandwiched concrete panels are composite materials composed of insulation and outer wythes. The panels are structurally effective complying with the need of strength and stability, thermal comfort, and acoustic performance for residential and light commercial

construction (Ramli Sulong et al. 2019). The skeleton of these panels consists of an EPS insulating foam core placed in between wire mesh grids on both sides. The outer faces termed as wythes are made from plastering/shotcrete. The main function of the core material is to separate the facings to maximize stiffness of the sandwich structure (Daniel Ronald Joseph et al. 2019b). The EPS panels are integral of the EPS as insulation, wire mesh as wythes reinforcement and truss type shear connectors integrating outer wythes (Figure 1.1). Extensive research has been conducted on the structural performance and mechanical behavior of EPS sandwich composite panels under various loading conditions, focusing on compressive strength (Benayoune et al. 2007, 2008, Smakosz and Tejchman 2014), flexural strength (Bush and Stine 1994, Salmon et al. 1997, D. Bush and Wu 1998), diagonal tension, composite action (Davies et al. 2004, Smakosz and Tejchman 2014) and shear strength (Lameiras et al. 2013a, 2013b, Hamed 2018, Huang and Dai 2019, Choi et al. 2019a). The materials EPS as insulation, shear connectors, wythes as parts of EPS panels are discussed under following subheadings.

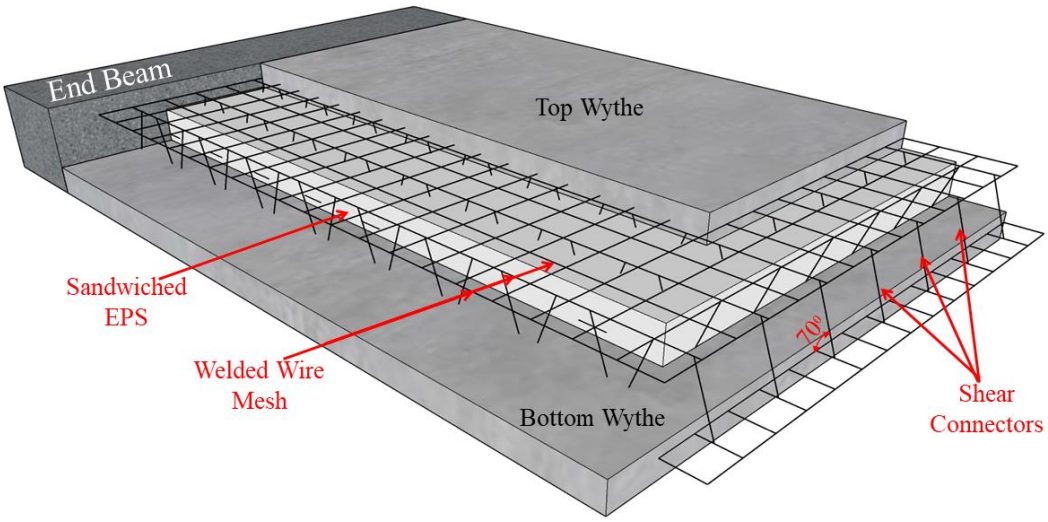

Figure 1.1 Schematic diagram of a typical EPS sandwiched concrete panel

1.2.1 Expanded polystyrene (EPS) Insulation

There is a wide variety of insulation materials, each having its own set of benefits and drawbacks. The insulation materials include Expanded Polystyrene (EPS), Extruded Polystyrene (XPS), Polyurethane Foam (PUR), Mineral Wool (Rock Wool and Glass Wool), Cellulose Insulation etc. EPS is advantageous as it is a cost-effective insulation material comprised of 98% air and 2% polystyrene with high efficiency, it is 100% recyclable (Plastics NZ 2024). Other materials like XPS have good thermal insulation properties, high compressive strength, moisture resistance and durability but its manufacturing cost is higher compared to

EPS, it is also difficult to recycle. Similarly, PUR is a product of mixing of polyol and polyisocyanate, it has high thermal performance and compressive strength but incurs high initial cost and environmental impacts. Mineral wool as an insulation material gives lower thermal resistance and it is heavier making it difficult for handling. Cellulose insulation is made from recycled paper products after treating them with fire retardants. Cellulose insulation is very likely to absorb moisture and requires appropriate moisture barriers. The EPS being cost effective in manufacturing, recyclable, light in weight, low-water absorption, high strength, and inert in nature is advantageous over other insulation materials and therefore commonly used in the building constructions.

The manufacturing of EPS includes the suspension polymerization of styrene monomer, resulting in translucent spherical beads. The refining process of crude oil for petroleum results in creation of several other hydrocarbons which includes ethylene and benzene. The catalytic reaction of ethylene and benzene forms ethylbenzene. Further, the ethylbenzene forms into styrene monomer by dehydrogenation. The styrene monomer is a hard and brittle plastic material having the approximate density of 630 kg/m^3 used as the raw material for EPS manufacturing (Figure 1.2). Further the production of EPS from raw material styrene monomer includes following steps (Figure 1.3):

i. *Pre-Expansion:* The process of suspension polymerization converts the raw styrene monomer into polystyrene beads. The process helps in controlling the size and purity of the polymer beads. Upon completion of the process and subsequent drying, the result is the formation of polystyrene beads. These polystyrene beads contain a low boiling point hydrocarbon (Pentane) to support the proceeding process. The hydrocarbon is also called as the blowing agent.
ii. *Expansion:* The formed polystyrene beads exposed to steam heat or warm air causes the vaporization of the entrapped pentane gas. The steam heat softens the boundary walls of the polystyrene beads, and the vaporised pentane gas exerts the pressure on the boundary walls resulting in the 20 to 50 times expansion of the polystyrene beads making pre-expanded beads.
iii. *Aging:* This process allows the pre-expanded beads to rest or age for a period after expansion and before moulding into a final product. This aging period is crucial for optimizing the properties and performance of the beads in the final product. The beads stabilize and condition to reach equilibrium.

iv. *Moulding*: The stabilized pre-expanded beads placed in moulds and subjected to steam, causing them to expand further. The further expansion of the pre-expanded beads in a confined mould results in fused packing of the EPS beads filling up the voids between cells. Thereafter, vacuum is created inside the mould resulting in cooling of the mould and removal of the moisture from the mould. The vacuum also eliminates the pentane gas from the polystyrene leaving no residual gasses inside the EPS foam. The outcome obtained in the form of EPS blocks or shaped products.

The beads are expanded and molded into various forms and sizes. The EPS manufactured by the polymerization of styrene monomer can be achieved in variable densities ranging from 10 – 35 kg/m^3. To produce varying densities, the size of the beads is modified, resulting in a corresponding variation in the density of the EPS. EPS with a density exceeding 20 kg/m^3 must be of the self-extinguishing variety and comply with the test procedures outlined in IS 4672:1984 (Bureau of Indian Standards 2004). The physical properties of EPS corresponding to the density of EPS are mentioned in Table 1.1. The EPS having density of 15 – 25 kg/m^3 is used in packaging materials, crafts, packaging requiring impact protection, lightweight insulation, and void filling; wall insulation, roof insulation, and other insulations; perimeter insulation for foundations etc. (ASTM C 578–04 2004) ("The BPF Expanded Polystyrene Group | Sustainability" n.d.). The structure of EPS consists of closed-cell plastic material composed of small hollow spherical beads. This unique closed-cell structure imparts EPS with its distinctive properties, making it a lightweight yet rigid foam with excellent thermal insulation and high impact resistance.

1.2.2 Concrete wythes

EPS panels are composed of concrete faces on two sides of the insulation termed as wythes. The thickness of wythes varies as per the design requirements, exposure conditions, finishing, connectors, and loads imposed (Einea et al. 1991). It is composed of reinforcement in terms of square welded wire mesh.(Sylaj et al. 2020, Jajodia and Gadve 2023). The amount of longitudinal reinforcement needed is influenced by several factors, including the panel's span, Overall width of outer wythes, the level of composite action, the load imposed on the panel, and the serviceability requirements. The reinforcement can include prestressing strands or wires, reinforcing bars, wire mesh, or a combination of these materials (Shewale et al. 2023). Transverse reinforcement is affected by factors such as the spacing of connectors, the thickness

of the wythes, applied stresses, and temperature changes. It may consist of either small reinforcing bars or wire mesh. The concrete wythes in EPS panels can be categorized into non-structural wythes and structural wythes.

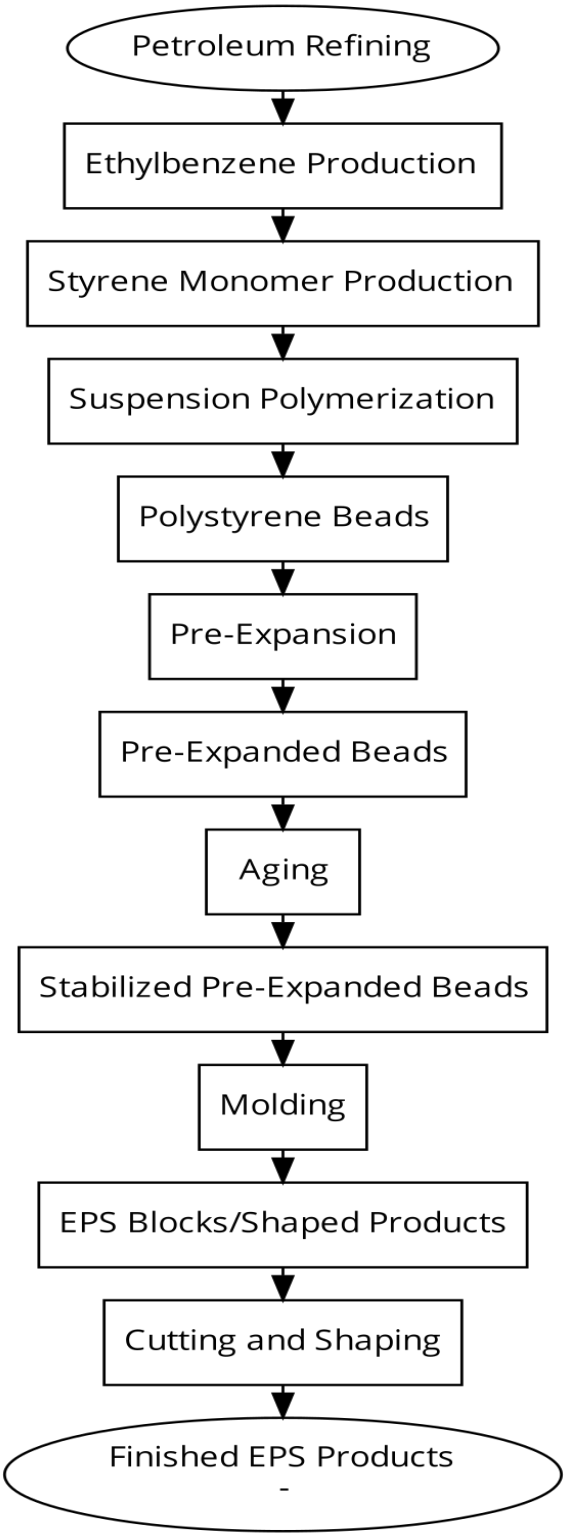

Figure 1.2 Flow chart outline - Stages in the production of EPS

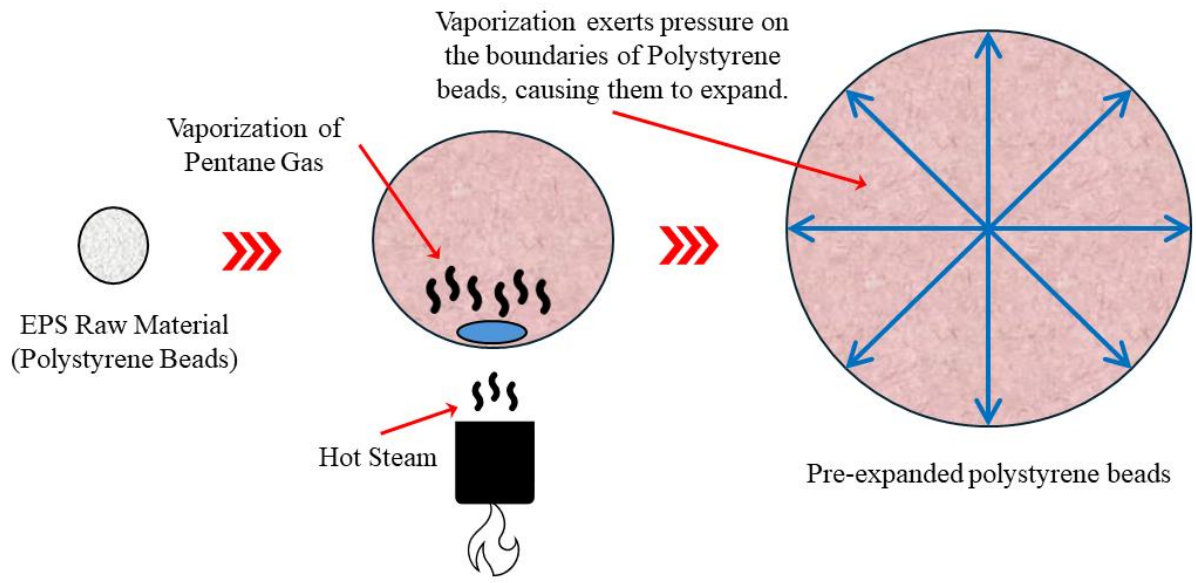

Figure 1.3 Vaporization of the polystyrene beads into pre-expanded beads

Table 1.1 Physical properties of expanded polystyrene (EPS)

Property		**Units**	**Low**	**Medium**	**High**
EPS Density		Kg/m^3	15-20	20-25	25-30
Flexural Strength		Kg/cm^2	2.0 – 2.5	2.5 – 3.0	3.0 – 4.0
Compressive Strength		Kg/cm^2	0.8 – 1.0	1.0 – 1.6	1.6 – 2.0
Thermal Conductivity		w/m^0K	0.030 – 0.034	0.030 – 0.034	0.029 – 0.030
Melting Range		^0C	100-120	100-120	100-120
Self-Ignition Point		^0C	300	300	300
Water Absorption	1 day	Volume %	0.2 – 0.5	0.2 – 0.4	0.2 – 0.4
	2 day	Volume %	0.3 – 0.8	0.3 – 0.7	0.3 – 0.7
	3 day	Volume %	2.0 – 4.0	2.0 – 3.0	2.0 – 3.0

Non-structural wythe is a facing used for aesthetics, and insulation protection from environment. Non-structural wythes are normally termed as cladding or a floating wythe (Pessiki and Mlynarczyk 2003). The non-structural wythes insignificantly contribute to the load bearing in the sandwiched panels. The thickness of the non-structural wythes is small to fulfil the minimum requirement to bear the environmental loads, self-weight, limit temperature variations, provide adequate cover to reinforcement, and keep the panel light in weight.

Structural wythes in the sandwiched panels are the facings of the panel which will bear the loads coming of the panel. Any sandwich panel can have one structural wythes or both structural wythes. In case of one structural wythe, the other facing acts as a floating wythe as

discussed in the previous paragraph. In case both the wythes are designed as structural wythes, then both are going to share the load imposed on the panels. The sharing of loads by structural wythes denotes the degree of composite action of the sandwiched panels. If both the structural wythes behave integrated or we can say monolithically then they are called as composite panels, if partial sharing of load occurs then it is called as semi-composite panels, and if no sharing of the loads occurs then it is called as non-composite panels (Tomlinson et al. 2016a, 2016b, Tomlinson and Fam 2016b).

The composite action or integral action of outer wythes in EPS panels can be understood using the strain profile diagram of the insulation panels under lateral loads (Figure 1.4). The strain diagram represents the two concrete wythes on the outsides termed as top wythes and bottom wythe separated by the insulation sandwiched in between. The panels which can be termed as composite panels will have the equivalent positive and negative strain profiles in top and bottom wythes. The top and bottom wythes of the non-composite panels behave independently and create independent strain profiles by bending along their own separate neutral axis. The top and bottom wythes of the semi-composite panels shares the load partially. Most sandwiched panels behave in a semi-composite manner and their degree of compositeness depends on the shear connectors used in the panels (David Salmon and Einea 1995, Uzal et al. 2018, Choi et al. 2019c, 2019a, 2019b).

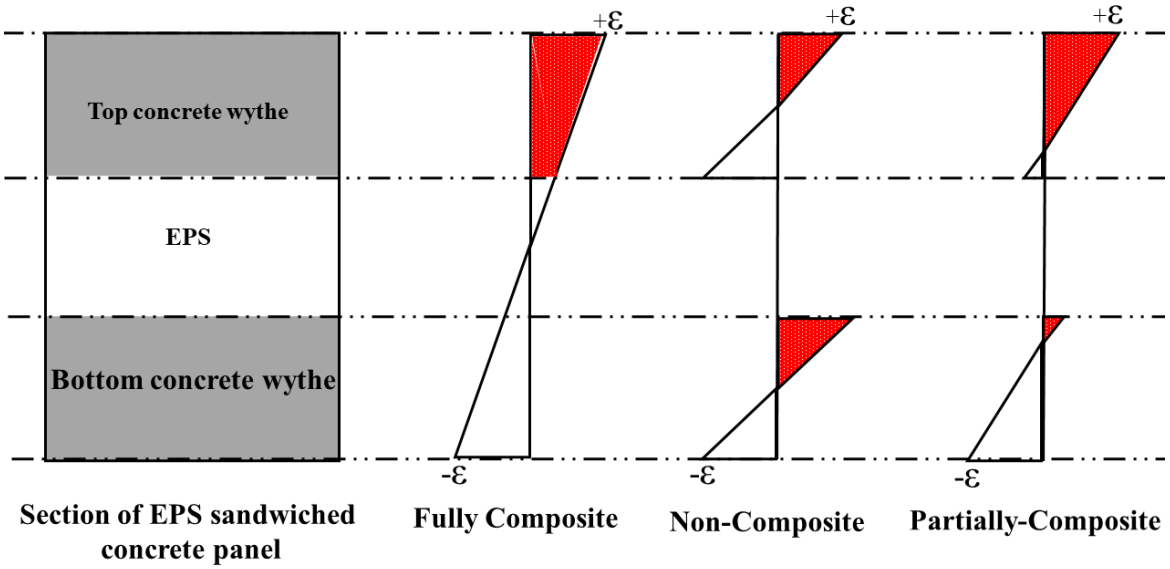

Figure 1.4 Strain profiles of fully composite, non-composite and partially composite sandwiched panels

1.2.3 Shear connectors

The connectors that join the outer concrete wythes of EPS panels are known as shear connectors. When EPS panels are subjected to compressive, diagonal, or lateral forces, a differential movement occurs between the two faces. During flexural forces, the bending curvature varies, leading to an accumulation of shear forces between the wythes along with compressive and tensile forces. The connectors between wythes resist and transfer these loads. The effectiveness of load transfer rests on shear connectors type and material. The composite action of the EPS panels is achieved based on the efficiency of load transfer between the concrete wythes. Shear connectors ensure the effective transfer of loads in EPS panels and are classified into two main types: continuous and discrete. Continuous shear connectors include steel or FRP trusses and FRP mats, while isolated shear connectors comprise threaded fiber reinforced polymer rods or steel and Channel pins (Lameiras et al. 2013a, 2013b, Hamed 2018, Huang and Dai 2019, Choi et al. 2019a). Other materials and forms for shear connectors include punched plates, diagonal bar shear connectives, perforated bond strips, T shaped connectors, commonly used steel trusses, and glass fiber reinforced polymer grid connectors (Zhao et al. 2018, Classen et al. 2018). Dowels and rib shear connectors provide straightforward yet effective methods for transferring shear forces through direct bearing and interlock mechanisms. These various shear connectors are used in construction to ensure effective load transfer and structural integrity, accommodating different design requirements and material properties. For design purposes, a partial bond force at the wythe-to-core interfaces should be considered (Shams et al. 2015). Increase in the diameter and angle of inclination of shear connectors enhances the through-thickness shear transfer and stiffness of composite sandwich panels (Woltman et al. 2013, Tomlinson and Fam 2016a, 2016b, Egbon and Tomlinson 2021). The research demonstrates that truss-type shear connectors are effective in achieving composite action of the panels (Bush and Stine 1994). The EPS panels used in the present research incorporated steel wire trussed shear connectors.

1.3 ENVIRONMENTAL EXPOSURE VARIABLES

The EPS panels and other materials are exposed to various environmental conditions during the design life. These materials are vulnerable to aggressive environments and degradation (Garhwal et al. 2021a). The exposure of construction materials to some aggressive natural and artificial environmental conditions results in loss of durability of the concrete. The EPS panels, being different from traditional load-bearing masonry structures, need to be assessed for environmental degradation when exposed to harsh conditions such as acid attack,

chloride attack, sulphate attack, and accidental fires (Vishnu et al. 2017, Garhwal et al. 2022). The following subheadings discuss these exposure conditions.

1.3.1 Chloride exposure

In countries like India, where almost 80% of the yearly rainfall occurs within just two months, and in regions with extensive coastlines and prevalent marine humid climates like the Middle East, EPS structures can undergo degradation (Glasser et al. 2008, Goyal et al. 2023). Atmospheric corrosion occurs when metals are exposed to atmospheric conditions that include moisture, oxygen, and pollutants such as sulfur dioxide, carbon dioxide, and chlorides. The presence of these elements leads to chemical reactions on the metal surface, forming corrosion products such as rust in the case of iron and steel (ASTM G31-72 2004, Sharma and Mukherjee 2011). Though the reinforced cement concrete provides a passivating layer (pH>13) of iron oxide (Fe_2O_3) around the embedded reinforcement which protects the reinforcement corrosion, but the ingress of chlorides and carbon dioxide reduces the alkalinity of the passive layer resulting in the corrosion of the reinforcement (Reis et al. 2005, Daniyal and Akhtar 2020, Sadeghi-Pouya et al. 2021, Ahmed et al. 2024). The effects of these exposures can be understood by knowing the procedure of the corrosion.

Corrosion is an electrochemical process where the same steel bar hosts both an anode and a cathode. In this process, iron atoms at the anode oxidize, releasing electrons and becoming positively charged cations (Fe++). At the cathode, oxygen reacts with water, gaining electrons to produce hydroxyl ions (OH-). This forms a corrosion cell within the reinforcement, as illustrated in Figure 1.5. Concrete acts as an electrolyte, enabling the transfer of electrons between the anode and the cathode. When RCC is subjected to alternating wetting and drying conditions, it becomes sufficiently conductive to function as an electrolyte. Corrosion can only occur if both anodic and cathodic processes happen concurrently. The anode and cathode can be positioned in proximity or physically isolated from each other. When they are in proximity on a microscopic level, the resulting corrosion cell is known as a microcell. If there is a larger distance between them, the corrosion cell is termed a macro-cell. The corrosion of steel reinforcement in RCC is caused by the presence of both microcells and macro-cells (Sharma and Mukherjee 2011).

Corrosion of steel in concrete can occur in the presence of carbon dioxide (CO_2) and chlorides (Cl^-), both of which contribute to the breakdown of the protective passive film on the steel surface. Commonly, chloride ions (Cl^-) can Permeate the concrete and access the steel

reinforcement, causing the deterioration of the protective oxide layer on the steel and facilitating the onset of corrosive processes. Chloride induced corrosion occurs into the following stages.

$Fe = Fe^{2+} + 2e^-$ (At the anode, iron loses electrons to form ferrous ions)

$Fe^{2+} + 2Cl^- = FeCl_2$ (Ferrous ions react with chloride ions to form ferrous chloride)

$FeCl_2 + 2H_2O + \frac{1}{2}O_2 = Fe(OH)_2 + 2HCl$

(Ferrous chloride reacts with water and oxygen to form ferrous hydroxide and hydrochloric acid)

$O_2 + 2H_2O + 4e^- = 4OH^-$

(At cathode, oxygen reacts with water and electrons to form hydroxyl ions)

$4Fe^{2+} + 4OH^- + O_2 + 2H_2O = 4Fe(OH)_3 = 2Fe_2O_3.3H_2O$

(Ferrous ions and hydroxyl ions react with oxygen to form iron hydroxide which eventually dehydrates to form hydrated ferric oxide (Rust))

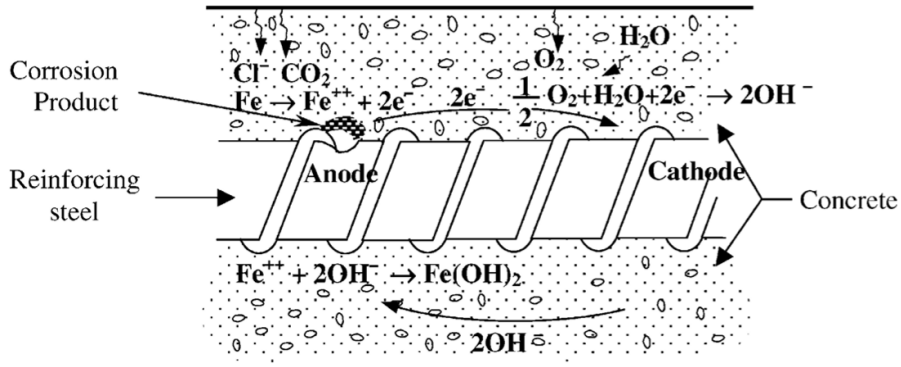

Figure 1.5 Schematic illustration of the embedded steel corrosion in concrete (Ahmad 2003)

The rust produced is 4 to 6 times the original volume of steel (Figure 1.6). This expansion induces tensile stress on the concrete, leading to the creation of cracks. The cracks gradually build up and spread to the surface of the concrete. In the end, the corrosion products result in the concrete breaking and cracking, which weakens the link between the steel and concrete. This leads to a decrease in the steel's cross-sectional area and, as a result, reduces its ability to handle loads (Ohtsu and Tomoda 2007, Bahekar and Gadve 2019). Thus, EPS panels are prone

to corrosion due to environmental effects. The factors causing a high degree of corrosion can reduce the durability of the EPS panels.

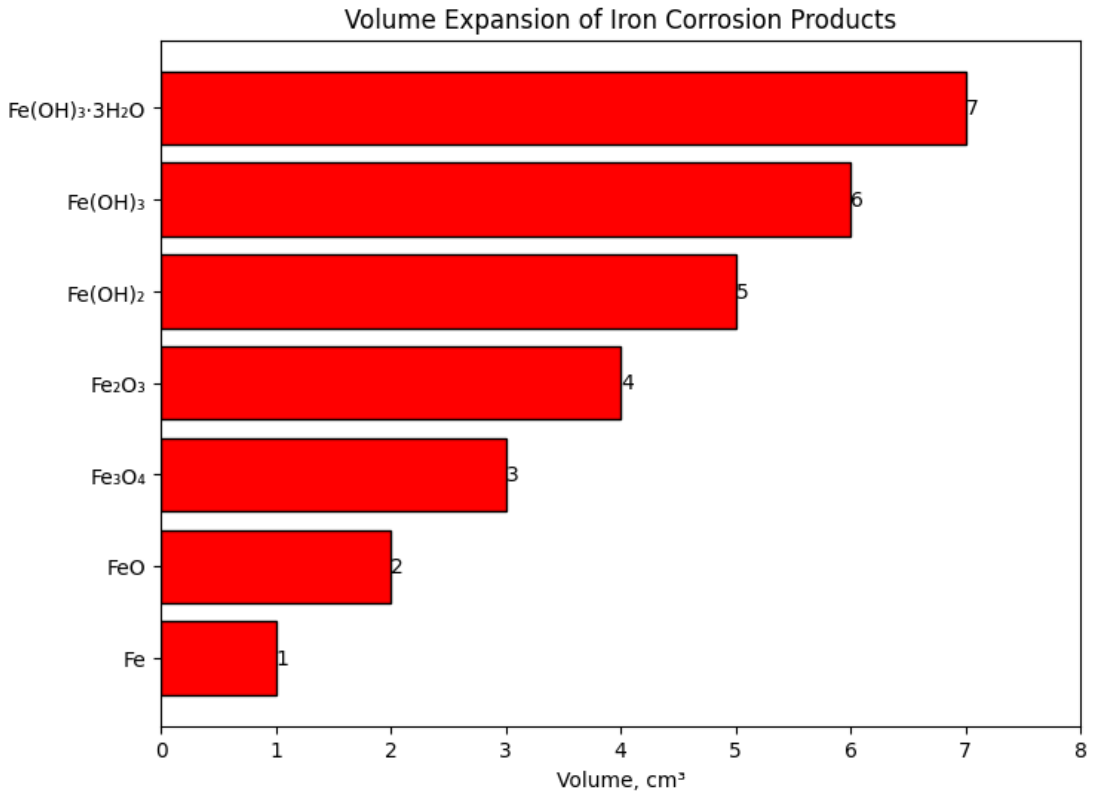

Figure 1.6 Volume expansion of the corrosion rust produced

1.3.2 Acid exposure

Acid attacks can be vastly diverse as linked to specific applications. The potential of Hydrogen (pH) and the acid type classify an acid attack's aggressiveness. The literature shows the degradation due to the presence of sulphuric acid is observed to be very severe, which generally initiates from industrial manufacturing procedures such as geothermal energy generation, mining activities, wastewater treated in sewage treatment facilities, acid rain, and sludge accumulation in sewer pipes. (Chang et al. 2005, Bassuoni and Nehdi 2007, Ji et al. 2021, Gaur et al. 2022) (Zivica and Bajza 2001). During an acid attack, the binder pastes matrix dissolves along with any soluble aggregate, leading to the formation of a visibly damaged layer on the concrete surface. The acid resistance of concrete is heavily influenced by the remaining mechanical strength of the degraded layer and its adhesion to the intact material (Breit 2004).

The EPS panels are susceptible to acid attack commonly encountered in industrial environments, wastewater treatment plants, and areas affected by acid rain (Breit 2004, Mohajan and Mohajan 2018). This exposure affects the concrete wythes that compromise the

integrity and durability of concrete (Bassuoni and Nehdi 2007, Janfeshan Araghi et al. 2015, Gutberlet et al. 2015, Barbhuiya and Kumala 2017). When concrete is exposed to acidic environments, chemical reactions occur between the acid and the calcium hydroxide and other alkaline components within the concrete. These reactions result in the formation of soluble salts, which leach away from the concrete matrix, leading to a loss of material and structural degradation. Sulfuric acid and hydrochloric acid are particularly aggressive, causing extensive damage that includes surface erosion, cracking, and weakening of the concrete's mechanical properties. It is essential to understand the durability of EPS panels under acids attacks to ensure the safety of structures.

1.3.3 Sulphate exposure

Sulphates are used in the manufacturing processes of galvanic cells as electrolytes. Soil may also contain excessive gypsum or other sulphates. Sulphate attack occurs when concrete is exposed to sulphate ions found in soil, groundwater, or industrial effluents. These ions react with calcium compounds in the concrete, particularly calcium hydroxide and tricalcium aluminate, forming expansive products like ettringite and gypsum. Sulphate attack is common due to sodium, calcium and magnesium sulphates (Soive and Tran 2017, Xie et al. 2020). Studies show sodium sulphates impact concrete structures the most. Sulphate from the source reacts with aluminate in the cement binder mix to form gypsum and ettringite (Gu et al. 2020). These reactions create internal pressure within the concrete matrix, causing cracking, spalling, and overall degradation of the material. The failure mode of concrete exposed to sulphate could be characterized as expansion and cracking. Sulphate attack is especially problematic in environments with high sulphate concentrations, common in arid and semi-arid regions, marine environments, and areas with contaminated water. The durability of EPS panels is compromised by exposure to sulphate ions, leading to sulphate attack on the concrete wythes. Understanding the mechanisms and impacts of sulphate attack is crucial for designing structures and assessing the durability of EPS sandwich concrete panels to ensure they can withstand harsh environmental conditions.

1.3.4 Heat exposure

Residential fires pose a significant threat to life, property, and safety. They can cause devastating damage and result in severe injuries or fatalities. Understanding the common causes of residential fires is essential for implementing effective prevention strategies and ensuring the safety of homes and their occupants. The leading cause of residential fires is

unattended cooking, grease fires, stove malfunctions, and distractions while cooking can quickly escalate into uncontrollable blazes. Most common fire cause is heating devices, portable heaters, electrical faults in wirings, improper use of electrical appliances: Improper storage of flammable liquids such as liquified petroleum gas, and paint thinners are also causes of accidental fires (Shea 2011, Xiong et al. 2017). Fire Resistance is a property of an element of building construction and is the measure of its ability to satisfy for a stated period, some or all the following criteria including load bearing capacity, Integrity and resistance to temperature (Figure 1.7).

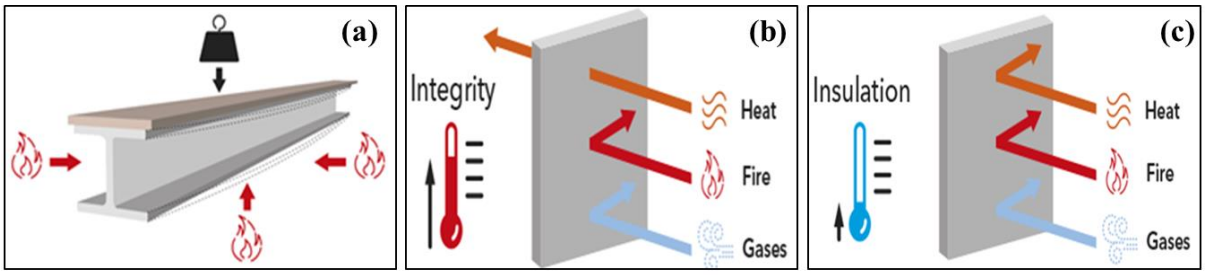

Figure 1.7 Failures in materials exposed to elevated temperatures and fires (COMFORTECH BUILDING PERFORMANCE SOLUTIONS).

The exposure of cement-based concrete to elevated temperatures causes significant deterioration in the microstructure (Poon et al. 2003, Pulkit and Adhikary 2022). Ettringite undergoes dehydration within the temperature range of 70^0 to 180^0 C. Additionally, the free water present in the pores evaporates at approximately 100^0 C. The distinct thermal coefficients exhibited by each phase in concrete, along with the decomposition of hydration products, result in the development of micro-cracks and subsequent deterioration of the concrete's strength. (Bastin and Sharma 2017, Malik et al. 2021). The increase in internal pores and micro-cracks at high temperatures in cement-based materials reduces structural safety (Gu et al. 2020).

EPS panels comprise of the different materials placed together. The material used has different behavior when exposed to elevated temperatures. The insulation material especially is a high impacted material in an EPS panel (Mazzuca et al. 2021, Tahir and Hamed 2021, Hasanzadeh et al. 2023). Though in EPS panel, the wythes function as a barrier impeding the direct transfer of heat to the insulation when it is exposed to elevated temperatures. The thermal resistance of the concrete wythes is low and long exposure of elevated temperatures results in high temperature ingress till insulation (Jithin and Joseph 2023). The insulation materials, such as EPS and Polyethylene Terephthalate (PET) foams lose mechanical properties when exposed to elevated temperatures affecting compression, shear, and flexural strength of the insulation.

The investigations illustrate a degradation ranging from 38% to 50%, which can lead to premature failures (Mazzuca et al. 2021, Tahir and Hamed 2021).

1.4 NON-DESTRUCTIVE EVALUATION TECHNIQUES

Non-destructive evaluation (NDE) techniques encompass a range of procedures employed to examine and evaluate the state of structures without damaging the structure. These approaches are crucial in the building and maintenance sectors since they enable the timely identification of flaws, analysis of materials, and monitoring of structural soundness. NDE techniques are vital for guaranteeing the security, dependability, and durability of diverse structures, such as buildings, bridges, pipelines, and aerospace components. NDE aids in taking early repair and restoration measures. They benefit in assessing the fitness and quality of the component materials without disturbing the function of the building.

Many NDE techniques are available for the detection of the deterioration of the structural components exposed to environmental degradations. The basic NDE is visual inspection, it involves examining the concrete surface for visible signs of damage, such as cracks, spalling, or discoloration. Borescopes and drones can be used to inspect hard-to-reach areas. This method relies on periodic examinations of the concrete surface, based on the structure's importance. Observations like surface cracks, concrete spalling, and exposed reinforcement are used to assess the deterioration of reinforced structures. However, this technique is limited to evaluating surface conditions and cannot quantify the extent of damage or detect reinforcement corrosion beneath the surface. Some NDE techniques used in the evaluation of structures includes Rebound Hammer Test, Ground Penetrating Radar, Half-Cell Potential, Infrared Thermography, Radiographic Testing, Electrochemical Impedance Spectroscopy, Impact Echo Technique, Ultrasonic Pulse Velocity and Acoustic Emission are discussed for their advantages and disadvantages of use (Perdrix et al. 2016).

Instrument based techniques majorly used in NDE of structures include Rebound Hammer Test (Schmidt Hammer), it evaluates surface hardness and estimates compressive strength of concrete. A hammer impacts the concrete surface, and the rebound distance is measured (Figure 1.8). Higher rebound values generally indicate stronger concrete. The rebound hammer test works on the principle that the rebound of an elastic mass depends on the hardness of the surface it strikes. In the context of concrete, a spring-loaded hammer impacts the surface, and the rebound distance of the hammer is measured. The rebound distance is then correlated to the compressive strength of the concrete. The rebound hammer has the limitation of the access of

the strength up to the shallow depth from the surface and is also affected by the surface conditions of the concrete.

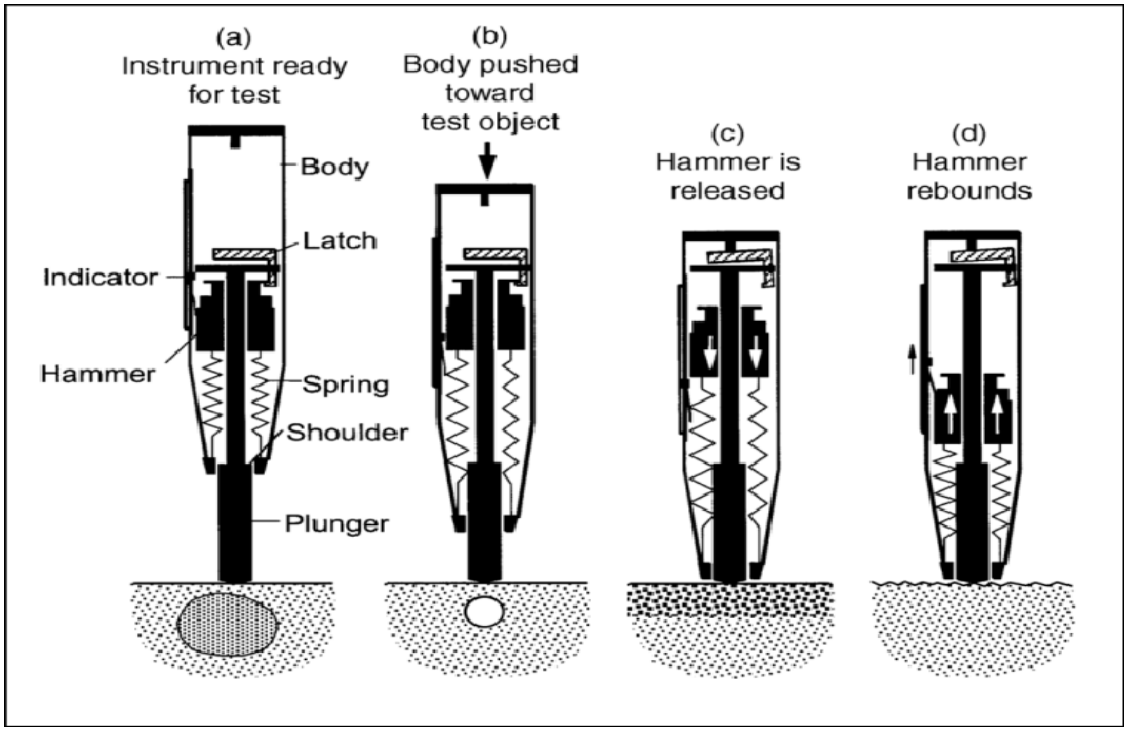

Figure 1.8 Schematic representation of the operation of the rebound hammer (Alyamaç et al. 2018b).

Ground Penetrating Radar (GPR) employs electromagnetic waves to identify variations in material characteristics within concrete, making it another instrument-based approach. It helps locate embedded objects, measure slab thickness, and identify voids or areas of delamination. This method employs high-frequency electromagnetic waves, typically in the range of 1 to 1000 MHz, which are transmitted into the concrete through an antenna. When these waves encounter different materials or interfaces, such as reinforcing steel, voids, cracks, or changes in material properties, they reflect to the surface. The reflected signals are then captured and analyzed to create a detailed image or profile of the subsurface features. The effectiveness of GPR can be influenced by factors such as the material properties of the concrete, the presence of moisture, and the frequency of the radar waves used.

The NDE technique of Half-Cell Potential is used to measure the electrochemical potential of reinforcing steel in concrete. This is the most common electrochemical method used to detect corrosion initiation in reinforced concrete (RC) structures. The half-cell potential (HCP) method measures the change in electrochemical potential of embedded rebar against a reference electrode placed on the concrete surface. Prior to doing the actual testing, the voltage

difference across different sites on the rebar is examined to verify the electrical continuity of the reinforcement. The objective is to achieve a resistance of less than 1 ohm, which indicates a consistent electrical connection. It is essential to moisten the concrete surface beforehand to achieve optimal contact with the reference electrode. The recorded measurements are plotted as contour maps, which help identify areas affected by corrosion. However, it is very expensive and uneconomical to monitor the entire structure continuously for changing corrosion conditions. Additionally, the measured results are influenced by factors such as the quality of the cover concrete, especially its moisture content, and the presence of chlorides and oxygen.

The emerging NDE technique of Infrared Thermography detects surface temperature variations using thermal cameras. It helps identify areas of moisture intrusion, delamination, and voids by detecting differences in thermal conductivity. This method operates on the principle that all objects emit infrared radiation as a function of their temperature. By capturing this radiation, infrared thermography can identify areas of heat loss, moisture intrusion, and subsurface defects in concrete and other materials. The technique is particularly useful for large-scale inspections, as it allows for rapid assessment without physical contact. The technique is very useful in identification of faults in electrical systems but has limited use in structural monitoring.

The NDE of Radiographic Testing uses X-rays or gamma rays to produce images of the internal structure of concrete. It is effective for identifying internal voids, cracks, and other defects without damaging the concrete. X-rays and gamma rays possess high energy levels, enabling them to penetrate through materials. The extent of penetration is contingent upon the energy level of the radiation as well as the dimensions and density of the material being examined. As radiation passes through a material, its intensity decreases due to absorption, scattering, and other interactions with the material. Flaws or voids within the material cause variations in radiation absorption, resulting in contrasting images on the radiographic film or detector. The testing with this method needs proper precautions as X-rays and gamma rays pose potential health risks to personnel if not handled properly. Limited accessibility to certain areas of complex structures may hinder the inspection process.

The NDE of Electrochemical Impedance Spectroscopy measures the response of impedance by applying small sinusoidal pulses at various frequencies. The collected data is subsequently evaluated to generate graphs comparing the imaginary and real components, as well as the amplitude and frequency. This aids in the analysis of corrosion kinetics and causes.

Although this technology has better data extraction capabilities, it is slower and has limited utility in actual scenarios. EIS provides detailed understanding of corrosion mechanisms in structures, but it is very complex in nature.

The Impact Echo Technique is based on the utilization of stress waves that are produced by impact. These stress waves travel through concrete and bounce back when they encounter imperfections inside the material or on its outside surfaces. This technology has the capability to identify many types of imperfections in concrete structures, such as delamination, cracks, honeycombing, voids, and debonding. It may be applied to several types of concrete buildings, including plain, reinforced, and post-tensioned ones. A proficient workforce is important for its implementation. Nevertheless, the outcomes derived from the Impact-Echo Method (IEM) may be considerably influenced by the existence of cracks and other flaws in concrete that are frequently seen in actual RC structures. As a result, this has a direct effect on the precision of the assessment. To effectively utilize this technology, it is necessary to maintain tight contact between the impacting device and the surface. However, this limitation restricts its practical usefulness in field applications.

Ultrasonic Pulse Velocity (UPV) measures the time it takes for an ultrasonic pulse to travel through concrete. This technique helps determine the uniformity, presence of voids, cracks, and other imperfections. High velocity indicates good quality, while lower velocities suggest flaws or deterioration. Ultrasonic Guided Waves (UGW) rely on the transmission of sound waves through a particular material. Based on the idea, sound waves propagate at a constant velocity via pre-established pathways within the medium. Ultrasonic waves are sound waves that have a frequency higher than 20 kHz, which is above what can be detected by humans.

The non-destructive techniques discussed in the previous paragraphs have several combined limitations. These methods face significant challenges in data collection and processing, as multiple probes must be installed to conduct tests, and variations in surface conditions can affect the results (Sharma et. al. 2018, Singh et al. 2022). Additionally, continuous monitoring of structures requires highly skilled personnel and expensive instruments. Other non-destructive techniques like radiography etc. face challenges in monitoring large RC structures. The extent of evaluation is shallow and some techniques like half-cell potential are used for only corrosion (Sharma and Mukherjee 2011). These techniques are difficult for practical use (Garhwal et al. 2021a & b). The NDE technique for continuously monitoring the structures needs durable instruments, precise data analysis, representation, ease

of use and effective data acquisition. The emerging wave propagation technique of Acoustic Emission (AE) is effective in accessing the internal concrete damage and can precisely locate the fault. The system is passive, with AE sensors put on the structure. These sensors listen passively for any activity that may result from degradation or deformation of the structure, providing information about the extent of damage.

1.5 ACOUSTIC EMISSION TECHNIQUE

The wave propagation techniques have been used in the aerospace industry, material testing, oil and gas industry, automotive industry and manufacturing industry. Recently wave propagation tools have been explored for structural health monitoring of concrete structures. AE technique is a non-destructive testing (NDT) method based on wave detection generated during the propagation of the cracks.

Acoustic Emission (AE) testing is a technique used to identify the emission of energy in the form of stress waves emanating from cracks or active faults in concrete. By utilizing sensors, the emissions are detected, providing valuable information on the commencement and spread of cracks. AE is classified as a passive monitoring approach since it detects temporary elastic waves generated by material displacement or cracks, using sensors positioned on the surface for monitoring purposes. Passive monitoring with AE does not require access to reinforcement, making it easier to apply in practice compared to active techniques. AE has considerable promise in evaluating the deterioration in various structural categories. The sensors of the device detect signals that indicate the deterioration of structures, allowing for the early detection of damage. AE has demonstrated considerable potential in the early identification and monitoring of corrosion, particularly in its first stages and the subsequent tracking of its advancement. The fracture initiation and development locations in EPS panels can be identified by analyzing different AE parameters, including AE hits, amplitude, and AE event, location plots. These factors help to identify regions of significant AE activity and the resulting damages.

1.5.1 Principle of acoustic emission technique

When a material undergoes stress or experiences structural changes, localized sources of elastic energy release, generating acoustic waves. These waves propagate through the material and are detected by sensitive piezoelectric sensors known as transducers. The emitted acoustic waves travel through the material, and their characteristics, such as amplitude, frequency, and arrival time, provide valuable information about the nature and severity of the underlying

damage or deformation (Figure 1.9). Detected acoustic signals are amplified, filtered, and analyzed to distinguish between background noise and relevant AE events. By analyzing the waveform parameters, such as wave rise time, duration, and energy release, it is possible to identify the type and location of structural defects or damage. Figure 1.9 shows a schematic diagram in which crack occurrence due to tension forces of corrosion is created due to which the transient waves are generated and travels in all directions. The surfaces mounted with the AE sensors receive them and transfer the electrical converted signal to the AE instrument set-up.

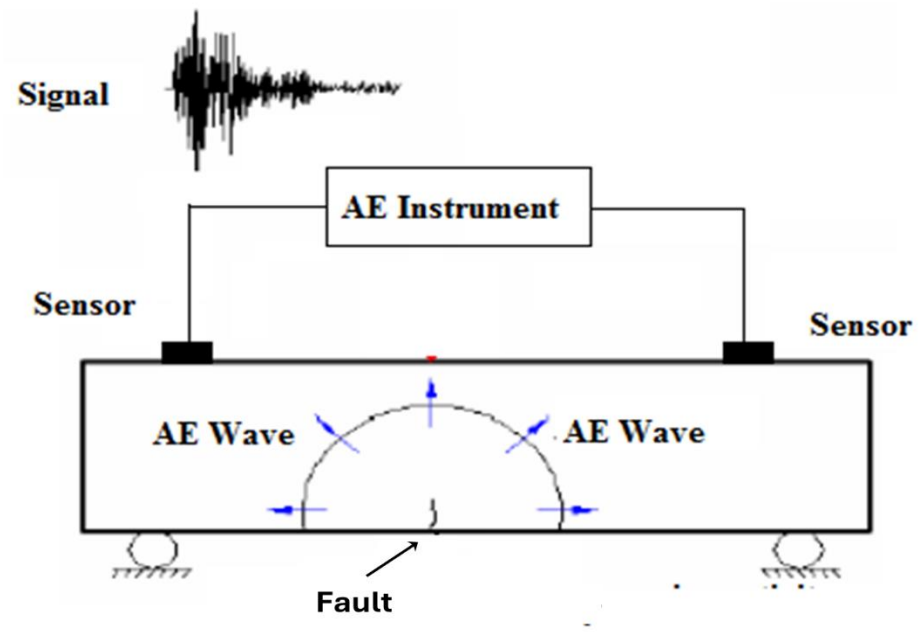

Figure 1.9 Schematic illustration of AE Monitoring Process (Ohtsu and Ono 1986)

1.5.2 Piezoelectric AE sensors

Acoustic Emission (AE) monitoring is a non-destructive testing method that detects and analyzes the high-frequency stress waves released by materials experiencing stress. The ears of the AE monitoring system are its sensors which capture the sounds effectively and transmit them to the monitoring system.

AE uses piezoelectric sensors to record the acoustic waves transmitted during the fracture in the material. Piezoelectric sensors are widely employed for AE monitoring. These devices operate by utilizing the piezoelectric effect, which is the capability of certain materials like quartz or carefully engineered ceramics to generate an electric charge when exposed to mechanical pressure. When an acoustic emission event happens, it produces stress waves that travel through the material. The waves reach the sensor and cause the piezoelectric material to

change shape, generating an electrical signal that is directly proportional to the magnitude of the wave. The sensors can be divided into two types:

i. *Resonant Sensors:* These devices are designed to operate within a specific frequency range that corresponds to the resonance of the piezoelectric element. This design enhances the signal at the resonant frequency, hence increasing sensitivity and boosting the signal-to-noise ratio within that specific frequency range.
ii. *Broadband Sensors:* These sensors have the ability to detect a broad range of frequencies, allowing for a more thorough study of the AE events across the entire spectrum.

The AE waves recorded can be evaluated as discussed in the following subsection.

1.5.3 AE signal analysis

The analysis of detected AE signals normally falls in two categories:

Waveform analysis process entails the capturing and analysis of AE data to quantify the magnitude of structural damage. The system captures the acoustic signal and assesses the extent of damage by analyzing the signal's behavior. This analytical approach can distinguish between the waveform of an audio signal and background noise. The drawback of using this approach is that it necessitates a substantial amount of storage for the data. Additionally, a pause or delay is necessary after each waveform to save it, resulting in a delay.

Parametric Analysis entails the capture of AE signals to offer both quantitative and qualitative assessment of damage in different structures. This technique offers a significant advantage over waveform analysis due to its superior recording and data storage speed. The metrics usually criteria for assessing the extent of harm are hits, counts, energy, signal strength, and amplitude (Figure 1.10).

The AE signal obtained for each crack is documented as the total number of hits. The area exhibiting elevated levels of AE hits is correlated with a rapid progression of fractures. Cumulative Signal Strength (CSS) is determined by summing the signal strength of each individual impact over time and the overall quantity of AE activity generated. The detection of micro or macro fractures can be determined by analyzing the amplitude of spikes formed in AE hit. Microcracks, which are often more numerous, produce acoustic signals with smaller

amplitude values, while macro-cracks, which are less common, generate acoustic signals with higher amplitude values. Rise angle and average frequency analysis of the concrete structures helps in distinguishing the nature of the cracks. The nature of the cracks, that is shear cracks or tensile crack are identified based on the value of rise angle and average frequency. The shear type cracks have longer rise time and lower average frequency and vice-versa in tensile cracks. The presence of diverse types of cracks, including micro-cracks and macro-cracks, leads to the production of various acoustic emissions with varied frequencies and amplitudes (Kawasaki et al. 2013a). The Ib-value is an AE indicator that serves as a connection between low-amplitude AE impacts caused by micro-cracks and high-amplitude AE hits caused by macro-cracks. Hence, micro-cracking causes an increase in Ib-values, which signifies the build-up of tension caused by the propagation of fractures. This technique can be effectively and conveniently used in the non-destructive evaluation of EPS panels.

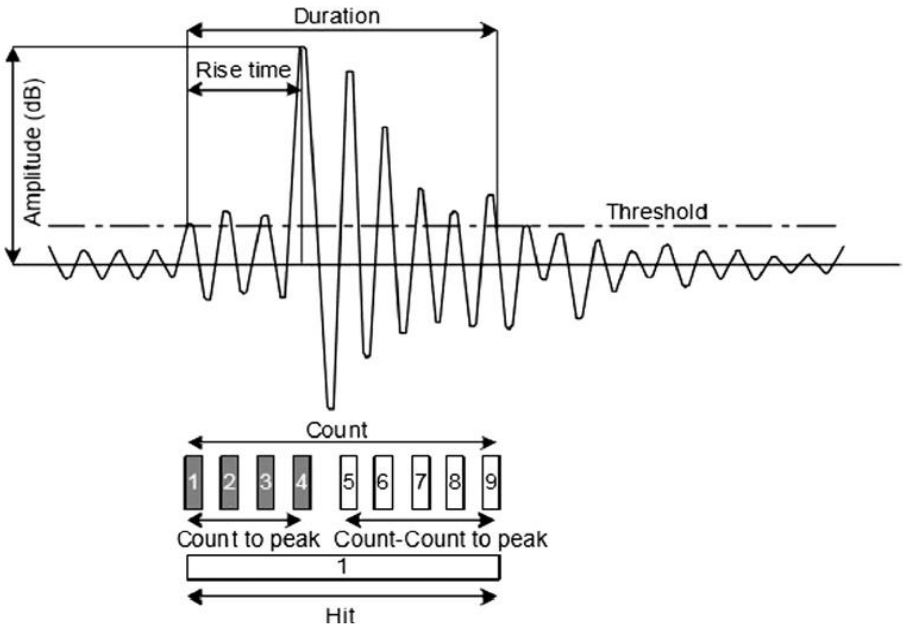

Figure 1.10 Various AE waveform parameters (Grosse and Ohtsu 2008)

1.6 OBJECTIVES OF THE STUDY

The objectives of the present study based on the research gaps identified in the available literature are outlined as follows:

- To conduct a comprehensive evaluation of Expanded Polystyrene (EPS) sandwiched composite panels subjected to chloride-induced corrosion, utilizing both destructive and non-destructive testing techniques to assess degradation and performance efficiency.

- Investigate the durability and degradation behavior of EPS sandwiched composite panels under acid and sulfate attack, employing a combination of destructive and non-destructive methods.
- Assess the thermal performance and mechanical stability of EPS sandwiched composite panels exposed to elevated temperatures, using experimental approaches to evaluate material resilience and fire resistance.

1.7 ORGANISATION OF THESIS

This thesis is organized into seven chapters, each addressing critical aspects of EPS sandwich panels and their performance under various conditions:

Chapter 1 Provides an overview of the construction industry's shift towards innovative materials and technologies. Highlights the advantages of EPS sandwich panels over traditional masonry, including cost-effectiveness, lightweight properties, rapid construction, and enhanced structural integrity. Emphasizes the importance of validating the long-term durability and reliability of new construction materials through thorough research.

Chapter 2 Examines existing research on EPS sandwich panels, detailing their properties, advantages, and performance compared to traditional materials. Available research on the potential threats posed by aggressive environmental conditions such as acid attacks, sulphate attacks, and elevated temperatures. Reviews the application of non-destructive evaluation techniques, particularly Acoustic Emission (AE), for monitoring the structural health.

Chapter 3 Describes the experimental setup for evaluating the flexural performance of EPS panels under different environmental conditions. Details the dimensions and specifications of the EPS panels used in the study. Explains the procedures for simulating chloride corrosion, acid attack, sulphate attack, and elevated temperatures. Outlines the AE monitoring process and the parameters for detecting damage in the panels.

Chapter 4 Presents the findings on the impact of varying levels of corrosion on the flexural strength of EPS panels. Analyzes the AE data to gain insights into the acoustic behaviour of the panels during loading.

Chapter 5 Examines the impact of acid and sulphate attacks on the durability of EPS panels. The panels are subjected to flexural testing in sulfuric acid and sodium sulphate environments, simulating aggressive chemical exposure. AE monitoring is employed to detect

micro-cracks and structural changes in real-time, providing insights into the panels' mechanical behaviour and durability.

Chapter 6 Investigates the degradation of EPS panels subjected to elevated temperatures and four-point flexural loading. The study assesses parameters such as yield load, ultimate load, deflection, ductility factor, stiffness, and composite action to evaluate the impact of thermal and mechanical stresses. The chapter also explores the application of Acoustic Emission (AE) monitoring as a non-destructive testing (NDT) technique to detect early signs of degradation under heat exposure.

Chapter 7 Summarizes the study's key findings, emphasizing the degradation in mechanical properties of EPS panels under aggressive environmental conditions. Highlights the importance of AE monitoring in providing reliable indications of damage and degradation. Discusses the implications of the results for the wider application of EPS panels in the construction industry. Suggests directions for future research to enhance EPS panels' long-term durability and resilience.

1.8 CLOSING REMARKS

This introduction chapter has provided a foundational understanding of EPS and its application as EPS-sandwiched concrete panels. The essential components of these panels, including outer wythes, reinforcement, shear connectors, and the concept of composite action are explored. This groundwork sets the stage for comprehensively investigating EPS panels' performance in various structural applications. Additionally, the causes and impacts of corrosion, acid attack, sulphate attack, and exposure to elevated temperatures on concrete structures and EPS panels are discussed. Understanding these degradation mechanisms is crucial for developing resilient construction materials capable of withstanding harsh environmental conditions. Furthermore, the principles of the AE technique and its relevant variables are introduced.

By establishing this comprehensive overview, this chapter paves the way for the detailed research and analysis presented in subsequent chapters. The insights gained here will guide our exploration of innovative solutions to enhance the durability and performance of EPS-sandwiched concrete panels, ensuring their effectiveness in modern construction.

CHAPTER 2

LITERATURE REVIEW

2.1 GENERAL

The advancement of technologies and the emergence of new materials keep evolving in the construction industry. The emerging new material provides faster, more cost-effective, pleasant, and stronger alternatives to conventional materials and procedures. Nevertheless, the adoption of these developing materials requires a deliberate approach, involving thorough research to confirm their dependability and establish trust. Although these materials often demonstrate satisfactory strength, a comprehensive examination of their durability is nevertheless necessary for all categories. Such material evaluated in this study is the emerging EPS sandwiched concrete panel, it is a novel material utilized in the building sector. Compared to traditional brick and stone masonry techniques, this material is cost-effective, lightweight, quick to construct, and economical. It enhances structural integrity and exhibits optimal performance during seismic events. Several conducted studies demonstrate that the structural ability of these panels exceeds that of brick masonry. However, there is a scarcity of study on the long-lasting nature of EPS panels.

The following sections provide an overview of the existing literature on EPS sandwiched concrete panels, acid attacks on concrete materials, sulphate attacks on concrete materials, and exposure of structural components to elevated temperatures. In addition, the literature on non-destructive techniques of AE utilized in structure health monitoring is reviewed.

2.2 EPS SANDWICHED CONCRETE PANELS

EPS sandwiched concrete panels have been used in cold countries for decades. The EPS panels provide both high structural strength and are light in weight. The light weight of the EPS panels due to low density EPS foam sandwiched in between the structural concrete wythes makes it easy to use and cast. EPS sandwiched concrete panels are frequently utilized as load-bearing walls in residential structures. Much research has been carried out on EPS panels and the same are briefed in the following sections.

2.2.1 Flexural behavior of EPS panels

(Bush and Stine 1994) tested flexural strength of composite Precast Concrete Sandwich Panel (PCSP) having full scale size. The loading was applied in the cycles to examine the

fatigue in the panels. The cyclic loading resulted in reduced stiffness, and it was concluded that the debonding of the insulation and concrete wythe resulted in 15% loss of stiffness. The tests demonstrated a significant level of composite action and exhibited ductility by undergoing substantial deformations prior to failure.

(Salmon et al. 1997) studied the full-scale flexural testing of the pre-cast EPS sandwiched panels. Full compositeness was assumed during the calculation of the ultimate moment. Threaded connectors were determined to be superior to embedded connectors due to their reduced anchorage loss. The panels demonstrate partially composite behavior under service loads, which is reflected in their load-deflection performance.

(Pessiki and Mlynarczyk 2003) Performed lateral load tests on four full-scale precast concrete sandwich wall panels. The panels were positioned horizontally and affixed with consistent sideways force. The study found that panels with designated solid concrete areas exhibited greater flexural resistance. It was suggested that, in order to produce the necessary composite action in precast sandwich wall panels, solid concrete regions should be included for shear transmission between the wythes for design purposes.

(Benayoune et al. 2008) Conducted a comprehensive investigation, combining theoretical and experimental approaches, to assess the test specimens. The obtained results were then compared with empirical data. The testing determined that the failure modes had similarities to those observed in the solid slab. The finite element analysis precisely predicted the load-deflection curves obtained from the experiments and the strain in the shear connectors. It has been noticed that the stiffness of the shear connectors has a substantial influence on the load-bearing capability of the panels. A two-dimensional finite element model was proposed using the available data to accurately measure the extent of composite action with truss-shaped shear connectors.

(Hassan and Rizkalla 2010) Examined the correlation between the total thickness of the precast sandwich panel and its ability to sustain loads. The study emphasizes the influence of the degree of curvature and slip-strain behavior. It accomplishes this by creating a design chart that can be used to predict the flexural capacity of wall panels with different shear-reinforcement ratios. The approach was further confirmed using finite-element analysis, which demonstrated a strong correlation between the projected displacements and stresses and the experimental data, up to the service-load level.

(Raju et al. 2014) Examined the conduct of 3D-Panels for structural purposes. The study found that the axial compressive strength of the wall panel is influenced by both the compressive strength of the concrete utilized and the aspect ratio of the panel. The shear strength of the panels is directly correlated with the quantity of diagonal connectors present. The flexural strength is contingent upon the combined factors of the overall thickness, concrete strength, and the level of composite action facilitated by the diagonal connectors. The insulation thickness for the sandwiched panel can be determined based on the desired thermal resistance to be attained. The maximum load that the panels can withstand is mostly determined by the compressive strength of the mortar and the thickness of the panel.

(Choi et al. 2015) Performed testing on Insulated Concrete Sandwich Wall Panels (ICSWP) in both positive and negative lateral directions to simulate wind pressure and suction. The sandwiched panels were assessed based on their ultimate strength and initial stiffness to determine their composite action. The adhesive contact between concrete and insulation was strengthened by the absorptive characteristic of EPS foam, as observed. The inclusion of EPS foam enhanced the flexural response and composite behavior of the sandwiched panels. The tensile strains caused by both positive and negative directional loading affected the bond between the insulation and concrete layers. The behavior of the panels changed depending on the direction of the load. The combined effects of mechanical bonds can be utilized to enhance the structural integrity of the ICSWP by using continuous GFRP shear connectors.

(Chen et al. 2015) Examined the characteristics of expanded polystyrene (EPS) insulation employed in sandwiched panels. The study focused on analyzing the static and dynamic compressive and tensile behavior of EPS panels with densities ranging from 13.5 kg/m^3 to 28 kg/m^3, under various strain rates. Empirical relationships were developed using calculated values of dynamic strengths, Young's modulus of elasticity, and energy absorption. These relationships were then used to simulate the properties of EPS in numerical simulations of dynamic responses in structural insulated panels with EPS foam core subjected to impact and blast loads.

(Amran et al. 2016) evaluated the flexural load taking capacity of the insulation sandwiched panels having concrete wythes of the precast foamed concrete sandwiched panels (PFCSPs) manufactured using foamed concrete with a compressive strength of 25.73 MPa. The test results were assessed based on the highest possible flexural strength, the profile of moment-vertical deflection, the correlation between load and strain, the variation of strain across the

depth of the slab, the influence of aspect ratio, the crack patterns, and the maximum load at which flexural failure occurs. The comparison of the experimental and Finite Element Analysis (FEA) model data exhibited a substantial level of accuracy. The study determined that the PFCSP slab is a viable and efficient alternative to conventional concrete slab systems in buildings.

(Tomlinson and Fam 2016b) emphasized on evaluation flexural response of partially composite insulated concrete sandwich wall panels analytically. The model-based analysis revealed that the increase of reinforcement ration in the sandwiched panels improves the flexural load resistance capacity. The reinforcement strengthens the outer wythes and greater shear transfer is required to achieve the composite action. The use of low strength shear connectors results in reduced composite action. The ductile failure can be ascertained if the reinforcement ratio of the connectors is improved with the wythe reinforcement. Specifically, this adjustment causes the failure to occur through the yielding of the longitudinal steel reinforcement rather than a brittle failure of the connectors.

(Daniel Ronald Joseph et al. 2018) Conducted a flexural capacity test on EPS sandwiched concrete panels subjected to four-point bending loads. The study employed truss-shaped shear connectors and observed that these connectors accomplish composite action till failure. The fluctuation in the thickness of panels affects the ability to bear loads under bending. The ductility of the panels is influenced by the size of the wire mesh reinforcement in the concrete wythes. The wire mesh size further enhances the dispersion of the cracks. It was noted that the shear connectors influenced both the overall load carrying capability of the panels and the composite action between the wythes of the panels. The analysis found that the panels failed due to a combination of flexural and shear forces. The study determined that the ability of the sandwich panels to withstand flexural loads is directly correlated with their thickness.

(O′Hegarty et al. 2019) Examined the sandwich panel with a thin concrete cladding technology. The study aimed to substitute the traditional steel reinforcement with FRP grids and connectors. The study employed high strength fiber reinforced concrete, which eliminated the need for concrete covering and hence reduced the overall thickness of the sandwiched panels. Carbon fiber reinforced grid shear connectors were utilized. The sandwiched panels were subjected to full-scale flexural testing using outer wythes of different thicknesses, specifically 40 mm and 25 mm. The results obtained from these tests were utilized to validate

the precision of the finite element model (FEM). It was noted that the shear connectors did not effectively achieve substantial composite activity.

(Daniel Ronald Joseph et al. 2019b) The flexural characteristics of prototype precast insulated concrete sandwich panels were examined by utilizing truss-shaped continuous shear connectors. The study examined the effects of varying panel thickness and wire mesh quantity on the outcome. The investigation determined that the truss-shaped shear connections effectively achieve composite action under normal operating stresses. The study found that the thickness of the panel directly affects the flexural rigidity of the EPS panels. Further experiments are advised to expedite the development of standards for designing EPS sandwiched concrete panels.

(Hou et al. 2019) investigated the flexural behavior of four full-scale specimens. They observed that all specimens exhibited full composite action when resisting bending moments. The panel with ribbed exterior reinforced concrete panels showed reduced flexural resistance at both yield and the ultimate limit state. This study introduced a series of analytical models that used the test data to further analyze the flexural behavior of the proposed sandwich wall panel. Comparisons of the results indicated that the models provide accurate predictions and can be used for future applications.

(O'Hegarty and Kinnane 2020) Analyzed the flexural characteristics of sandwich panels with high strength concrete faces and evaluated their composite behavior using various techniques such as flexural strength, strain distribution across the top and bottom concrete layers, comparison of applied and internal moments, the stiffness method, and the ultimate load method. Strength-based procedures were discovered to produce varying levels of composite action in comparison to stiffness-based methods. Panels that possess efficient shear transfer and composite action will exhibit a higher overall capacity for bending moment and stiffness compared to panels made of the same material and having the same shape, but with connectors that fail to achieve an equivalent level of shear transfer. Continuous shear connectors offer superior rigidity in comparison to discrete shear connectors.

(Bishnoi et al. 2021) Examined the enhancement of ductility in EPS sandwiched concrete panels subjected to flexural loading by integrating geosynthetic grids in the concrete wythe. Two distinct types of geosynthetic grids were utilized, specifically plastic geogrid and polyester geogrid. The study determined that the use of geosynthetic grids enhanced the flexural strength and ductility of panels. The findings demonstrate a 28% rise in the flexibility of plastic geogrid

(SPGG) and a 36.8% increase in the flexibility of polyester geogrid (SGi200) as compared to the control sample that used wire mesh as wythe reinforcement.

(Chakraborty et al. 2021) Examined the flexural characteristics of sandwich beam panels that include reinforcement and an EPS core. The comparison between the span to depth ratio fluctuation and the cracking moment of the panel was conducted. The analysis revealed that the strain profiles exhibit substantial variance in the bending of the two wythes. The stresses in the panels, as determined by sectional analysis and composite beam theory, differed because these theories did not account for the shear deformation of the EPS core. The correlation between the flexural breaking moment and the a/d ratio is accurately predicted.

(Ahmad and Singh 2021b) Examined the influence of building techniques and boundary circumstances on the flexural strength of Reinforced Concrete Sandwich Panels (RCSP). The RCSP utilized corrugated EPS and wire mesh as reinforcement. The study considered the construction methods of pouring and spraying concrete, as well as the boundary circumstances related to the existence of reinforced concrete beams along the supported margins. The thickness of the wythes and EPS was modified in addition to the variation of procedures and end circumstances. The study found that the thickness and construction technique of the wythes significantly affect the initial behavior of panels until they develop cracks, but their influence on the ultimate load capacity is minimal.

(Borodinecs and Jacnevs 2023) Investigated the application of structural insulated panels (SIPs) in single-family dwellings located in Baltic climates. The study conducted in Riga using DELPHIN simulations concluded that there was no presence of hazardous interstitial condensation, and the risk of mold was low. The orientation of a wall has a considerable impact on how moisture moves throughout the year. This emphasizes the need of considering the specific climate conditions of a location when applying Structural Insulated Panels (SIPs) to ensure safety.

(Shmulsky et al. 2023) Examined the deflection characteristics of structural insulated panels (SIPs) when subjected to bending forces and the gradual deformation that occurs over time. During the testing of full-scale Structural Insulated Panels (SIPs), it was observed that the deflection caused by shear forces exerted on the foam material ranged from 44% to 73% of the total deflection. The foam's modulus of stiffness was reduced, and shear-based deflection was raised as a result of creep testing.

(Alharthi et al. 2024) This study investigated the flexural characteristics of hollow concrete beams that were reinforced with GFRP bars. A total of seven beams were tested, each having different longitudinal apertures. The findings indicated that circular cavities exhibited superior performance compared to square ones. A precise analytical model successfully forecasted the loads, while a parametric investigation emphasized the substantial influence of hole position and concrete strength on the behavior of the beam.

(Huang et al. 2024) addressed the damage of lightweight wall panels and connectors during seismic events, lacking general predictive methods. Using the Maximum Information Coefficient method, a seismic analysis framework was established. Experiments and simulations on EPS concrete panels revealed nonlinear and hysteresis behaviors. A system model and correlation evaluation using refined MIC aid in damage prediction of nonstructural elements.

The flexural response of the EPS sandwiched concrete panels have been studied by experimental, numerical and modelling analysis by many researchers. The sandwiched concrete panels strength, ductility, stiffness and composite action was tested and tried to improve with the variation of the shear connectors size, type and material. Numerous studies have worked on substantially improving the thickness, strength and bonding of the concrete wythes utilizing different methods. The literature tells that the truss-shaped shear connections significantly achieve the composite action under service loads. Though the threaded FRP connectors can significantly improve composite action, they do not facilitate ease of construction in these types of sandwiched panels. The studies show that the thickness of the panel affects the flexural rigidity of the EPS panels. The ductility can be improved by varying the reinforcement of the concrete wythes of insulated panels.

2.2.2 Compression behavior of EPS panels

(Salmon et al. 1997) studied the full-scale testing of the vertically positioned pre-cast EPS sandwiched panels. The panel is comprised of steel and FRP based shear connectors. The panels sustained high loads with anchored FRP based shear connectors, the anchorage loss was minimized in case of threaded shear connectors. It was observed that the panels behaved in a partially composite action under service loads.

(Benayoune et al. 2007) studied the axial behavior of the reinforced composite sandwich panels. The experiment included the recording of the strains in shear connectors, concrete

wythes and propagation of cracking. The load deformation plots were also examined. The test results aided the modeling for finite element analysis of the panels. The study highlighted that the empirical formulas as recommended by ACI design practices on precast solid walls are appropriately applicable on the sandwich panels. The results obtained from the FEA helped in proposing a semi-empirical formula for the sandwich panels.

(Ede and Ogundiran 2014) analyzed the thermal characteristics and compressive strength of the sandwiched concrete panels comprising of the insulation of the EPS at core. The sandwiched panels studied varied with the thickness of the insulation. The axial testing of the insulated panels showed it as a substantial replacement for the conventional wall construction technique.

(Raju et al. 2014) conducted a study on the behavior of 3D-Panels in structural applications. The axial load carrying capability of panels is determined by the concrete grade and the aspect ratio chosen for the 3D wall panel. The shear strength of 3D panels is determined by the ability of the diagonals utilized in the panels to transfer shear loads. The impact of the wall slenderness ratio on the ultimate strength of the panels was examined by altering the height of the walls.

(Tomlinson and Fam 2016b) Examined the ability of EPS panels to withstand axial loads by assessing their load-bearing capability. The testing configuration applied a non-centralized load on the sandwiched panels. The failure modes were classified as concrete crushing, flexural yielding, connections yielding, rupture, stability failures, and progressive failure of connectors. The experimental data was used to verify the analytical models. The investigation determined that there is a clear correlation between the level of composite activity and the span of the panels. An observed trend was that the degree of composite activity increased as the span of the insulated panels increased. The degree of composite action was influenced by the size and center-to-center distance of the longitudinal shear connectors, in addition to the span. A significant level of participation, around 31%, was observed in composite activity due to the presence of insulation.

(Tomlinson and Fam 2016a) Examined the collective influence of axial force and load on the effectiveness of insulated panels equipped with FRP shear connectors and basalt FRP longitudinal reinforcement. The insulation panels utilized high strength concrete wythes with a compressive strength of 60 MPa. These wythes were combined with a layer of Expanded Polystyrene (EPS) insulation, which had a density of 27 kg/m³ and a thermal conductivity of

0.029 W/mK. The level of composite action was assessed using the load and moment (PM) interaction curve. The study revealed that the composite action diminished as the axial load increased. An increase in the applied load causes a reduction in the stiffness of the shear connection, which in turn affects the failure mode.

(Amran et al. 2018) Examined the structural performance of full-scale Precast Foamed Concrete Sandwich Panels (PFCSP). The panels underwent testing under axial stresses with different thicknesses. The LUSAS software package was employed to forecast the Nonlinear Finite Element Analysis (FEA). The FEA data and experimental results demonstrated a commendable level of accuracy and an enhancement in the slenderness function.

(Rao and Poluraju 2020) Conducted an experimental investigation on full-scale precast reinforced concrete sandwich panels used as walls. Full size panels with clearly defined aspect ratios of 3.0 and 2.63 were subjected to lateral loading in the plane. The end conditions were altered by introducing or removing end beam stiffeners. The sandwich walls were subjected to a constant axial load, as well as incremental and repetitive lateral stress, which was administered using a displacement control system. The experimental results were compared with the lateral strength determined by calculations derived from various codes of practice. The addition of additional longitudinal reinforcement and end stiffeners significantly enhanced the lateral strength, crack resistance, stiffness, ductility, and energy absorption and dissipation capabilities of the precast sandwich slim walls.

(Ahmad and Singh 2021a) Examined the structural behavior of Reinforced Concrete Sandwich Panels (RCSP) containing an EPS core when exposed to axial and in-plane shear forces. The panels consist of a corrugated EPS core, welded wire mesh, and orthogonal shear connectors. The empirically determined values of the axial load and shear strength were compared to the calculated values acquired through analytical methods. The experimental values and analytically derived values were closely correlated. The analytically computed shear strength estimates were determined to be overestimated.

(Rajeshwaran and Logeshwari 2023) evaluates sandwich wall infills in framed structures, using EPS cores and concrete layers, as replacements for traditional walls. These panels offer low weight, easy installation, good insulation, and cost-effectiveness. Tests on panels with varying core thicknesses showed high load capacity, minimal deflection, and effective strain performance, proving their superiority over conventional walls.

(Bishnoi et al. 2024) Examined the shear strength of concrete sandwich panels in the in-plane diagonal direction. The panels were modified by integrating geogrids to assess their ability to deform and bear loads. The specimens that included plastic geogrid demonstrated a 13.7% and 26% enhancement in shear capacity and load-bearing capability, respectively, as compared to the control specimen. The study determined that including geogrids into sandwich panels can enhance the load-bearing capacity, shear capacity, and deformation ability of the EPS sandwiched concrete panels.

The research available on the axial response exhibits significant load resisting capacity of the insulated concrete panels for structural applications. The panels with varied shear connectors were tested and it can be concluded that the anchored shear connectors assist in higher load taking capacity and composite action. The insulation is found to be participating in load sharing ranging from 17% to 40% as reported in the studies. The composite action is observed to be diminishing with the increase in the axial load.

2.2.3 Shear Stiffness and composite action

(Bush and Stine 1994) studied the behavior of truss type shear connectors and concrete rib shear connectors in composite PCSP systems. The truss shaped shear connectors were welded together and placed in the longitudinal direction of the panels. The truss type shear connectors provide ample composite action in longitudinal direction and significantly improved the stiffness and the flexural load taking capacity of the EPS panels. It also observed that the construction details have impact on the shear distribution between insulation, shear connectors and concrete wythes.

(David Salmon and Einea 1995) compared the partial composite action of panels with discrete shear connectors and their volume changes. The volume changes was attributed with the temperature variation around the wythes. The results obtained from testing were used for the validation of the model. The model was used to predict the bowing effect on the panels when the temperature gradient occurs across the outer wythes. The study concluded that variations in layer stiffness do not impact the bowing effect.

(Salmon et al. 1997) studied the full-scale testing of the vertically positioned pre-cast EPS sandwiched panels. The EPS panels consisted of steel and FRP based shear connectors. The composite behavior and flexural strength were evaluated through bending experiments, while shear strength was also assessed using a push-off test. Full compositeness was assumed when

calculating the ultimate moment. The panels exhibit partially composite behavior under service loads, as evidenced by the load-deflection behavior.

(Pessiki and Mlynarczyk 2003) conducted lateral load tests on four full-scale precast concrete sandwich wall panels. Various types of shear connectors were utilized including solid concrete areas, and metal connectors. The study compared the solid concrete regions, and steel M-ties. The results show that the use of solid concrete regions achieved full composite action and varied with the number of solid concrete regions between the outer layers of the panels. The M-ties achieved low composite action and strength.

(Benayoune et al. 2008) studied the variation of the steel shear connector and their diameter to evaluate the ultimate strength and change in compositeness of the panels. The finite element analysis accurately estimated the shear connectors strain. It was concluded that the shear connectors stiffness and change in diameter has a significant impact on the degree of composite action. The truss shaped shear connectors achieve higher composite action in panels.

(Hassan and Rizkalla 2010) Suggested a methodology for assessing the shear-flow ability of insulating materials with the carbon FRP shear grid. The insulation materials made of both expanded and extruded polystyrene did not exhibit the same behavior as the plane section near ultimate stresses. It is recommended to use a simplified design table to calculate the nominal moment ability of EPS and XPS foam-core panels at different levels of composite interaction. The approach was further validated by finite-element analysis, which demonstrated a strong correlation between the projected displacements and stresses and the experimental data, up to the service-load level.

(Naito et al. 2011) Evaluated the durability and reaction of fourteen distinct varieties of shear connectors. The study measured the several ways in which failures occurred and the corresponding reactions, creating simple graphs that show the strength of each relationship. The results exhibited significant variation in the strength, stiffness, and pliability of the links, with an average shear strength of 9.3 kilonewtons. The ties exhibited characteristics of elasticity, brittleness, plasticity, and hardening. The flexural behavior of sandwich wall panels was estimated by establishing trilinear constitutive relationships derived from the obtained data.

(Carbonari et al. 2012) Examined the attributes of the perpendicular shear connectors in lightweight sandwich panels. The loading conditions of the three experimental programs were

altered in order to determine their influence on the panel's behavior. It was noted that the connectors have no effect on the stiffness of the construction. The specimens displayed significant deformability and susceptibility to cracking when subjected to typical service loads. It was suggested that the structural response could be improved by incorporating reinforced concrete beams between the slabs and their supporting elements. An established and verified model can aid in accurate forecasting of the configuration of the sandwiched panels.

(Gara et al. 2012) modeled and tested full scale sandwiched wall panels. EPS panels had 35 mm concrete wythes reinforced with 3 mm wire mesh. The orthogonal connectors integrating outer wythes were studied. Testing involved axial and eccentric compression loads. As insulating thickness increases, rigidity decreases. As the slenderness ratio increases, panel load capacity drops. Due to welding, mesh failure at connections with smaller effective cross-sections reduced panel ductility. The denser wire mesh efficiently redistributed the stresses.

(Woltman et al. 2013) Examined multiple shear joints for insulated prefab concrete sandwich wall panels using glass fiber reinforced polymer interconnections. The cohesive connection between the concrete and insulation was a significant factor in 28% of the shear transmission. The incorporation of concrete studs enhances the load-bearing capacity of the structural wythe and reduces the unsupported span of connectors between the two wythes.

(Kim and You 2015) Analyzed sandwich wall panels using grid-type glass FRP shear connectors. The glass fiber reinforced polymer (FRP) shear connectors are utilized to improve the thermal efficiency of the expanded polystyrene (EPS) panels. In addition, the panels were subjected to variations in insulation thickness, specifically 100 mm of EPS and XPS. The EPS panels were laterally tested to assess the level of composite interaction between both concrete wythes. The study determined that the glass Fiber grid shear connectors effectively enhanced the composite action, resulting in a significant improvement in flexural resistance capacity. The EPS insulation facilitates more effective load distribution between wythes in comparison to XPS insulation.

(Tomlinson and Fam 2016a) A study was done to examine the combined impact of vertical and lateral stresses on the durability of basalt Fiberglass shear links and basalt FRP longitudinal strengthening. The composite action, assessed using both strength and stiffness approaches, diminished as the axial load increased. The decrease in rigidity of the shear connection is the primary reason for this deterioration, which consequently affects the overall rigidity of the wall and modifies its failure mechanisms.

(Daniel Ronald Joseph et al. 2019a) Performed an investigation on small-scale precast concrete panels that were subjected to shear pressure throughout their thickness. The study analyzed the thickness of the EPS core, the distance among the wythes with and without EPS, and the variation in shear connector lines. The test results demonstrate that the truss type shear connectors effectively achieve a substantial degree of composite activity. The addition of the Expanded Polystyrene (EPS) improves the transfer of shear forces between the layers of the sandwiched panels. The rigidity of the EPS panels is directly determined by the number of shear connectors. The panels consistently fail due to panel buckling.

(Choi et al. 2019b) Examined the PCSP with a grid-type glass fiber-reinforced polymer shear connection. The shear capacity of PCSPs was determined using the suggested design equation. The test program consisted of 22 double-shear push-out specimens, each featuring various combinations of two types of insulation, insulation width, and grid distances for the shear connectors. The data was employed to calculate the hardness index and shear modulus values. The investigation revealed that augmenting the thickness of the insulating wythe resulted in a reduction in both the maximum shear flow and shear modulus of the PCSP system.

(Hou et al. 2020) Inspected the panel consisting of two Steel Reinforced Concrete Layers (SRCLs) separated by an EPS layer. The panel consists of various types of glass FRP shear connectors. The connectors included web members, circular perforated webs, slotted perforated webs, and solid conventional webs. Shear connections with solid concrete webs demonstrated superior flexural capacity and composite action. The analytical models were created utilizing the transformed cross-section technique and the principles of elastic beam theory. The model demonstrated precise accuracy in predicting the flexural response of the panel up to its yield limit.

(Chen et al. 2020) Conducted a study and comparison of the assessment of the degree of composite action using the displacement technique, strain method, and load method. Flexural testing was conducted to assess alongside the composite behavior of the sandwiched panels. A non-linear Finite Element model was constructed that effectively correlated with the test findings. The validated model was used to conduct a parametric analysis, in which the stiffness and size of the shear connectors were varied.

(Kinnane et al. 2020) The field of research on building cladding using precast concrete sandwich panels is expanding. Insulating two layers of concrete can effectively increase thermal resistance. Steel thin plate connectors are still utilized to vertically support the outer

layer of concrete and transfer lateral pressure from the rain-screen to the structural layer. The design of steel shear connectors must adhere to both thermal and strength capacity limitations in order to achieve optimal performance. A comprehensive empirical investigation investigates the structural shear behavior of precast concrete sandwich panels with steel plate connections of different dimensions, which impact load capacities, stiffness, and failure processes.

(O'Hegarty et al. 2021) Thin precast concrete sandwich panels, featuring high-strength fiber-reinforced concrete and high-performance insulation, are tested for structural and thermal performance. Connected with fiber-reinforced polymer grids, these panels save weight and material, offer manufacturing efficiencies, and meet structural and thermal requirements. The final design, tested on a demonstration building, proves suitable for standard precast facilities.

(Egbon and Tomlinson 2021) examined how insulation kinds and shear connectors affect insulation sandwiched concrete panel composite behavior. Walls with EPS insulation have more composite activity than those with conventional insulation. Insulation surface roughness and concrete bonding affected panel composite operation. The test parameters include glass FRP bar diameter (9.5 and 16.0 mm), insulation (XPS, EPS, PIR), and notch (trapezoidal, rectangular). The results determined toughness index and shear modulus. The study indicated that increasing insulating wythe thickness decreased PCSP system shear flow and modulus.

(Pan et al. 2022) proposed a new type of shear connectors and evaluated the performance of the insulated concrete panels. The C-shaped glass FRP connectors were laid open to shear, tensile, and compression tests to evaluate their performance under different conditions. The increase in the length of the connector resulted in the failure from shear connector to the anchorage bond. The anchor failed due to anchorage rebars and concrete interaction, according to tensile and compression testing.

(Moka and Siva Chidambaram 2023) evaluated two novel connections for joining precast concrete beams using couplers and U-bolts through three-point bending tests. Findings show couplers ensure efficient stress transfer with ductile failure, while U-bolts enhance energy dissipation but suffer interface failure without proper surface treatment. Both methods demonstrated varied performance based on connection elements and materials.

(Shah and Shah 2023) explores a novel SIP design using 170 mm thick polystyrene sheets with 3 mm electro-welded mesh on both faces, enhancing structural integrity. The galvanized mesh acts like reinforced concrete, offering benefits such as ease of installation, cost-

effectiveness, faster construction, lightweight, fire resistance, flexibility, thermal properties, and easy transportation, making it suitable for various design loads.

The studies on the type of shear connectors and their corresponding impact on mechanical properties are reviewed. It understood that the increase in slenderness ratio of the panels results in reduction of load taking capacity. The ductility of the panels is impacted by the size of the welded wire mesh. Glass FRP connectors were weaker in tensile strength compared to steel connectors, failing through longitudinal delamination but remaining intact within the concrete layer. EPS insulation provided better load sharing between wythes than XPS insulation. Solid concrete web shear connectors enhanced flexural capacity and composite action.

2.3 EXPOSURE CONDITIONS

The panels are effective in resisting the load but are misgauged to be durable. Many factors including chlorides, acid rains, sulphates, carbon dioxide and other aggressive chemicals largely affect the existing concrete structures. The passage of time aids deterioration and damage due to corrosion, acid attack, sulphate attack and accidental heat exposures. The impact of various levels of exposure and their corresponding deterioration needs to be evaluated. This section reviews the research available of the acid and sulphate attack on concrete, corrosion of reinforcement and heat exposure of concrete structures and insulation panels.

(Xiao and König 2004) examined experimental studies from the past two decades to compare the mechanical properties of concrete exposed to high temperatures. Mechanical behavior: strength, elastic modulus, peak strain, and Poisson's ratio. The derived yield force and elastic modulus of rebar were examined. Finally, the study examines how high temperatures affect Chinese concrete-reinforcement bar bonds. The study concluded that high temperatures degrade concrete’s mechanical properties, with tensile strength being more affected than compressive strength. Water cooling significantly reduces strength, and rebar is more sensitive to heat than concrete. Further research on explosive spalling and bond strength under heat is recommended.

(Glasser et al. 2008) examined the changes in microstructure because of exposure of concrete to chlorides and carbon dioxide. An explanation of external sulphate attack is provided, detailing the processes that result in the formation of ettringite and Thomasite. The composition of Portland cement is affected by temperature and thermal fluctuations,

particularly during the early stages of hydration. This study emphasized the limitations of accelerated tests and empirical methods while highlighting modeling as a promising approach to predict concrete performance in varied conditions. Combining targeted experiments with modeling can enhance durability predictions, leading to more sustainable and cost-effective concrete construction.

(Yu et al. 2013) Investigated the effects of sulfate attack on concrete and analyzed the factors contributing to concrete expansion in the presence of sulphates. The crystallization theory is utilized to explain the phenomenon of sulfate attack. Correlations were established between the expansion and the alteration of mono-sulphate crystals inside the C-S-H to ettringite. When the amount of substance of the solution reaches the point of criticality, it produces the necessary pressure for the formation of ettringite crystals within tiny empty spaces in the C-S-H. The confinement and significant saturation of the solution result in the creation of ettringite, which leads to the growth of the paste.

(Kazem et al. 2015) Investigated the impact of prolonged exposure on the shear transfer process between FRP/foam and concrete in sandwich panels. Environmental exposure causes the gradual deterioration of GFRP over time. A timeframe of 7 months was offered for exposure. The study suggested incorporating 30% of the overall capacity of the shear connectors into the design.

(Soive and Tran 2017) studied the model based physical and chemical factors to predict the penetration of sulphate ions into fully saturated cementitious materials. The previously conducted experiment results were used for the numerical profiles of sulphate concentration in the material. The study revealed that the degree of supersaturation increases in correlation with the concentration of the aggressive sulphate solution, without a significant rise in the total sulphate content within the material. These findings align with the principles of crystallization pressure theory.

(Bastin and Sharma 2017) tested alternative strengthening methods to restore reinforced concrete beams injured by high temperatures. Reinforced concrete beams were built, heat treated, reinforced, and tested to determine the effects of factors. Study variables included strengthening technique and thermal damage. For strength and stiffness restoration, externally bonded FRP proved best.

(Vishnu et al. 2017) The study assessed the durability of EPS sandwiched panels exposed to alternate wetting-drying cycles and impressed current corrosion. It found significant reductions in flexural and in-plane shear strength, with impressed current corrosion causing the most damage, particularly to steel reinforcements. The pin-connected shear connectors failed to achieve effective composite action between the EPS and concrete layers, further weakening the panels. These results highlight the need for improved connection designs and protective strategies to enhance the structural performance of EPS panels in environments prone to harsh weather or corrosive conditions.

(Sanchez et al. 2017) Research has shown that the corrosion of steel rebar has a major negative impact on the condition of reinforced concrete structures. Multiple corrosion pathways lead to the formation of geometric defects and decrease the mechanical integrity, with the presence of interstitial hydrogen resulting in embrittlement. This study investigates the impact of local, dents, and corrosion stress on the performance of rebar. The research reveals that the strength of the rebar is influenced by the morphology of corrosion and the amount of weight loss. Furthermore, the study provides an explanation for the variability observed in experimental results.

(Sun et al. 2019) studied the elastic deformation characteristics of concrete when subjected to sulphate exposure. The study focused on the creation of a comprehensive computational model to predict the time-based elastic deformation characteristics of concrete materials. The model included the flow of ions, pore size and corresponding diffusion and ettringite induced internal tension in the concrete. The model was correlated with the experiments results. It was observed that when the ettringite concentration is more than 50% the internal stress stabilizes. Additionally, it demonstrates that the diffusion coefficient of sulphate ions declines as time progresses because of the accumulation of reaction products.

(Irico et al. 2020) Evaluated the corrosion resulting from highly concentrated sulfuric acid exposure at a pH of around 2 on two different types of Self-Compacting Concrete (SCC). The study found that the quantity of acid solution renewal during the exposure time has an impact on the amount of mass lost and the rate at which concrete degrades. The methods significantly contributed to the degradation of the concrete, resulting in a loss of 2.5 kg/m^2 after being exposed for a period of six months. Implementing granulometric cement optimization only led to a modest enhancement in the acid resistance of concrete. The observed discrepancy, in

comparison to SCC-OPC, indicates that the impact of cement type diminishes in importance when dealing with low water-to-cement ratio concrete and efficient concrete techniques.

(O'Hegarty et al. 2020) studied thin, lightweight precast concrete sandwich panels with high-performance insulation, it was observed that they show promise but need better thermal performance analysis. Experimental and finite element studies reveal significant thermal bridging, leading to higher heat loss. Optimized designs could reduce the U-value by 59%, improving efficiency compared to standard thicker panels.

(Daniyal and Akhtar 2020) explored electrochemical techniques for accurate measurement of the rate of corrosion in steel samples. Number of corrosion control methods containing electrochemical chloride extraction, surface treatments of steel and concrete, cathodic protection, chemical corrosion inhibitors and the utilization of mineral admixtures. Each method comes with some advantages and disadvantages and the need arises to originate more economical non-destructive corrosion monitoring and prevention techniques.

(Xue et al. 2020) studied the durability of precast sandwiched concrete panels with glass FRP shear connectors under alkaline conditions. The alkaline conditions created demonstrated the environment during the elevated temperatures. scanning electron microscope images were observed to study the effects of varying durations and magnitudes of temperature exposure on the glass FRP connectors. The findings revealed that tensile and compressive strength of the glass FRP connectors were significantly reduced due to the exposure. Despite these changes, the glass FRP connectors were still able to retain their minimum tensile strength.

(Sakthivel et al. 2021) The use of supplementary cementitious materials (SCMs) is growing in construction, but long-term data on their effects on shrinkage and creep are limited. This study investigated shrinkage in blended concretes with varying water-to-binder ratios and binder contents, finding that fly ash and slag did not significantly affect drying shrinkage compared to conventional concrete. Experimental and model-predicted shrinkage strains showed notable differences.

(Malik et al. 2021) Stressed the importance of assessing the level of harm resulting from heat exposure in order to choose the most appropriate retrofitting approach. Concrete's composition can be established by assessing the properties of each of its parts after being subjected to high temperatures. Distinct crystallographic configurations of materials lead to distinct thermal expansion properties in the cement-sand matrix and coarse aggregates. The

objective of this study is to do a concise and evaluative examination of the thermal and mechanical characteristics of various types of concrete and its components under high temperatures.

(Andrade et al. 2021) studied to reduce clinker production and emissions, the industry seeks alternatives like bentonite, a common clay. This study found bentonite, used without precalcination, promising for reinforced structural concrete, showing favorable mechanical strength and resistance to sulfates, carbonation, and chlorides.

(Klak et al. 2022) examined the effects of fire on reinforced concrete structures, highlighting the reduction in strength and elasticity of concrete and steel as temperatures rise. It finds that fire decreases the load-bearing capacity of beams, slabs, and columns, with deformation worsening over time. Increased cross-sectional thickness improves fire resistance, while fire negatively impacts structural members, especially beams and columns. Slabs experience significant bending moment redistribution and deflection as temperatures rise. The study stresses the importance of individually evaluating structural elements to optimize fire-resistant design and ensure structural integrity.

(Huang et al. 2022) Conducted a study on the effects of fire on precast concrete sandwich panels (PCSPs) with fiber-reinforced polymer (FRP) enhanced geopolymer concrete for the two layers and FRP tubes as the connectors for shear resistance. The fire was visible on a single side of the panel for a duration of 4 hours. The tests demonstrated that the axial strength of the panels decreased by 88% after exposure. Furthermore, the choice of reinforcement, the thickness of the reinforced concrete wythe, and the kind of connector are critical factors that impact the structural integrity of the precast concrete sandwich panels (PCSPs) following a fire.

(Ahmad et al. 2022) Corrosion of reinforcing steel in concrete is a major durability issue in RC structures exposed to chloride and carbonation. This study developed a novel approach to induce uniform, natural-pattern corrosion in rebars. The setup involved a DC power supply capable of maintaining the required voltage and current density over the experiment's duration. The positive terminal of the power supply is connected to the steel bars inside the RC beam (serving as the anode), while the negative terminal is attached to a stainless-steel plate (acting as the cathode). Initially, a higher voltage is needed due to the concrete's and steel bars' high resistivity, but as the corrosion progresses, this voltage decreases because the resistivity drops.

RC beams were corroded to varying degrees and tested under flexural stress, demonstrating the method's efficacy and accuracy.

(Jyoti Basu et al. 2022) Conducted a rigorous analysis of the performance of EPS sandwiched concrete panels under fire and bullet loads. The thermos-mechanical model of the sandwich panel entails studying the transient heat transport and connecting it with temperature-displacement analysis. An increase in temperature causes the stresses to be redistributed, resulting in a decrease in the strength, stiffness, and overall lifespan of the panels. A three-point bending test is used to quantify the stress distribution across different temperature regions. The ABAQUS software is employed for doing Finite Element Analysis (FEA) on these panels.

(Garhwal et al. 2022) studied the impact of the corrosion on the durability of the EPS sandwiched concrete panels tested under four-point flexural loading. The study examined these panels' strength, stiffness, ductility, and composite action. The ultimate flexural load-carrying capacity decreases by 6.98%, 13.93%, 20.62%, and 60.45% after 5, 10, 15, and 20 days of accelerated corrosion, respectively.

(Abolhasani et al. 2022) Formulated an extensive experimental protocol to investigate the microstructural, mechanical, and fracture characteristics of Calcium Aluminate Cement Concrete (CACC) following exposure to elevated temperatures. The residual fracture parameters, such as fracture toughness, fracture energy, and characteristic length, were calculated following the guidelines provided by RILEM. The scanning electron microscope scans showed that the gaps between the particles expanded as a result of the rising internal vapor pressure, showing an increase in the number of pores within the concrete structure. Nevertheless, with the rise in temperatures, there was a concurrent decline in both fracture toughness and flexural strength. Furthermore, the findings indicated that at temperatures exceeding 400 °C, the reduction in weight of the concrete primarily occurs as a result of the vaporization of chemically bonded water and the breakdown of cement hydration compounds, both of which are chemical reactions.

(Giriraju et al. 2022) This study examines the impact of chloride-induced corrosion on the tensile behavior of 7-wire strands in prestressed concrete. Corrosion led to complete ductility loss at 12% section loss. Using CT scanning, pitting severity was quantified, and analytical models were developed to predict mechanical properties and pitting factor for field applications.

(Yanjie et al. 2022) Examined the mechanical properties and degradation mechanisms of concrete subjected to varying temperature gradients. The experimental program included temperature gradients ranging from 40-4 °C, 60-4 °C, 80-4 °C, to 100-4 °C. The technique of sonic emission, which does not cause damage, was used to investigate the properties of concrete. The findings demonstrated a significant decline in the structural strength of concrete with increasing temperature, accompanied by an increase in the maximum deformation. As temperature gradients rise, the failure properties of concrete gradually shift from being fragile to becoming malleable. An abrupt surge in the frequency of AE ringing counts can serve as an indicator of concrete damage worsening. Decreasing the value of b while loading can serve as an indicator of concrete failure resulting from temperature gradients, therefore suggesting the existence of visible fissures.

(Andrade et al. 2023) evaluated hydrotalcite, both natural and synthetic, as a substitute for 10, 20, and 30% of ordinary Portland cement. The substitution improved chloride resistance and maintained mechanical strength but showed variable carbonation resistance over time.

(Li et al. 2023) The fire performance of structural insulated panels (SIPs) was examined by altering the epoxy resin adhesive (EA) with expandable graphite (EG), ammonium polyphosphate (APP), and calcium carbonate (CaCO3) to produce a flame-retardant adhesive (FREA). The study discovered that FREA (Fire-Resistant Epoxy Adhesive) had enhanced fire resistance, resulting in a 33% increase in char yield, a higher limiting oxygen index, and a superior UL94 V-0 rating when compared to the normal EA (Epoxy Adhesive). In addition, FREA decreased the rate at which heat is released and lowered the amount of harmful emissions, so improving the fire safety of SIPs without affecting their functionality.

(O'Hegarty et al. 2024) Improving building performance is crucial for reducing greenhouse gas emissions and energy consumption. However, a gap between design and actual performance, often attributed to occupant behavior, complicates this effort. This study addresses the technical reasons for this gap, focusing on moisture in insulation and thermal bypass. Using thermal resistance analogies and computational fluid dynamics, it finds that moisture and bypass can significantly increase heat loss and energy consumption. The results highlight the importance of not only designing but also adequately installing insulation to ensure optimal performance.

(Pillai et al. 2024) expected premature corrosion and failures. Reviewing corrosion assumptions and developing methods for "corrosion-free" PSC structures is crucial. Key points

include determining the chloride threshold for S-C systems and introducing non-invasive techniques like chemical treatments and cathodic protection to control corrosion in PT structures with voids.

The literature on the exposure of concrete and reinforced structures to corrosive environments, acid attack, sulfate attack, and elevated temperatures highlights significant degradation in both physical and mechanical properties. Corrosion of structural elements is shown to severely reduce load-bearing capacity, while acid attacks lead to concrete deterioration and, with prolonged exposure, reinforcement corrosion. Sulfate attacks, particularly due to the formation of ettringite, cause concrete expansion and deterioration, especially in environments with high saturation. Elevated temperatures negatively affect the characteristics of concrete components, as scanning electron microscopy (SEM) reveals increased pore formation due to internal vapor pressure. This results in reduced fracture toughness and flexural strength at higher temperatures. However, there is a notable gap in the literature regarding the exposure of insulated sandwich panels to these conditions, with limited research on corrosion and no studies found for acid attack, sulfate attack, or elevated temperatures.

2.4 NON-DESTRUCTIVE ACOUSTIC EMISSION TECHNIQUES

The AE technique is a highly effective method for evaluating the deterioration of structures. Through the provision of timely notifications, it empowers the protection team to expeditiously execute repairs, leading to a decrease in expenses and an extension of the durability of structures. According to ASTM E 1316 (2006), Acoustic Emission refers to the occurrence of transient elastic waves emitted due to the sudden release of energy from locations of fault within a material. AE technique is the process of identifying vibrations generated by waves, which are subsequently recorded by AE sensors upon reaching the material's surface. Piezoelectric sensors convert mechanical vibrations into electrical signals, which are subsequently amplified and transmitted to a data acquisition system. The AE technique is useful in detecting the deterioration of structures well before failure. Many researchers have studied the application of AE technique on different materials and structural members to understand the AE parameters related to deterioration.

(Idrissi and Limam 2003) Conducted research on the process of chloride corrosion of steel that is encased within concrete. An endeavor is undertaken to identify the deterioration induced by corrosion by the acoustic emission method. The experimental results show that

electrochemical techniques can evaluate the corrosiveness of the medium used. The acoustic emission had a discernible pattern that indicated both the initiation and advancement of corrosion. Hence, it was highly practical to highlight the acoustic properties of the concrete deterioration linked to the porosity of the mortar and the chloride content. The results indicate a robust correlation between variations in acoustic activity and the magnitude of corrosion density.

(Kawasaki et al. 2013b) Utilized Accelerated Electron Transmission (AET) to investigate the processes of corrosion in reinforced concrete. The onset of reinforcement corrosion can be detected by a drop in the Rise Angle (RA) value and a rise in the Average Frequency (AF) as observed by the Acoustic Emission (AE) parameter. During the later stages, as the cracks caused by rust became more numerous, there was a noticeable increase in the RA value and a decrease in the AF values. The variability of the Ib-value during cracking caused by corrosion was greater than the reported values during the commencement stage. The study determined that Ib-value analysis is an effective method for identifying both the initiation of corrosion and the advancement of cracks caused by corrosion.

(Shahidan et al. 2013) utilized acoustic emission measures such as amplitude, rising time, average frequency, and signal strength to identify and quantify the extent of damage in beams of size 150 × 250 × 1900 mm tested under flexure in the laboratory. The stress strain graphs, and the AE activities were correlated, and it found that the AE effectively established fractures and levels on damage with increase of load.

(Farnam et al. 2015) analyzed the AE waveform to obtain the variation in characteristics of a crack that forms in a cement-based composite material. The cracks that formed in the aggregate were found to have an acoustic emission frequency range of 300 kHz to 400 kHz. The cracks generated in the cement paste matrix ranged in frequency range of 100 kHz to 300 kHz. The early-stage cracks were observed to be of the frequencies ranging from 300 kHz to 400 kHz demonstrating the aggregate cracking. The AE events at later stage of loading were in the frequency range of 100-300 kHz demonstrating the cracks in cement paste.

(Zaki et al. 2015) Utilized the AE method to evaluate and monitor the impact of corrosion on the performance of a Reinforced Concrete (RC) beam during a three-point flexure test. AE's data analysis indicates a distinct correlation between the RA value and AF values, which are indicative of varying degrees of corrosion. The damage index derived from the AE research conducted during the early stages of damage has demonstrated its usefulness as an indication

for assessing the corrosion damage of RC beams under initial loads. The implementation of a Weibull damage function was utilized to estimate the remaining flexural capacity of the beam. Moreover, it was shown that when corrosion intensifies, the incidence of tensile fracture also rises.

(Sharma et al. 2018) examined the utilization of the AE and Ultrasonic Guided Waves (UGW) technique to monitor the spread of corrosion in RC structures. The AE approach is highly efficient in monitoring the onset and advancement of corrosion as compared to the UGW. The commencement of corrosion could not be detected using UGW as there was no change in the waveforms. An increase in the number of AE impacts was noticed from the first day, and the position of cracks was detected using an AE X-Y plot. The stages of corrosion can be clearly identified using both AE and UGW techniques. The integration of guided wave and AE techniques can yield ideal outcomes for the assessment and detection of corrosion.

(Alyamaç et al. 2018) focused countries in seismic zones face significant earthquake risks, prompting governments to focus on urban regeneration. This study aims to determine the optimal non-destructive testing (NDT) method for assessing building material strength in urban regeneration projects. A feasibility analysis evaluated standard NDT methods based on cost and accuracy, highlighting the need for a practical, efficient method for large-scale projects.

(Sharma et al. 2020) Examined the bending characteristics and breakage patterns of reinforced concrete beams that employ both steel and glass FRP reinforcement. Acoustic Emission (AE) measurements, such as amplitude, number of AE events, Acoustic Factor (AF), and Resonance Amplitude (RA), demonstrate a strong correlation with the onset and advancement of cracking in steel Reinforced Concrete (RC) and glass Fiber Reinforced Polymer (FRP) RC beams. The AF-RA value effectively distinguishes and categorizes the various failure scenarios in the two types of beams.

(Yu et al. 2020) examined the corrosion damage along the bar in concrete using the AE technique. AE parameters were correlated with the degree of corrosion. The data obtained from analyzing the distribution of corrosion damage can be utilized to predict possible failures. Mathematical modeling can be used to analyze the bond slip relationship and assess the structural deterioration to estimate the life expectancy.

(Garhwal et al. 2021b) assessed the behavior and performance of full-size beams of 4 meters subjected to different amount of corrosion. The non-destructive technique of AE was

utilized while testing the beams under flexure. The AE hits recorded during the flexural testing precisely showed the different stages of failure. As the amount of corrosion increased, it was visible in the AE parameters of AE hit as compared to control beam.

(Garhwal et al. 2021a) studied the AE response of the glass FRP sheets repaired beams. The beams were subjected to corrosion and then repaired with micro-concrete and retrofitted with glass FRP sheets. The advantages of using glass FRP repair in corroded RC beams were found to be advantageous in regaining the strength of the beam and the same was observed in the AE activities of the repaired beams. The AE hits and their amplitudes increased after the repair of the beam. The growing frequency of AE impacts and the repeated occurrence of AE cracking phases after the repair of corroded beams provide evidence for the efficacy of the AE method in monitoring restored buildings. This technique would enable the identification of subsurface damage, even following the implementation of FRP repair.

(Prem et al. 2021) conducted a study with the objective of identifying the causes of failure, specifically shear, shear-flexure, and flexure, using the non-destructive approach of AE. Nine distinct under-reinforced beams were constructed with variations intended to induce failure in shear, mixed, and flexure modes. AE monitoring was undertaken during the testing, and several parameters of AE were examined, including amplitude, energy, rising angle, average frequency, signal intensity, b-value, severity index, and historic index. The study found a correlation between the characteristics of the AE and the type of failure.

(Singh et al. 2022) Utilized AE Technique to discover the specific failure modes and locations within the Beam Column Joints (BCJ). The AE findings were analyzed based on cumulative AE hits, cumulative energy, rise angle, average frequency, and improved b-value. The improved b-value analysis has shown a significant correlation with the experimental results, indicating that macroscopic fracture occurs in a reinforced concrete beam-column joint (RC BCJ) under stress conditions. The AE event map provides a lucid and precise visual depiction of the progression of fissures in the concrete. AE data can be used to differentiate between tensile and shear fractures that occur at the joint.

(Yanjie et al. 2022) Examined the effects of four temperature gradients (40-4 °C, 60-4 °C, 80-4 °C, and 100-4 °C) on the strength, maximum deformation, and failure of concrete. The mechanisms of deterioration were also observed using AE ringing counts and b value. The findings demonstrated a significant decline in the resilience of concrete as the temperature escalated, accompanied by an increase in the maximum deformation. An rapid surge in the

frequency of AE ringing counts can serve as an indicator of the deterioration of concrete damage. During the loading phase, a reduction in the b value can serve as an indication of concrete failure resulting from temperature gradients, suggesting the existence of visible fractures.

(Burud and Chandra Kishen 2023) examined the long memory phenomenon in concrete fracture processes, quantifying it with the Hurst exponent from acoustic emission measurements. Analyzing magnitude and inter-event times for three beam sizes under monotonic and fatigue loading, strong long memory is found under fatigue loading. Local Hurst exponent variations differentiate monotonic and fatigue loading, aiding damage detection.

(Singh et al. 2023) studied AE and digital imaging to investigate fracture in concrete under tensile load. Analysis identifies four fracture stages: elastic, microcrack growth, stable crack growth, and major crack growth until failure. The fracture process zone (FPZ) is mapped using AE event distributions. Logistic b-value growth aligns with crack progression, aiding failure prediction.

(Radhika and Chandra Kishen 2024b) This work used acoustic emission (AE) to examine the fracture pattern and damage processes in plain concrete subjected to both monotonic and fatigue loads. By examining AE data collected from twelve beam samples, the study concludes that conducting an examination of average frequency, rising angle, and intensity can effectively detect structural degradation and predict possible collapse. The application of K-means clustering identifies four unique damage processes.

(Radhika and Chandra Kishen 2024a) studied use of acoustic emission (AE) and Bayesian analysis to investigate fatigue crack growth in plain concrete under three-point bending. A log-linear relationship between AE parameters and fatigue crack growth is established, with AE energy identified as the best parameter for characterizing fatigue behavior. The model is validated and shown to be independent of loading frequency and specimen size.

2.5 SUMMARY OF LITERATURE REVIEW

Flexural Behavior: The flexural strength and stiffness of EPS panels are highly dependent on the type and configuration of shear connectors. Truss-shaped connectors, for example, significantly enhance composite action and load-carrying capacity. The addition of reinforcement such as geogrids further improves ductility and crack resistance. Moreover,

panel thickness and concrete strength play a crucial role in flexural performance, with thicker panels exhibiting higher load capacities.

Compressive Behavior: EPS panels with anchored FRP-based shear connectors exhibit substantial load-bearing capacity under axial compression. The insulation within the panel also contributes to load sharing, with composite action diminishing as axial load increases. Studies indicate that modifying panel dimensions, particularly thickness, can optimize their compressive strength, making them suitable for structural applications.

Shear and Composite Action: The behavior of EPS panels under shear loads is influenced by the type of shear connectors used. Solid concrete webs and truss-shaped connectors offer superior composite action and stiffness. Studies also show that increasing insulation thickness reduces shear flow and stiffness, while certain insulation types like EPS enhance load distribution between concrete wythes.

2.6 GAPS IN RESEARCH AREA

The following gaps have been identified in the existing literature and require further investigation:

- Long-Term Durability: The studies on the long-term performance of EPS panels, especially under varying environmental conditions such as high humidity, freeze-thaw cycles, and chemical exposure are limited.
- Fire and Elevated Temperature Resistance: There is limited research on the behavior and performance of EPS panels when exposed to fire and elevated temperatures. Though research exists on the behavior of concrete at elevated temperatures, studies on the composite action of EPS panels under the influence of elevated temperatures are lacking.
- Standardization of Design Guidelines: Despite the availability of empirical and finite element models, a standardized design framework for EPS panels is still lacking. Limited data is available on the durability of EPS panels for developing recommendations for design.
- Non-destructive testing: The formation of the non-destructive testing tools for the evaluation of the structural materials is crucial. The research consists of a gap in evaluation of the EPS panels for mechanical parameters using non-destructive tools.

2.7 CLOSING REMARKS

The literature review has provided a comprehensive examination of EPS-sandwiched concrete panels, it covered the critical areas such as the corrosion of concrete structures, acid and sulphate attacks, heat exposure, and the use of AE testing in concrete structures. The review highlights the efficacy of the AE technique in identifying failures in various types of reinforced concrete. Despite its effectiveness, the AE approach has not yet been employed for the examination and monitoring of insulating sandwiched panels. This review suggests that the AE technique holds significant potential for NDT and the evaluation of EPS-sandwiched concrete panels that have deteriorated due to aggressive environmental conditions.

This chapter establishes a solid foundation for understanding the current state of research and identifies key areas for future exploration, particularly in applying AE techniques to EPS-sandwiched concrete panels. The insights gained from this review will inform and guide the subsequent experimental work and analysis, ensuring a thorough investigation into the durability and resilience of these innovative construction materials.

CHAPTER 3

EXPERIMENTAL DETAILS AND METHODOLOGY

3.1 GENERAL

This chapter outlines the materials and methods used to investigate the performance of EPS panels under various conditions. The focus is on assessing material properties, subjecting the panels to corrosion, acid, sulphate environments, and elevated temperatures. Additionally, the AE technique is employed as a Non-Destructive Testing (NDT) method to assess EPS panels degradation. This chapter comprises three subtopics: materials used, exposure conditions, mechanical testing and AE monitoring.

3.2 MATERIALS USED

3.2.1 Cement

Ordinary Portland Cement (53 grade), which is compliant with the IS 12269:2013 has been used and is comparable to ASTM C150-17. standard was utilized. The results of the physical properties of cement are mentioned in Table 3.1.

Table 3.1 Physical properties of cement

Property	**Obtained Value**	**Recommended Value**	**Test Method**
Standard Consistency (%)	31	27-33	IS 4031 (Part 4)
Fineness of cement (%)	0.6	-	IS 4031 (Part-1)
Specific Gravity	3.12	3.15	IS 4031 (Part 11)
Setting Time (minutes) (a) Initial Setting Time (b) Final Setting Time	 90 330	 30 (minimum) 600 (maximum)	IS 4031 (Part 5)
Compressive Strength (N/mm^2) (a) 3 days (b) 7 days (c) 28 days	 29 39.5 57	 27 37 53	IS 4031 (Part 6)

3.2.2 Fine Aggregates

Locally naturally occurring fine aggregates were explored and chosen for the mix in the present study. Table 3.2 lists the locally available river sands, and their gradation determined with sieve analysis as per the procedure recommended by IS 383: 2016. As per the grading of the fine aggregates IS 383: 2016 divides it into four grades (Table 3.3). From the available fine aggregates Pathankot coarse sand was used for the mix categorized as Zone-II (Figure 3.1). The physical properties of the sand were determined, and the results of physical properties are presented in Table 3.4.

Table 3.2 Sieve analysis results for sand

IS Sieve Designation	**% Passing**			
	Black Stone Dust	Markanda Sand	Pathankot Coarse Sand	Yamuna Nagar Sand
10 mm	100	100	100	100
4.75 mm	100	98.5	95	99.5
2.36 mm	98	89	74.5	99
1.18 mm	76.5	65	45.5	98.5
0.600 micron	69.5	56.5	37.5	97
0.300 micron	39.5	39.5	20	74.5
0.150 micron	16.5	10.5	8	16.5
Pan	0	0.5	0.5	0.5

Table 3.3 Grading Zones of fine aggregates (IS 383:2016)

IS Sieve Designation	**% Passing**			
	Grading Zone-I	Grading Zone-II	Grading Zone-III	Grading Zone-IV
10 mm	100	100	100	100
4.75 mm	90 - 100	90 – 100	90 – 100	95 – 100
2.36 mm	60 – 95	75 – 100	85 – 100	95 – 100
1.18 mm	30 - 70	55 – 90	75 – 100	90 – 100
0.600 micron	15 – 34	35 – 59	60 – 79	80 – 100
0.300 micron	5 – 20	8 – 30	12 – 40	15 – 50
0.150 micron	0 - 10	0 - 10	0 - 10	0 - 15

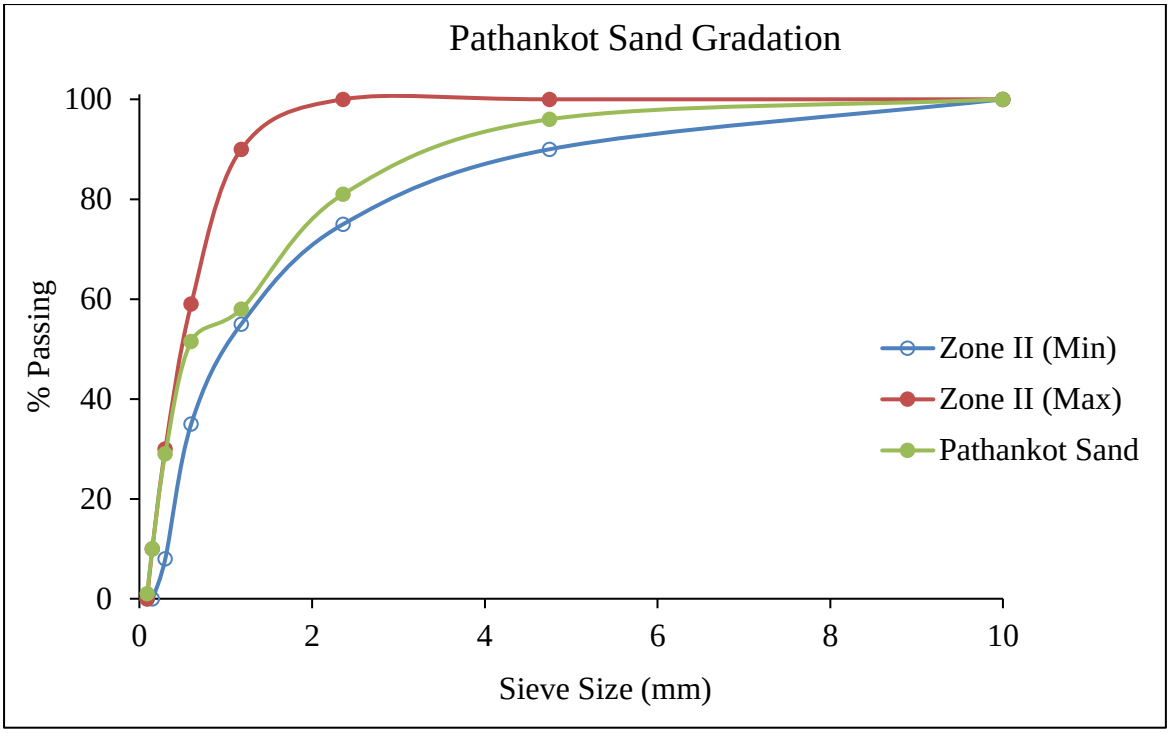

Figure 3.1 Comparison of gradation of sand

Table 3.4 Physical properties of sand

Property	**Value**
Fineness Modulus	3.2
Specific Gravity	2.8
Bulk Density (kg/m^3)	1460
Water Absorption (%)	1.2
Silt Content (%)	< 3.0
Particle Shape	Rounded to sub-rounded
Gradation	Zone-II
Maximum size (mm)	4.75

3.2.3 Expanded Polystyrene (EPS) insulation

Expanded Polystyrene (EPS) is a light, closed-cell plastic made from small hollow spherical beads. This special closed-cell design gives EPS its notable characteristics, resulting in a lightweight yet sturdy foam that offers superb thermal insulation and high impact resistance. Being inert, EPS does not decay and offers no nutritional value to pests, making it unappealing to vermin like rats and termites. Low density EPS (15 kg/m^3) with a thickness of

50 mm was used for the sandwich panels in the study. The physical properties of EPS as provided by the supplier are listed in Table 3.5.

Table 3.5 Physical properties of expanded polystyrene (EPS) -by supplier

Property		**Values**
EPS Density (kg/m^3)		15
Thermal Conductivity (W/m·K)		0.031
Melting Range (^{0}C)		90
Self-Ignition Point (^{0}C)		300
Water Absorption (Volume %)	1 day	0.2
	2 days	0.3
	3 days	2.0

3.2.4 Welded wires

The EPS panels incorporated wires to serve as both reinforcement and shear connectors. A 50 mm square wire mesh was utilized for the wythe reinforcement. The wire mesh on each side was connected by continuous truss-shaped shear connectors, inclined at 70 degrees. According to ASTM A1064 recommendations, the square grid wire mesh and shear connectors were welded to ensure the reinforcement integrity (ASTM A1064 / A1064M-18a 2018). The wires were galvanized (coated with zinc) to prevent rusting. Each wire had a diameter of 3 mm and an average tensile strength of 651.6 N/mm², as provided by the manufacturer.

3.2.5 Mix proportions

The wythes of the EPS panels were designed to be shotcrete after the initial placement of the EPS skeleton, following the guidelines outlined in the CBRI manual (CBRI 2017). The present research simulated the shotcrete mix using a cement-sand mortar mix in 1:3 ratio. The mortar mix for the panels consisted of 1 part cement to 3 parts coarse sand with a water cement ratio of 0.45. The compressive strength of the mix obtained using 70.5 mm cubes after 28 days was 30 N/mm^2. Another mix using a 1:2:3 ratio (Cement: Sand: Aggregates) was used for the stiffened end beams of the EPS panels. The coarse aggregates were used in a proportion of 60% of 20 mm size aggregates and 40% 10 mm size aggregates.

3.3 CASTING OF PANELS

A total of fifty-one EPS sandwiched concrete panels were cast for the study. The total number of specimens included triplicates of each parameter. Each panel measured 1000 × 600 × 130 mm (length × width × thickness), as shown in the schematic sketch in Figure 3.2. The top and bottom concrete wythes of all panels had a uniform thickness of 40 mm. Continuous truss-shaped shear connectors were spaced 100 mm apart along the longitudinal span of the panels. The 50 mm thick EPS was placed in the center of the panel, with a distance of 15 mm between the EPS and the wire mesh. A concrete layer of 25 mm was provided over the reinforcement.

The casting process is illustrated in Figure 3.3. The panel skeleton (EPS, mesh grid, and shear connectors) was cut to size and placed in the mold. The panels casted for corrosion were provided with electric wires connecting the wire mesh before plastering (Figure 3.3a). The mortar mix was then applied to the upper side of the EPS panel. A mold cap was used to flip the panel and plaster the lower wythe. After plastering the wythes, the end beams were cast with the concrete mix. After 24 hours, the panels were removed from the molds, laid horizontally on the ground, and covered with jute bags for curing (Figure 3.4). To ensure proper curing, water was sprinkled periodically (every 2 hours during the day and every 6 hours at night) to maintain moisture. The panels were cured for a total of 28 days.

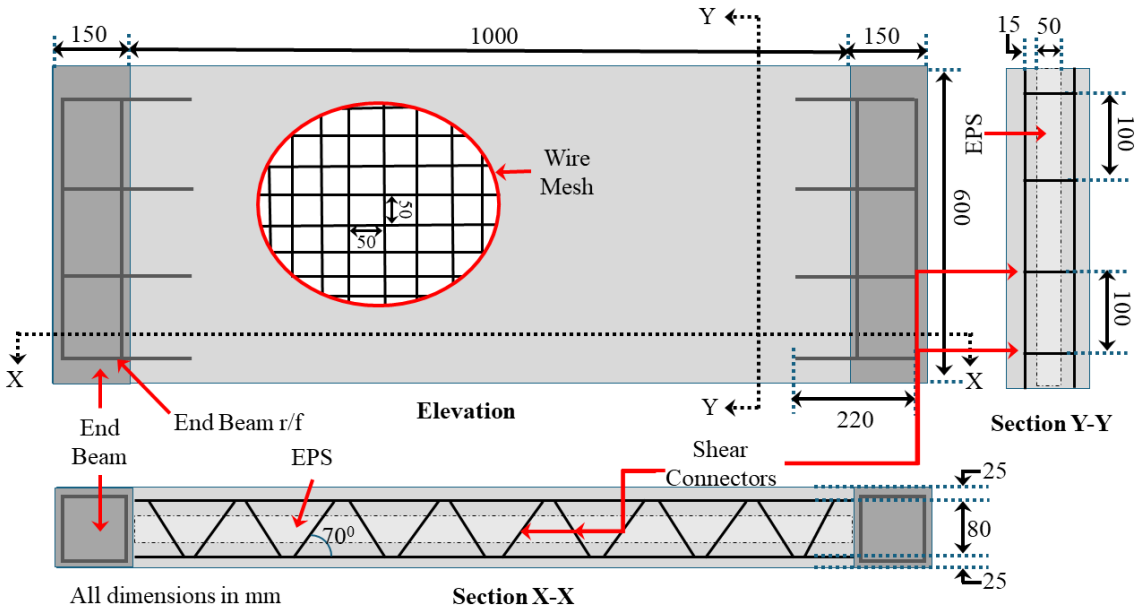

Figure 3.2 Schematic EPS sandwiched concrete panels

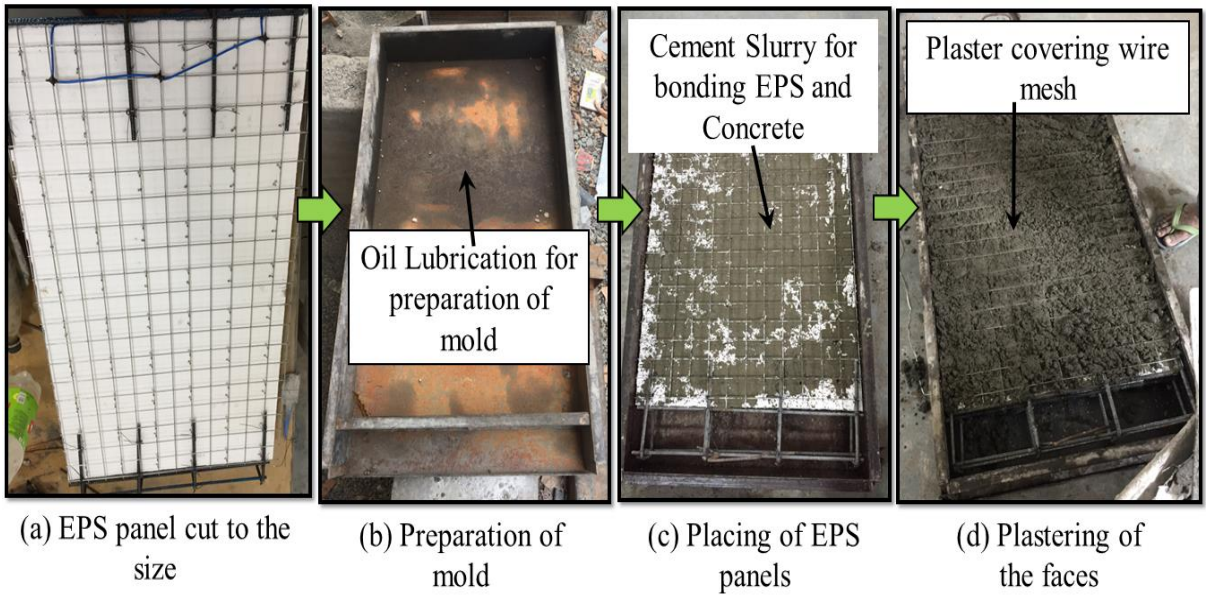

Figure 3.3 Casting of EPS sandwiched concrete panels

Figure 3.4 Curing of EPS sandwiched concrete panels

3.4 EPS PANELS AND ENVIRONMENT EXPOSURE

EPS panels are popular for rapid construction worldwide due to their versatility and exceptional combination of high compressive strength and durability. However, exposure to harsh natural and artificial environments can decrease the durability of the concrete in these panels. Unlike conventional load-bearing masonry constructions, EPS panels require evaluation for environmental deterioration when subjected to severe conditions such as acid

attack, chloride attack, sulphate attack, and accidental elevated temperatures. This section discusses the methodology used for exposing the panels to different environmental conditions.

3.4.1 Accelerated corrosion

Corrosion refers to the gradual degradation of materials, particularly metals, due to chemical reactions with their environment. This process weakens the structural integrity and durability of buildings and infrastructure, leading to potential safety hazards and increased maintenance costs. Factors like moisture, salts, and pollutants accelerate corrosion. Protective measures and regular monitoring are crucial for ensuring structures' long-term stability and performance.

EPS structures are susceptible to degradation in regions with high annual rainfall or extensive coastlines and humid climates. An accelerated corrosion technique was employed to simulate different deterioration stages in the EPS panels rapidly (Bahekar and Gadve 2017, Ahmad et al. 2022). A constant voltage DC power supply (details provided in Figure 3.5) was used for this process. The EPS panels were subjected to a constant voltage of 10 V for varying durations to induce accelerated chloride corrosion in the central 600 mm length. A stainless-steel mesh served as the cathode, and the wire mesh reinforcement acted as the anode. The central portion was continuously dripped with a 3.5% NaCl solution to maintain conductivity (Figure 3.6). The corrosion current was recorded daily at 6-hour intervals.

Figure 3.5 APLAB regulated DC power supply

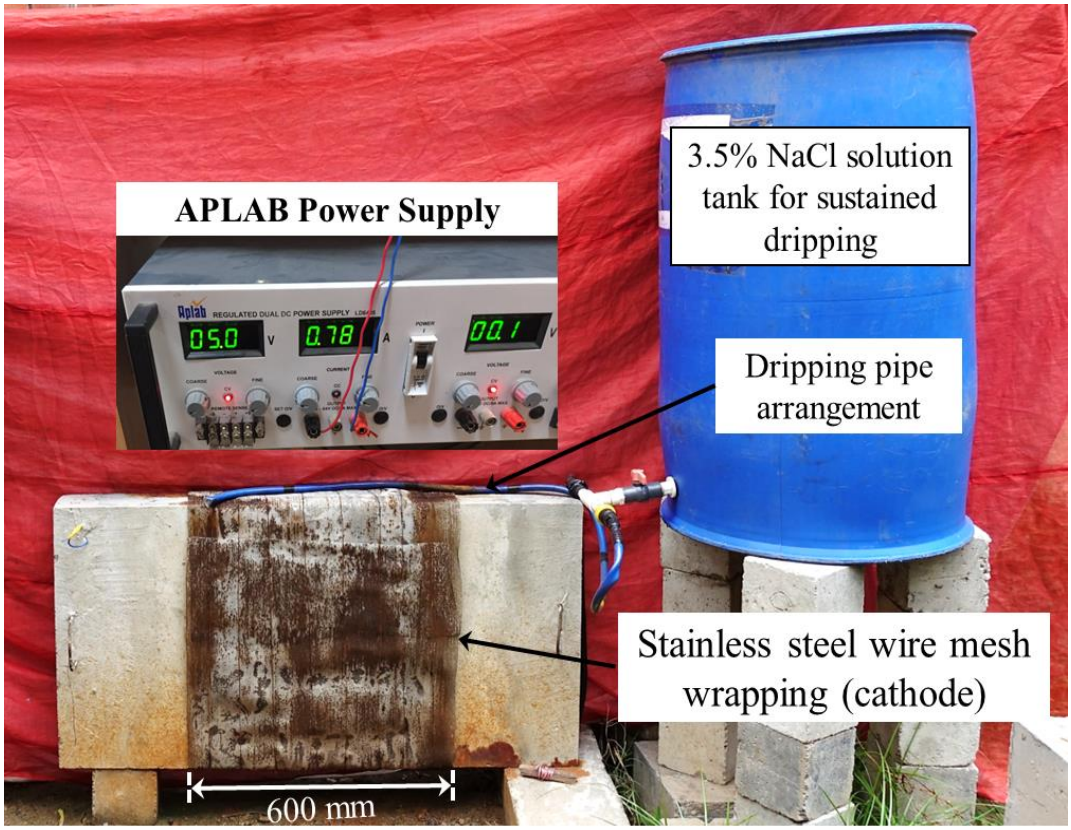

Figure 3.6 Corrosion set-up for EPS Panels.

The duration of exposure for accelerated corrosion was determined through a pilot study in which EPS panels were subjected to corrosion using a power supply. The current was monitored regularly, and the time at which the flow of current decreased was recorded. The point when current starts to decrease denotes that the conductive material is degraded and based on the observations durations of exposure as mentioned in Table 3.6 are decided. The nomenclature for the corroded EPS panels is illustrated as EPS-C05, where "EPS" indicates the panel type, "C" signifies corrosion, and "05" represents the number of days of accelerated corrosion. Similar nomenclature was adopted for other exposure conditions, with "A" denoting acid attack, "S" denoting sulphate attack, and "H" denoting heat exposure (details provided in Table 3.6

Following exposure to different corrosion durations, the EPS panels were visually inspected, and their mass loss was estimated using Faraday's Laws. The physical calculation of mass loss was impractical owing to the distributed wire mesh in wythes, estimated loss was calculated using Faraday' law. The recorded current during accelerated corrosion was used to calculate the panel's total electric charge (Q) using Equation 3.1. Mass loss was then estimated using Equation-3.2.

$$Q = \int_{t_1}^{t_2} I(t) \quad (3.1)$$

$$m = \frac{Q.M}{n.F} \quad (3.2)$$

where,

m = Mass of the substance deposited or released (gm)
Q = total electric charge (Coulombs)
M = Molar mass of the substance (55.8)
n = valence number of ions of the substance (2)
t_1 = Initial Time
t_2 = Final Time
I = Current in Ampere
F = Faraday's constant (96485 C/mol)

Table 3.6 Nomenclature and exposure details of EPS panels

Nomenclature	**Exposure Condition**	**Magnitude of Exposure**
EPS-00	-	Control Specimen
EPS-C05	Accelerated Corrosion	5-days
EPS-C10	Accelerated Corrosion	10-days
EPS-C15	Accelerated Corrosion	15-days
EPS-C20	Accelerated Corrosion	20-days
EPS-A07	Acid Attack (H_2SO_4)	7-days
EPS-A14	Acid Attack (H_2SO_4)	14-days
EPS-A21	Acid Attack (H_2SO_4)	21-days
EPS-A28	Acid Attack (H_2SO_4)	28-days
EPS-S90	Sulphate Attack (Na_2SO_4)	90-days
EPS-S180	Sulphate Attack (Na_2SO_4)	180-days
EPS-S270	Sulphate Attack (Na_2SO_4)	270-days
EPS-S360	Sulphate Attack (Na_2SO_4)	360-days
EPS-H50	Elevated Temperature	50^0 C
EPS-H100	Elevated Temperature	100^0 C
EPS-H150	Elevated Temperature	150^0 C
EPS-H200	Elevated Temperature	200^0 C

3.4.2 Acid and Sulphate Exposure

Acid and sulphate attacks are significant chemical deterioration processes that affect concrete structures. Acid attack Occurs when concrete reacts with acidic substances like sulfuric or hydrochloric acid. This reaction forms soluble salts that leach out, causing surface erosion, spalling, and structural weakening. It is commonly observed in industrial settings and areas exposed to acid rain. Sulphate attack Occurs when concrete is exposed to sulphate ions, typically found in soil or groundwater. These ions react with concrete components to form expansive products, resulting in cracking, spalling, and losing strength. This concerns environments with high sulphate concentrations, such as certain soils and industrial wastewater.

For accelerated acid exposure, the EPS panels were immersed in an acid solution for varying durations (7, 14, 21, and 28 days) after a 28-day curing period. Polyethylene water tanks were used to accommodate the panels (Figure 3.7). The tanks were covered to provide a controlled environment, minimize evaporation, and prevent contamination from fumes. The water level was maintained below the top end beams to avoid corrosion of the handling hooks. A constant pH method was used, with the pH maintained at 1 ± 0.2 using a sulfuric acid (H_2SO_4) solution (Alexander et al. 2013). The pH measurement was done by taking samples and testing them with a pH meter (Make of the pH meter was EUTECH CyberScan pH 510), and adjustments were made with additional H_2SO_4 as needed. The solution was replaced entirely every 7 days. Details of the immersed specimens (EPS panels and concrete cubes) for calculating mass loss and residual strength are provided in Table 3.6.

A similar setup was used for the exposure to the sulphate environment as was used for the acid attack (Figure 3.7). The sulphate solution was prepared by mixing 5% sodium sulphate (Na_2SO_4) in water. The pH of the solution was checked periodically and maintained in the range of 6.0 to 8.0. Along with the EPS panels, prism beams of size 285 mm × 75 mm × 75 mm and cubes of size 70.5 mm were immersed in the solution. The immersed prism beams and cubes were checked for changes in length and mass due to sulphate attack every two weeks (Sun et al. 2019). The sulphate exposure for the EPS panels varied as 90 days, 180 days, 270 days, and 360 days, as mentioned in Table 3.6.

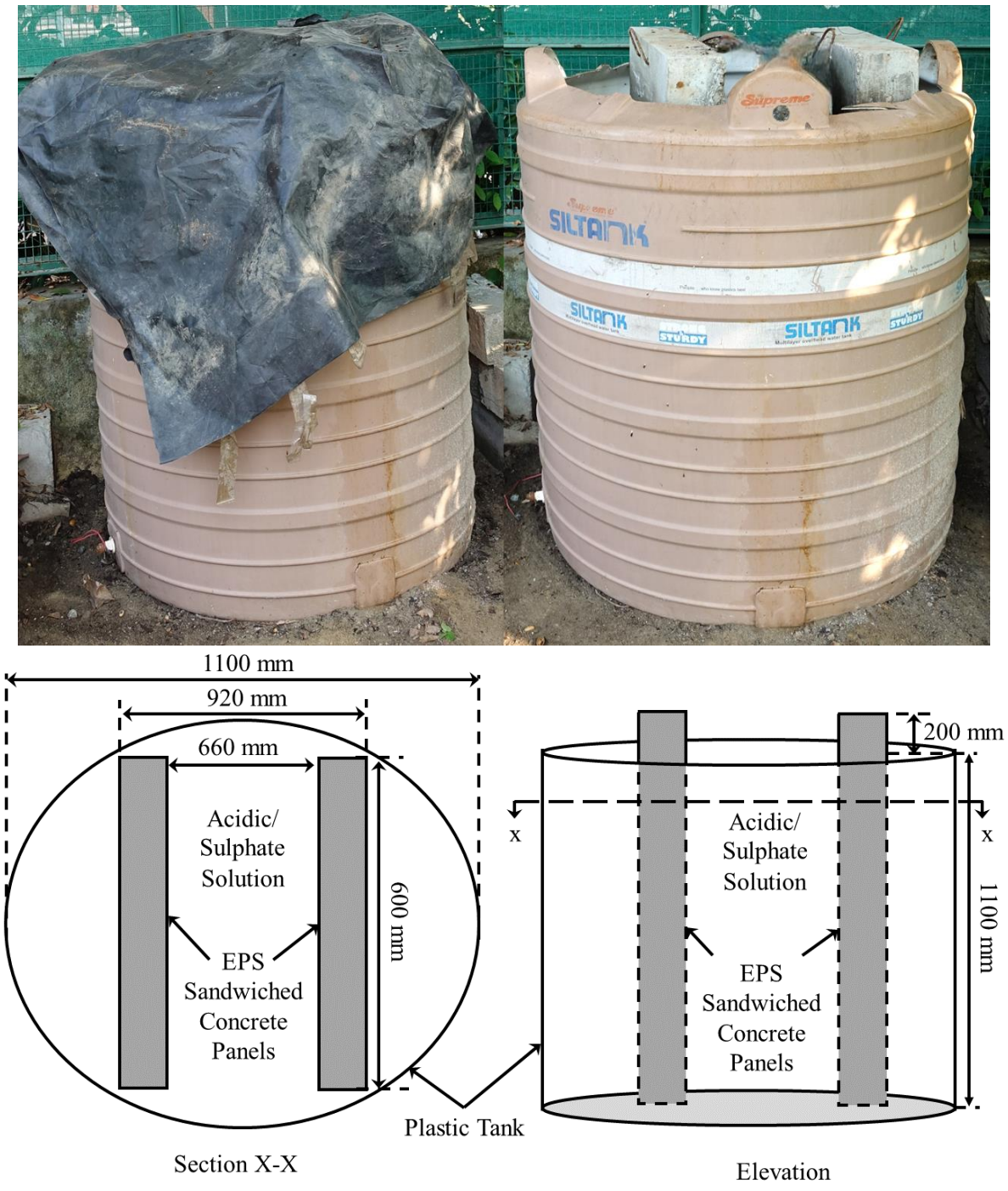

Figure 3.7 Schematic of acid and sulphate exposure set-up

3.4.3 Heat exposure

Despite their significant potential, EPS panels face challenges when exposed to high temperatures. Over recent years, extensive research has been conducted to understand the mechanisms of heat degradation in concrete (Poon et al. 2003, Pulkit and Adhikary 2022). Ettringite dehydrates and decomposes between 70°C and 180°C, while free water in the pores

evaporates around 100°C. The different thermal expansion coefficients of concrete phases and the decomposition of hydration products lead to micro-cracks and weaken the concrete.

After casting and curing for 28 days, the EPS panels were exposed to elevated temperatures using two hot plates, each sized 400 mm × 400 mm and encapsulating five cartridge heaters (Figure 3.8). The test setup was configured in a mold with dimensions of 190 mm in depth, 700 mm in width, and 1400 mm in length. The panels were placed horizontally within the mold, with hot plates positioned beneath the bottom wythe (Figure 3.9). The hot plates were aligned with the centroid of the EPS panel. To prevent heat loss, the cavity area around the EPS panel was filled with glass wool. Thermocouples were attached to the hot plates, and the heating rate was set at 10°C/min. The EPS panel was subjected to heat of varying intensities from the bottom wythe at a constant rate for 3 hours after reaching the target temperature (Figure 3.10). The opposite side of the panel (top wythe) was exposed to the environment, which was at room temperature (~26°C). Details of the exposure for different panels are provided in Table 3.6.

Figure 3.8 Square 400 mm heating plate used for the elevated temperature set-up

3.5 FLEXURAL TESTING OF EPS PANELS

Flexural testing of EPS panels evaluates their ability to resist bending under load. EPS panels are subjected to wind pressure, seismic pressure, and eccentric loads during use in structures. In the test, EPS-sandwiched concrete panels are subjected to a controlled load applied at specific points while the deflection at the midpoint is measured. This setup helps determine the panels' flexural strength, stiffness, and deformation characteristics. The results provide insights into the structural performance and durability of EPS panels in construction.

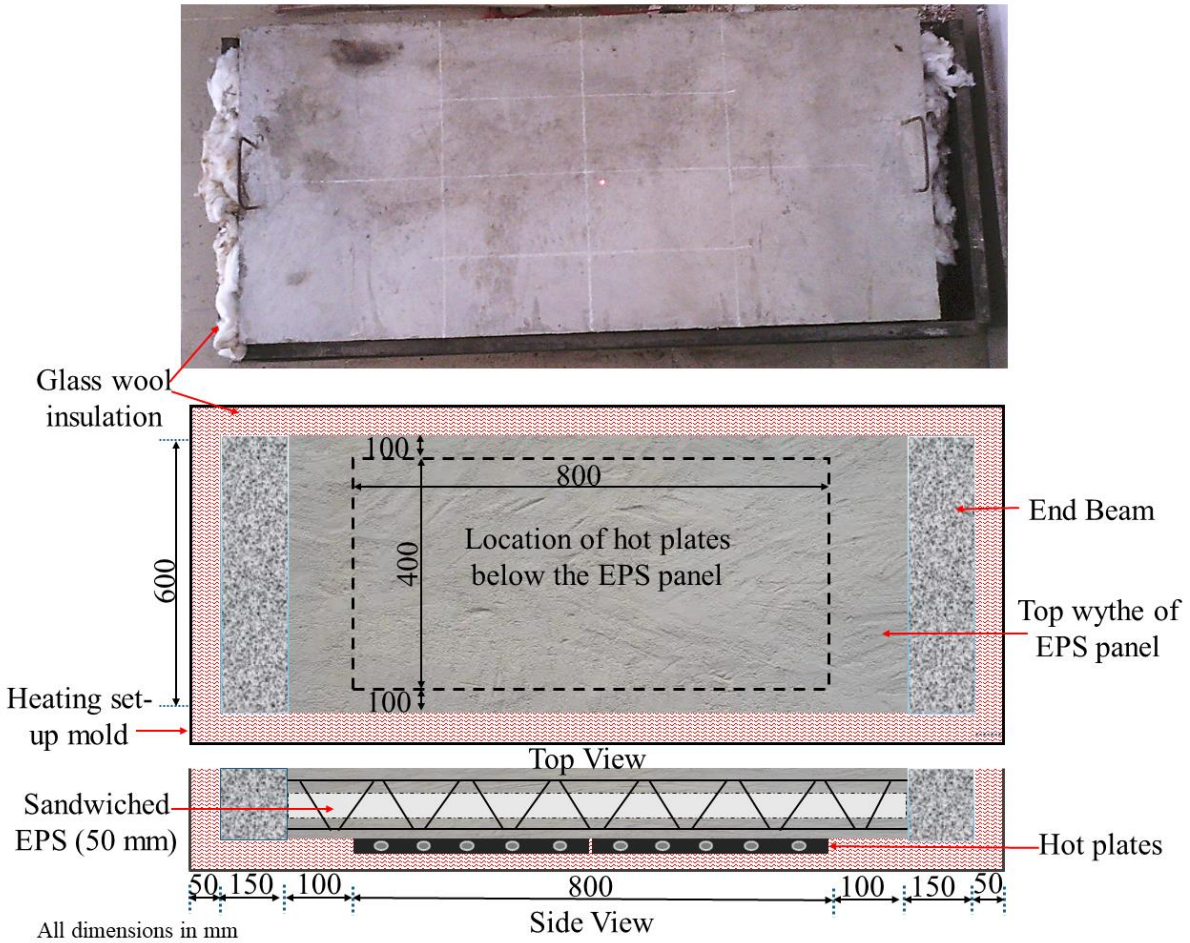

Figure 3.9 Heat exposure set-up of EPS panels.

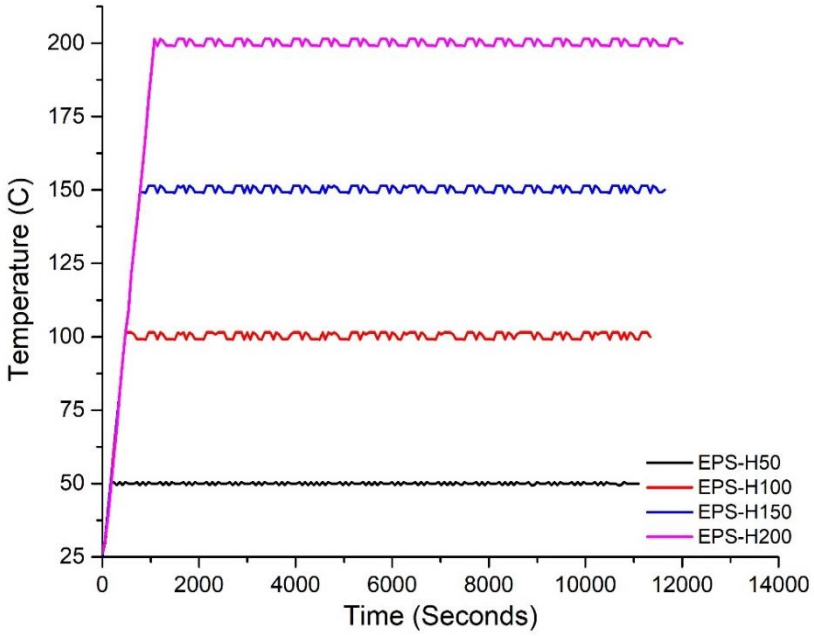

Figure 3.10 Heat exposure vs time graph for heat exposed EPS panels

The unexposed EPS panels, along with the panels exposed to different environments, were tested under flexure. The setup for four-point flexural loading is depicted in Figure 3.11. The

total span for the flexural testing is 990 mm, with the load applied at two points, each positioned 330 mm apart from the other and the supports. The end supports for the testing were arranged with flat plates and bearings to avoid local stress concentration near the supports. The load was applied at a displacement rate of 1 mm per minute using a 500 kN servo-controlled hydraulic actuator. The load cell was attached to the hydraulic actuator, which was connected to the data logger for data collection. The deflection at the midpoint of the EPS-sandwiched concrete panels was measured using a Linear Variable Displacement Transducer (LVDT) with a range of 50 mm and an accuracy of 0.001 mm (Gefran PY2 Series LVDT Sensor) connected to the data logger.

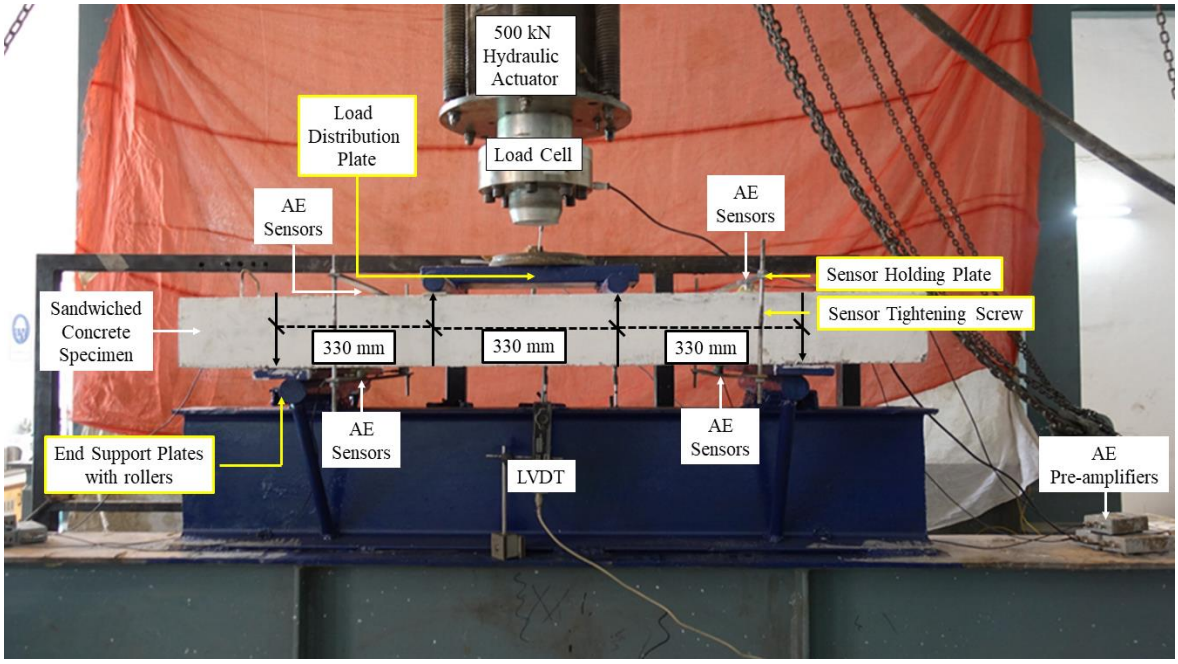

Figure 3.11 Flexural testing set-up

3.6 ACOUSTIC EMISSION MONITORING

Currently, AE technology, a non-destructive testing method, is experiencing significant advancements. The approach for analyzing AE waveforms is undergoing rapid development. An in-depth examination of AE waveforms can ascertain several AE parameters, including AE hits, hit count, signal amplitude, rise time, length, and signal strength (Figure 3.12). An AE hit refers to an acoustic signal that surpasses a predetermined threshold limit. Threshold limits are determined based on elements such as frequency, damping properties of the transducer, and the structure. The area beneath the AE waveform is directly linked to the swift release of energy in a substance and the energy associated with AE. The integral of the rectified AE signal is referred to as signal strength, measured in pico-volt-seconds. The difference in signal strength

is typically expressed as Cumulative Signal Strength (CSS). The AE technique has developed extensive capabilities for evaluating damage in different structural components, particularly for assessing corrosion in reinforced concrete studies (Miller et al. 2002, Garhwal et al. 2021a).

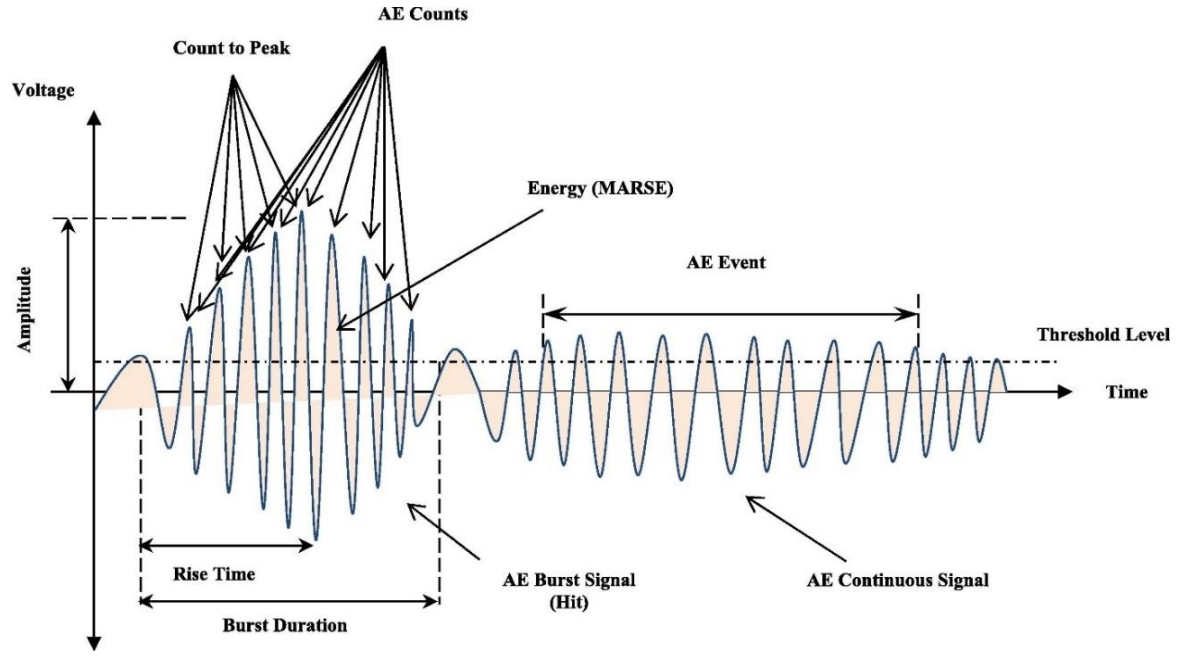

Figure 3.12 Parameters of AE waveform (Ali et al. 2019)

The current study employed the passive acoustic emission (AE) technique to observe and evaluate the mechanical behavior of EPS-sandwiched concrete panels exposed to different environments and tested under flexural loading. The Micro-II AE data acquisition system (SAMOS MISTRAS, PAC) was configured with 8 AE channels, AE sensors, preamplifiers, and filters to collect AE data (Figure 3.13). AE sensors detect signals and waveforms produced by concrete cracks. The AE signals generated have a primary spectrum band that falls between the frequency range of 3 to 60 kHz. Piezometric AE sensors with a resonance frequency of 60 kHz (R6 α) were used to detect the passive AE signals generated by deformations in EPS panels. The compact size of the sensors, with dimensions of 19 mm in diameter and 22.4 mm in height, facilitated easy mounting on the EPS panels (Figure 3.14).

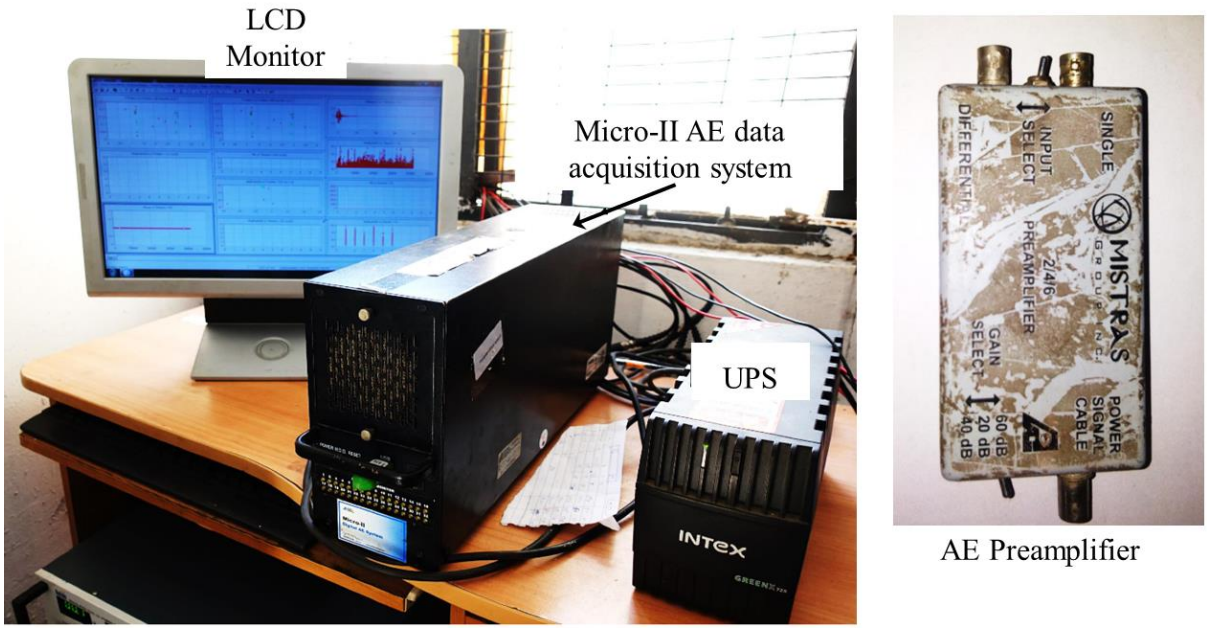

Figure 3.13 AE data monitoring system equipment

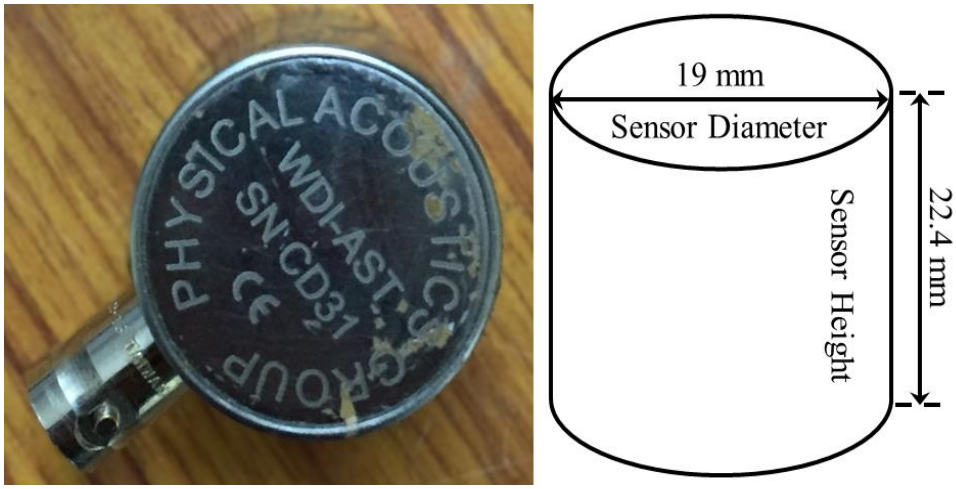

Figure 3.14 R6ά AE sensor dimensions

To acquire AE data during flexural testing of EPS panels, six surface-mounted AE sensors were affixed to the sandwiched panels (Figure 3.15). The sensors were placed in a triangular pattern on both faces of the panel (wythes). Roller bearing grease was applied to ensure a seamless connection between the AE sensors and the surface of the EPS-sandwiched concrete panels. The sensors were secured using flat plates grooved with designated sensor sites to allow for unrestricted installation (Figure 3.11). Each groove was equipped with a sturdy foam foundation to exert sufficient pressure on the sensors, ensuring continuous contact with the surface while preventing any harm to the sensors. The plates on opposite faces were interconnected using a double-sided threaded adjustable screw arrangement. A threshold of 45 dB was set to prevent the acquisition of AE signals from being affected by external noise. The

signal captured by the sensors is too feeble for analysis and is thus enhanced using a pre-amplifier (Figure 3.13). The AE signals were continually captured during the flexural testing of EPS panels. The AE Win program was used to extract AE parameters and examine the features of these AE signals.

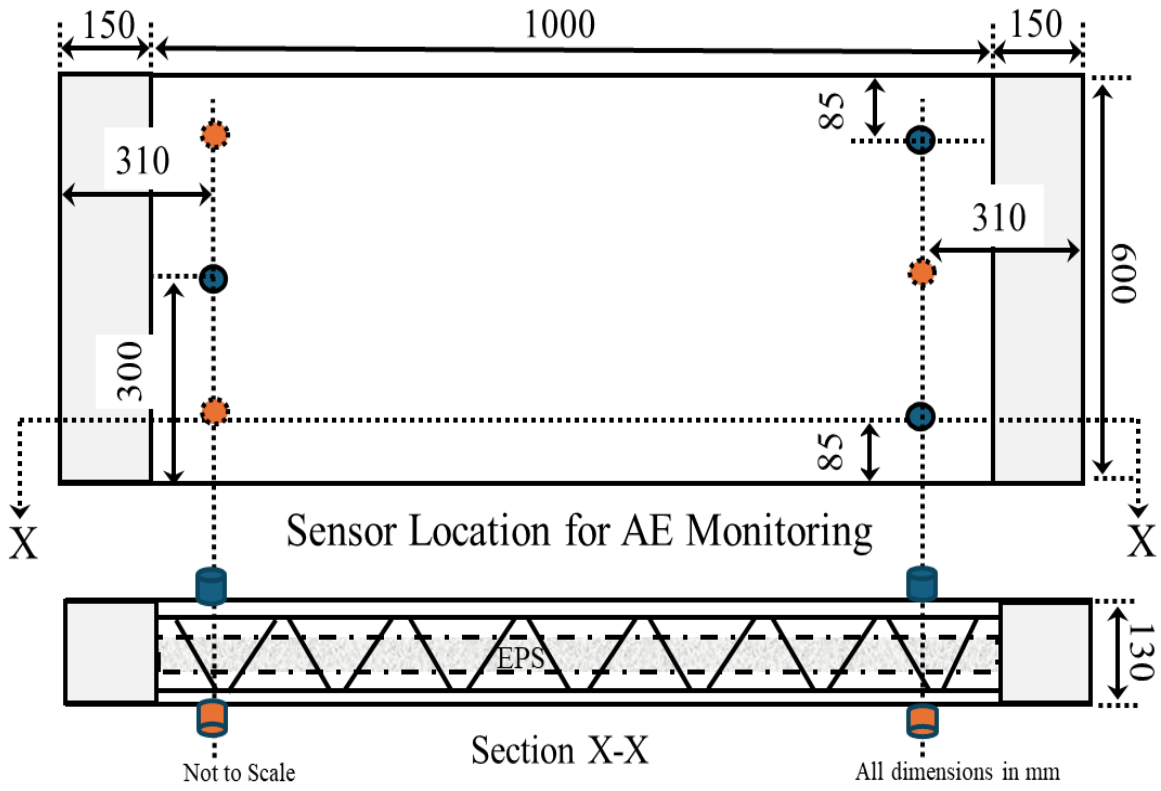

Figure 3.15 AE sensor's location on EPS panel

In this study, cumulative AE hits, signal strength, Average Frequency (AF), duration, amplitude, X-Y event plots, and AE energy have been used to relate the damage in EPS-sandwiched concrete panels exposed to different environments.

3.7 CLOSING REMARKS

This chapter has provided a comprehensive overview of the research program and methodology employed in the study of EPS panels. Detailed descriptions of the materials used for constructing EPS panels were presented, along with the specific methods used to simulate corrosion environments and induce acid and sulphate attacks. Additionally, the methodology for exposing EPS panels to elevated temperatures was outlined, ensuring a thorough understanding of the environmental stressors applied to the panels.

The chapter also detailed the instrumentation used in the experiments, with particular emphasis on the tools and techniques for AE NDT during flexural testing of the EPS panels post-exposure. By laying out these methods and procedures, this chapter sets the foundation for analyzing the data and interpreting the results in subsequent chapters. The comprehensive methodology ensures that the findings will be robust, providing valuable insights into the durability and resilience of EPS panels in challenging environments.

CHAPTER 4

EVALUATION OF CORROSION EFFECTS ON FLEXURAL PERFORMANCE OF EPS PANELS

4.1 GENERAL

Expanded Polystyrene (EPS) panels are a lightweight, prefabricated building material composed of rigid polystyrene beads fused together by a heating process. These beads contain a high air volume, making EPS panels highly insulative and buoyant. This combination of properties makes them a popular choice for various applications in construction, including EPS panels, which offer excellent thermal resistance, help regulate indoor temperatures and reduce energy consumption. They can be used as lightweight roof decks or as part of insulated roof assemblies. EPS panels can be used for interior or exterior non-load-bearing walls, providing insulation and some structural stability. EPS can be incorporated into wall panels, cladding systems, and other building envelope elements.

However, a major concern with EPS panels used in concrete structures is the potential impact of corrosion on their performance. Steel reinforcement embedded within concrete is susceptible to degradation due to atmospheric corrosion, where moisture, oxygen, and contaminants like chlorides initiate the formation of rust. This rust occupies a larger volume than the original steel, creating internal stresses that can lead to cracking and spalling of the surrounding concrete. In light of this challenge, establishing reliable and non-intrusive methods for monitoring corrosion in steel reinforcement within concrete buildings is crucial. This chapter presents a comprehensive analysis of an experimental investigation undertaken to examine how varying levels of corrosion affect the flexural performance of EPS panels. The investigation utilized EPS panels with different corrosion levels (labeled EPS-00, EPS-C05, EPS-C10, EPS-C15 and EPS-C20) and subjected them to out-of-plane four-point flexural loading. The primary objective was to assess the impact of corrosion on the flexural strength of these panels.

Furthermore, the study incorporates a non-destructive technique called acoustic emission (AE) monitoring. This technique analyzes sound waves within the material during deformation or damage. By employing AE monitoring, the researchers aimed to gain insights into the interior acoustic behavior of the panels under stress. This approach holds promise for the non-destructive evaluation of structural integrity in EPS panels, offering valuable information about

their performance and potential failure mechanisms under corrosive conditions. The findings of this investigation aim to contribute to developing more efficient maintenance and monitoring strategies for EPS panels in various construction applications.

4.2 VISUAL OBSERVATIONS

Accelerated impressed current corrosion was employed to deteriorate EPS-concrete panels. Reddish-brown corrosion product was released throughout the process, emanating from the interface between the concrete layer and insulation, as well as from cracks in severely corroded panels. Visual observations were conducted after corrosion on each panel was complete. To improve visibility, the EPS panels were cleaned with a light brush and water to remove accumulated rust on the surface. Images of the corroded panels are presented in Figure 4.1. Panels that developed cracks were highlighted with red markers before imaging.

During the corrosion of EPS-C05, no reddish hue was observed for the first two days. However, as the process progressed to the fifth day, reddish-brown corrosion became evident without any surface cracks. EPS-C05 exhibited the least corrosion, with only rust stains near the interface of the insulation and concrete layer (Figure 4.1a). No visible surface cracks due to corrosion were observed in this panel. The presence of rust oozing out through the interface between the insulation and concrete layer in EPS-C05 indicates that chloride water can easily penetrate this area despite the bonding achieved by pouring cement paste. Significant corrosion was observed in EPS-C10, which also developed small surface cracks on the concrete layer after 10 days of corrosion (Figure 4.1b). These minor cracks likely originated from the expansive forces exerted by the rust generated near the wire mesh embedded within the concrete layer.

Substantial cracks were observed on the concrete layer of EPS-C15, extending from the edges towards the center of the panel (Figure 4.1c). Rust was observed seeping from small fractures around the edges of the EPS panels. The severely corroded EPS-C20 panels generated a full-width crack near the center. A dark brown rust produced during corrosion was observed oozing out through the entire length of the crack. A few minor cracks were also observed in addition to the full-width crack (Figure 4.1d). Visual observations during the corrosion process revealed that initial corrosion is not visible on the surface and is concealed between the concrete layer and the insulation of the EPS panels. Intensified corrosion over a longer period begins to show stains near the edges of the EPS panels, and prolonged corrosion results in cracks on the surface of the concrete layer.

The EPS panels were further inspected visually after undergoing four-point flexural loading. Figure 4.2 shows the internal condition of severely corroded EPS panels after cracking. The deterioration of the shear connectors is clearly visible, with cavities forming around them as they pierce through the EPS insulation. These cavities can promote a corrosive environment when moisture is present. Figure 4.2 also illustrates that the corrosion of the shear connectors extends to the wire mesh embedded in the concrete.

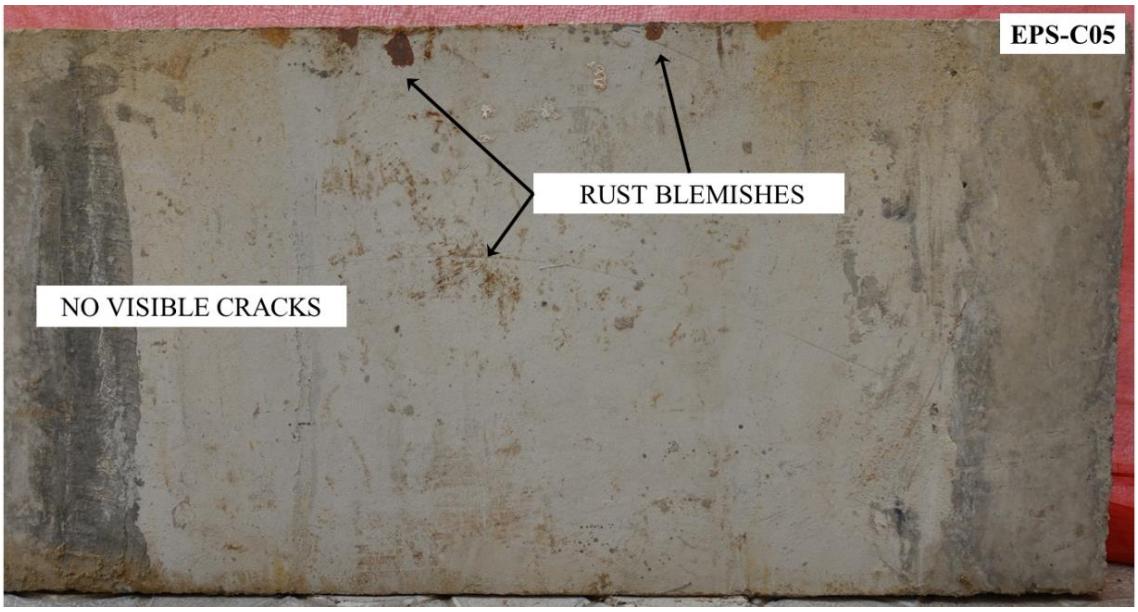

(a) EPS-C05

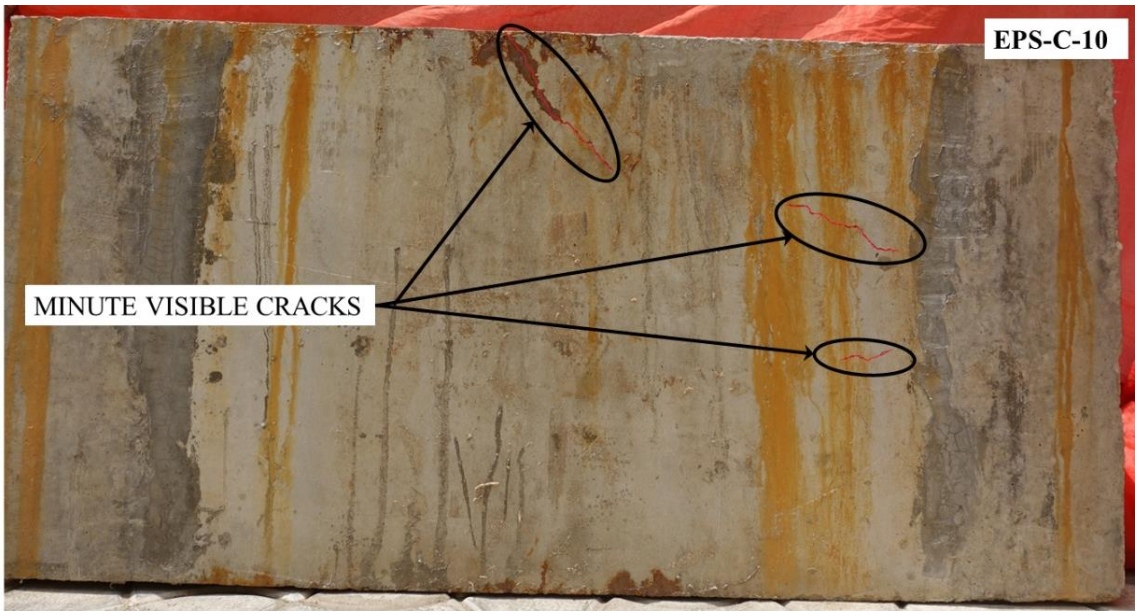

(b) EPS-C10

Figure 4.1 Visuals of EPS sandwiched concrete panels corroded to varying levels (Cont.)

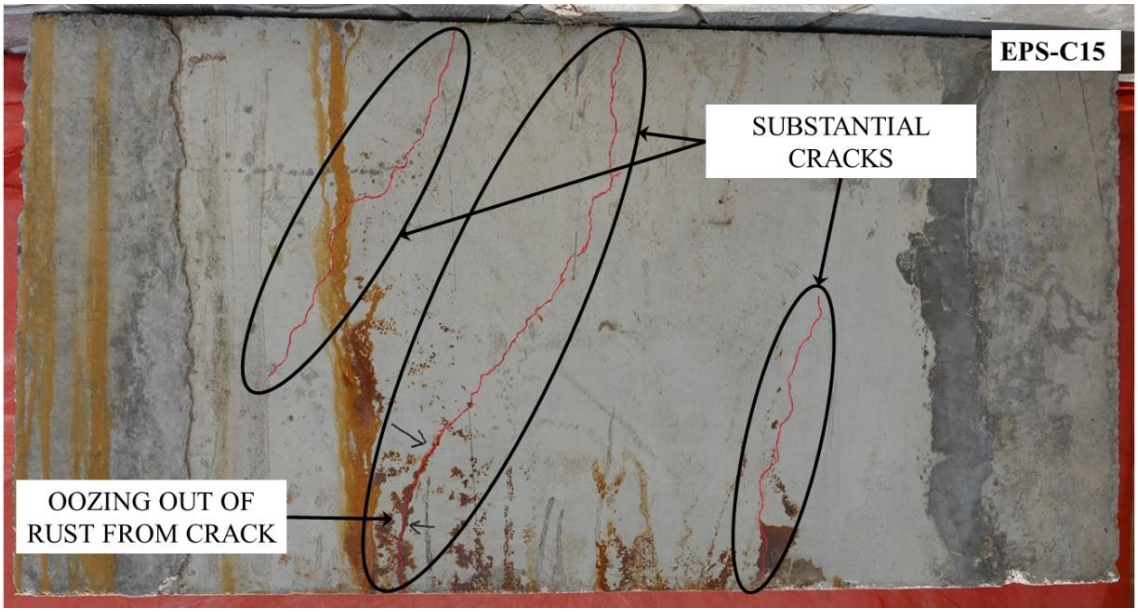

(c) EPS-C15

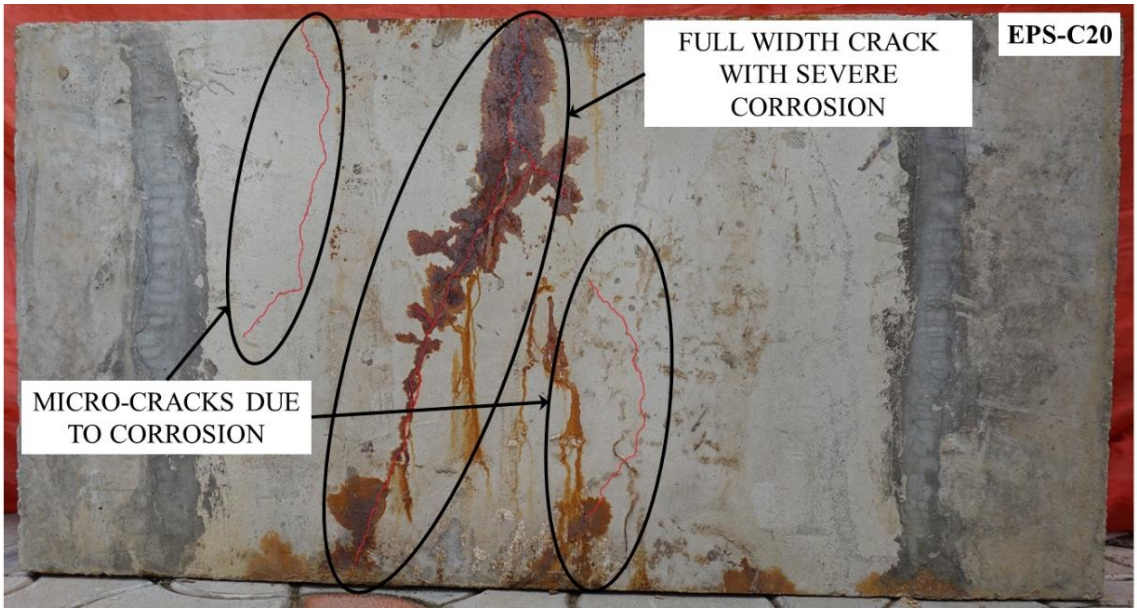

(d) EPS-C20

Figure 4.1 Visuals of EPS sandwiched concrete panels corroded to varying levels.

To assess the extent of corrosion, the concrete cover of the wire mesh was chipped away, revealing that corrosion initiated around the joints of the wire mesh and spread in all directions. The corrosion found to be concealed around the EPS beads of the insulation. This explains why initial corrosion is not visible on the surface of the EPS panels, as the corrosion remain hidden around the EPS beads (Figure 4.2 & Figure 4.3).

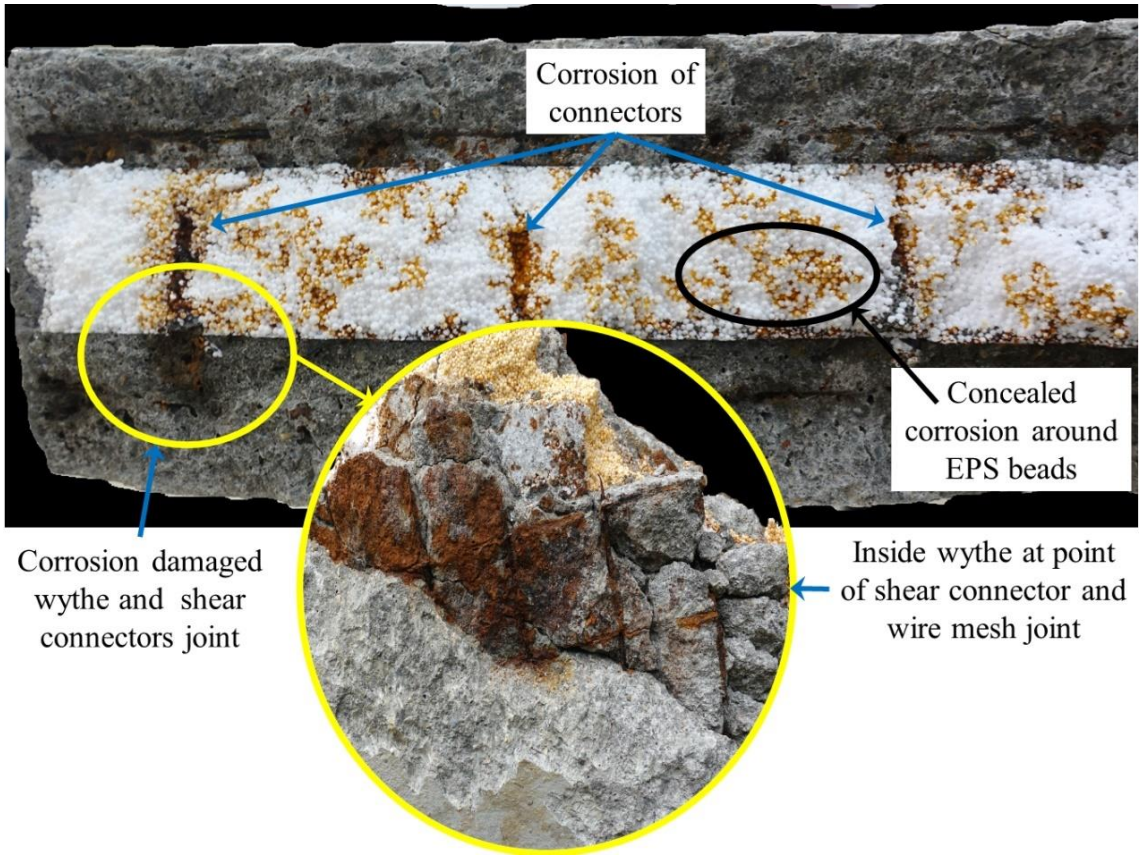

Figure 4.2 Inside view of the EPS panel after corrosion

Figure 4.3 Extricated EPS and wire mesh after panel testing

4.3 CORRELATION BETWEEN CORROSION CURRENT AND EXPOSURE DURATION IN EPS PANELS

Accelerated corrosion was controlled by applying a constant voltage of 10 V. The corresponding current varied with the extent of corrosion, signifying the transfer of electrons

during the corrosion process. An ammeter integrated into the constant voltage source measured the corrosion current at 12-hour intervals. Figure 4.4 illustrates the relationship between exposure duration and the variation in impressed current for corroded EPS panels.

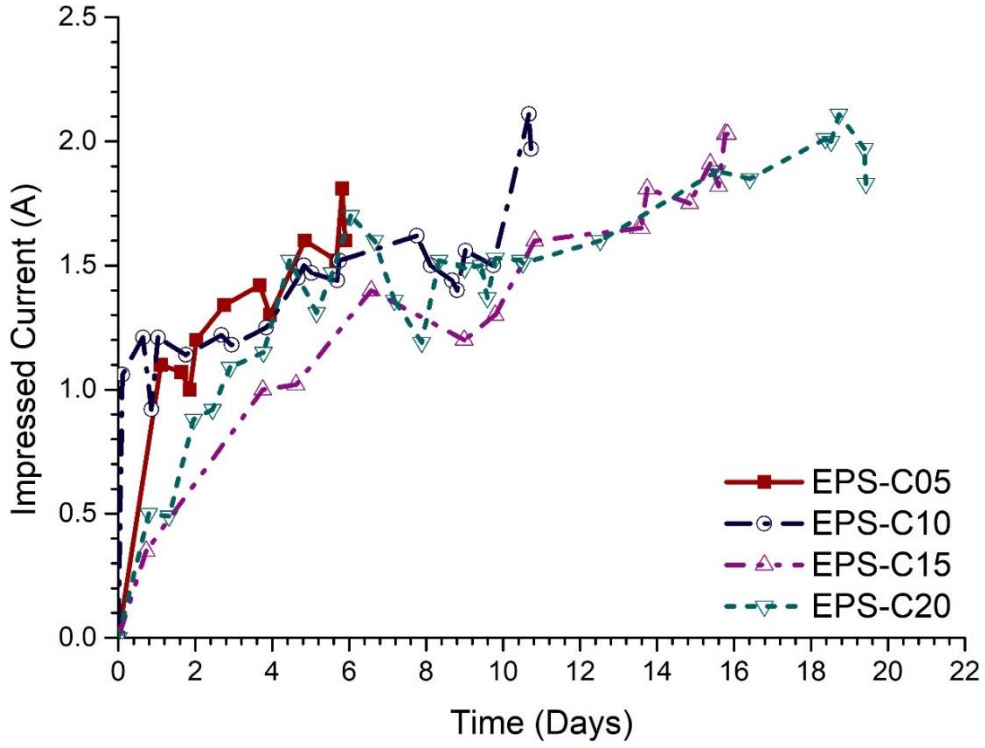

Figure 4.4 Variation in impressed current with time.

Initially, there was a gradual and insignificant rise in corrosion current across all samples during the first 48 hours. On the second day, a small decrease in the current value was observed, attributed to the initial resistance from the galvanization of steel connectors and the alkaline protective shield of the concrete. Over the next two days, the corrosion current showed a noticeable increase, indicating the corrosion progression until the 8th day. Following this period, a dramatic decrease in current was noted in all samples exposed for 8 to 10 days, reflecting the resistance the passive oxide layer provided on the steel surface. After this timeframe, the corrosion current experienced a renewed escalation, signifying the gradual breakdown of the protective oxide layer. This breakdown allowed additional penetration of corrosive chloride ions and decreased the system's electrical resistance. The appearance of corrosion cracks in cases of severe corrosion effectively demonstrated the overall increase in corrosion current.

Therefore, it is evident that the electrochemical technique indicates the likelihood of corrosion through the observed rise in corrosion current, although it does not precisely quantify

it. The variation in corrosion current observed with increasing corrosion exposure duration in all tested specimens over 5, 10, 15, and 20 days demonstrates the consistency and replicability of the studies. The current recorded for all the specimens was used to calculate the mass loss of reinforcement in the EPS panels using Faraday's law, as described in section 3.4.1 (Equations 3.1 and 3.2). The calculated mass loss is mentioned in Table 4.1. Based on the calculated mass loss, it is observed that the corrosion rate increases over time, as evidenced by the higher mass loss in EPS-C20 compared to previously corroded EPS panels when monitored daily.

Table 4.1 Mass loss of corroded EPS panels.

Nomenclature	Mass Loss (%)	Duration of Exposure
EPS-00	0	No exposure
EPS-C05	6.67	5 Days (120 hours)
EPS-C10	8.41	10 Days (240 hours)
EPS-C15	10.76	15 Days (360 hours)
EPS-C20	18.13	20 Days (480 hours)

4.4 MECHANICAL TESTING PARAMETERS OF CORRODED EPS PANELS

This section examines the mechanical testing parameters of the EPS-sandwiched concrete panels exposed to varying degrees of corrosion The EPS panels tested under four-point flexural loading.

4.4.1 Load-displacement behaviour

The load-deflection graph of the control specimen (EPS-00) is segmented into three distinct zones, as illustrated in Figure 4.5. Zone-I refers to the region with high stiffness and load resistance without any cracks in the EPS panel. EPS-00 remained in Zone-I until a load of 6 kN was applied. Zone-II refers to the region where cracks occur in the EPS panel, but it remains in an elastic state, or the state before yielding of the panel. Zone II is marked by assessing the yield load using bilinearization of the load-deflection curve of EPS panels. EPS-00 remained in the cracked elastic state when the load was applied beyond 6 kN and up to 19.5 kN (Figure 4.5). Zone-III in the load-deflection curve is referred to as the cracked plastic zone,

which is the ductile region post-yielding and up to failure of the EPS panels. The control panel EPS-00 displayed a large deflection in Zone-III and ultimately failed at a load of 34.95 kN.

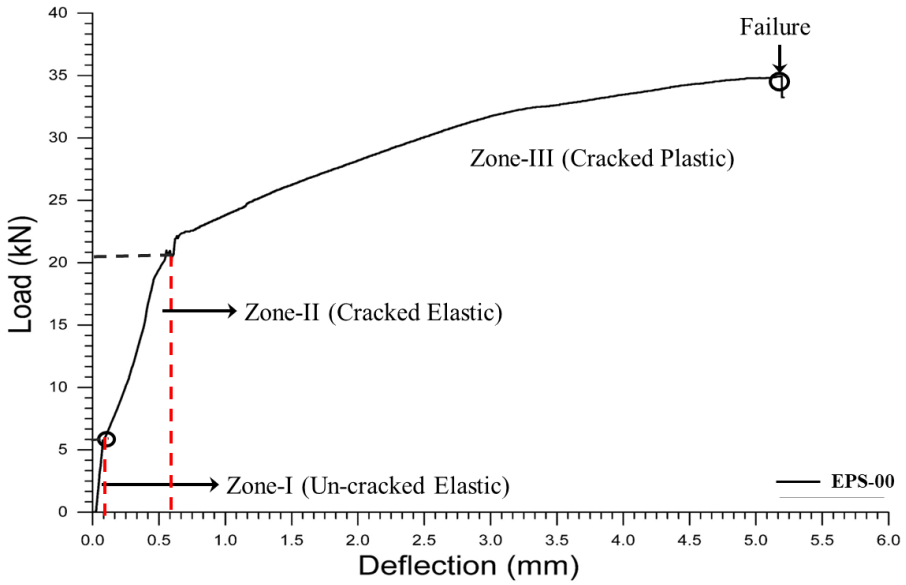

Figure 4.5 Load deflection curve of control EPS panel (EPS-00)

Visual observations during segmented Zones-I, II, III, and the failure of EPS-00, as mentioned in Figure 4.5, are presented in Figure 4.6. Zone-I shows no cracks during flexural loading of the control specimen. As the load increased beyond 6 kN (Zone-II), EPS-00 generated micro-cracks in the lower wythe, which extended to the upper wythe as the load increased up to 19.5 kN (Figure 4.6). As the load increased further (Zone-III), EPS-00 generated numerous cracks in both wythes. Cracks in the top wythe were observed near the edges. In contrast, the bottom wythe expanded the generated cracks (Figure 4.6). The EPS-00 panel ultimately failed due to significant cracking and splitting along its width in the middle (Figure 4.6). The observed failure demonstrates the effectiveness of the shear connectors in distributing the load between the two wythes.

The corroded EPS panels were similarly observed for load-deflection behavior. It was observed that the panels developed early cracking and failed at a reduced ultimate load compared to the control EPS panel. The initial crack in the EPS-C05 panel occurred at a similar load of 6.3 kN (Zone-I). Subsequent small fissures near the support emerged quickly after the initial crack in Zone-II, and it yielded a load of 14 kN (Figure 4.7a). In Zone-III, a large crack in the lower wythe generated near the mid-span of the panel expanded with the increment of load, and the panel failed at a load of 32.51 kN (Figure 4.7a).

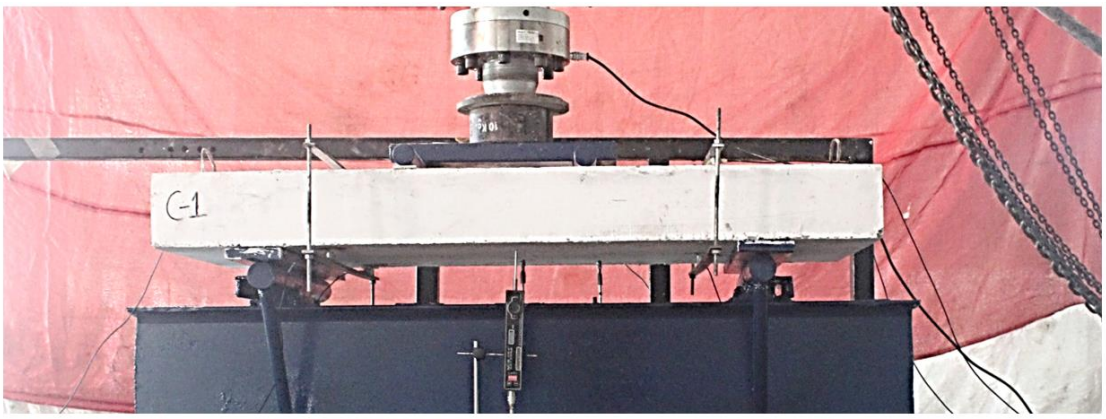

Zone –I (Un-cracked Elastic)

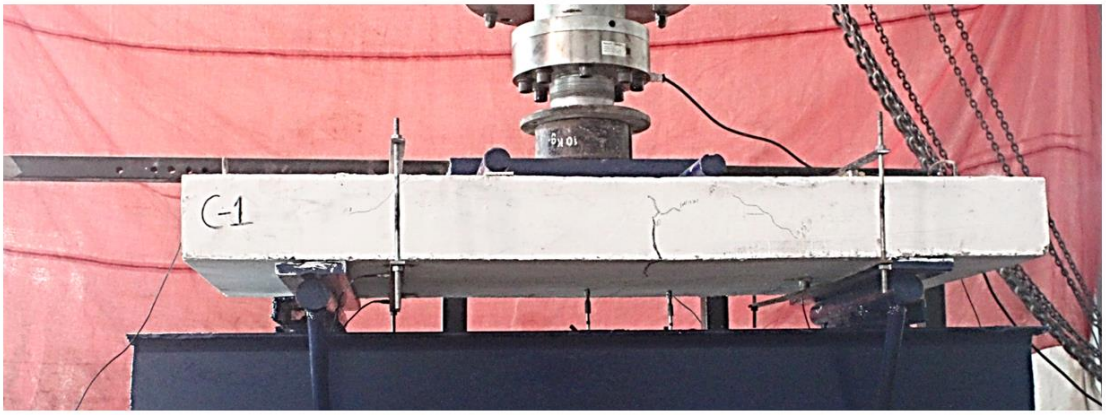

Zone-II (Cracked Elastic)

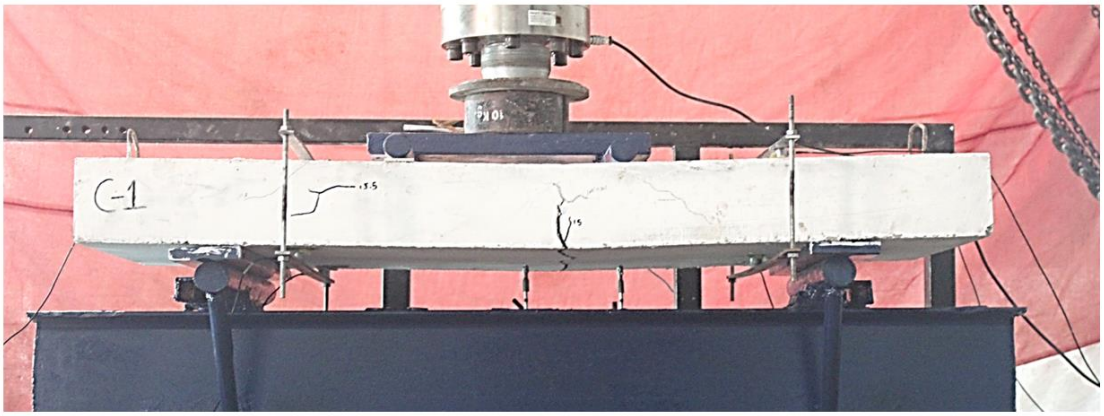

Zone –III (Cracked Plastic)

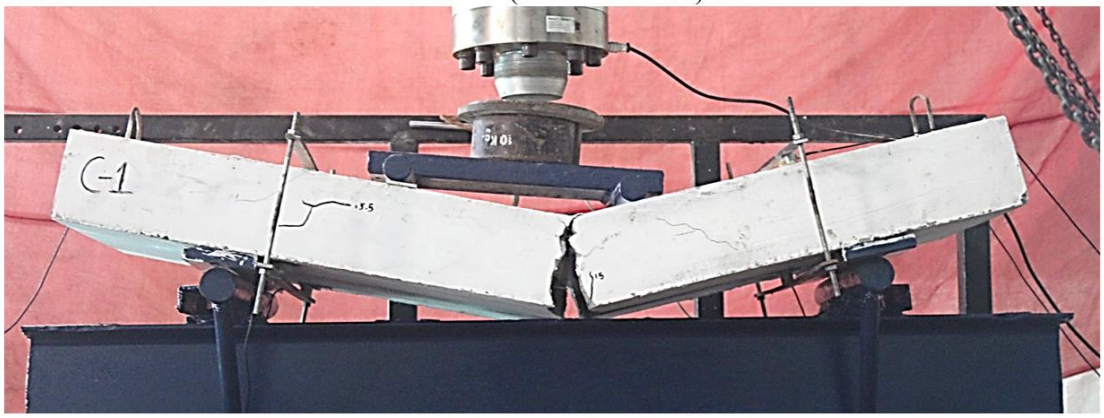

Failure of EPS panel

Figure 4.6 Cracks during different Zones of flexural testing (EPS-00)

The corroded EPS-C10 panel and beyond comprised pre-existing minor cracks due to corrosion (Section 4.2). Zone-I of EPS-C10 is assumed to last until existing cracks extend or new cracks emerge during flexural testing. EPS-C10 generated a new crack at a lower load of 5 kN compared to the control panel (Figure 4.7b).

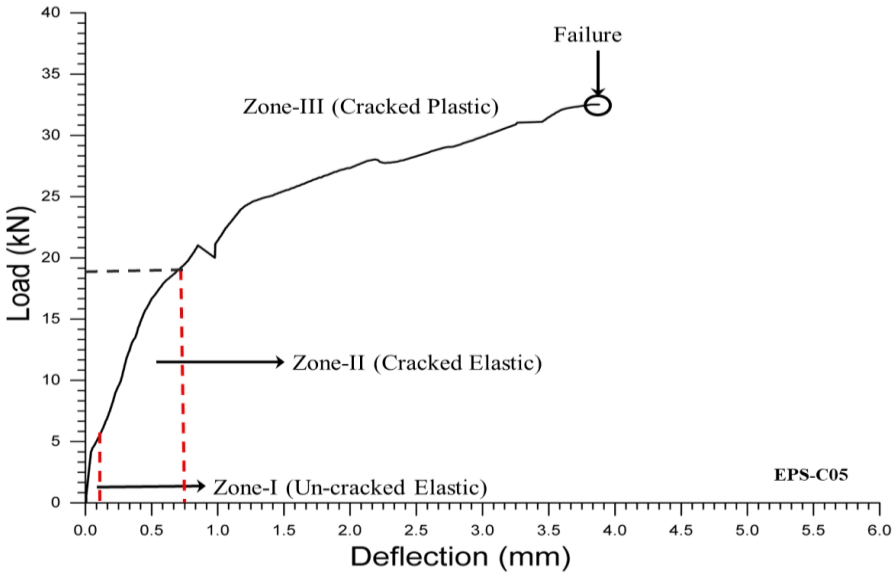

(a) EPS-C05

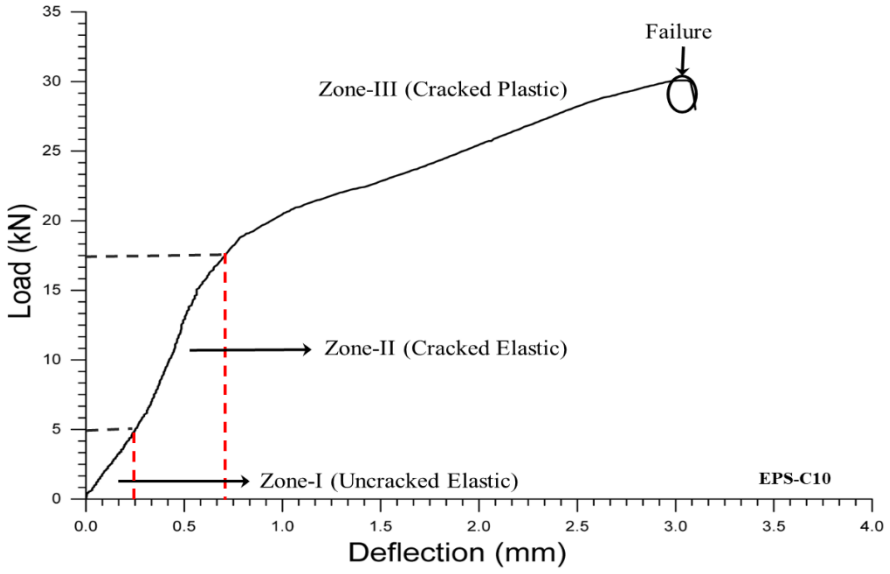

(b) EPS-C10

Figure 4.7 Load-deflection curve of corroded EPS panels (Cont.)

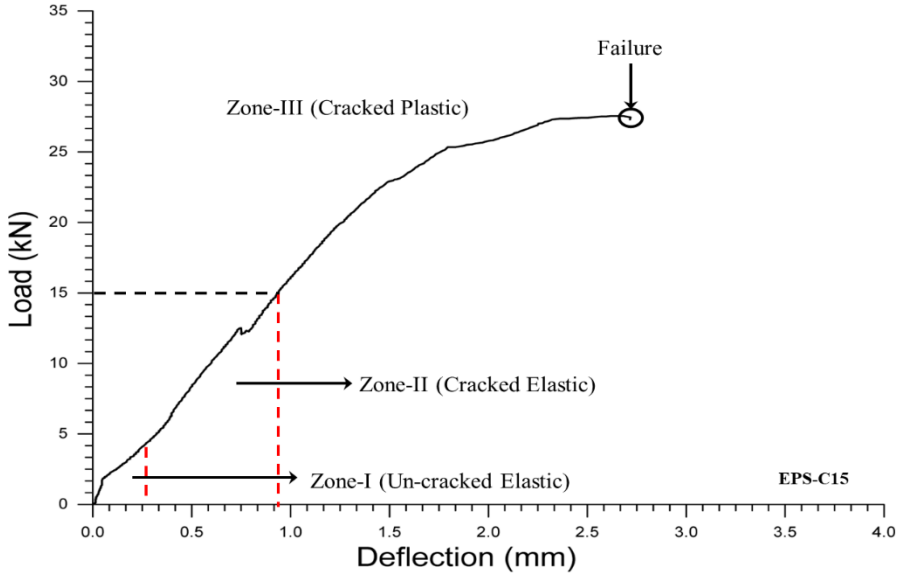

(c) EPS-C15

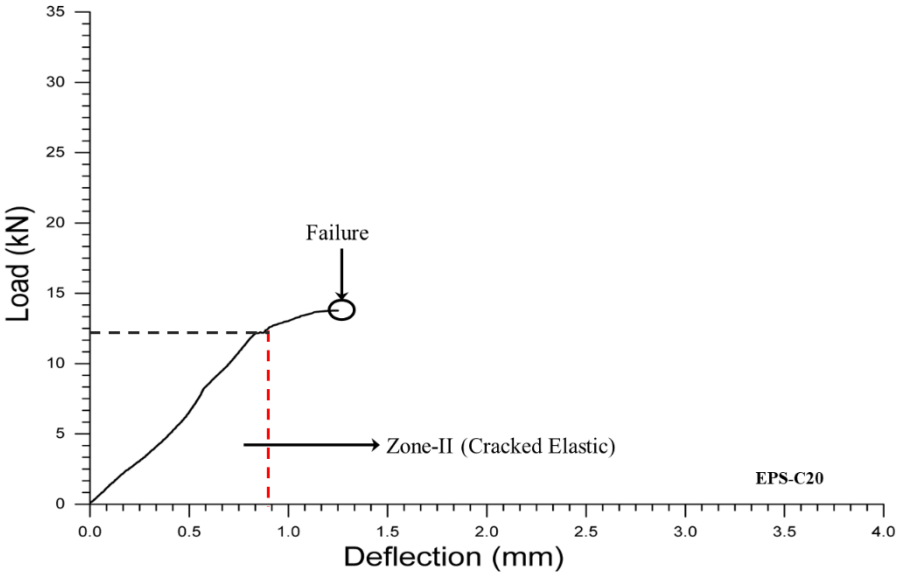

(d) EPS-C20

Figure 4.7 Load-deflection curve of corroded EPS panels

With the increment of loads in Zone-II, numerous cracks were generated in the lower wythe, and the panel yielded at a load of 18.5 kN. Further, the panel collapsed at an ultimate load of 30.08 kN with a fracture of uniform thickness suddenly emerging and extending along the thickness from the lower wythe to the upper wythe. EPS-C15 and EPS-C20 yielded at lower loads of 15 kN and 12.5 kN, respectively. The failure of EPS-C15 occurred at a load 20.62% lower than the failure load of the control panel (Figure 4.7c). A drastic reduction is observed in the flexural load-carrying capacity of EPS-C20, which failed at a load of 13.82 kN, 60.45% lower than the control panel (Figure 4.7d).

From the load-deflection plots of the control and corroded EPS panels, it is observed that failure emerged along the fissures generated due to corrosion. The EPS panels with increasing levels of corrosion show brittle behavior when subjected to flexural loading. The panels EPS-C05, EPS-C10, EPS-C15, and EPS-C20 exhibited decreases of 6.98%, 13.93%, 20.62%, and 60.45%, respectively, in their ultimate flexural load-carrying capacity compared to the control panel. Therefore, it can be inferred that progressive corrosion results in a decreased capacity to bear loads.

4.4.2 Ductility and energy absorption of corroded EPS panels

The derived parameters obtained from the load-deflection curve are mentioned in Table 4.2. Here, Py represents the yield load, Pu represents the ultimate load, Δy represents the mid-span deflections at yield load, and Δu represents the maximum deflection of the EPS panel.

Table 4.2 Various parameters under flexural loading

Panel	First crack (kN)	Ultimate Load (Pu) (kN)	Yield Load (Py) (kN)	Deflection at Yield (Δy) (mm)	Ultimate Deflection (Δu) (mm)	Ductility Factor (DF = Δu/ Δy)	Yield Energy (Ey) (kNmm)	Ultimate Energy (Eu) (kNmm)	Composite Action (*k*) %
EPS-00	6	34.95	19.5	0.7	5.21	7.44	9.69	146.58	34.11
EPS-C05	6.3	32.51	18	0.8	3.88	4.85	9.90	95.82	23.41
EPS-C10	5	30.08	18.5	0.8	3.10	3.87	8.14	65.54	24.25
EPS-C15	4	27.74	15	0.9	2.68	2.97	6.92	50.45	7.70
EPS-C20	0	13.82	12.5	0.8	1.25	1.56	5.51	10.22	10.08

The deformability or ductility of structural components is regarded as a crucial measure for assessing the performance of EPS sandwiched concrete panels. Ductility refers to the ability of structural components to undergo deformation without fracturing once they have reached their yield point. An assessment has been conducted on how corrosion impacts the ductility of the panel. The Ductility Factor (DF) is the ratio of the ultimate deflection (Δu) to the yield deflection (Δy) as mentioned in Table 4.2. A notable decrease in the ductility factor is found in corroded panels compared to the control panel, with EPS-C05, EPS-C10, EPS-C15, and EPS-C20 displaying reductions of 37.93%, 62.81%, 69.74%, and 85.01%, respectively. Corroded specimens exhibit a substantial decrease in the Ductility Factor (DF), indicating that they become significantly more brittle and less capable of sustaining deformation without failure.

This reduction in DF underscores the detrimental impact of corrosion on the structural integrity and flexibility of the EPS panels. The panels exhibiting progressive corrosion display signs of heightened fragility.

The energy absorbed, calculated from the load-deflection curve, is the area under the load-deflection curve. Eu represents the energy the specimen absorbs until it reaches its ultimate load and fails. In contrast, Ey represents the amount of energy absorbed until the yielding of the EPS panels. The comparison of energy absorbed benefits in direct comparison as it combines load and deflection and can be used for performance, ductility, material comparison, and performance monitoring. Table 4.2 indicates a significant decrease in the ability to absorb energy as corrosion progresses. The yield energy of panels EPS-C15 and EPS-C20 is significantly affected. The comparison of ultimate energy absorbed during flexural testing shows that increased corrosion has drastically decreased energy absorption. The moderately corroded panel EPS-C10 shows a considerable reduction of 55.28% in ultimate energy. In comparison, EPS-C15 and EPS-C20 show a drastic decrease in performance with 65.58% and 93.02% decreases in overall energy absorption compared to the control EPS panel. The decrease in energy absorption results from higher corrosion levels in the shear connections of the panels, which leads to less resistance to force and a weakened link between the shear connectors and wire mesh. As corrosion develops, pre-existing corrosion fractures cause a significant and abrupt decrease in Eu.

The observations of the mechanical testing results of the EPS panels show that during flexural testing, the initial crack appeared in the bottom wythe of panels, except for EPS-C20. Before reaching the yield threshold, the initial fracture occurred in all specimens. The EPS-00 and EPS-C05 specimens exhibited shear and flexural cracks up to the point of yielding during testing, ultimately failing under flexural stress. Therefore, as corrosion levels in EPS panels rise, the ultimate load-carrying capability decreases, making it necessary to conduct regular inspections and take corrective measures promptly to prevent disastrous failures.

4.5 DEGREE OF COMPOSITE ACTION

EPS sandwiched concrete panels sustain loads by sharing or compositely resisting the load with the outer wythes, shear connectors, and insulation. The degree to which these components share the load determines the degree of composite action. EPS panels can be classified as fully composite, partially composite, or non-composite (Section 1.2.2), with most sandwiched panels exhibiting semi-composite behavior. The degree of compositeness of EPS panels can be

identified using Equation 4.1 (Pessiki and Mlynarczyk 2003). Here, *k* denotes the degree of composite action, I_{exp} is an experimental moment of inertia of the tested EPS panel, Ic is the theoretical moment of inertia of a fully composite EPS panel, and Inc is the theoretical moment of inertia of a non-composite EPS panel.

$$k\ (\%) = \frac{I_{exp} - I_{nc}}{I_c - I_{nc}} \times 100 \qquad (4.1)$$

The example calculation for composite action is as follows:

$$I_{exp} = \frac{23\ PL^3}{648\ \delta\ E}$$

Here, P = Yield Load, L = Length of the EPS panel, δ = Deflection at yield, E = Modulus of elasticity

$$I_{exp} = \frac{23 \times 19.5 \times 1000 \times 1000^3}{648 \times 0.7 \times 25000} = 39550264.55\ mm^4$$

$$I_{nc} = 2 \times \frac{B \times t^3}{12} = 2 \times \frac{600 \times 40^3}{12} = 6400000\ mm^4$$

Here, B = Width of the EPS panel, *t* = Thickness of each wythe of EPS panel

$$I_c = \frac{B \times t_1^2}{12} + Bt_1y_1^2 + \frac{B \times t_2^2}{12} + Bt_2y_2^2$$

Here, t_1 = Thickness of top wythe, t_2 = Thickness of bottom wythe, y_1 = Distance of centroid of top wythe from centroid of EPS panel, y_2 = Distance of centroid of bottom wythe from centroid of EPS panel

$$I_c = \frac{600 \times 40^2}{12} + 600 \times 40 \times 45^2 + \frac{600 \times 40^2}{12} + 600 \times 40 \times 45^2 = 103600000\ mm^4$$

Placing the values in Equation 4.1 gives the composite action of the EPS panel:

$$k\ (\%) = \frac{39550264.55 - 6400000}{103600000 - 6400000} \times 100 = 34.10\ \%$$

The loss of composite action results in a corresponding loss in the strength of the EPS panel. The composite action calculated using the above equation is mentioned in Table 4.2. It is observed that all the panels behave in a partially composite manner. The control panel, EPS-00, has a degree of composite action of 34.11, which decreases with increased levels of

corrosion in the EPS panels. Compared to the control panel, there is a loss of 77.42% and 70.44% in composite action for EPS-C15 and EPS-C20, respectively.

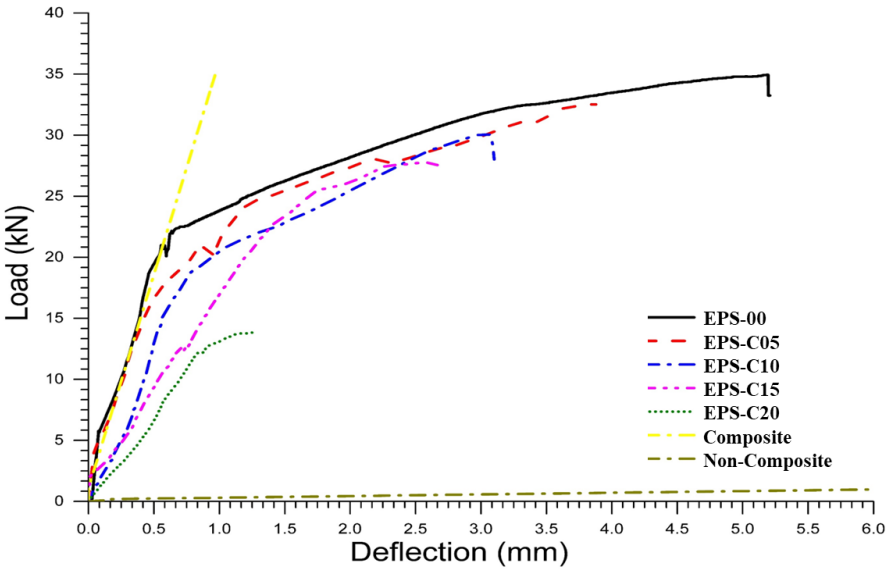

Figure 4.8 Combined Load deflection curves for EPS panels corroded to different levels.

The load-deflection curves of EPS panels, fitted between the approximate theoretical slopes of fully composite and non-composite EPS panels, are represented in yellow and dark green (Figure 4.8). By comparing the load-deflection slope up to the elastic limit, it is observed that EPS-00 and EPS-C05 coincide with the theoretical curve for fully composite panels. The loss of compositeness is observed in EPS-C10 due to induced corrosion. Similar behavior is observed in highly corroded EPS-C15 and EPS-C20, where the shear connectors were found to be severely corroded, as noted during visual observation (Section 4.2). The load-deflection curves of all the panels deviate from the fully composite slope beyond the elastic limit. The curves demonstrate that none of the panels behaved in a non-composite manner (Figure 4.8).

It is observed that after the elastic limit, composite action decreases regardless of corrosion severity. This may be due to the bending of the shear connectors under higher loads. The loss of stiffness and composite action is directly caused by the degeneration of shear connectors, as highlighted by Tomlinson & Fam in their literature study (Tomlinson and Fam 2016a). The shear connectors experience significant damage because of corrosion. The decrease in ductility of the panels exposed to corrosion is a result of the corrosion of the wire mesh, which serves as reinforcement in the wythes.

4.6 PASSIVE ACOUSTIC EMISSION MONITORING

Acoustic emission (AE) monitoring is a non-destructive technique used to detect and locate damage in structures. It involves using sensors to capture high-frequency acoustic waves generated by the rapid release of energy from localized sources within a material, such as cracks or deformations. By analyzing AE hits, their amplitudes, and XY plot events, this method can identify the initiation and progression of damage well before it becomes visible. AE monitoring is particularly effective for tracking structural integrity under stress, providing valuable data for preventive maintenance and ensuring safety.

4.6.1 Cumulative AE hits & their amplitudes

An AE hit is an acoustic signal surpassing a predetermined threshold limit. The cumulative AE hits signify the aggregation of damage caused by advancing cracks and escalating flexural loading in EPS panels. The hits observed in the samples immediately indicate the existence of cracks as loads are applied and damage occurs. The cumulative AE hits and load vs. time graph for the control panel EPS-00 is presented in Figure 4.9. Efforts are made to relate the cumulative AE hits with the three zones defined in load-deflection curves. The plot shows that the EPS panels show micro-cracking during the initial loading stage, and the number of hits keeps increasing with the load. The gradual increase of slope demonstrates the occurrence of micro-cracking in the early stage, termed Stage-I (Figure 4.9). Stage-I of the cumulative AE hits corresponds to the yielding load of the load-deflection curve, showing that micro-cracking occurs until the yielding of the EPS panels, visible through the gradual increase of cumulative AE hits. Just after Stage I, there is a calm phase termed Stage II, characterized by the absence of any notable increase in AE impacts (Figure 4.9). After Stage II, the number of AE hits consistently and quickly increases with the load until the material fails completely at 34.95 kN, indicating the occurrence of macro-cracking, termed Stage-III (Figure 4.9). The degradation advances as visible fissures develop in the panel.

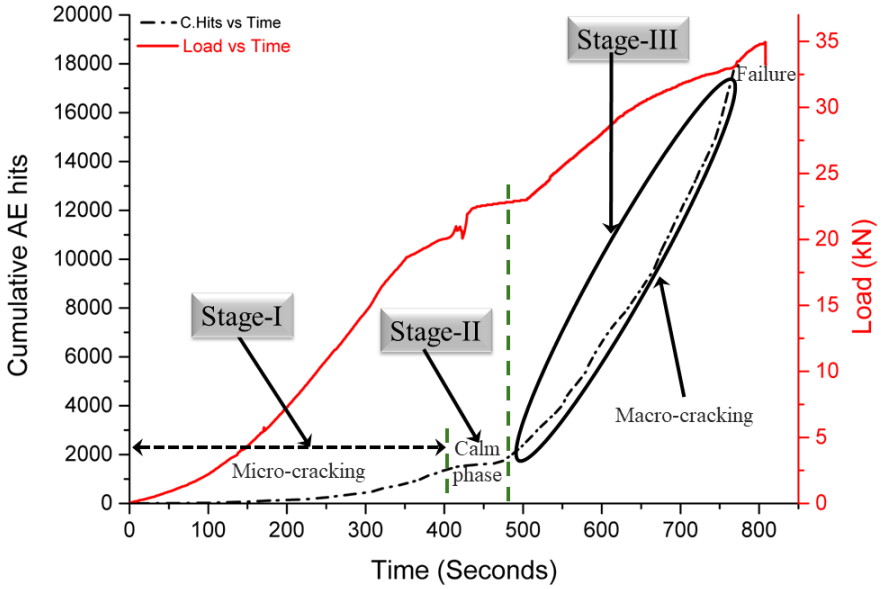

Figure 4.9 Variation in AE Hits Vs Time in control panel (EPS-00)

For corroded EPS panels tested under flexural loading, the cumulative AE hits plot, shown in Figure 4.10, provides critical insights into the panels' structural integrity. Initially, due to the presence of pre-existing corrosion cracks, the number of AE hits in all corroded EPS panels is relatively low compared to the uncorroded control panel, EPS-00. As corrosion progresses, the early micro-cracking stages and calm phases become less pronounced, leading to a noticeable reduction in cumulative AE hits over time.

In severely corroded EPS panels, the initial micro-cracking and calm phase gets merged with no clear variation in occurrence of AE hits in these stages. Although there is no clear variation, EPS-C20 exhibits very few AE hits during the initial loading phase, which is understood to be a calm phase caused by the presence of corrosion cracks and the subsequent widening of these cracks (Figure 4.10d). The AE hit plot of EPS-C05 & EPS-C10 shows a similar plot to control panel with decreased intensity of hits in each stage (Figure 4.10a & b). It is observed that failures in EPS-C10, EPS-C15, and EPS-C20 occurs abruptly. This is characterized by a sharp increase in the curve's slope during Stage III, indicating a sudden failure. These panels exhibit fewer and less pronounced macro-cracking phases compared to the control sample, suggesting a brittle failure mode. The cumulative AE hits plot thus serves as a vital tool for assessing the brittleness of EPS panels. Panels with extensive corrosion show a significant decrease in AE hits, reflecting the depletion of the AE cracking stages.

The findings highlight the critical impact of corrosion on the structural performance of EPS panels. The diminished AE hits and the absence of distinct micro-cracking stages in

heavily corroded panels underline the severity of corrosion damage, which compromises the panels' ability to withstand flexural loads. This analysis underscores the importance of monitoring AE hits in predicting failure and assessing the durability of EPS panels in corrosive environments. It also suggests the need for enhanced corrosion protection measures to ensure the longevity and reliability of these construction materials.

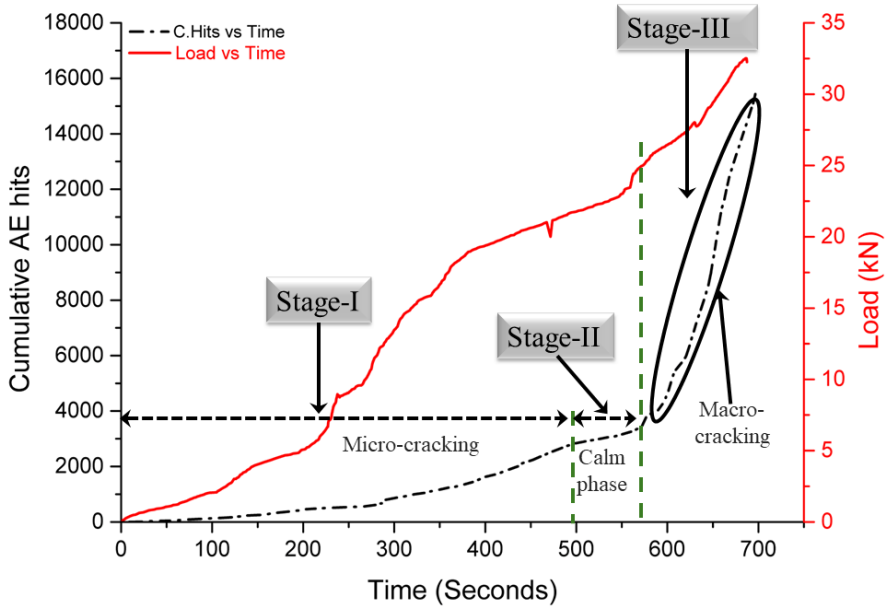

(a) EPS-C05 AE Hits Vs Time

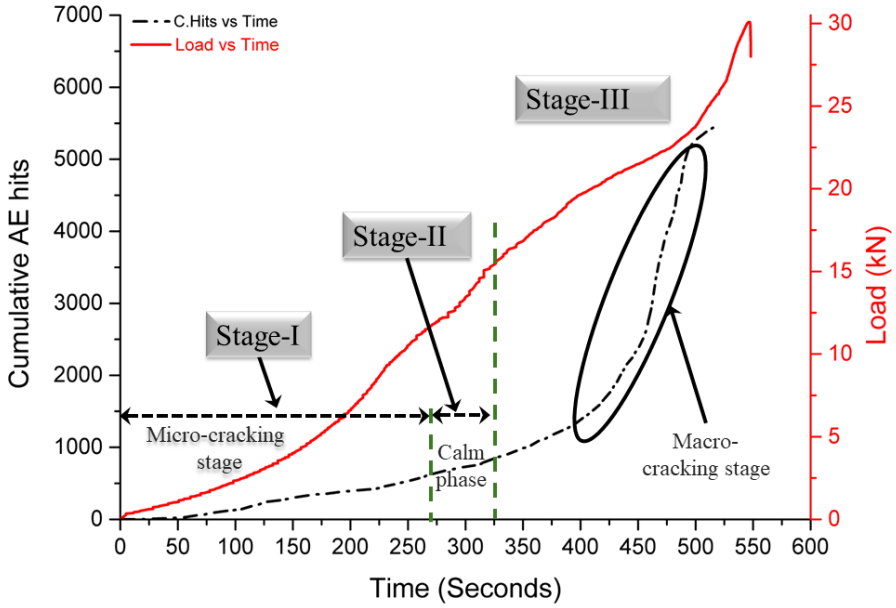

(b) EPS-C10 AE Hits Vs Time

Figure 4.10 Variation in AE Hits Vs Time with varying corrosion (Cont.)

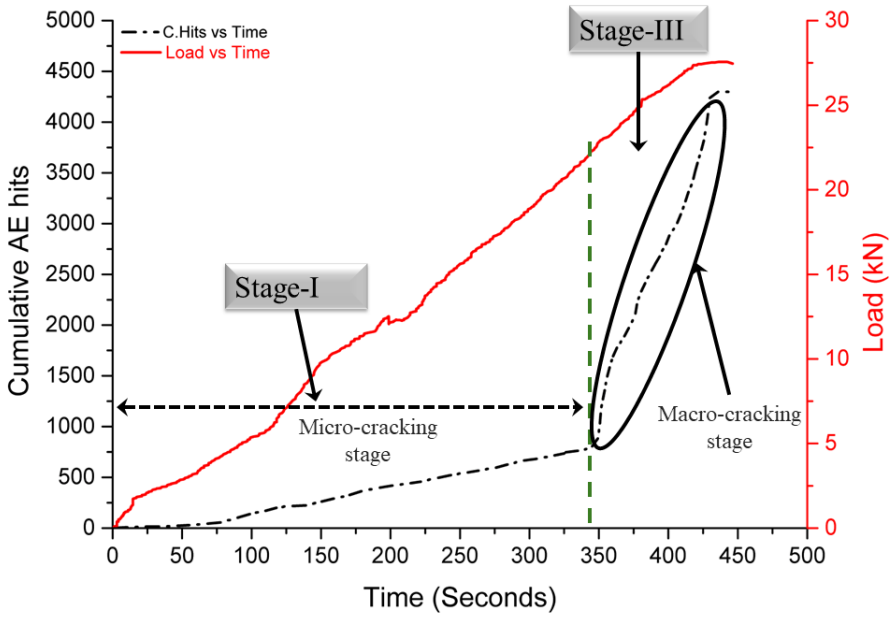

(c) EPS-C15 AE Hits Vs Time

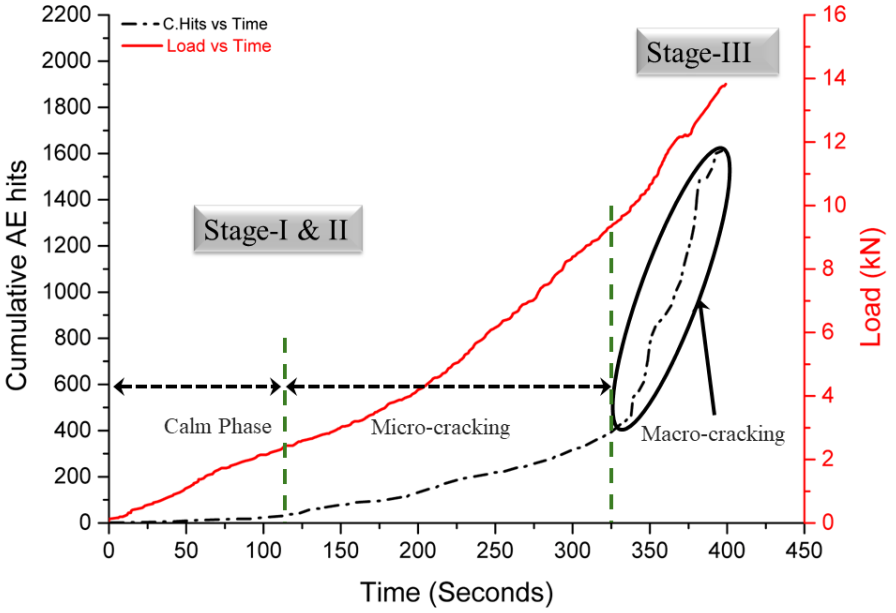

(d) EPS-C20 AE Hits Vs Time

Figure 4.10 Variation in AE Hits Vs Time with varying corrosion.

The amplitudes of AE hits correlate to increasing load and corrosion damage indicating the extent of damage of each hit because of internal deformations or cracks. The low amplitudes (50–60 dB) seen in Stage-I of the EPS panels (EPS-00) indicate the presence of micro-cracking. These microcracks are not apparent on the surface but are internal cracks of the EPS panels (Figure 4.11). During Stage-II, there are notable occurrences of AE signals without consistent amplitudes, suggesting a temporary absence of new fractures. Stage-III exhibits AE hits with a

high amplitude (70-80 dB), indicating the merging of small fractures into larger cracks, resulting in significant surface cracks. Therefore, the amplitude of AE signals serves as an indicator of the extent of damage sustained by panels.

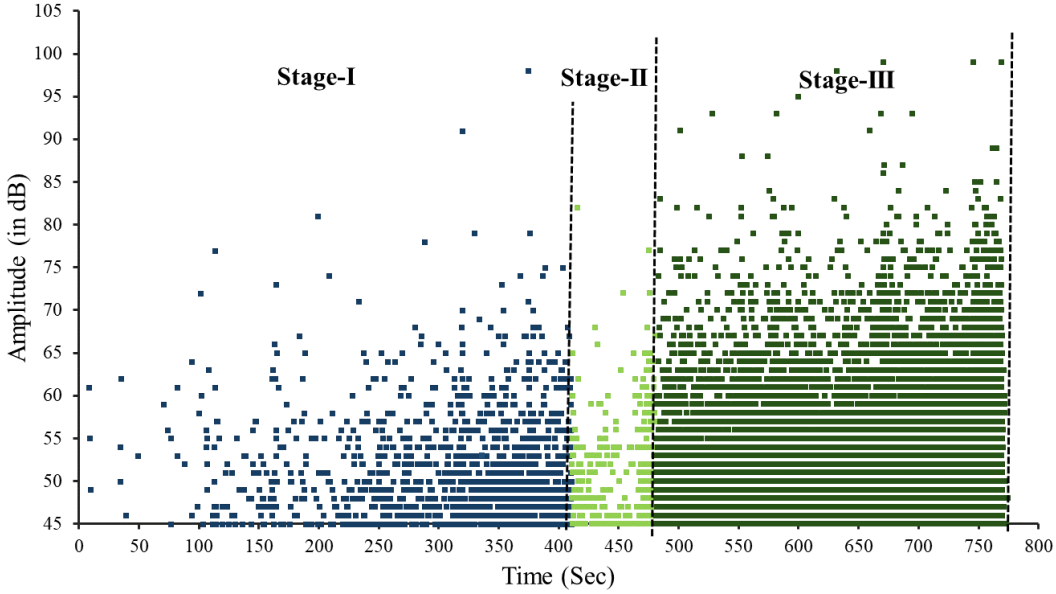

Figure 4.11 Amplitude of AE hits with time in EPS-00.

The amplitude for corroded EPS panels is represented by scatterplots in Figure 4.12. It is observed that the amplitudes of EPS-C05 are like control panels. The amplitudes in stage-III show lower average of amplitudes in EPS-C05 (Figure 4.12a). In EPS-C10, stage-I hits capped below 50 dB, followed by a lower amplitude hit in stage-II while amplitude in stage-III were similar as observed for EPS-C05 (Figure 4.12b). In highly corroded EPS-C15 & EPS-C20 panels, Stage-I & II are not clearly divided as both the stages show very low average of amplitudes (< 47 dB). The absence of Stage-I indicates already damaged panels. These panels show sudden increase in amplitude of hits in stage-III (55dB – 60dB) and depict the panel breaking suddenly (Figure 4.12c & d). Therefore, the amplitude of AE hits over time is a good indicator of crack severity and damage in EPS panels and can serve as an effective non-destructive testing monitor for damage diagnosis.

In conclusion, EPS panels that have undergone corrosion, the amplitudes of the corroded EPS panels weakened in all stages. Stage-I shows average amplitude below 50 dB in all corroded specimens as compared to control panels (Figure 4.12 a-d). The amplitude of stage-III in corroded EPS panels was reduced and delayed when subjected to average impacts of 60-65 dB amplitudes, which are lower than the amplitudes experienced in control panels.

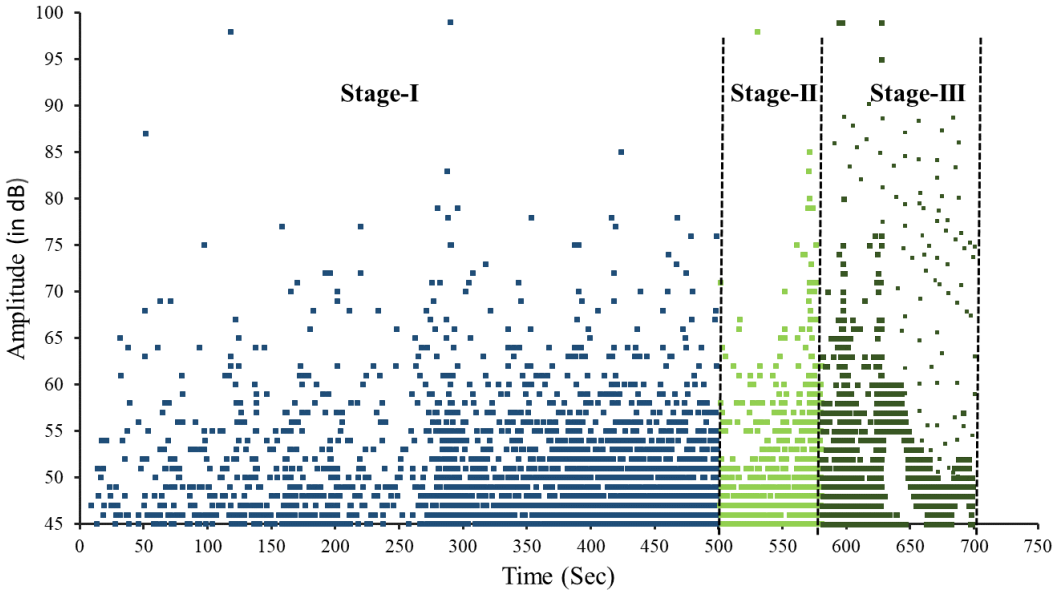

(a) Amplitude of AE hits with time in EPS-C05

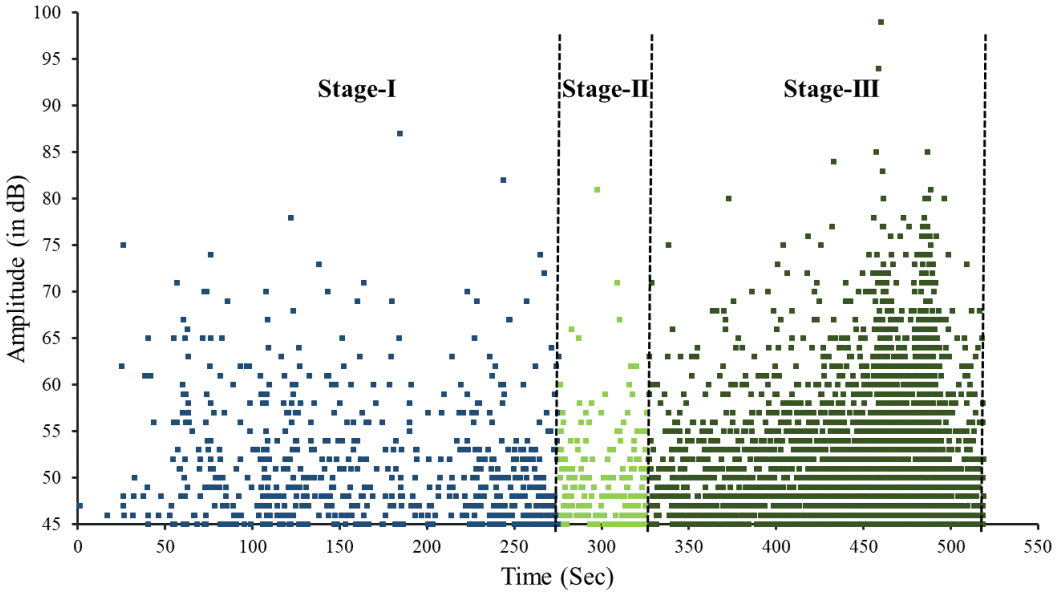

(b) Amplitude of AE hits with time in EPS-C10

Figure 4.12 Amplitude of AE hits with time of corroded EPS panels (Cont.).

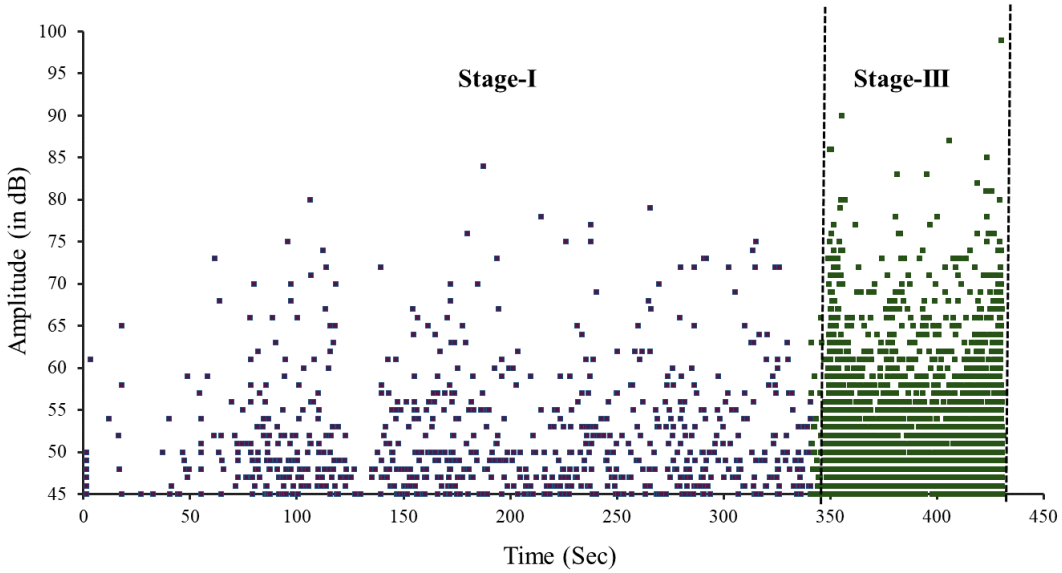

(c) Amplitude of AE hits with time in EPS-C15

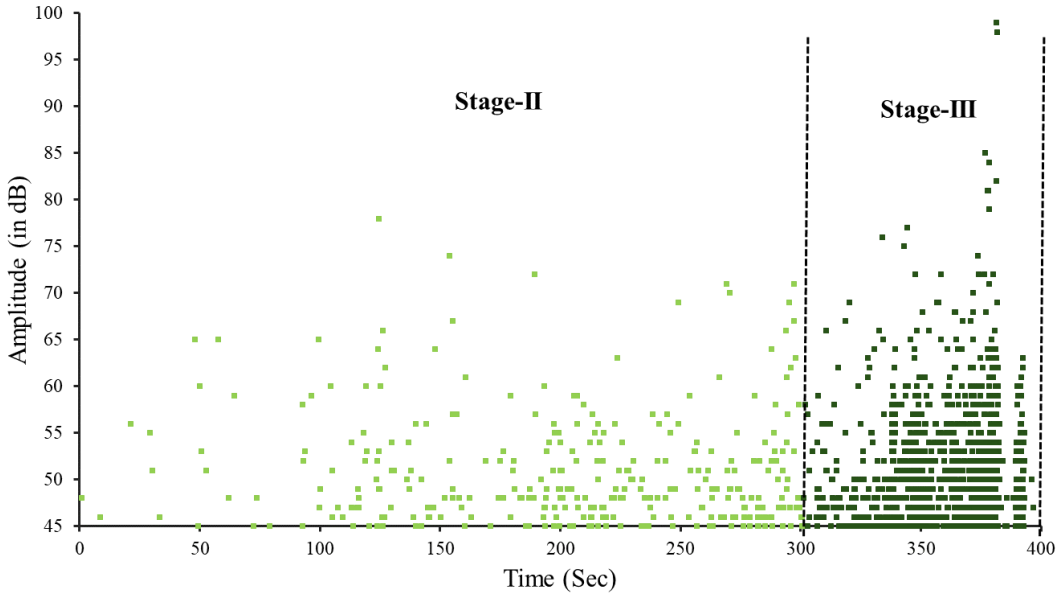

(d) Amplitude of AE hits with time in EPS-C20

Figure 4.12 Amplitude of AE hits with time of corroded EPS panels.

4.6.2 Acoustic Emission (AE) X-Y Event Plots of corroded EPS panels

Acoustic Emission (AE) XY event plots are an effective tool in structural health monitoring, accurately depicting deformation positions and damage within materials. The locations of faults are identified using the intersection method, which involves measuring the distance of the fault from each sensor based on the wave velocity in the material. The intersection point, detected using three or more AE sensors, is determined with the help of specialized software. The XY event plot visually illustrates the coordinates of these

occurrences, offering a graphical representation of the distribution and evolution of damage over time. This technique facilitates real-time identification of defects, even before they are visible to the naked eye, allowing for prompt maintenance and the prevention of catastrophic failures. In this study, AE sensors are arranged in a triangulation pattern to monitor the advancement of AE impacts and occurrences (Section 3.6, Figure 3.15). This configuration enables the timely identification of damaged and impacted regions well before their visibility, aiding in forecasting vulnerable areas. The AE XY event plots exhibit a strong resemblance to the visual images of the sandwich panel. In the final stages of loading before failure, the AE event plots precisely correspond to the observed surface crack patterns on the EPS panels.

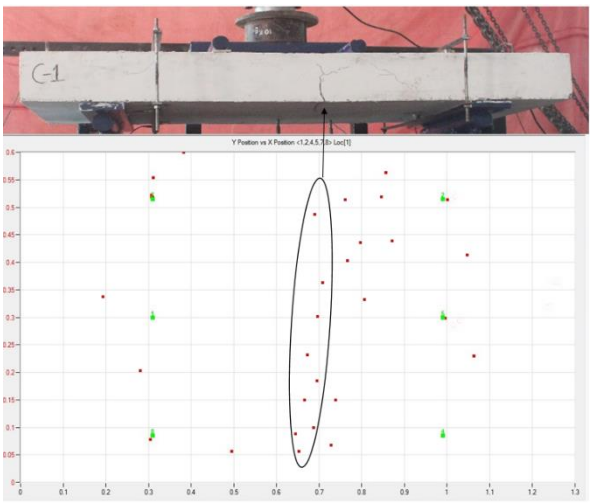

(a) Elastic Zone

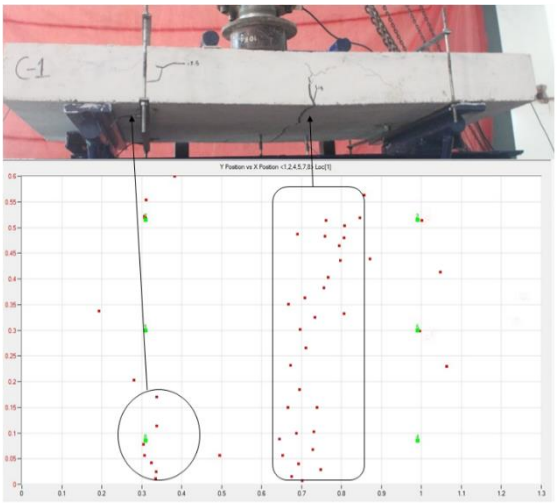

(b) Cracked Elastic Zone

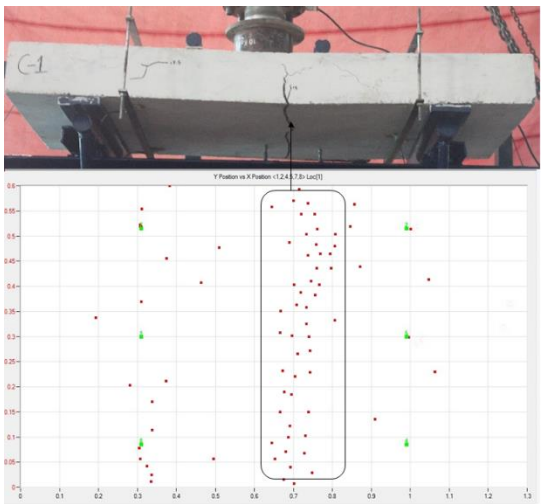

(c) Plastic Zone

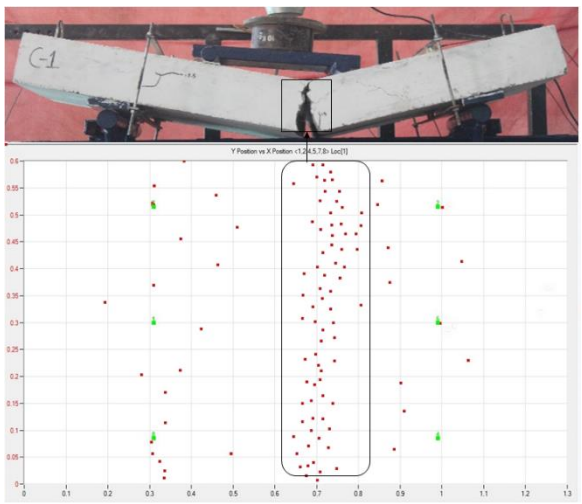

(d) Failure

Figure 4.13 AE X-Y event plots with increasing flexural loading – EPS-00

During the initial loading phases, internal cracks in the bottom wythe are indicated by AE events, visible in the elastic zone as shown in Figure 4.13a. With increased loading, AE events

appear near the supports and become visible on the surface (Figure 4.13b). As loading continues, the evolution of AE events aligns with the actual cracking pattern of the panel, with central cracks causing an increase in the number of events in that specific area (Figure 4.13c). In the ultimate failure stage, a significant crack extending from the bottom wythe to the top wythe is identified by a substantial number of AE events occurring in the same region (Figure 4.13d).

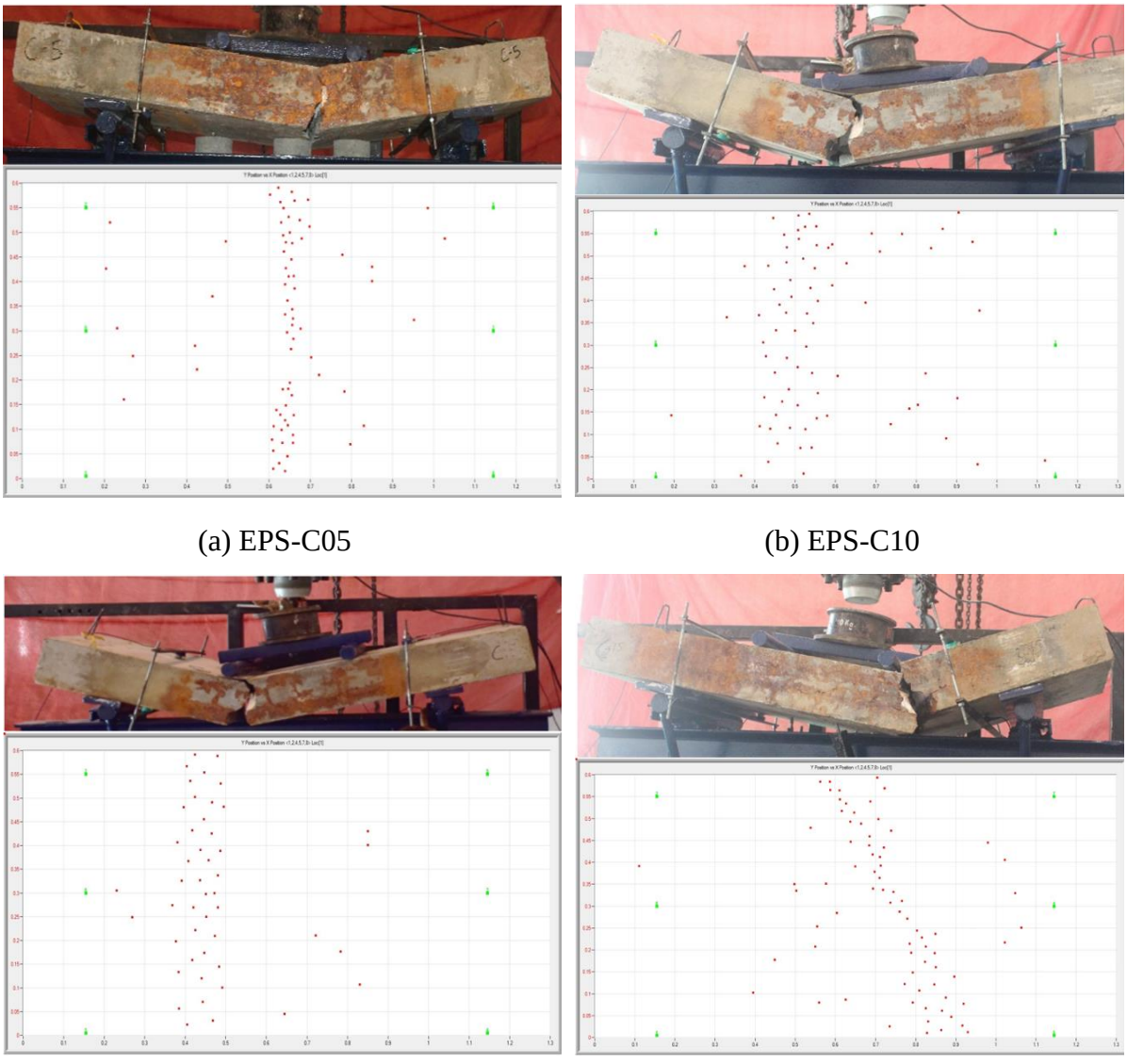

(a) EPS-C05 (b) EPS-C10

(c) EPS-C15 (d) EPS-C20

Figure 4.14 AE X-Y event plots for corroded specimens

For EPS panels subjected to varying levels of corrosion, the number of AE events significantly decreases compared to the control panel. Figure 4.14 illustrates the AE event plots alongside the actual cracked images of the corroded EPS panels (EPS-C05, EPS-C10, EPS-C15, and EPS-C20). The recorded AE event locations in all specimens correspond accurately

with the visual failure locations. The number of AE events diminishes as corrosion levels increase, which can be attributed to pre-existing corrosion cracks in the samples. Particularly in the highly corroded EPS-C15 and EPS-C20 panels, macro cracks were already present before loading, leading to fewer AE events.

Therefore, it can be concluded that AE monitoring during the flexural loading of EPS panels with varying levels of corrosion effectively identifies the initiation and progression of cracks through cumulative AE hits and their amplitudes. It also predicts damaged locations using AE XY event plots. The sequential stages of AE hits under incremental loading highlight the efficacy of the AE technique in accurately monitoring EPS panels subjected to combined corrosion and loading. This method can greatly contribute to developing a damage monitoring strategy for EPS panels.

4.7 CLOSING REMARKS

This chapter comprehensively analyzes corrosion's visual and mechanical effects on EPS concrete panels. Visual observations revealed significant deterioration, particularly around shear connectors, emphasizing the extent of corrosion-induced damage. Flexural testing results showed a substantial reduction in stiffness, yield energy, ultimate energy, and composite action of the panels with increasing corrosion levels, highlighting the importance of regular inspections and maintenance to prevent catastrophic failures. The chapter further explores the application of Acoustic Emission (AE) monitoring during flexural testing. This technique provided valuable insights into the internal damage mechanisms within corroded EPS panels. Analysis of the AE data, including cumulative AE hits, amplitude distribution, and AE X-Y event plots, effectively captured the initiation and progression of cracking. The strong correlation between AE data, visual observations, and mechanical testing results demonstrates the effectiveness of AE in detecting and predicting structural damage. This integrated approach offers a robust framework for assessing the structural health of EPS panels, paving the way for improved damage monitoring and maintenance strategies.

CHAPTER 5

EVALUATING THE EFFECTS OF AGGRESSIVE ACIDIC AND SULPHATE ENVIRONMENTS ON EPS PANELS

5.1 GENERAL

Acid and sulphate attacks pose substantial risks to the durability and soundness of concrete structures. An acid attack occurs when acidic solutions, such as sulfuric acid or hydrochloric acid, penetrate the concrete, causing the dissolution of calcium hydroxide and calcium silicate hydrate, the main binding components in concrete. Consequently, there is a decline in both physical and mechanical properties, resulting in the wearing away of the outer layer and increased porosity. On the other hand, sulphate attack occurs when sulphate ions react with the hydration products of cement, forming expansive compounds such as ettringite and gypsum. These compounds generate internal stresses, leading to cracking, spalling, and ultimately undermining the structural integrity of the concrete. Both chemical attacks are exacerbated by environmental factors such as moisture, temperature changes, and corrosive chemicals.

Studying the performance of EPS panels in aggressive acidic and sulphate-rich environments, particularly in marine conditions, is crucial. The degradation caused by exposure to acids and sulphates is not readily observable through visual inspection and becomes apparent only when the deterioration reaches significant levels. Therefore, non-destructive monitoring and evaluation techniques, such as AE, might enable the early detection of damage caused by aggressive agents and simplify the process of evaluating EPS panels using destructive techniques.

In this chapter, EPS panels will undergo flexural testing in environments contaminated with sulfuric acid and sodium sulphate. The tests will be accompanied by AE monitoring, which detects the release of energy from micro-cracks and other structural changes within the panels. This approach provides real-time data on the onset and progression of damage, offering insights into the panels' mechanical behavior and durability under aggressive chemical exposure. The results from the flexural tests, combined with AE data, will help evaluate the integrity and performance of EPS panels in aggressive environments, guiding future improvements in the design and application of these materials in construction.

5.2 ACID AND SULPHATE EXPOSURE

Following the curing process, the EPS panels underwent acid and sulphate exposure by immersion in sulfuric acid (H_2SO_4) and sodium sulphate (Na_2SO_4) solutions. The exposure durations were 7, 14, 21 and 28 days for acid and 90, 180, 270, and 360 days for sulphate. Flexural testing was employed to assess the extent of degradation of the EPS panels after these designated exposure periods.

5.2.1 Acid exposure

Acid attacks are a common cause of corrosion in cement-based structures, leading to significant deterioration through both mass loss and strength reduction. This study aims to intensify the acid attack by maintaining a consistent pH level of 1.0 ± 0.2 in the exposure solution. Sulfuric acid (H_2SO_4) was added to water to achieve this specific pH range. After initial submersion in the sulfuric acid solution, the pH level rose rapidly but eventually stabilized, likely due to the reduced alkalinity of the wythe mortar in the EPS panels (Figure 5.1). The pH slope for all EPS panels increased during the first 4 to 8 days of exposure, with variations caused by the periodic addition of sulfuric acid to readjust the pH to 1.

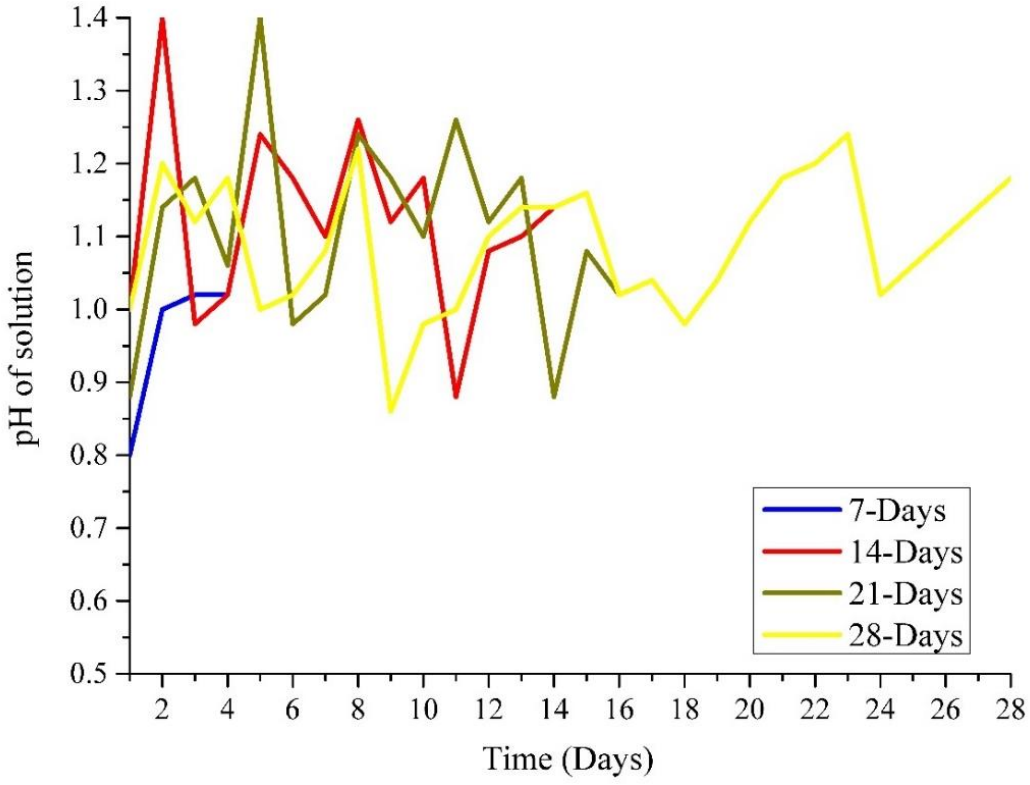

Figure 5.1 Variation of pH in acidic solution

5.2.2 Acid attack impacts cement mix

To comprehensively evaluate the impact of acid attack, 70.5 mm mortar cubes were submerged in the acidic solution and examined at regular intervals for mass loss and residual strength. Figures 5.2a and 5.2b illustrate the relationship between the acid exposure period and both mass loss and residual compressive strength. After 28 days, the residual strength of the mortar cubes showed a significant decline. While mass loss was minimal initially, it progressively increased, reaching 10% after the 28-day period. This consistent degradation highlights the aggressive nature of the acid attack and its detrimental effects on the structural integrity of the EPS panels. These findings underscore the importance of protective measures and periodic assessments to mitigate the adverse effects of acidic environments on cement-based structures.

5.2.3 Sulphate attack impact of cement mix

To investigate the effects of sulphate attack, prism beams (285 mm × 75 mm × 75 mm) and cubes (70.5 mm) were submerged in a 5% sodium sulphate (Na_2SO_4) solution alongside EPS panels. The purpose was to observe any alterations in length and mass caused by the sulphate exposure. The pH of the solution was maintained within a range of 6.0 and 8.0. Length and mass measurements were taken initially before immersion, followed by weekly measurements for the first 6 weeks and biweekly measurements thereafter for 360 days. Figure 5.3 (a & b) displays the percentage change in mass and length of prism beams subjected to sulphate exposure.

During the initial days of exposure, there was a significant and consistent increase in the mass of prism beams. Specifically, over a period of 25 days, the mass increased by 0.43%. Following this initial phase, the mass continued to gradually increase until day 54. After this point, no notable changes in mass were detected, and the mass remained relatively stable up to day 360.

Similarly, the length of the prism beams exhibited a gradual rise, reaching an increase of 0.043% of the gauge length by day 210. However, further exposure beyond this period did not result in significant changes in length. The data suggests that while initial exposure to the conditions led to measurable changes in both mass and length, the effects stabilized over time, indicating a period of acclimatization followed by equilibrium. This information is crucial for understanding the long-term durability and stability of materials under similar exposure conditions.

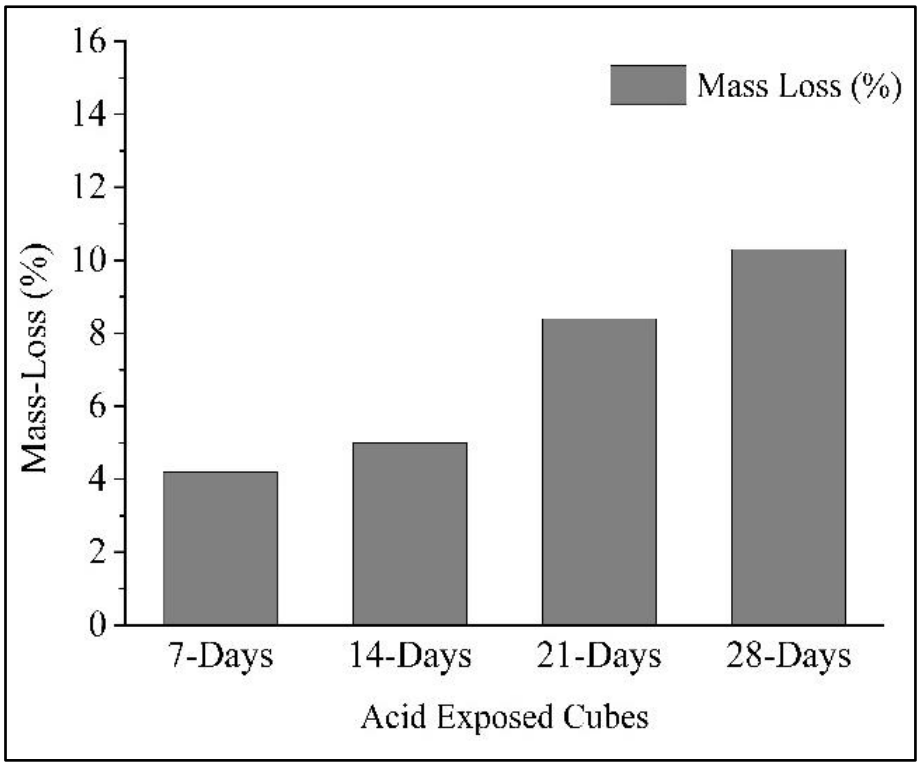

(a) Mass loss due to acid exposure

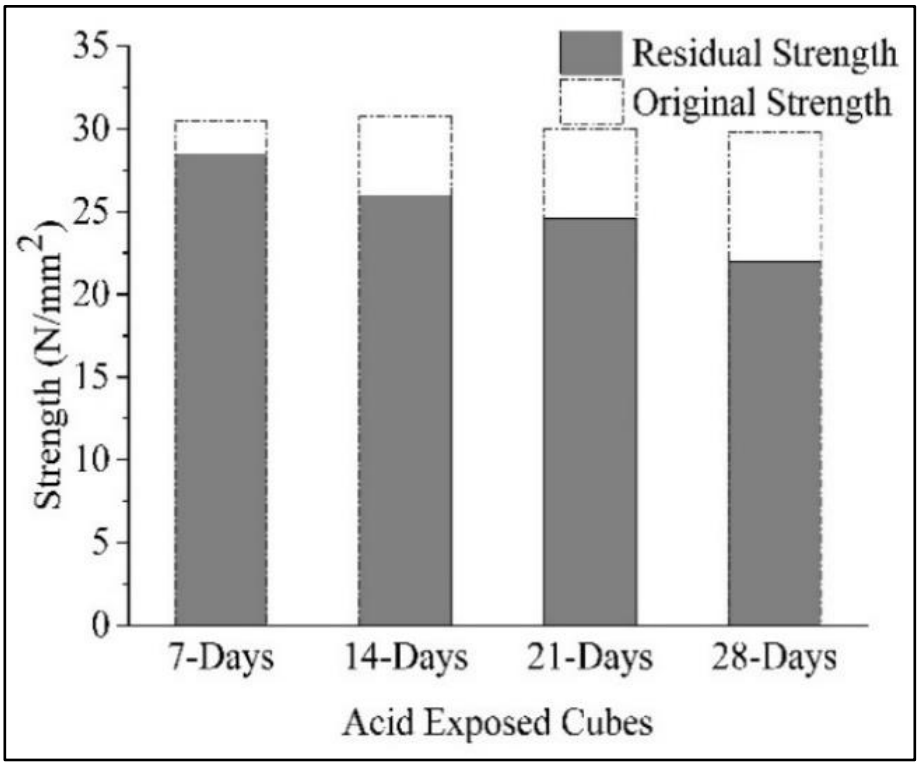

(b) Strength of acid-exposed cube

Figure 5.2 Aggressive acid exposure effect on mortar

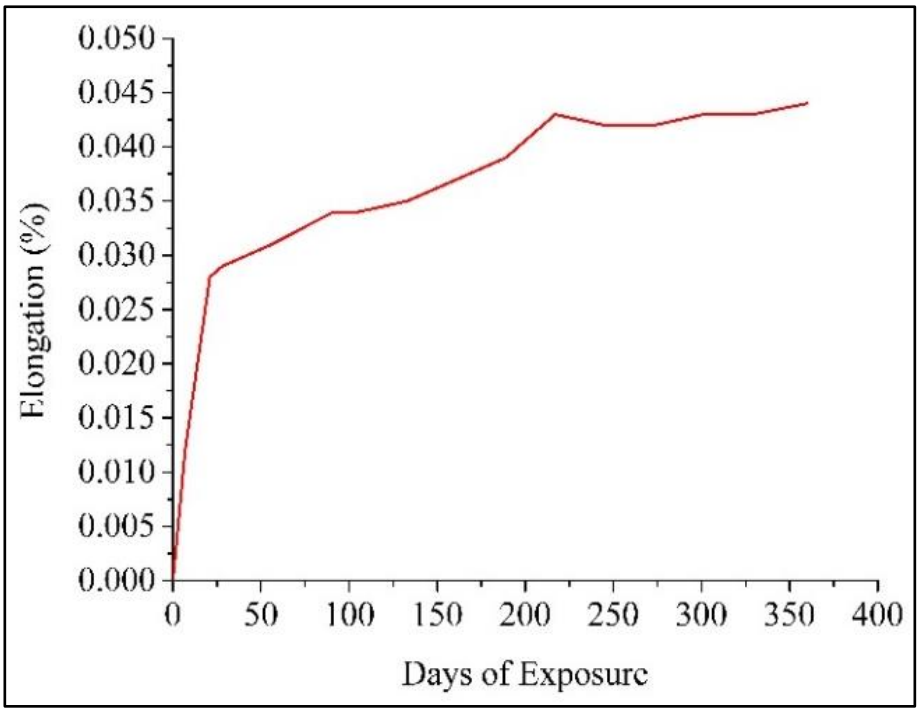

(a) Elongation of sulphate exposed beams

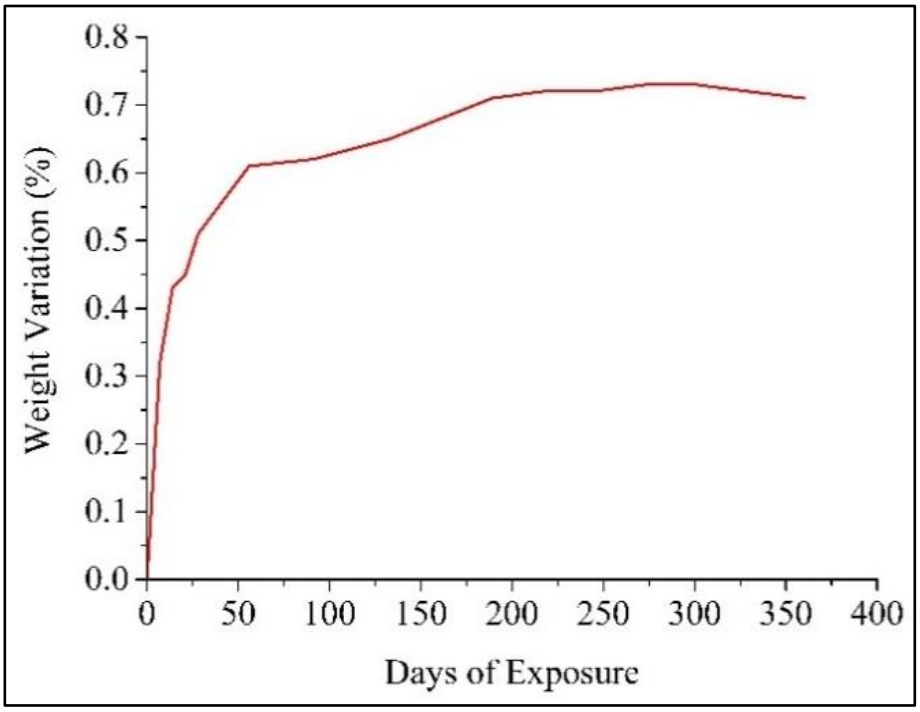

(b) Weight change of Sulphate cubes

Figure 5.3 Aggressive sulphate environment exposure effect on concrete

5.3 VISUAL OBSERVATIONS OF EXPOSED PANELS

Before flexural loading, a visual inspection was conducted on the EPS-sandwiched concrete panels subjected to acid and sulphate attacks. Figures 5.4a and 5.4b display the visual

representation of the EPS panels (EPS-A28 and EPS-S360) exposed to severe acid and sulphate conditions. The images of the uncovered panels were acquired after gently cleaning the mortar surface to eliminate any loose particles. The acid-exposed EPS panels exhibited localized mortar degradation on the surface in the EPS-A7, 14, 21, and 28 samples. Panels exposed to acid for longer periods showed greater mortar deterioration, characterized by wider areas with patches of damage. After 28 days of acid exposure, the EPS panel showed rust areas around the interface of the wythe and EPS (Figure 5.4a).

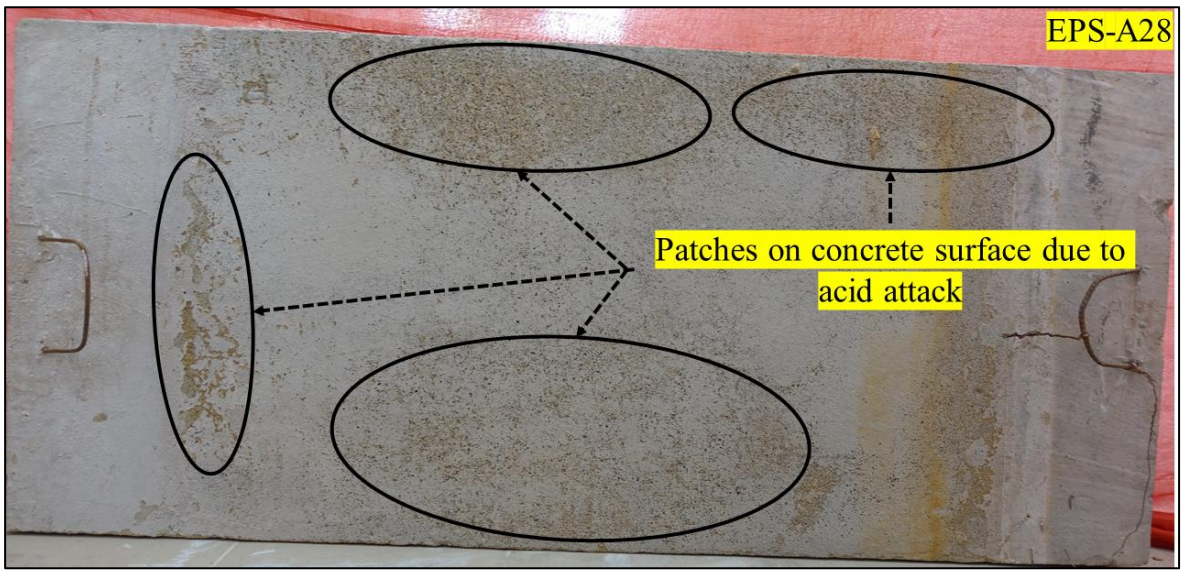

(a) Acid Exposed (EPS A28)

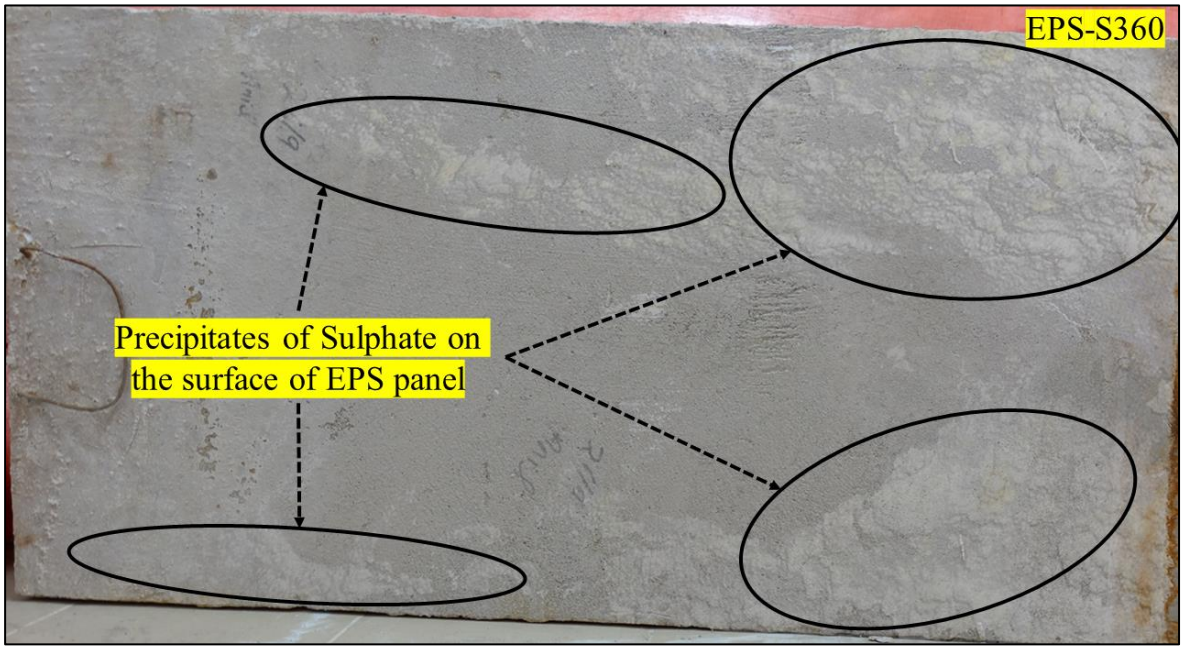

(b) Sulphate exposed (EPS S360)

Figure 5.4 Visuals of EPS panels subjected to aggressive environments

In contrast, the panels exposed to sulphate did not exhibit any surface degradation. However, sulphate precipitates were observed near the margins of the EPS panels (Figure 5.4b). Visual observations did not reveal any noticeable variations based on the duration of exposure to the acidic and sulphate environments. When exposed to an acidic environment, the EPS panels showed visible signs of deterioration on the mortar surface. However, detecting any internal damage within the EPS panels is challenging. Therefore, employing a NDT approach is crucial. NDT can detect internal decay in its early stages, well before visible damage becomes apparent.

The visual inspection of EPS panels post-failure in flexural testing is shown in Figure 5.5. For sulphate-exposed panels, the failure pattern was similar to the control specimen, with breaks occurring between the loading points. Acid-exposed panels showed varied failure patterns based on exposure duration. EPS-A7 and EPS-A14 behaved similarly to the control panel. However, EPS-A21 exhibited horizontal cracking along the interface of insulation and concrete wythe, and the highly acid-exposed EPS-A28 showed both horizontal and shear cracking near the supports, as well as middle cracks between the loading points.

These observations indicate that while sulphate exposure primarily affects ductility, acid exposure introduces complex failure patterns, especially with prolonged exposure. Understanding these changes is essential for predicting the long-term performance and durability of materials used in sulphate-rich and acidic environments.

5.4 MECHANICAL TESTING OF ACID AND SULPHATE EXPOSED EPS PANELS

5.4.1 Load-deflection behaviour of acid exposed EPS panels

The flexural performance of acid-exposed EPS panels is crucial for their structural applications. The load-deflection curves presented in Figure 5.6 illustrate the varying behaviors of EPS panels with different levels of acid exposure. The load-deflection curves of acid exposed panels are compared with the control panel as discussed in Section 4.4.1

The flexural behavior of acid-exposed EPS panels is detailed in Figure 5.6, highlighting the distinct response at varying exposure durations. In EPS-A07 (Figure 5.6a), the initial fracture occurs at a load of 10 kN, accompanied by a deflection of 0.8 mm, indicating elastic behavior in Zone-I.

(a) EPS-A7

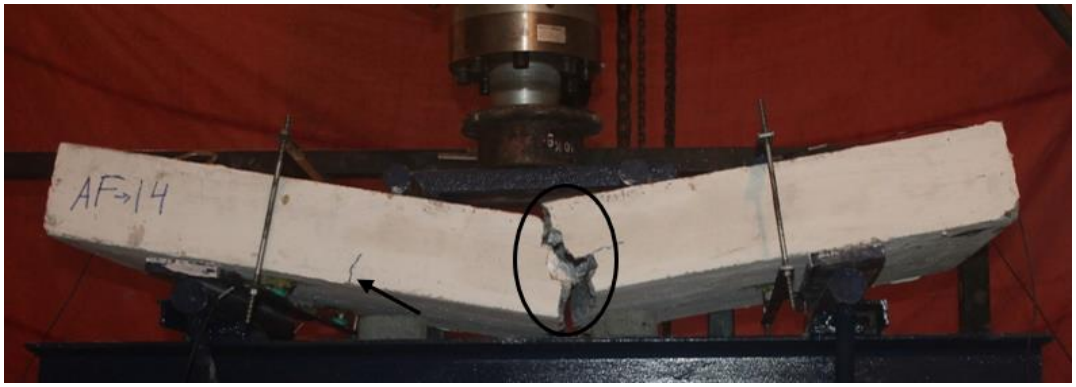

(b) EPS-A14

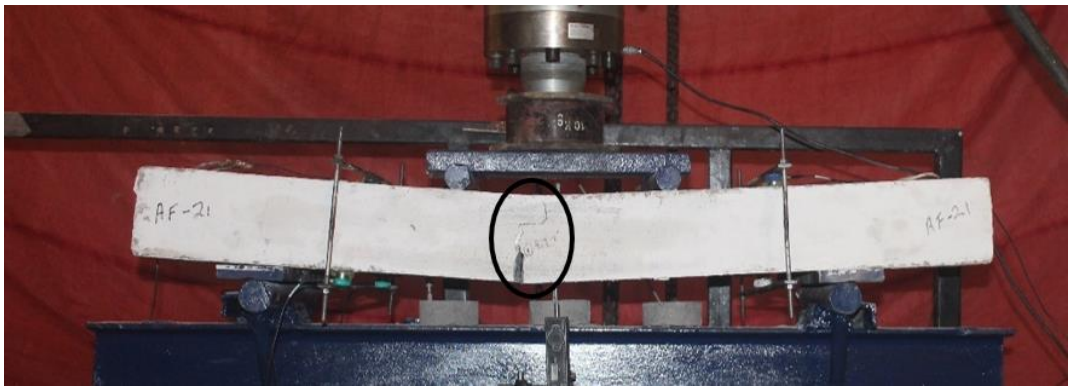

(c) EPS-A21

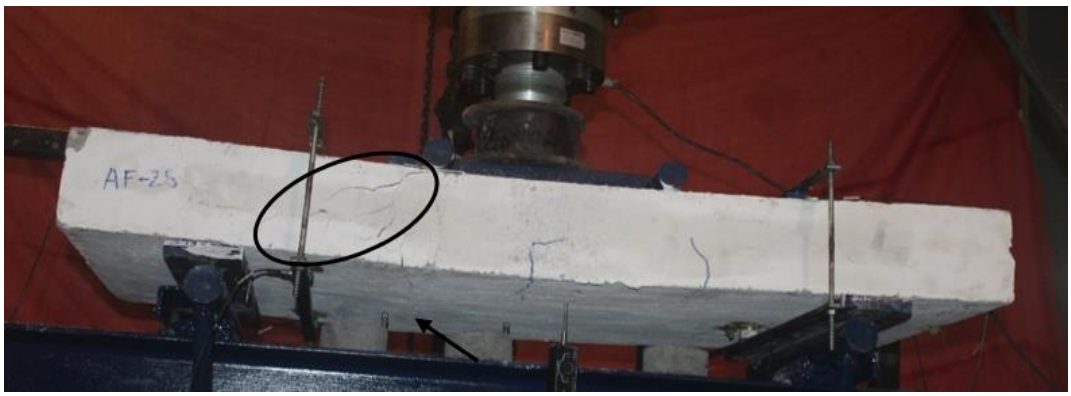

(d) EPS-A28

Figure 5.5 Failures in acid exposed EPS panels

After this initial crack, the panel transitions into Zone-II, exhibiting cracked elastic behavior as the load increases. Zone-III marks the onset of plastic behavior, characterized by a rapid increase in deflection until the panel ultimately fails at 35 kN and 5.5 mm deflection. This transition through the three zones illustrates the material's ability to absorb and distribute stress before failure.

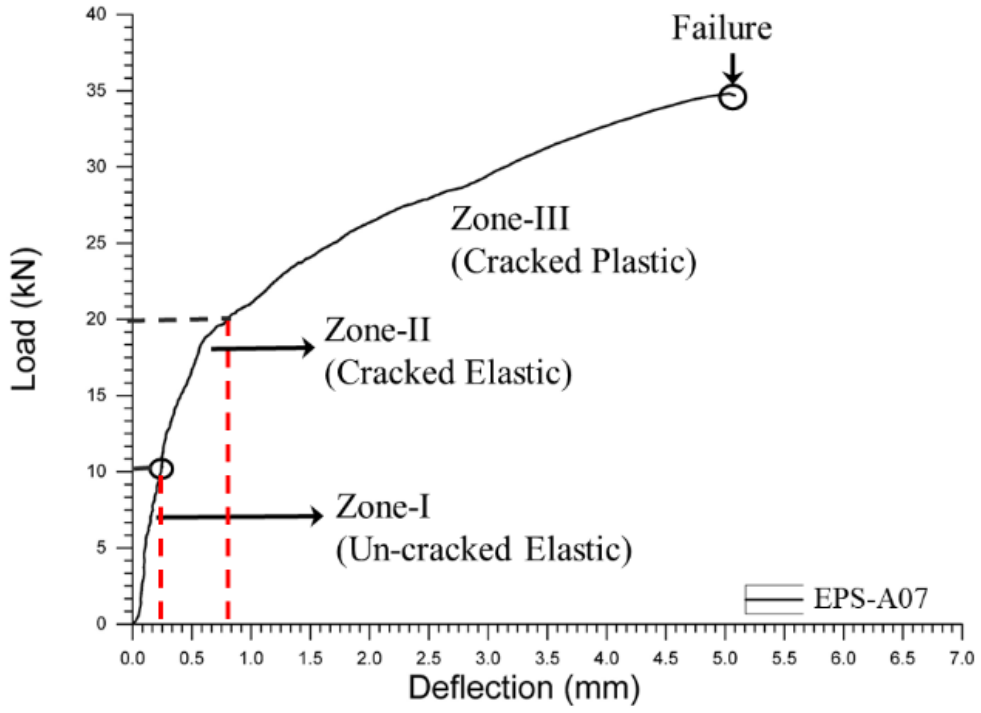

(a) Load deflection plot of EPS-A07

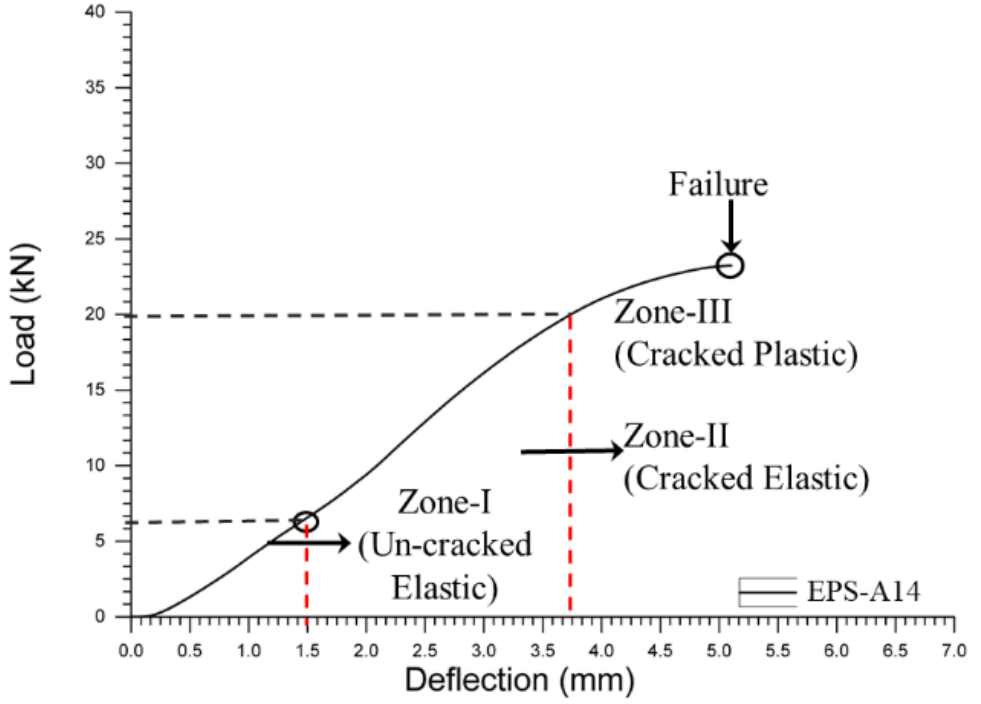

(b) Load deflection plot of EPS-A14

Figure 5.6 Load deflection plots of acid exposed EPS panels (Cont.)

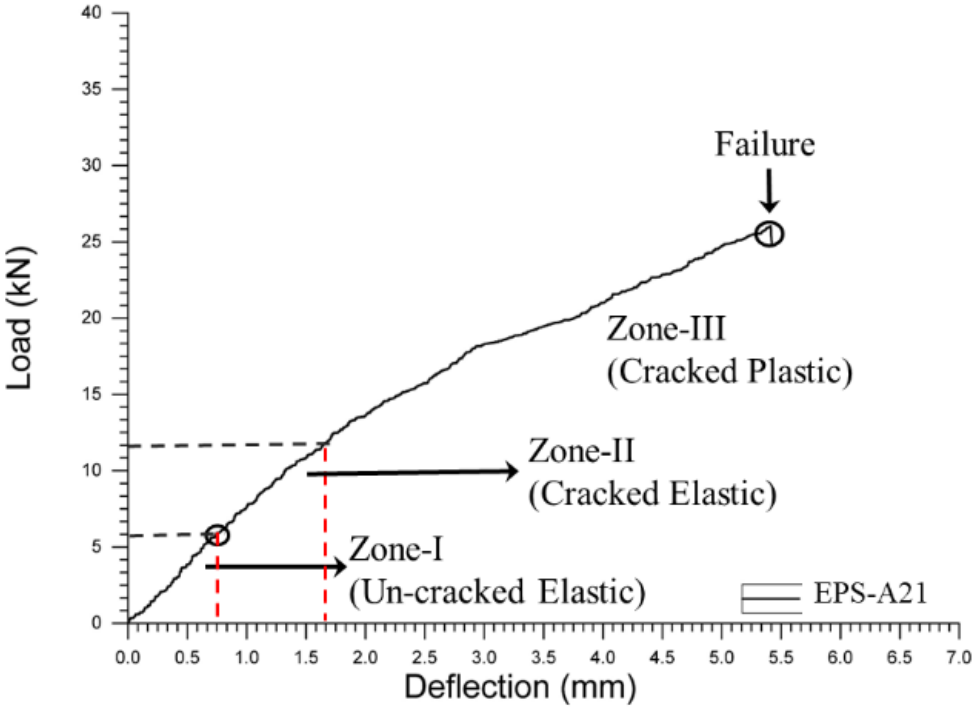

(c) Load deflection plot of EPS-A21

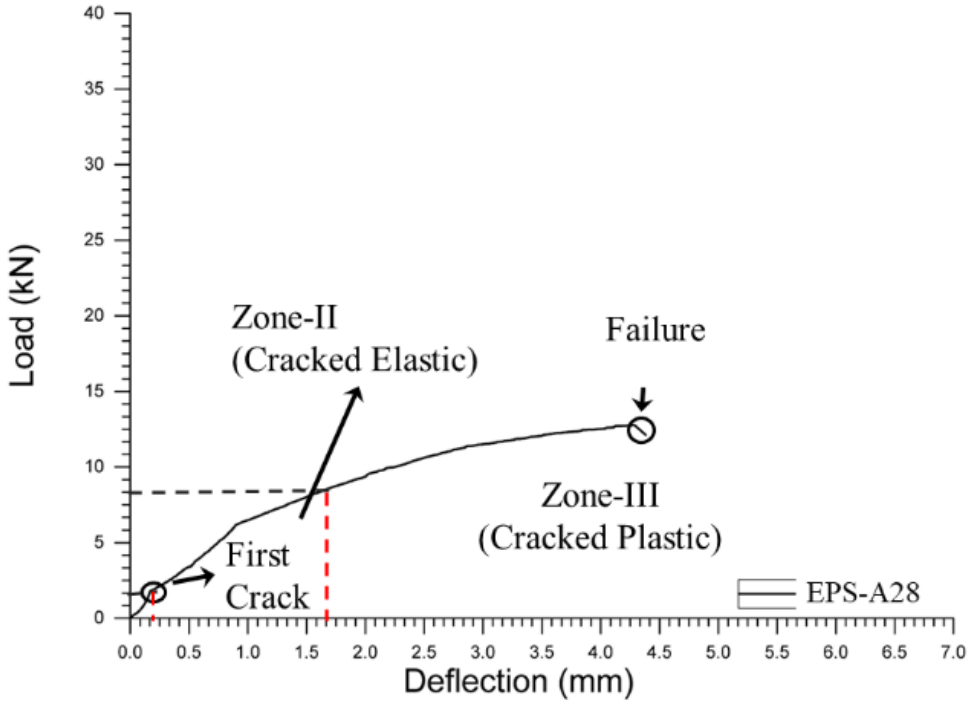

(d) Load deflection plot of EPS-A28

Figure 5.6 Load deflection plots of acid exposed EPS panels

Similarly, EPS-A14 (Figure 5.6b) exhibits an initial fracture at 6 kN with a 1.4 mm deflection, leading to failure at a lower load of 28 kN. The reduced load capacity compared to EPS-A07 suggests the impact of prolonged acid exposure. In EPS-A21 (Figure 5.6c), the initial

fracture occurs at 8 kN with a 1.2 mm deflection. As loading continues, a notable decrease in stiffness and strength is observed, resulting in a diminished load-carrying capacity. This reduction indicates the detrimental effects of sustained acid exposure on the material's structural integrity.

The most severe acid exposure is seen in EPS-A28 (Figure 5.6d), which shows a intense reduction in load capacity. The first crack occurs at a significantly lower load of 1.97 kN, progressing into Zone-II with a slower load increase compared to the control panel. In Zone-III, the panel demonstrates rapid deflection with minimal load increase, failing at approximately 20 kN. This pronounced reduction in load-bearing capacity and increased deflection highlights the severe impact of acid exposure on the structural performance of the EPS panels.

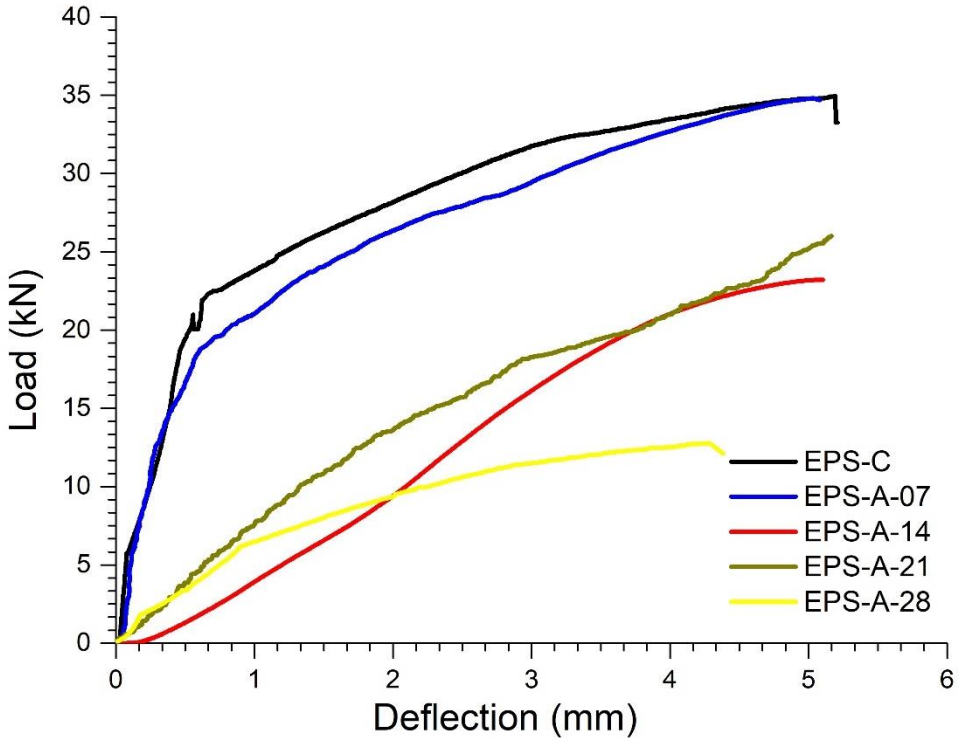

Figure 5.7 Combined load-deflection plots of acid exposed EPS panels.

A combined comparative graph of the load-deflection curves for acid-exposed EPS panels, shown in Figure 5.7, encapsulates these findings. The graph illustrates the progressive deterioration in flexural performance with increased acid exposure, underscoring the material's reduced structural resilience under aggressive environmental conditions. The ductility of specimens exposed to the acidic environment for 21 days or less remains largely unaffected, likely due to the minimal impact on reinforcement within this exposure period. However, in

EPS-A28, the extended exposure duration leads to noticeable corrosion on the reinforcement, which significantly impacts ductility. This comprehensive analysis of flexural behavior under acid exposure is crucial for understanding and predicting the long-term durability and reliability of EPS panels in acidic environments.

Table 5.1 Mechanical testing parameters of acid and sulphate exposed EPS panels

Panel Designation	First crack load (kN)	Ultimate load (Pu) (kN)	Yield load (Py) (kN)	Deflection at yield (Δy) (mm)	Ultimate Deflection (Δu) (mm)	Ductility Factor (DF = Δu/Δy)
EPS-00	6	34.95	19.5	0.7	5.21	7.44
EPS-A7	6.192	34.81	20.08	0.63	5.08	8.07
EPS-A14	6.618	28.76	16.73	1.53	5.10	3.34
EPS-A21	5.97	26.01	12.48	1.57	5.16	3.45
EPS-A28	1.97	13.02	8.62	1.43	4.68	3.27
EPS-S90	7.16	32.03	20.32	0.83	5.25	6.32
EPS-S180	6.36	31.07	19.02	1.51	5.09	3.75
EPS-S270	5.21	26.98	17.58	2.04	5.05	2.48
EPS-S360	5.64	20.02	8.82	1.48	4.98	3.36

5.4.2 Ductility and energy absorption of acid exposed EPS panels

Ductility, a material's ability to deform plastically before failure, is crucial for structural applications. It allows energy absorption and dissipation, enhancing a structure's resilience to dynamic loads and stress concentrations. Higher ductility improves safety and longevity by warning before a catastrophic collapse. Table 5.1 shows that acid exposure significantly reduces the EPS panels' ductility factor (DF) compared to the control panels by 55.11%, 53.63%, and 56.05% after exposure to an acid environment for 14, 21, and 28 days, respectively.

The load-deflection curves for all acid-exposed panels exhibit clear elastic and plastic regions, transitioning from uncracked to cracked elastic, and finally to cracked plastic behavior. The panels exhibit varying ultimate loads and deflections, highlighting the influence of acid exposure. Panels exposed for 7-days show minimal changes compared to the control. These

curves provide valuable insights into the mechanical behavior and failure mechanisms of EPS panels under flexural loading.

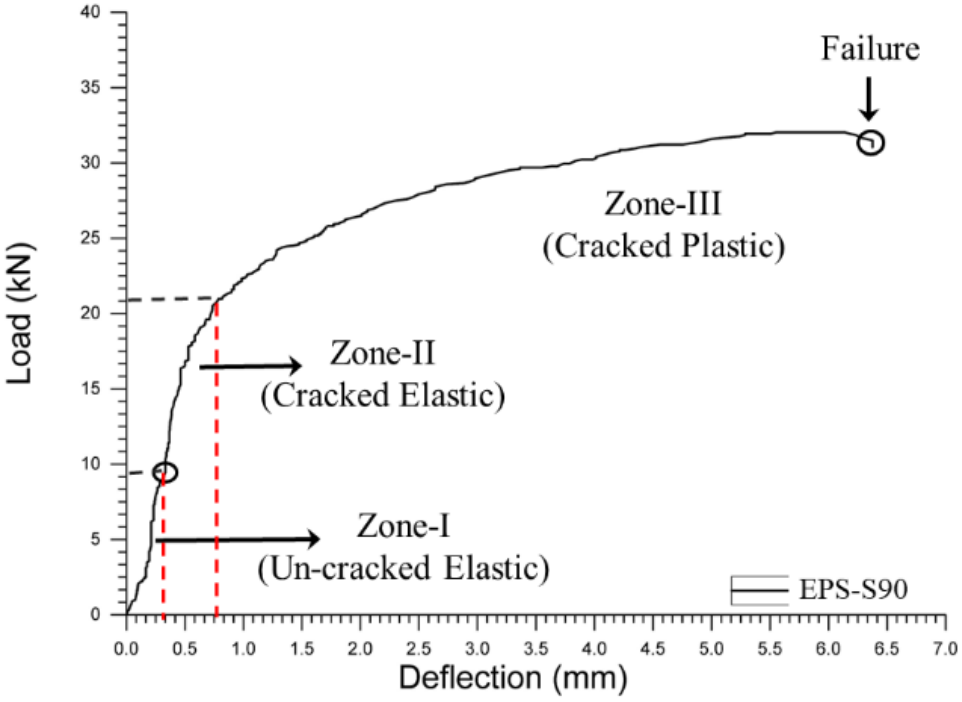

(a) Load deflection plot of EPS-S90

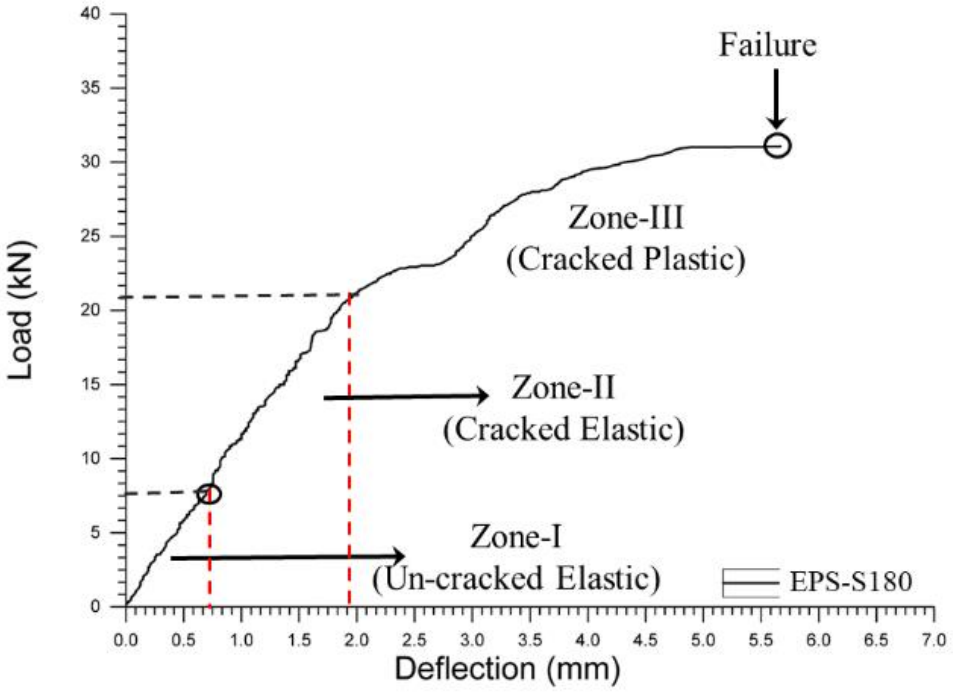

(b) Load deflection plot of EPS-S180

Figure 5.8 Load deflection plots of sulphate exposed EPS panels (Cont.)

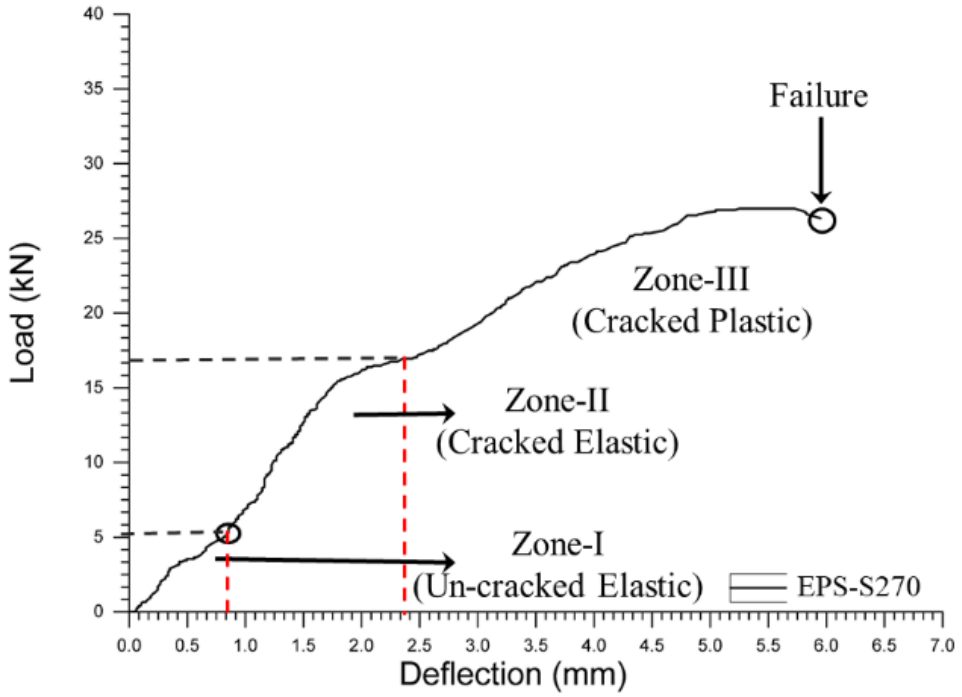

(c) Load deflection plot of EPS-S270

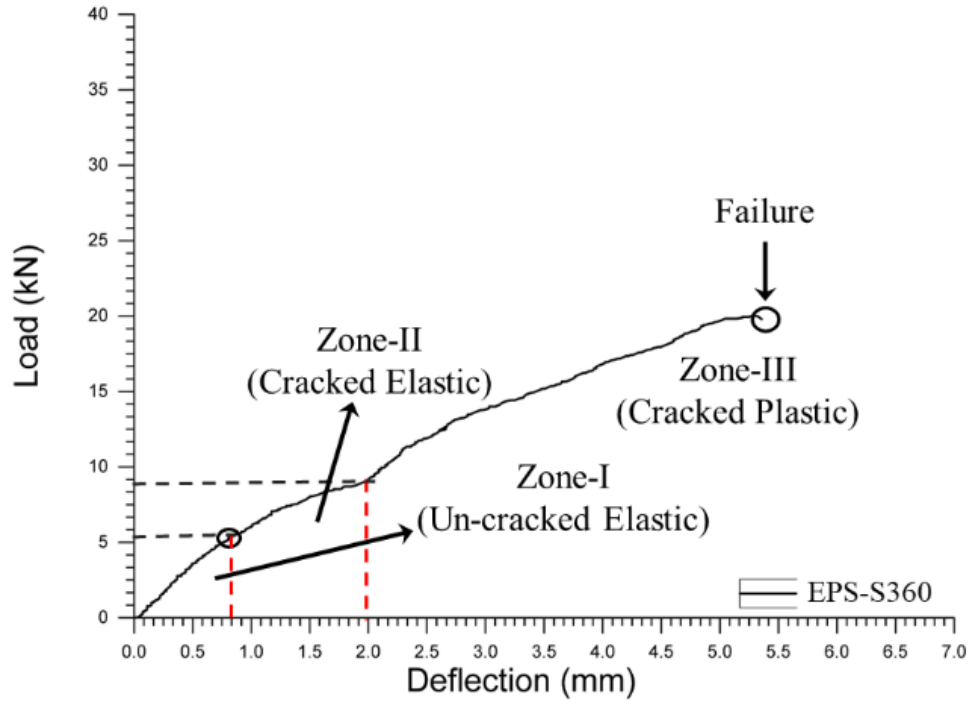

(d) Load deflection plot of EPS-S360

Figure 5.8 Load deflection plots of sulphate exposed EPS panels

5.4.3 Load-deflection behaviour of Sulphate Exposed EPS Panels

The flexural performance of the sulphate-exposed EPS panels was evaluated (Figure 5.8), similar to the acid-exposed EPS panels. Compared to the control panel (EPS-00), it is observed that increased sulphate exposure leads to changes in both the initial stiffness and final load-

carrying capacity. The EPS-S90 panel exhibited nearly identical behavior to the EPS-00 panel, demonstrating comparable starting stiffness and failing at a nearly identical load of 32.03 kN (Figure 5.8a). The initial stiffness of EPS-S180 significantly decreased, with failure occurring at a load of 31.07 kN, compared to the control panel, which failed at 34.95 kN (Figure 5.8b). Additionally, there is a significant decrease in the initial rigidity of EPS-S270 and EPS-S360 panels. These panels experienced failure at loads that were 22.8% and 42.71% lower than the control panel, respectively (Figures 5.8c and 5.8d). This suggests a progressive deterioration with longer exposure durations of 270 and 360 days. Combined load-deflection plot of sulphate exposed EPS panels is shown in Figure. 5.9.

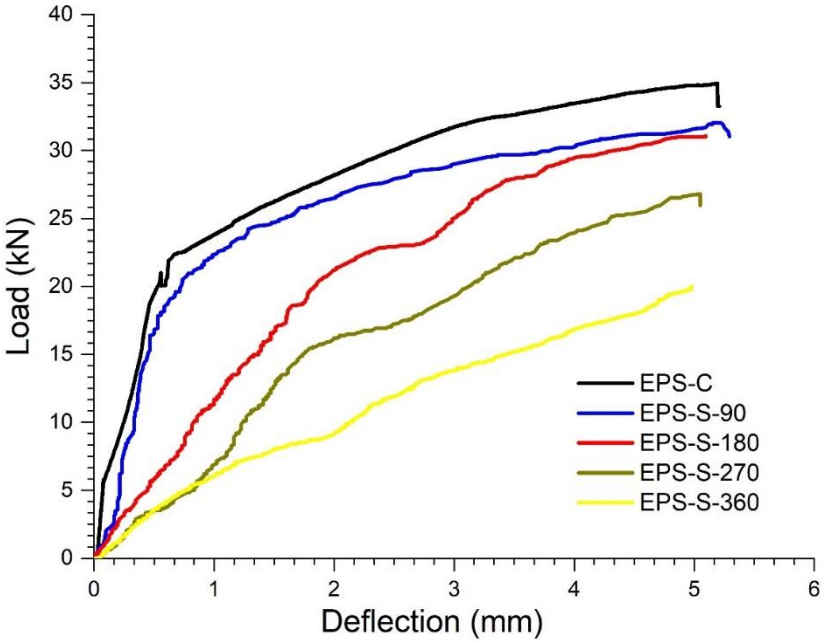

Figure 5.9 Combined load-deflection plots of sulphate exposed EPS panels

5.4.4 Ductility of the sulphate exposed EPS panels

The data presented in Table 5.1 illustrates the impact of sulphate exposure on the ductility of EPS panels over a period of 360 days, as measured by the Ductility Factor. Ductility, which refers to the ability of a material to deform under tensile stress, is a crucial property for construction materials. The data shows a significant decrease in ductility between 180 and 270 days, followed by a slight recovery at 360 days.

Initially, at 90 days of exposure (EPS-S90), the Ductility Factor is relatively high at 6.32, indicating good ductile properties. However, a marked decline is observed at 180 days (EPS-S180), where the Ductility Factor drops to 3.75. This trend continues, with the lowest value recorded at 270 days (EPS-S270), where the Ductility Factor is 2.48. This substantial reduction

suggests that prolonged sulphate exposure severely compromises the ductility of EPS panels, making them more brittle and less capable of withstanding tensile stress. Interestingly, by 360 days (EPS-S360), the Ductility Factor is calculated to 3.36. This minor increase could indicate some level of adaptation or stabilization, but it cannot be concluded as further research over extended durations would be necessary to support such conclusions. Still, the ductility factor remains significantly lower than the initial 90-day value.

5.4.5 Implications of acid and sulphate exposure

Extended exposure to acid and sulphate attacks deteriorates the mortar and corrodes the reinforcement within EPS panels. This degradation leads to a substantial loss of initial stiffness, ultimate load-carrying capacity, and reduced ductility. The decrease in ductility highlights the critical need for early health monitoring strategies for EPS panels, especially in harsh environments. Implementing such monitoring systems can significantly reduce the risk of structural failures in EPS panel structures, ensuring their long-term durability and safety.

5.5 AE MONITORING OF ACID AND SULPHATE EXPOSED EPS PANELS

5.5.1 Cumulative AE Hits

The monitoring of EPS panels during flexural testing was conducted using the Acoustic Emission (AE) technique. Various AE parameters, such as the number of AE hits, their amplitudes, RA, and AF, were recorded and analyzed. Cumulative AE hits indicate the buildup of damage due to progressive cracking within the material. The amplitude of an AE hit corresponds to the severity of the damage sustained by the panel. As loads and degradation increase, cumulative AE hits serve as a direct indicator of crack formation in the concrete panels.

The control EPS panel (EPS-00) increases cumulative AE hits when subjected to flexural loading (Figure 5.10a). This rise is directly proportional to the increase in load. Initially, the rate of AE hit increase is very gradual, with low amplitudes, indicating slow initial micro-cracking (Stage I, Figure 5.10a & b). No visible fractures are observed on the EPS panel surface during this stage. Stage II shows a period with minimal increase in AE hits and amplitudes remaining below 50 dB, indicating no new crack formation for a brief time. The initial formation of surface cracks occurs when the load reaches 19.5 kN. Subsequently, a consistent and sharp rise in AE hits is observed, with high amplitudes exceeding 50 dB.

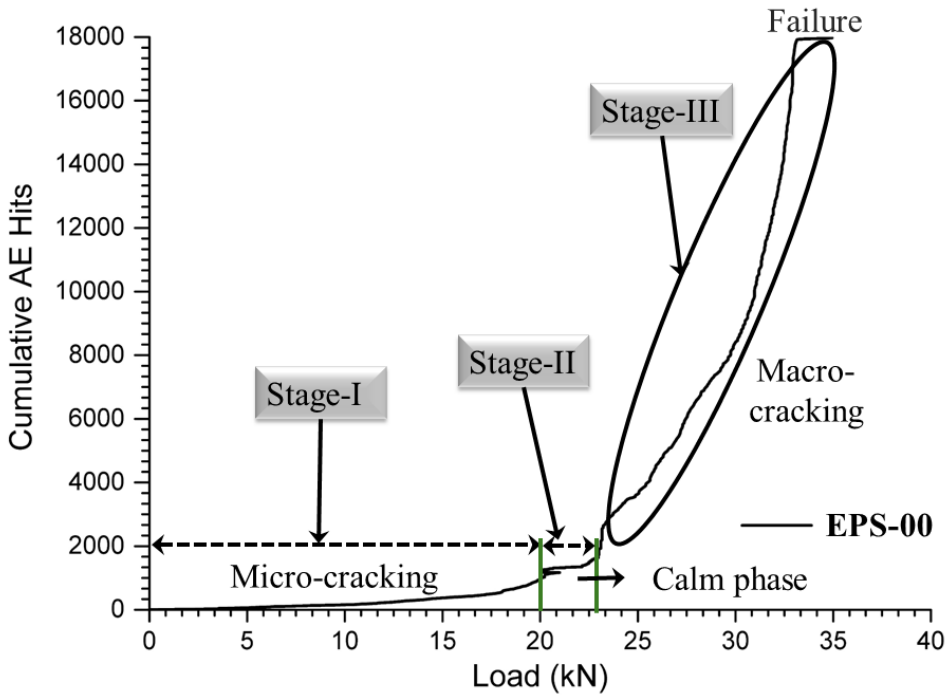

(a) AE hits vs load

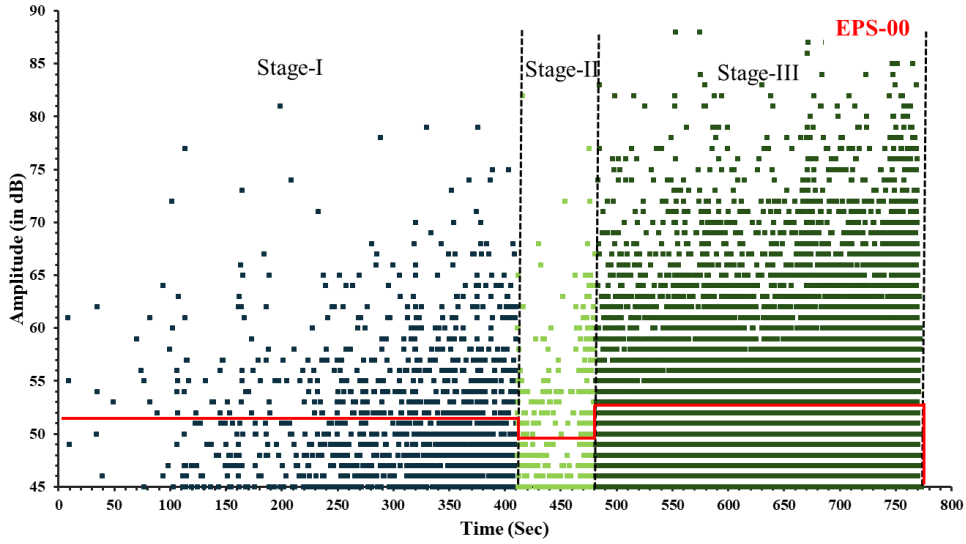

(b) Amplitude vs Time

Figure 5.10 AE plots of control EPS panel (EPS-00)

This signifies the merging of micro-cracks into macro-cracks, resulting in significant surface cracks as the load increases. Ultimately, the panels fail at a load of 34.95 kN. This process, referred to as macro-cracking, primarily occurs during Stage III. In this phase, damage progresses through the development of noticeable fractures in the control EPS panel. Therefore, AE plots provide a visual representation of damage's gradual development and intensity. They can be utilized as non-destructive testing techniques to gain valuable insights and be directly applied on-site.

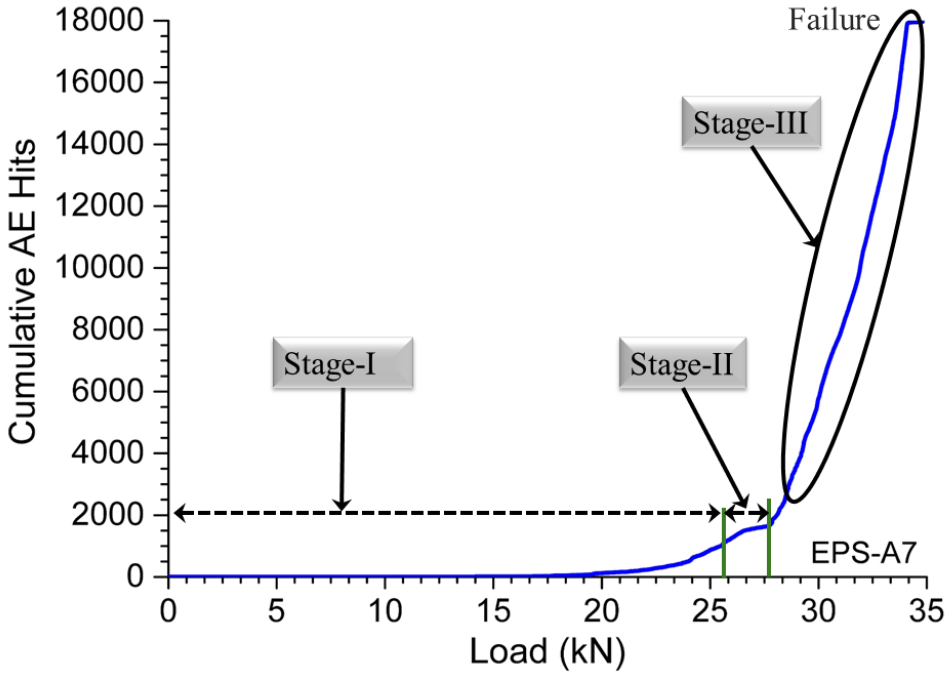

(a) AE Hits vs Load

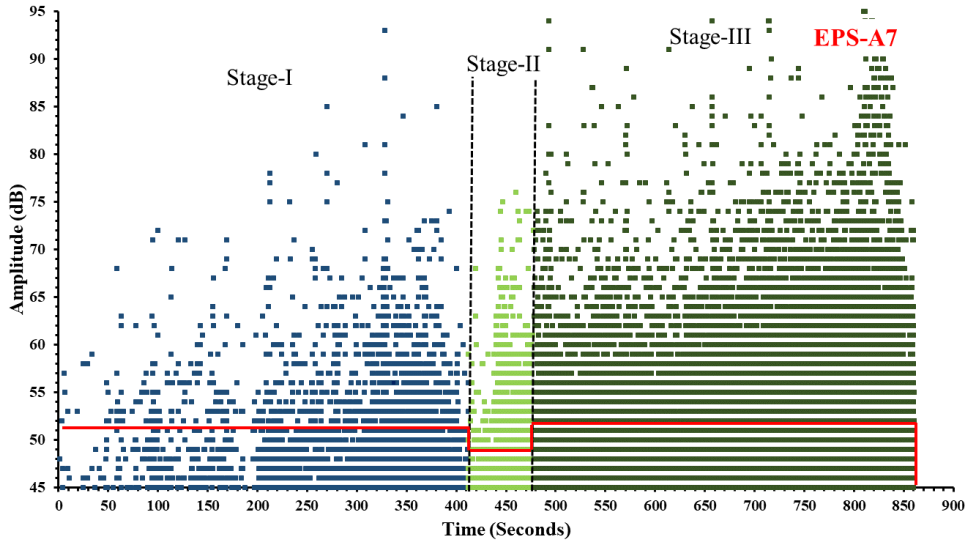

(b) Amplitude vs Time

Figure 5.11 AE plots of acid exposed EPS-A07 panel

5.5.2 Effect of acid exposure on AE

In contrast to the control panel, EPS panels exposed to acidic environments exhibit a noticeable decrease in cumulative AE hits with increased exposure duration. The amplitudes corresponding to acid exposure (EPS-A7 to EPS-A28) also decrease (Figs. 5.11 – 5.14).

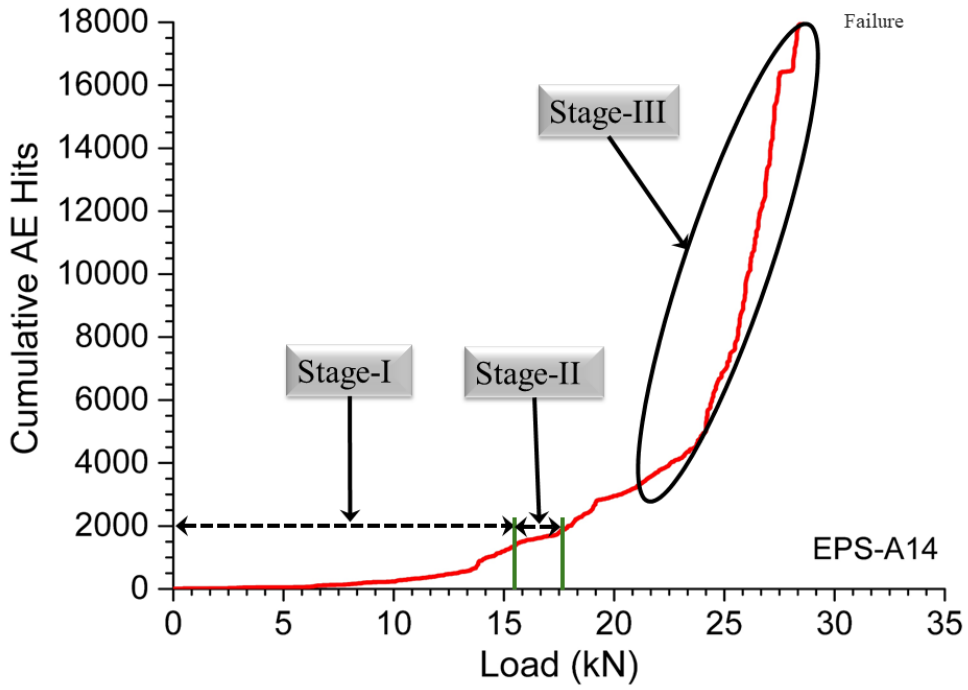

(a) AE Hits vs Load

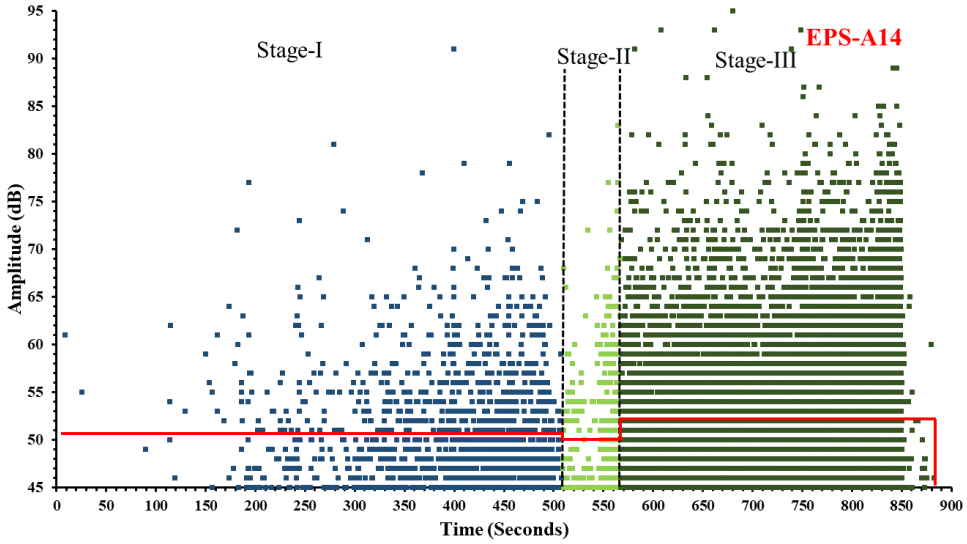

(b) Amplitude vs Time

Figure 5.12 AE plots of acid exposed EPS-A14 panel

The reduction in hits and amplitudes is minimal in EPS-A7 (Figure 5.11a & b) and EPS-A14 (Figure 5.12 a & b) panels. However, extended acid exposure significantly reduces the frequency of hits and amplitudes, as observed in the EPS-A21 and EPS-A28 panels (Figs. 5.13 & 5.14). For EPS-A21, Stages I and II show no significant changes in hits and amplitudes (less than 50 dB) compared to the control panel, which displays notable variance. In EPS-A28, Stages I and II exhibit impact and amplitudes below 47 dB. However, the panel fails

immediately due to macro-cracking following initial micro-cracking, which has an average amplitude around 49 dB (Figure 5.14b). This suggests pre-existing cracks and damage within the panel.

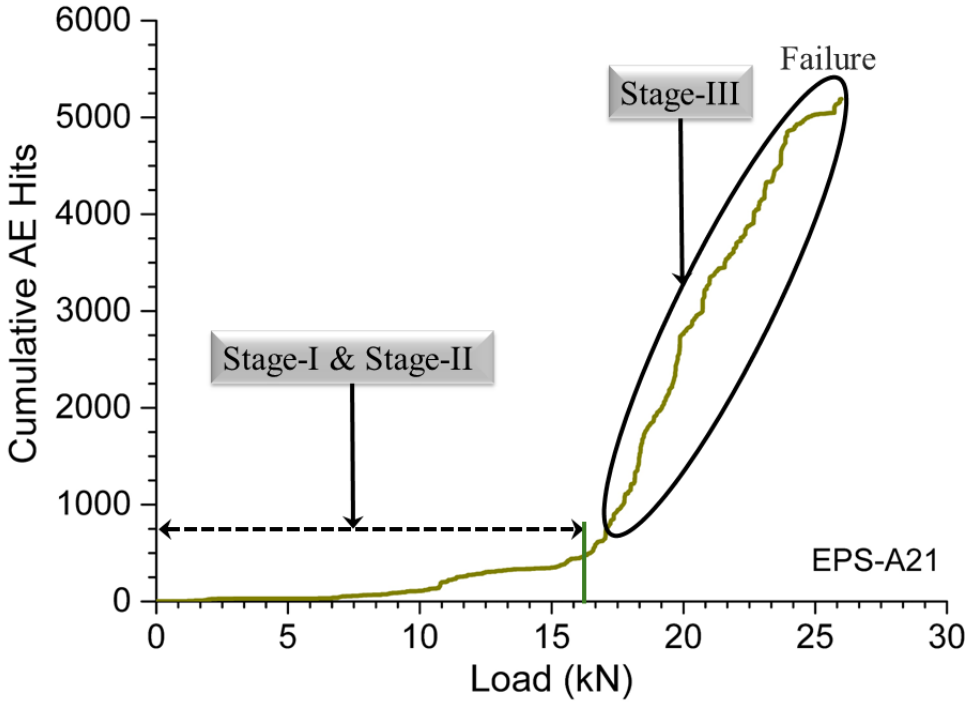

(a) AE Hits vs Load

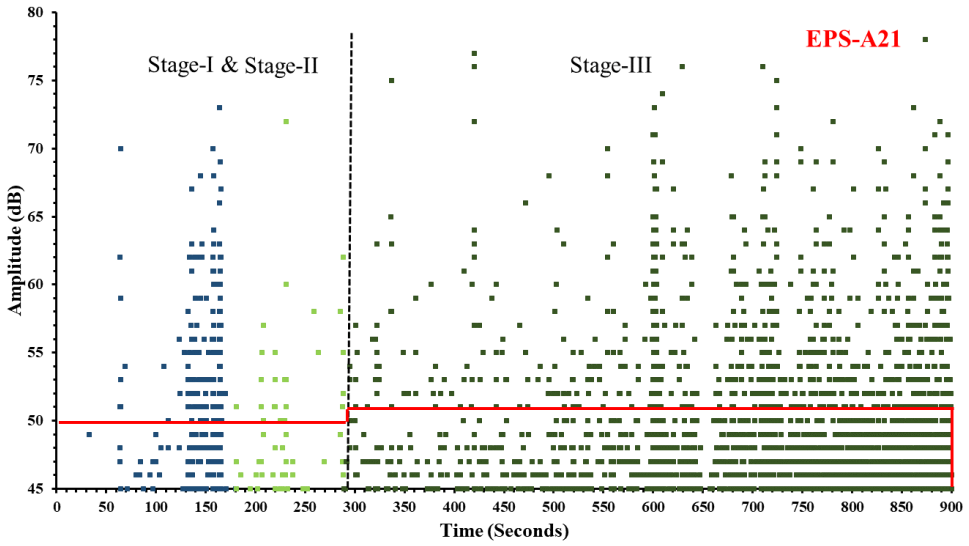

(b) Amplitude vs Time

Figure 5.13 AE plots of acid exposed EPS-A21 panel

This trend is consistent with the relationship between the plot of accumulated AE hits and the load for acid-deteriorated samples (EPS-A7, EPS-A14, EPS-A21, and EPS-A28). The

significant reduction in the quantity of impacts and the strength of amplitudes, compared to the control panel, clearly indicates damage in EPS panels exposed to acid. This damage can be effectively detected using the AE approach, highlighting the importance of continuous monitoring for early detection of structural degradation

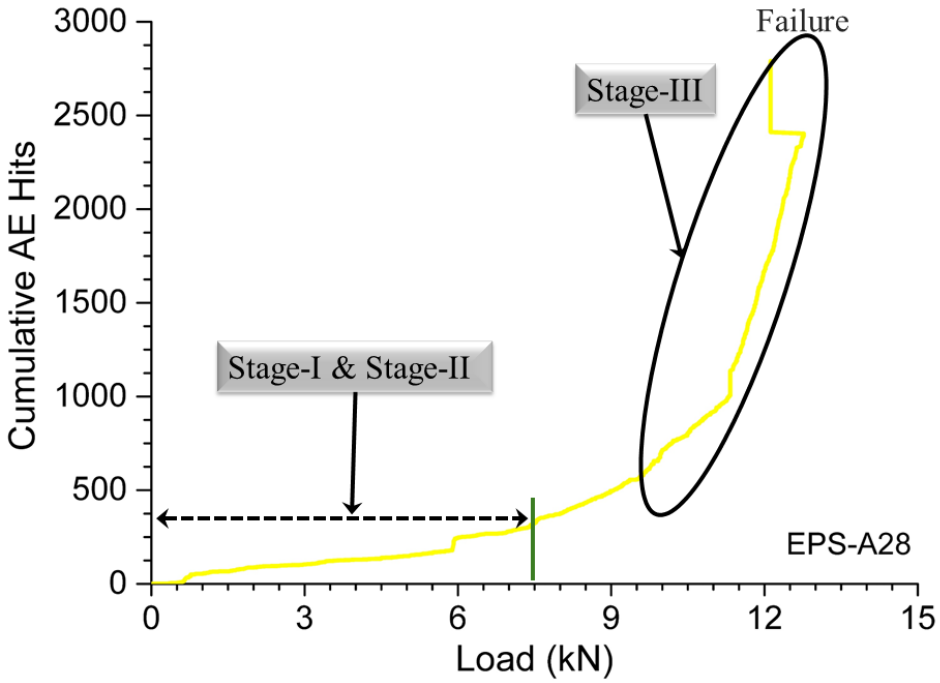

(a) AE Hits vs Load

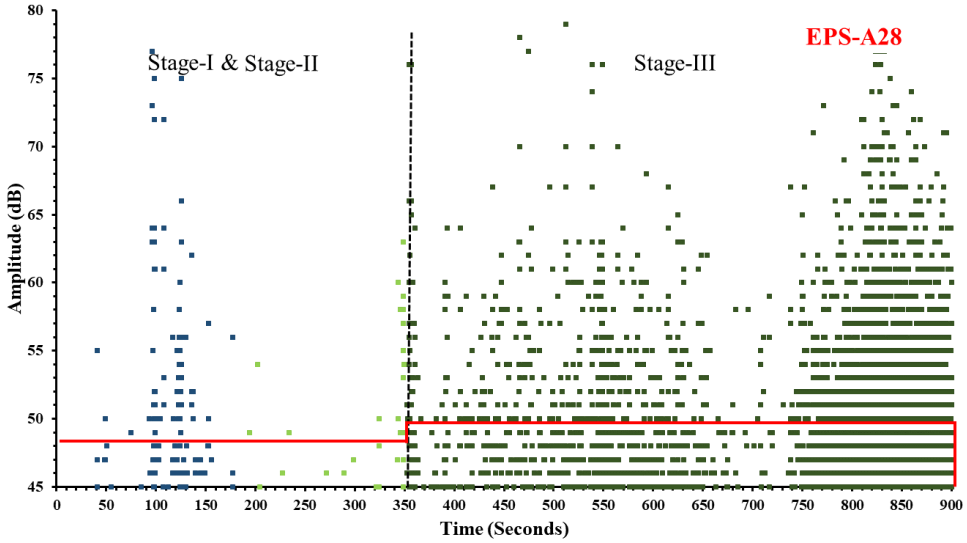

(b) Amplitude vs Time

Figure 5.14 AE plots of acid exposed EPS-A28 panel

This information underscores the necessity for structural health monitoring of EPS panels, especially in harsh environmental conditions, to ensure the longevity and safety of these

materials. Implementing AE monitoring techniques can provide critical insights into the onset and progression of damage, allowing for timely maintenance and repair, ultimately enhancing the durability and performance of EPS panels in aggressive environments.

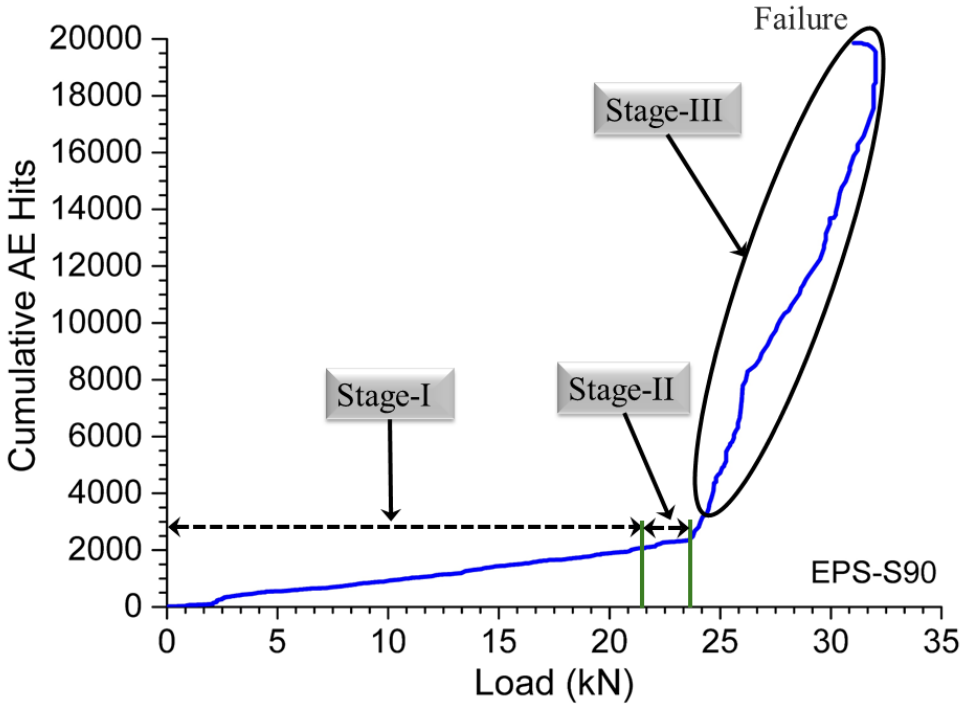

(a) AE Hits vs Load

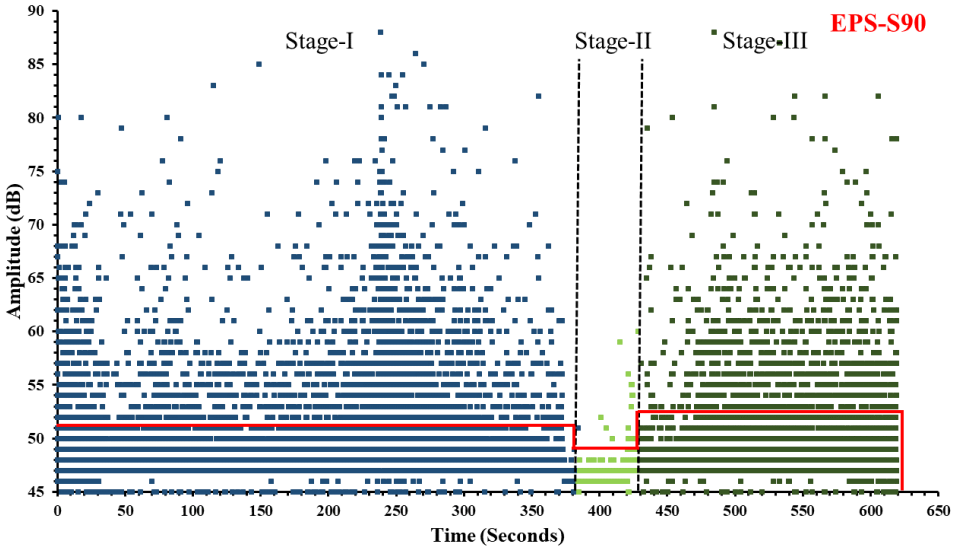

(b) Amplitude vs Time

Figure 5.15 AE plots of sulphate exposed EPS-S90 panel

5.5.3 Effects of sulphate exposure on AE

The AE hits and amplitudes measured during flexural testing of sulphate-exposed EPS panels are depicted in Figures 5.15 to 5.18.

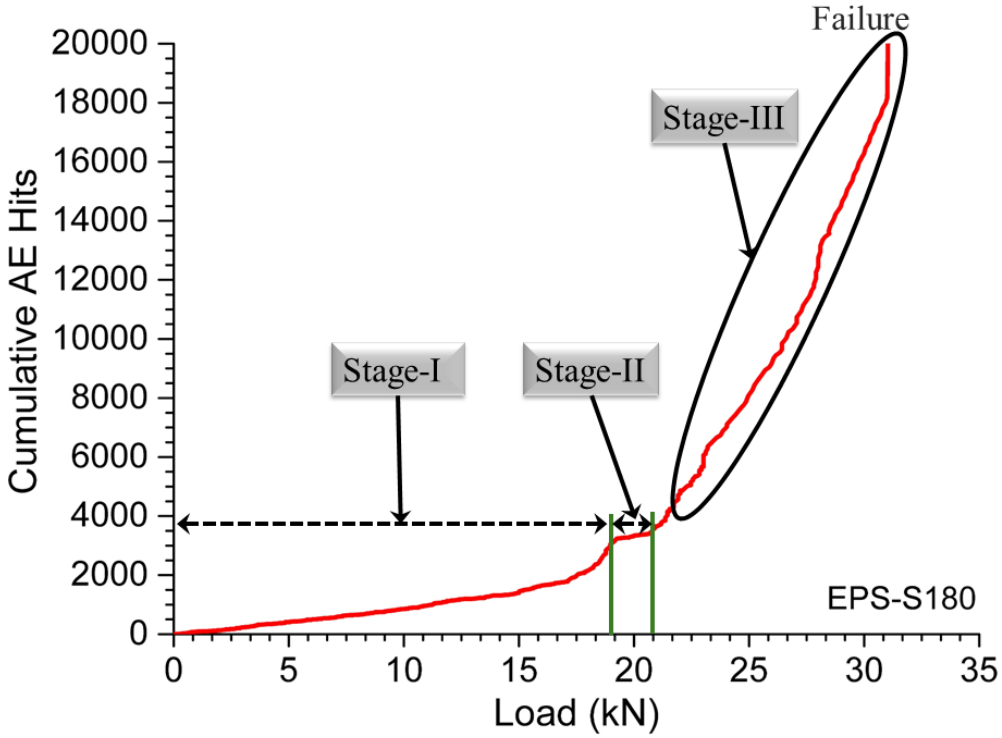

(a) AE Hits vs Load

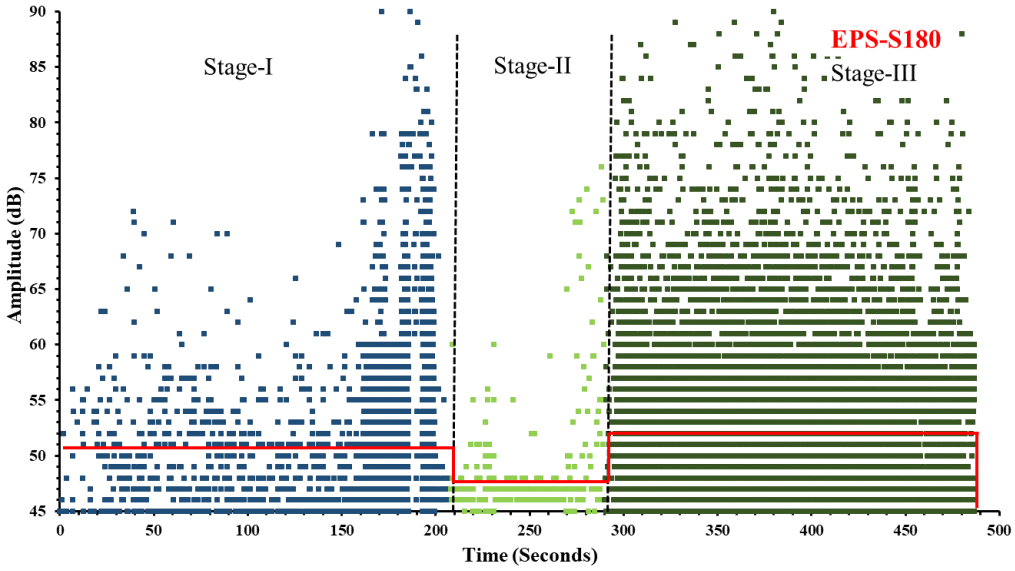

(b) Amplitude vs Time

Figure 5.16 AE plots of sulphate exposed EPS-S180 panel.

These figures reveal a more pronounced occurrence of early micro-cracking in panels EPS-S90 and EPS-S180 compared to the control panel, as shown in Figures 5.15 and 5.16. The greater impacts observed in these panels indicate active micro-cracking due to sulphate exposure, which is likely exacerbated by the flexural loading applied during testing.

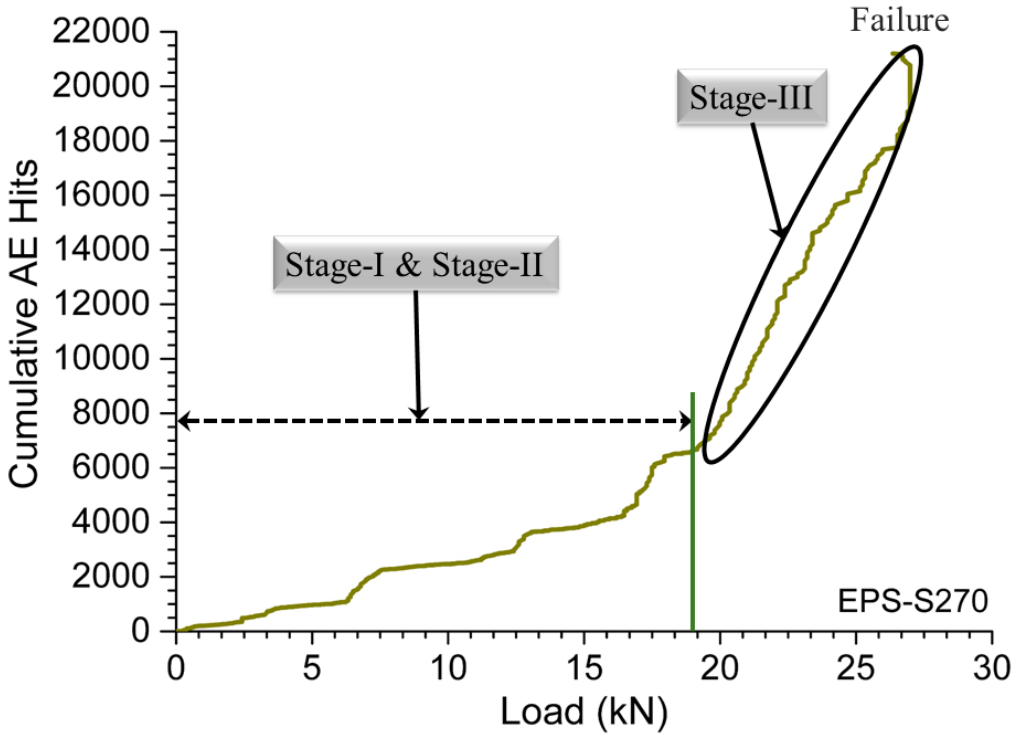

(a) AE Hits vs Load

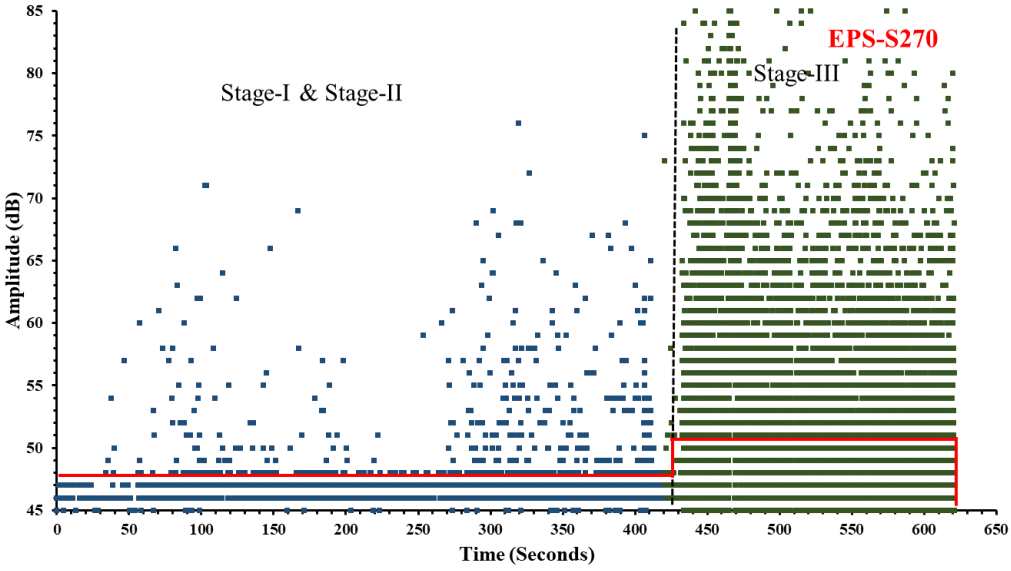

(b) Amplitude vs Time

Figure 5.17 AE plots of sulphate exposed EPS-S270 panel

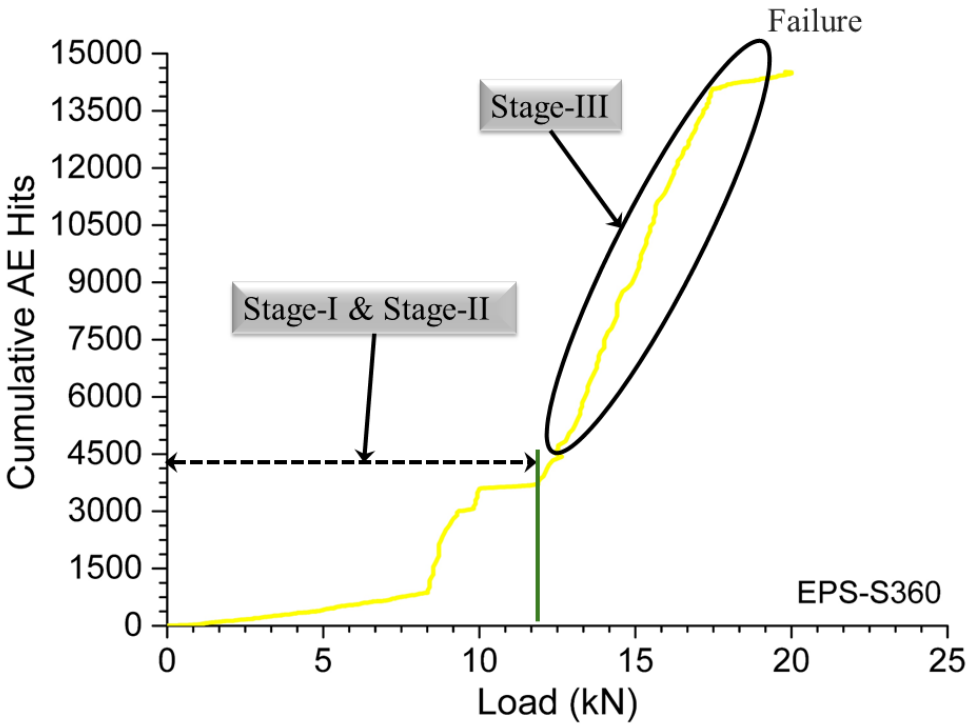

(a) AE Hits vs Load

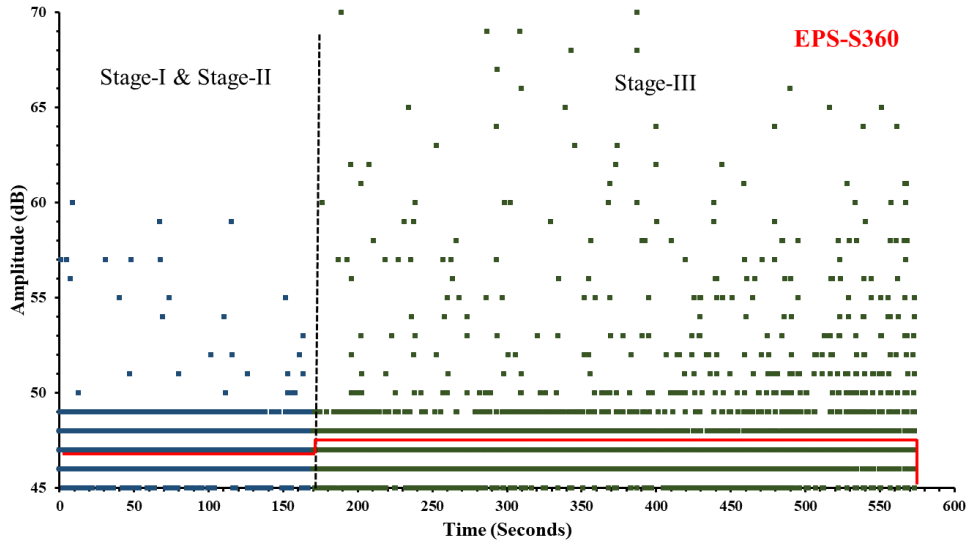

(b) Amplitude vs Time

Figure 5.18 AE plots of sulphate exposed EPS-S360 panel

This phenomenon can be attributed to the increased generation of gypsum resulting from sulphate exposure to the cement, which fills the internal spaces within the panels. This gypsum crystallization process is evidenced by the mass increase observed in Figure 5.3b (Najjar et al. 2017). The formation of gypsum within the air gaps exerts pressure on the mortar's boundary

walls, causing expansion and leading to the formation of internal microcracks. These micro-cracks become active under flexural stress, as demonstrated by the increased AE impacts.

Interestingly, despite the substantial amount of gypsum generated, the amplitude intensity of the AE signals did not significantly differ from that of the control panel. Figures 5.15b and 5.16b illustrate that the amplitudes of EPS-S90 and EPS-S180 remained comparable to the control panel. This indicates that while the presence of gypsum and the associated micro-cracking is more pronounced in sulphate-exposed panels, the severity or intensity of individual cracking events is not markedly different from the control.

Figures 5.17 and 5.18 (EPS-S270 & EPS-S360) further reinforce these observations, showing the AE impacts and amplitudes for panels exposed to sulphate for longer durations. These panels exhibit similar trends, with early micro-cracking but consistent amplitude levels when compared to the control. This consistency in amplitude suggests that the micro-cracks generated by gypsum formation, while more frequent, do not necessarily result in more severe individual cracking events.

The AE data underscores the complex interaction between sulphate exposure and the structural integrity of EPS panels. The increased micro-cracking activity highlights the potential for reduced durability and longevity in sulphate-rich environments, while the consistent amplitude levels suggest that the overall severity of damage may not be as pronounced as the frequency of micro-cracking events might imply. Understanding these dynamics is crucial for assessing the long-term performance and reliability of EPS panels in sulphate-exposed conditions.

The presence of significant interior cracks is indicated by the decreased AE hits and amplitudes (~47 dB) compared to the low flexural strength in EPS-S360 (Figure 5.18a & b). Therefore, it is crucial to closely observe the deterioration caused by sulphate attack before it reaches a point of severe damage. This can be done using a NDT tool such as AE monitoring, which can detect the gradual deterioration caused by both external forces and harsh environmental conditions (such as acid and sulphate). By doing so, timely measures can be taken to address the deterioration of EPS panels.

5.6 CRACK CLASSIFICATION USING RISE ANGLE AND AVERAGE FREQUENCY

Rise angle (RA) and Average Frequency (AF) are analyzed to categorize crack failure mechanisms in specimens, such as tensile and shear cracks. RA is the measure obtained by dividing the rising time by the maximum amplitude, with both measurements expressed in milliseconds per volt. The average frequency is calculated by dividing the counts by the total time span. The tensile cracks are characterized with high average frequency and low-rise angle while the shear cracks are categorized with low average frequency and high-rise angle.

The graphs represent the number of shear and tensile cracks during different stages of flexural testing. The dashed line is employed to distinguish between tensile and shear fractures. The fractures above the line indicate tensile cracks, while those below the diagonal line indicate shear cracks. The cracks established on the line are considered mixed (Figure 5.19- Figure 5.27). The RA vs AF plots provide a reliable indication of the variation in cracking pattern in EPS panels exposed to harsh acidic and sulphate assault conditions. The implementation of RA versus AF plots in AE monitoring can effectively identify crack failure patterns and cracking modes in EPS panels.

The charts comparing rise angle and Average Frequency are segmented into three stages corresponding to the stages used for cumulative hits. The control panel (EPS-00) represents the average plot in Stage I with tensile cracks (Figure 5.19a). The average of the values is marked on the graph, and it can be observed that it lies in the tensile zone. This indicates that during Stage I, the dominant type of cracks occurring in the EPS-00 panel are tensile cracks. In Stage II, a combination of tensile and shear types of cracks is observed, suggesting an equal number of tensile and shear cracks during this duration (Figure 5.19b). This stage highlights a transition period where both types of cracks are equally probable. Stage III categorizes the occurrence of shear cracks, as already formed cracks begin to slide against each other during this stage, making the presence of shear cracks more likely (Figure 5.19c).

Similarly, EPS panels subjected to acid and sulphate were studied using comparable plots. These studies revealed distinct patterns in the occurrence of tensile and shear cracks, providing insight into the material behavior under different environmental conditions. By analyzing these stages, it becomes evident how the mechanical properties of EPS panels are influenced by external factors, such as acidic or sulphate exposure. This comprehensive analysis aids in understanding the structural integrity and durability of EPS panels, contributing valuable information for their application in various field conditions.

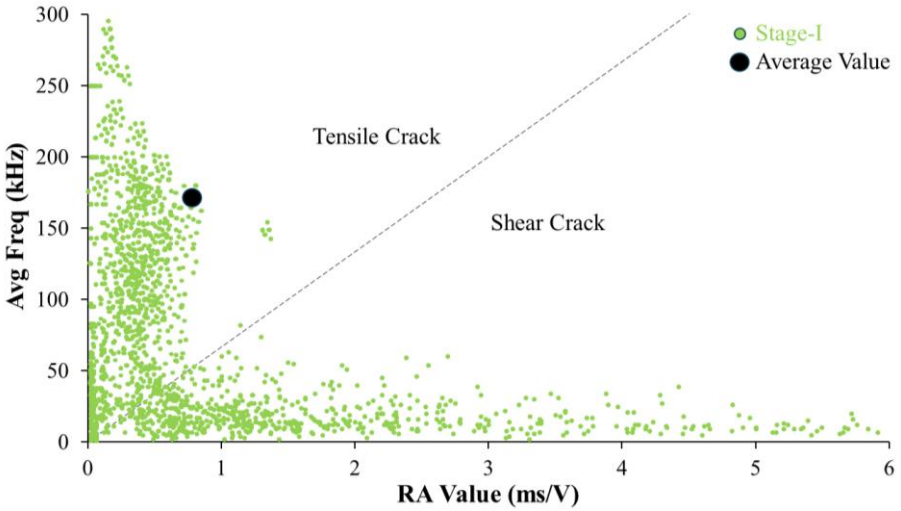

(a) RA vs AF Stage -I (EPS-00)

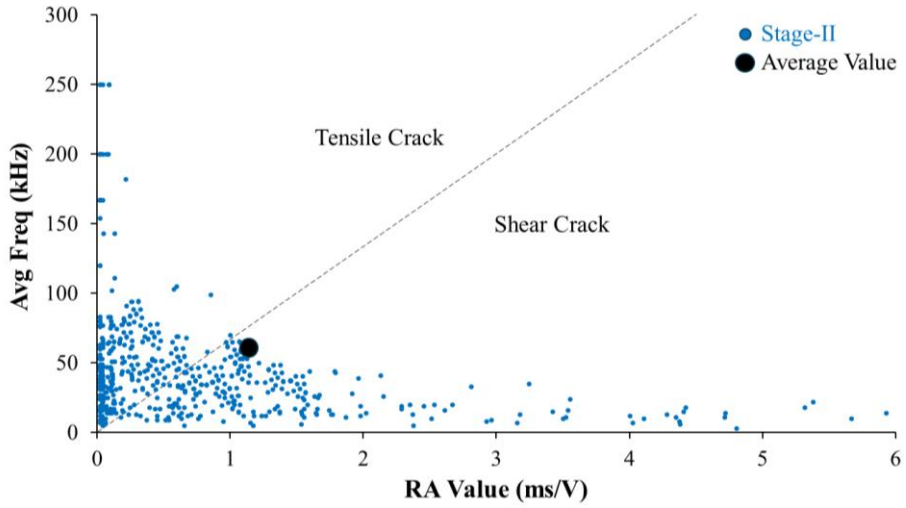

(b) RA vs AF Stage -II (EPS-00)

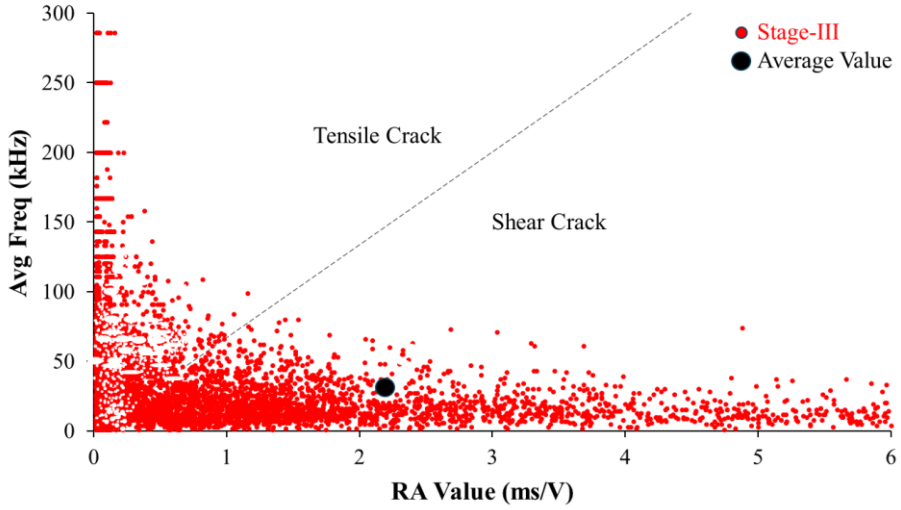

(c) RA vs AF Stage -III (EPS-00)

Figure 5.19 RA vs AF plot during stages in the control panel (EPS-00)

5.6.1 RA vs AF of acid exposed EPS panels

The EPS panels exposed to acid exhibited a transition from tensile cracks to shear cracks during Stage I of exposure. This density of the scatter plot is low due to a lesser number of AE hits during testing as discussed in Section 5.5.1. The shift of values of RA and AF are observed from the plots. The EPS-A07 shows tensile cracks as observed for the control panel during Stage-I though a dip is observed in AF values when the average is compared. In Stage-II mixed cracks are observed. Stage-III shows higher density of the shear cracks (Figure 5.20). The shift of tensile cracks increases to shear cracks in the case of EPS-A14, Stage-I shows average of RA & AF value shifting towards the dividing line (Figure 21). Stage-II & Stage-III didn't show major deviation in plots as compared to its predecessor EPS-A07.

The longer acid exposed EPS panel, EPS-A21 show evident shifting of the tensile cracks to shear cracks from the initial Stage-I. This panel clearly starts showing shear cracks in Stage-II and Stage-III (Figure 22). The extremely acid exposed EPS panel, EPS-A28 was observed in the three stages. The panel shows low tensile cracks and majorly shear cracks from Stage-I itself (Figure 23). This pattern suggests that acid exposure accelerates the transition from tensile to shear cracks, potentially due to the weakening of the material structure by the acid. The cumulative effect of acid exposure leads to a predominance of shear cracks as the stages progress, indicating a significant alteration in the mechanical behavior of the EPS panels. Understanding this transition is crucial for predicting the durability and structural integrity of EPS panels when subjected to acidic environments, thereby guiding better maintenance and application strategies for these materials in construction.

5.6.2 RA vs AF of sulphate exposed EPS panels

Similarly, the EPS panels exposed to sulphate attack are observed using RA and AF plots during the three stages. It is observed that no noticeable difference in crack types is observed up to 180 days of sulphate exposure of EPS panels (Figure 5.24 & 5.25). The testing of EPS-S90 and 180 revealed a higher number of cracks, and the cumulative hits recorded during the testing of the EPS panels confirmed this observation. The RA and AF plots detect the further exposure of EPS panels, and the higher occurrence of shear cracks can be observed during Stage II of testing of EPS panels as compared to the control EPS panel (Figure 5.26). The crack types shifted to shear types from the beginning of Stage I in the EPS-S360 panel (Figure 5.27). The early shifting and detection of shear cracks in RA and AF plots clearly demonstrate the deterioration of the EPS panels.

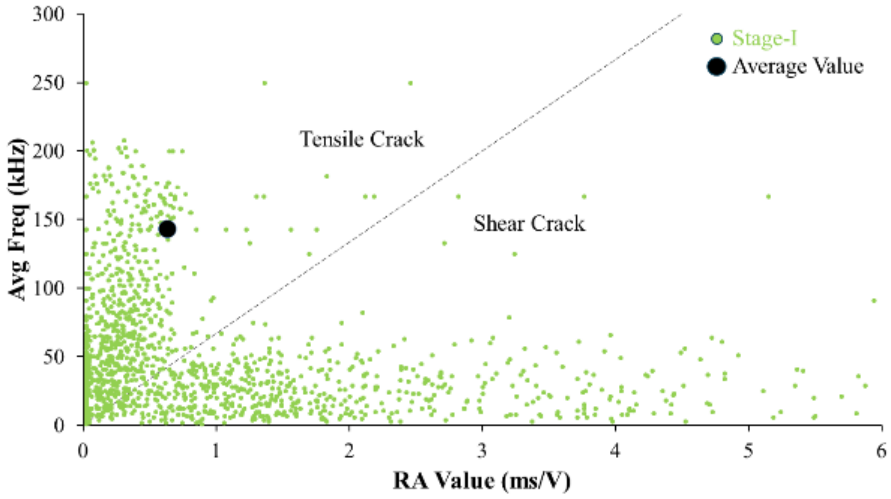

(a) RA vs AF Stage -I (EPS-A07)

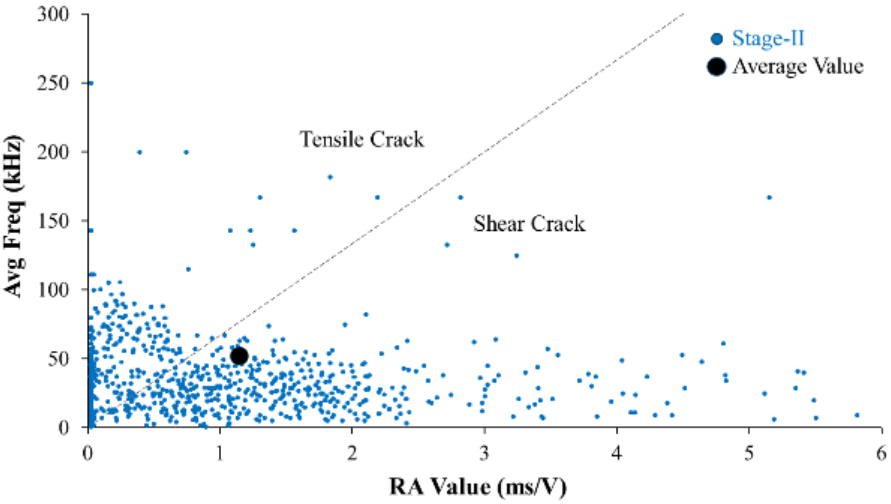

(b) RA vs AF Stage -II (EPS-A07)

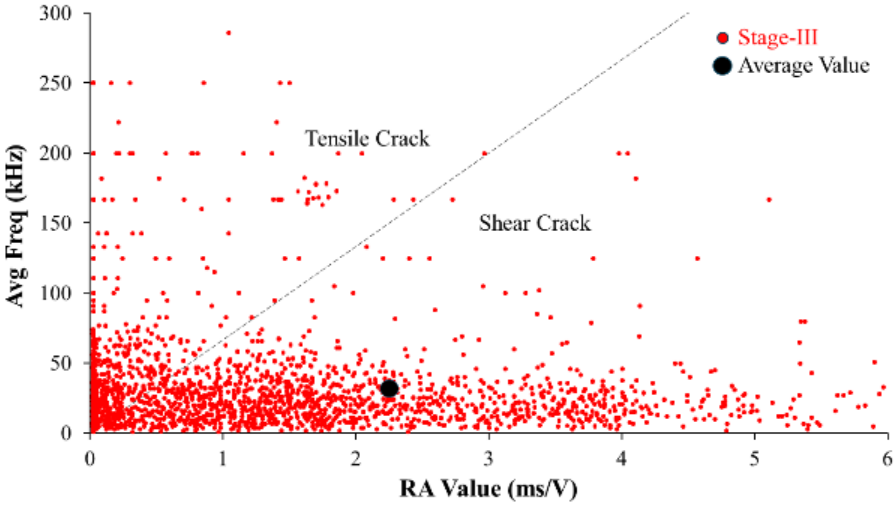

(c) RA vs AF Stage -III (EPS-A07)

Figure 5.20 RA vs AF plot during stages-in the acid exposed EPS-A07

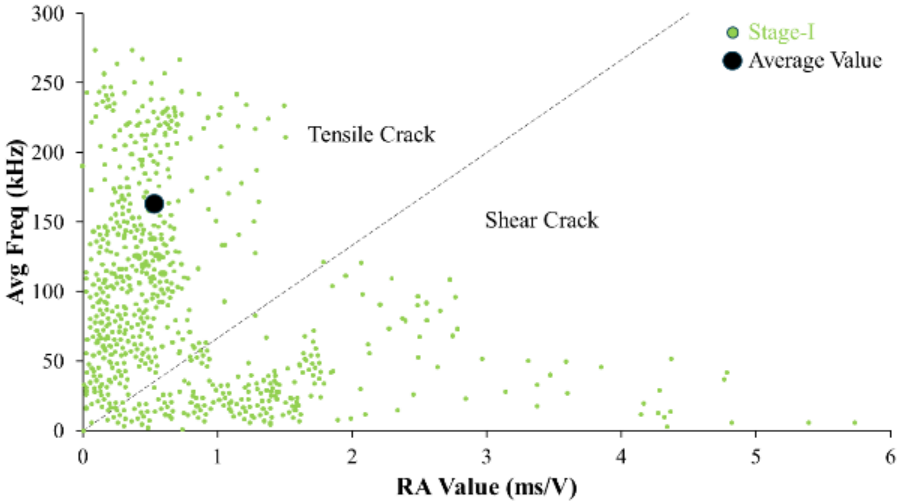

(a) RA vs AF Stage -I (EPS-A14)

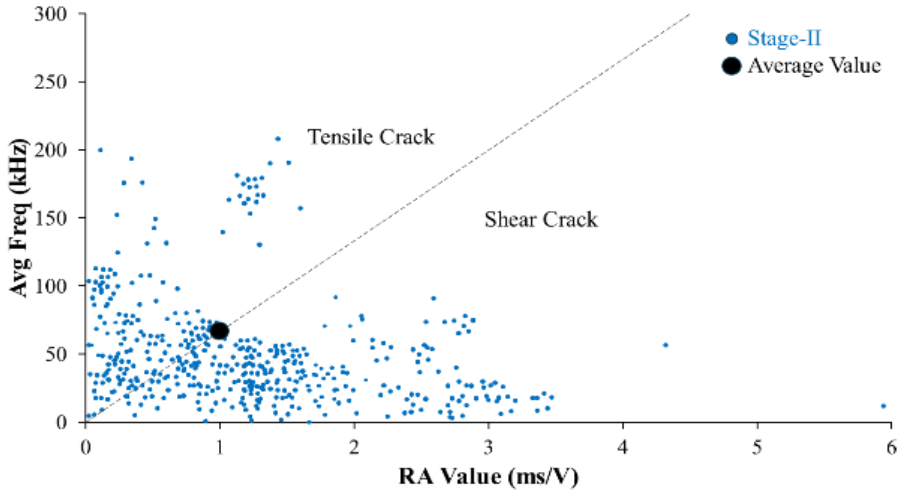

(b) RA vs AF Stage -II (EPS-A14)

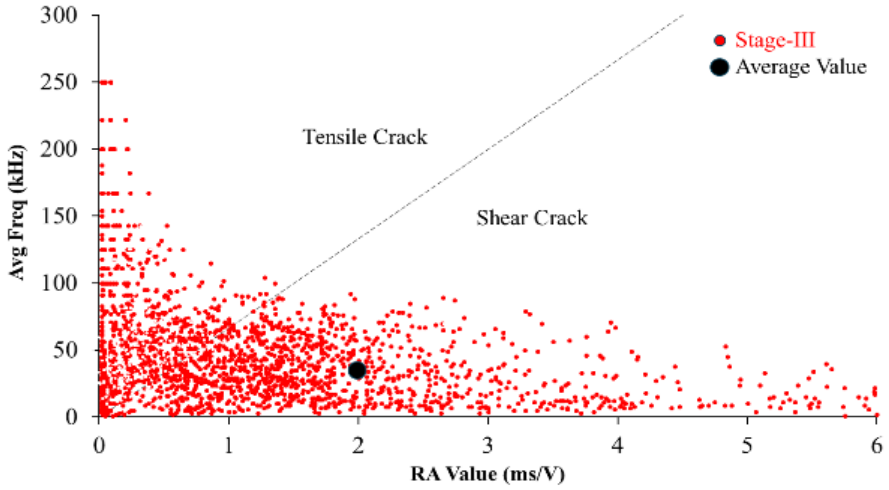

(c) RA vs AF Stage -III (EPS-A14)

Figure 5.21 RA vs AF plot during stages-in the acid exposed EPS-A14

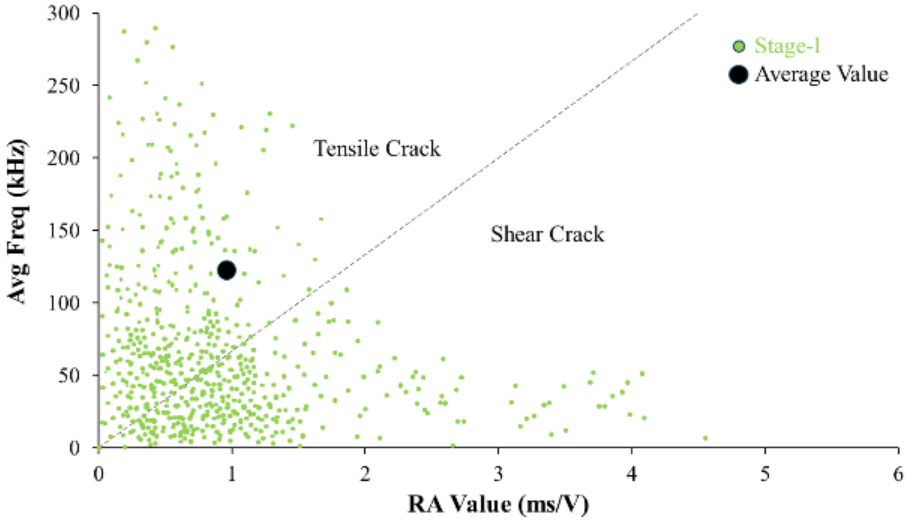

(a) RA vs AF Stage -I (EPS-A21)

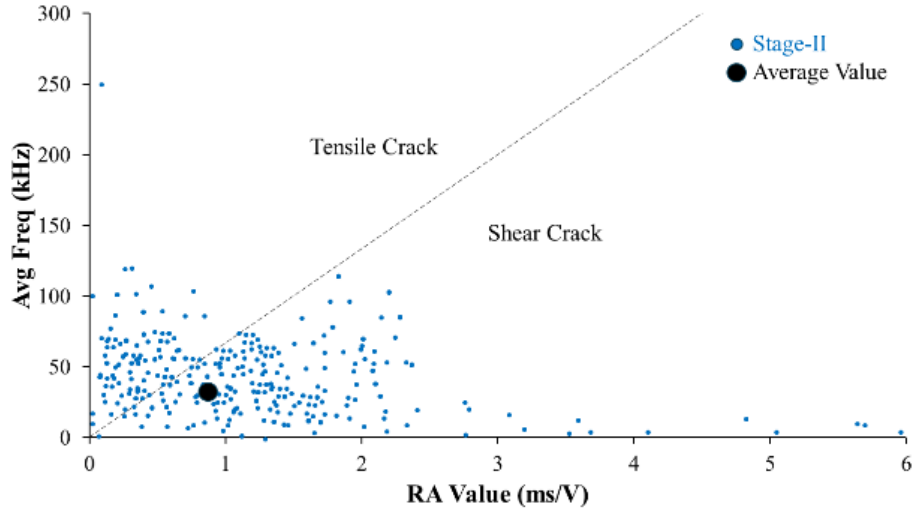

(b) RA vs AF Stage -II (EPS-A21)

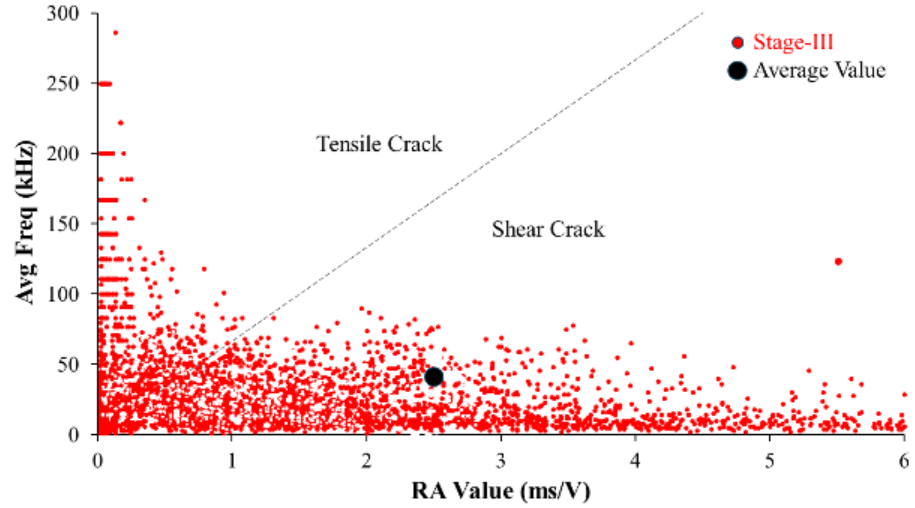

(c) RA vs AF Stage -III (EPS-A21)

Figure 5.22 RA vs AF plot during stages in the acid exposed EPS-A21

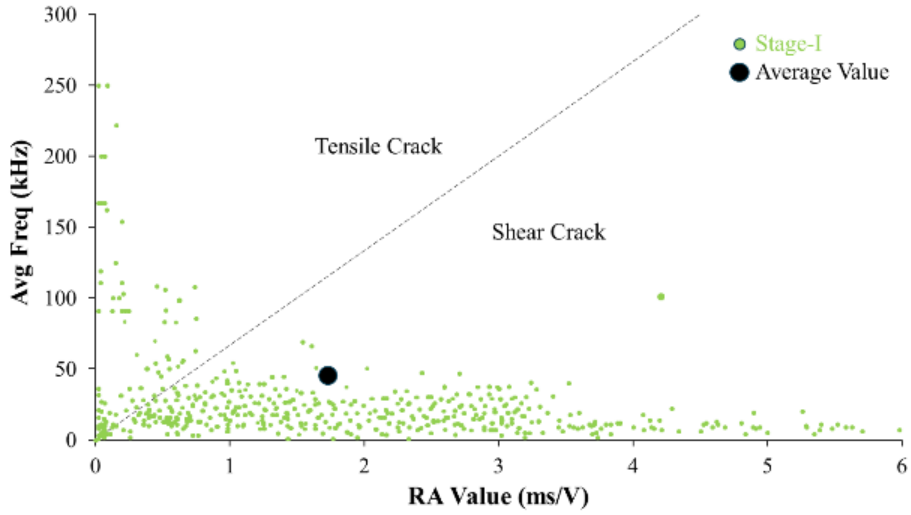

(a) RA vs AF Stage -I (EPS-A28)

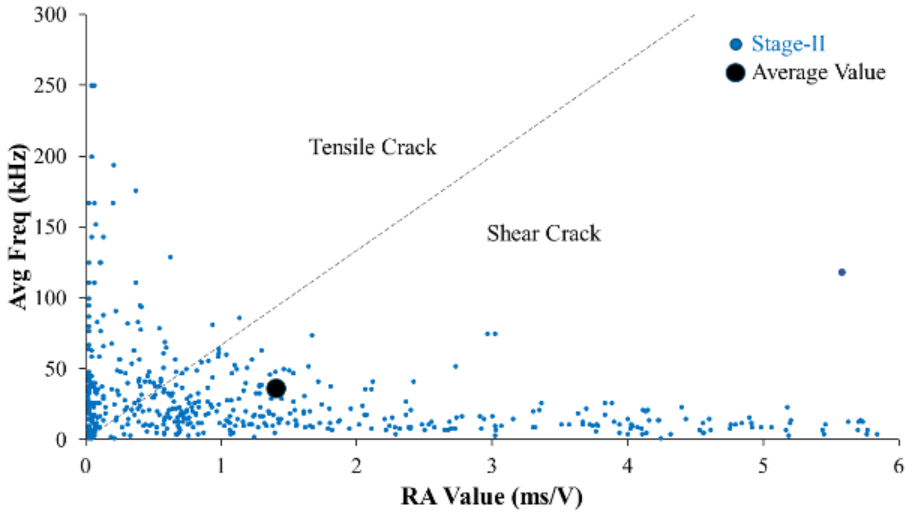

(b) RA vs AF Stage -II (EPS-A28)

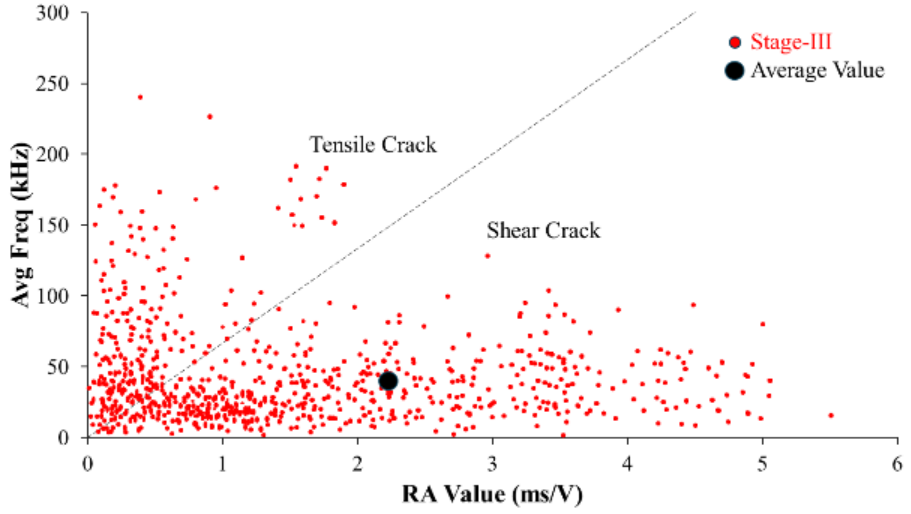

(c) RA vs AF Stage -III (EPS-A28)

Figure 5.23 RA vs AF plot during stages in the acid exposed EPS-A28 panel

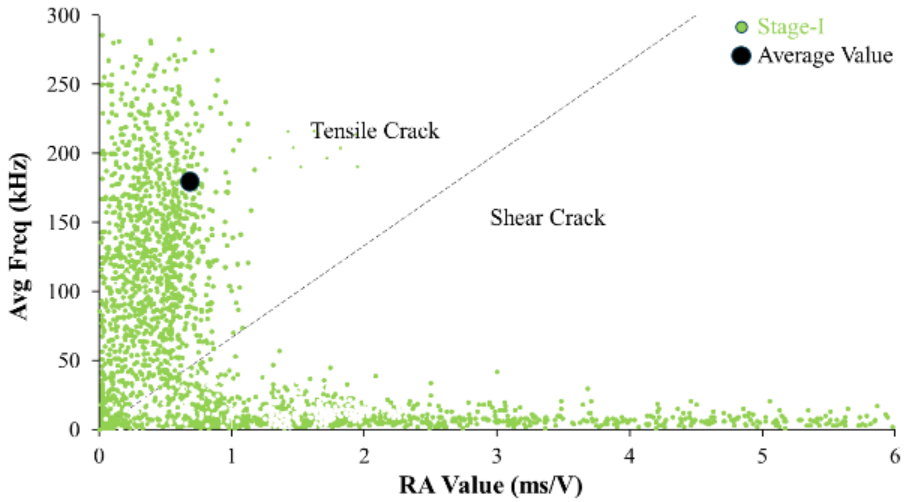

(a) RA vs AF Stage -I (EPS-S90)

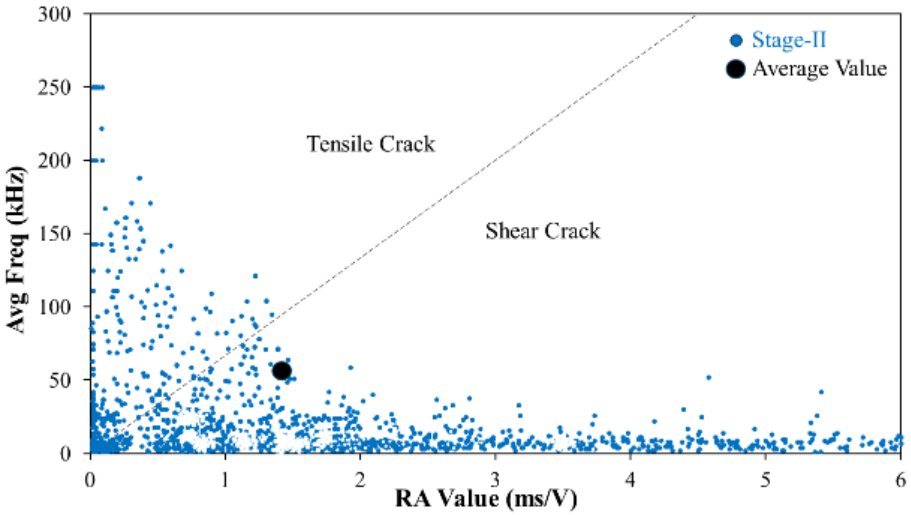

(b) RA vs AF Stage -II (EPS-S90)

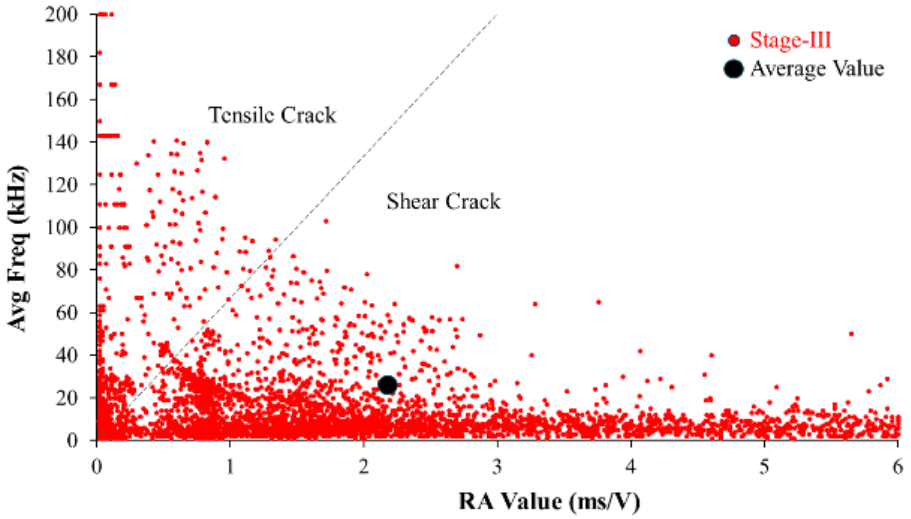

(c) RA vs AF Stage -III (EPS-S90)

Figure 5.24 RA vs AF plot during stages in the sulphate exposed EPS-S90 panel.

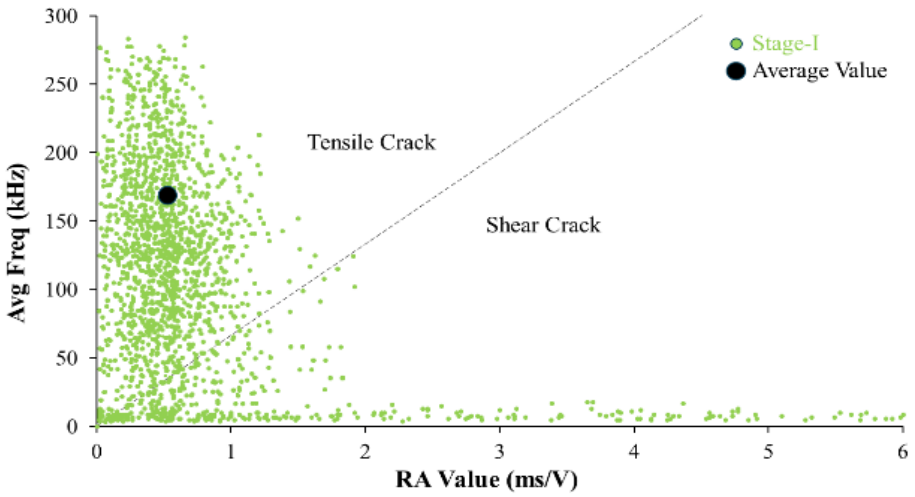

(a) RA vs AF Stage -I (EPS-S180)

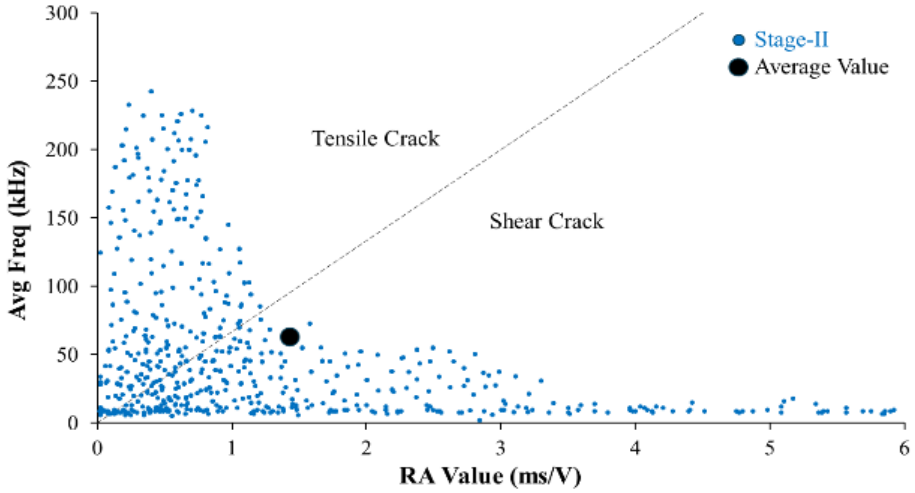

(e) RA vs AF Stage -II (EPS-S180)

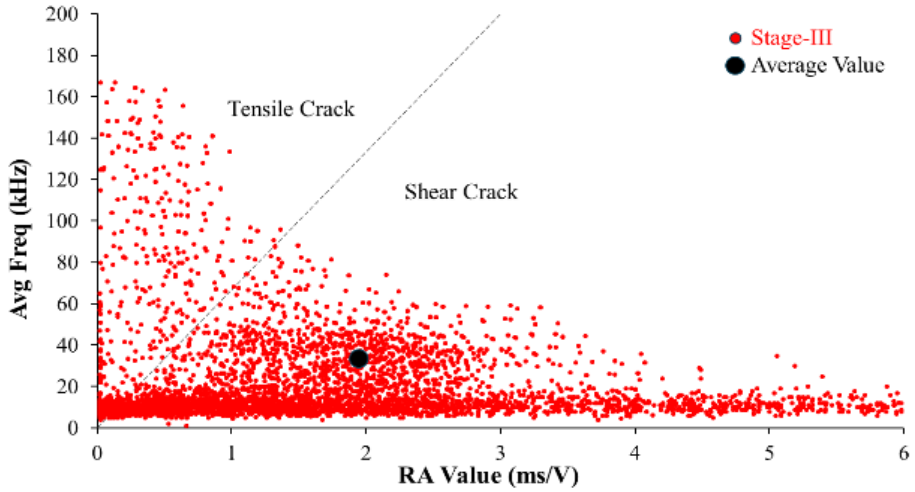

(c) RA vs AF Stage -III (EPS-S180)

Figure 5.25 RA vs AF plot during stages in the sulphate exposed EPS-S180 panel.

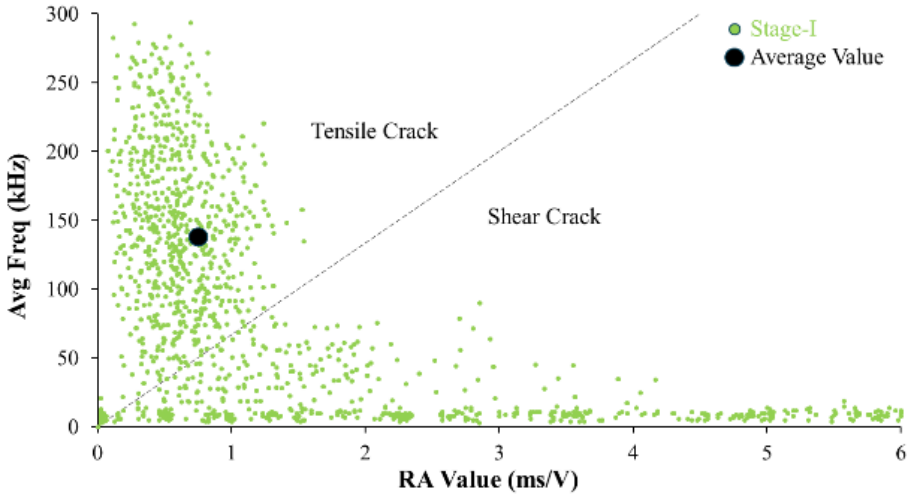

(a) RA vs AF Stage -I (EPS-S270)

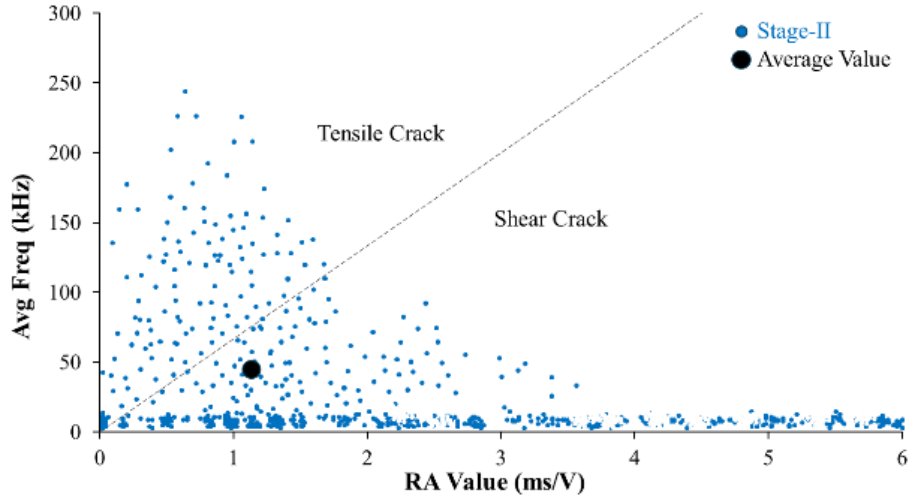

(b) RA vs AF Stage -II (EPS-S270)

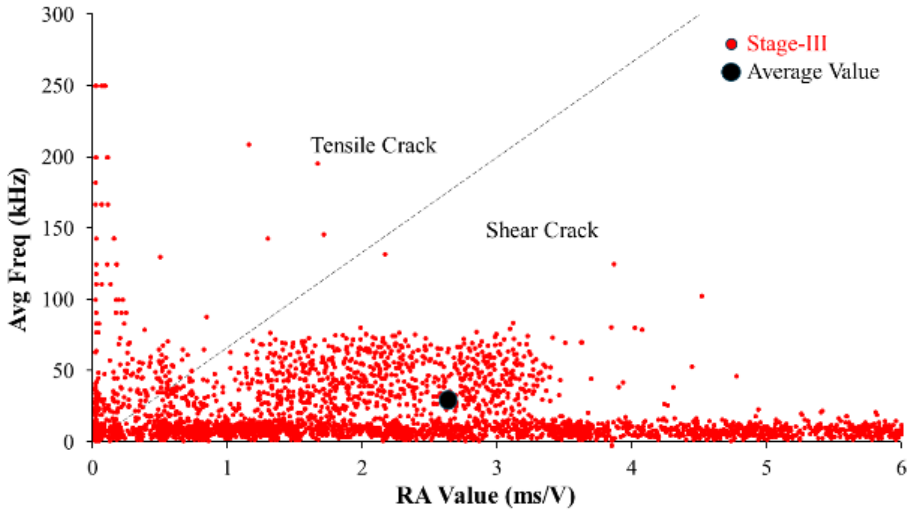

(c) RA vs AF Stage -III (EPS-S270)

Figure 5.26 RA vs AF plot during stages in the sulphate exposed EPS-S270 panel

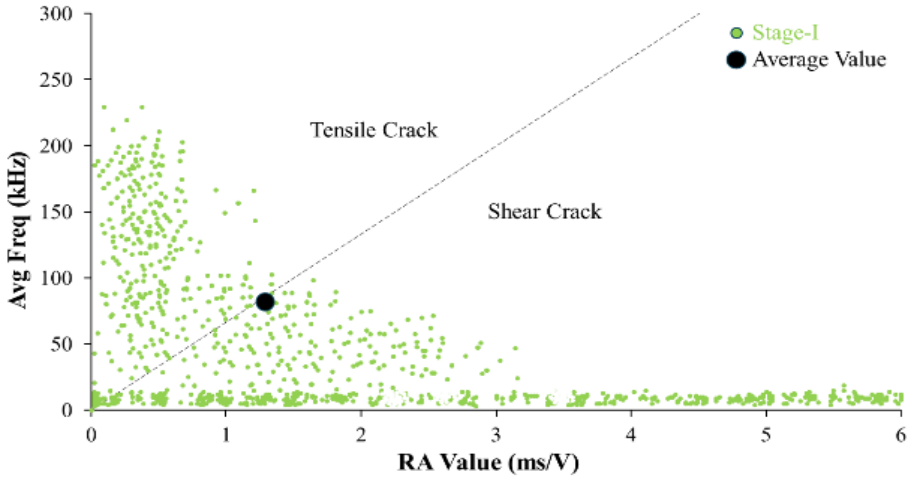

(a) RA vs AF Stage -I (EPS-S360)

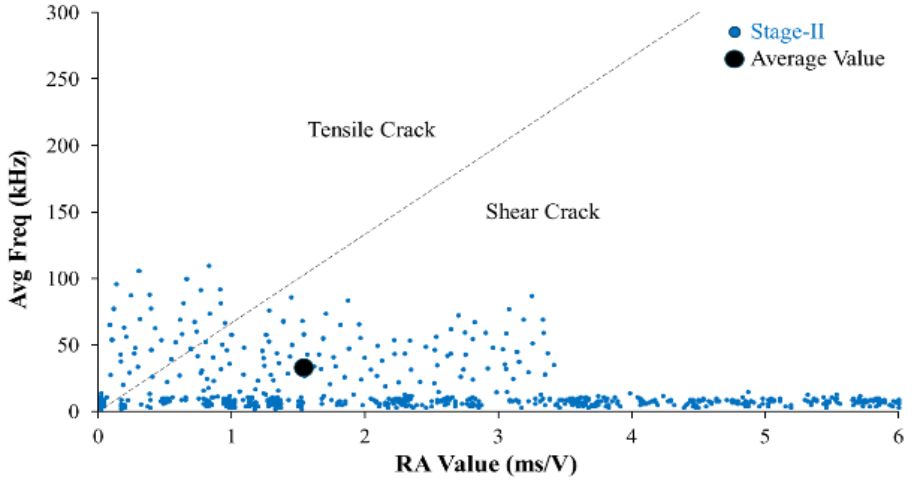

(b) RA vs AF Stage -II (EPS-S360)

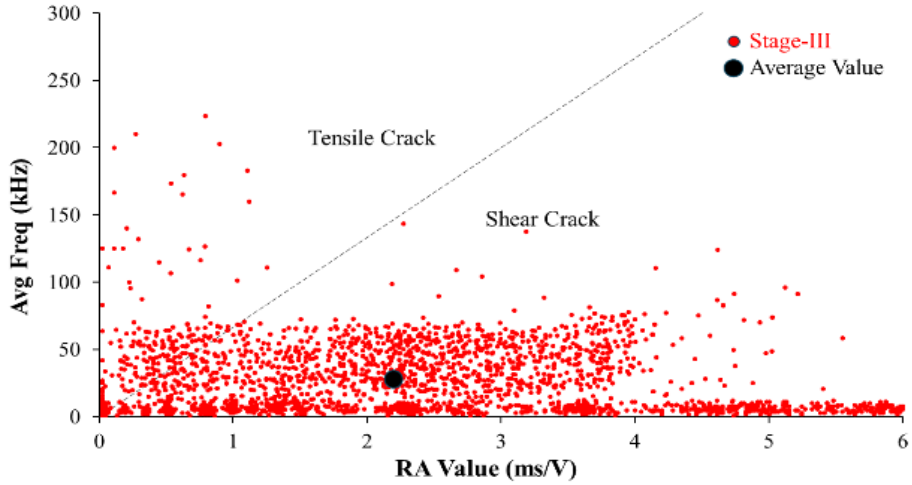

(c) RA vs AF Stage -III (EPS-S360)

Figure 5.27 RA vs AF plot during stages in the sulphate exposed EPS-S360 panel.

5.7 CLOSING REMARKS

This chapter has examined the effects of acid and sulphate exposure on EPS panels using four-point flexural testing. The study's findings emphasize the effectiveness of the AE technique in monitoring the behavior of EPS panels in aggressive environments. Significantly, the exposure to acid caused a substantial reduction in flexural strength, with the most pronounced fall occurring after 28 days, displaying an exponential decline. In addition, the AE effects and amplitudes clearly indicated the degradation of EPS panels from the beginning of the exposure.

The panels saw a significant decrease in the Ductility Factor due to exposure to acid, indicating that the material's flexibility was damaged. However, when exposed to sulphate, the panels initially maintained their strength at a level equivalent to the control panel for 180 days. After this point, a noticeable decrease in strength was noted. The degradation caused by sulphate was confirmed using AE tests, which indicated a rise in the total number of AE hits. This suggests the formation of interior voids because of the accumulation of gypsum.

The shift from tensile to shear cracks, as detected by AE analysis in the EPS panels exposed to both acid and sulphate, highlights the material's gradual degradation under these conditions. The relationship between AE impacts and damage presents a promising opportunity for non-destructive testing of EPS-sandwiched concrete panels, improving our ability to predict and mitigate long-term structural weaknesses. However, while Acoustic Emission (AE) testing is valuable for detecting cracks and faults, it often requires subjective data interpretation. This subjectivity, combined with a lack of standardized criteria for AE data evaluation, may lead to inconsistencies in fault detection and severity categorization.

The findings offer useful insights into the performance and durability of EPS panels in harsh settings, which can lead to enhanced monitoring and maintenance plans for construction materials.

CHAPTER 6

PERFORMANCE OF EPS PANELS UNDER ELEVATED TEMPERATURES

6.1 GENERAL

This chapter presents an experimental investigation on the performance of EPS panels subjected to elevated temperatures and four-point flexural loading. The primary objective is to assess the degradation of these composite panels under combined thermal and mechanical stresses. The parameters of yield load, ultimate load, yield deflection, ultimate deflection, ductility factor (DF), stiffness, and composite action established from flexural loading are used to evaluate the degradation of the EPS panels.

EPS concrete panels are widely used in construction due to their ease of fabrication, cost-effectiveness, and good structural performance under typical loads. However, their behaviour under elevated temperatures raises significant concerns. Numerous studies have investigated heat degradation mechanisms in concrete, showing that elevated temperatures cause significant deterioration in the concrete's microstructure. Ettringite dehydrates and decomposes between 70 and 180 degrees Celsius, and free water in the pores evaporates around 100 degrees Celsius. The differing thermal coefficients of each concrete phase, combined with the decomposition of hydration products, lead to micro-cracks and weakened concrete. Increased internal pores and micro-cracks at elevated temperatures reduce structural safety. Studies have shown that EPS loses its mechanical properties at high temperatures, exhibiting significant reductions in compression, shear, and flexural strength. This degradation can range from 38% to 50%, potentially leading to premature failures in panels exposed to fire or extreme heat conditions (Ede and Ogundiran 2014, Choi et al. 2019b, Tahir and Hamed 2021).

Beyond evaluating the performance of EPS panels under elevated temperatures, this chapter explores the utilization of a non-destructive testing (NDT) tool to monitor their degradation before critical structural damage occurs. Acoustic Emission (AE) has proven to be an effective technique for assessing damage and deterioration in various structures. This study will investigate the potential of AE for monitoring heat-exposed EPS panels by analyzing specific AE wave parameters like hits, amplitude, duration, average frequency (AF), rise angle (RA), and cumulative signal strength (CSS).

6.2 THERMAL BEHAVIOUR OF EPS PANELS

This section explores the thermal response of EPS panels used. Here, we investigate the impact of elevated temperatures on the physical characteristics of low-density EPS (15 kg/m³) commonly employed for insulation purposes.

6.2.1 Observation of EPS panel at elevated temperature

Prior to subjecting the cast EPS panels to combined thermal and mechanical loading, a preliminary investigation was conducted to understand the standalone behavior of the EPS skeleton under elevated temperatures. This involved visually inspecting the EPS skeleton (without the concrete wythes) within a hot-air oven. The EPS skeleton was initially exposed to a temperature of 50°C for 15 minutes. This initial exposure did not produce any noticeable changes to the EPS or the shear connectors, as illustrated in Figure 6.1a. Subsequently, the temperature was increased to 100°C using the same procedure. This significant temperature rise resulted in substantial shrinkage of the EPS, as evident in Figure 6.1b. The individual EPS beads were observed to shrink and stretch around the shear connectors. Manufacturer specifications for the EPS material indicated a glass transition temperature of approximately 120°C. Based on this information, the EPS skeleton was further exposed to this specific temperature for 15 minutes. This exposure caused a more pronounced shrinkage effect, causing the EPS to consolidate towards the center of the sample (Figure 6.1c). This visual observation suggests a transition in the material's physical state, potentially accompanied by the bursting of EPS beads and the thermoplastic stretching of the polystyrene material. Notably, the EPS volume decreased with increasing temperature, leading to a corresponding increase in density. Additionally, a color change from light to dark was observed, further indicating a transformation within the material. It is important to note that further exposure to even higher temperatures was not conducted within the scope of this study.

In contrast to the clear visual changes observed in the isolated EPS skeleton, no apparent alterations were detected in the cast EPS panels exposed to elevated temperatures. The panels underwent a three-hour exposure regime at varying temperatures, including 50°C, 100°C, 150°C, and 200°C. The internal changes may include micro-cracking and alterations in material properties, which cannot be reliably detected through visual inspection alone.

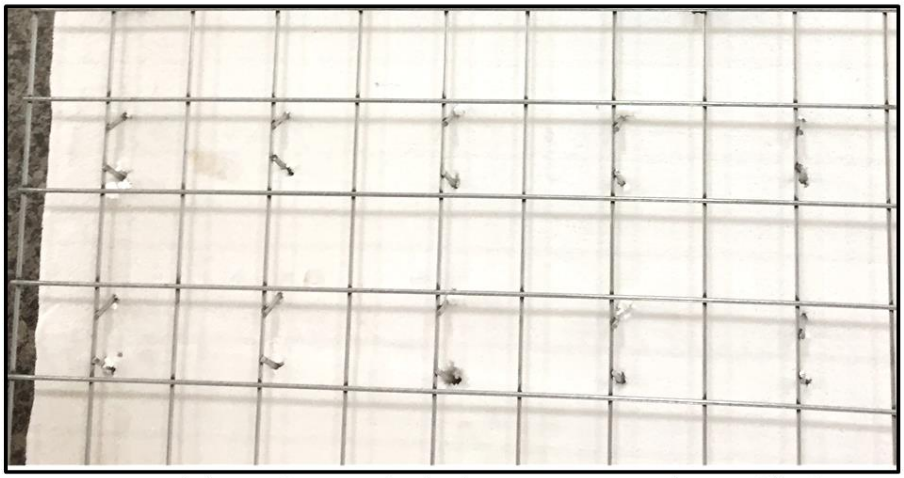

(a) EPS panel skeleton exposed to 50^0 C

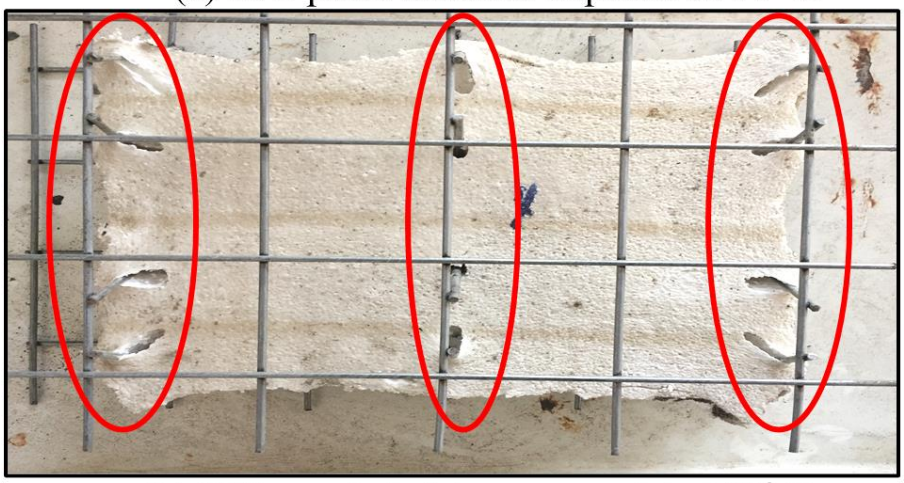

(b) EPS panel skeleton exposed to 100^0 C

(c) EPS panel skeleton exposed to 120^0 C

Figure 6.1 Exposure of EPS skeleton to elevated temperature

The implementation of NDT techniques for EPS concrete panels exposed to high temperatures plays a critical role in ensuring their long-term performance and safety. NDT methods enable the early detection of potential issues within the EPS core, facilitating timely

maintenance and repair interventions. This proactive approach contributes to maintaining the structural integrity of the panels, preventing catastrophic failures, and extending their service life. As such, NDT techniques become highly valuable tools for structural health monitoring of EPS concrete panels subjected to extreme thermal conditions.

6.2.2 Visual observations of elevated temperature exposed EPS panels

The EPS panels were tested under flexure after exposure to designed temperatures. The visuals of failures are shown in Figure 6.2. It is observed that the EPS panels exposed to temperatures up to 100^0 C show similar failure as of control panel. These panels developed cracks in the lower wythe of the EPS panel. A crack developed between the points of loading, and it was observed that the increased loading caused minor cracks near the edges of the lower wythe (Figure 6.2a & b). These panels ultimately failed with the expansion of middle crack in the lower wythe. The top wythe didn't show any signs of crack till failure.

The EPS panel exposed to temperature of 150^0C showed numerous cracks on the lower wythe during initial stage of loading. The increment of loads resulted in cracks under the support and near the edges. The horizontal crack was visible near the middle of the EPS panel's thickness, which did not appear in the control panels. The EPS-H150 developed an inclined cracks originating from top wythe and extending towards the support (Figure 6.2c). The panel ultimately failed by splitting along the crack under the support.

The EPS panel exposed to 200^0 C temperature, EPS-H200, when tested under flexure showed numerous cracks as observed in EPS-H150. The horizontal crack was observed near the interface in this panel. The panel developed cracks near the support on top wythe before ultimately failing (Figure 6.2d). The EPS-H200 ultimately failed by splitting already occurred cracks below the loading point.

The behavior of EPS-H150 and EPS-H200 was observed to be different during four-point flexural loading tests. The EPS-H150 panel was broken to examine the internal structure (Figure 6.3). It was found that the EPS insulation inside the panel was completely vandalized. The EPS beads were burst and the shrunken material adhered to the outer concrete surfaces. The shear connectors were bent in many locations inside the EPS panels. The horizontal cracks observed in EPS-H150 and EPS-H200 may result from the absence of sandwiched insulation in the panel, leading to less load sharing between the wythes.

(a) EPS-H50

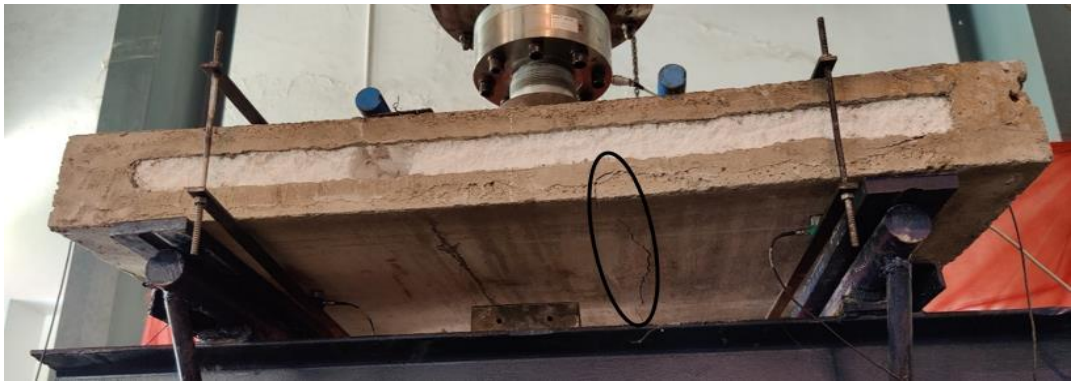

(b) EPS-H100

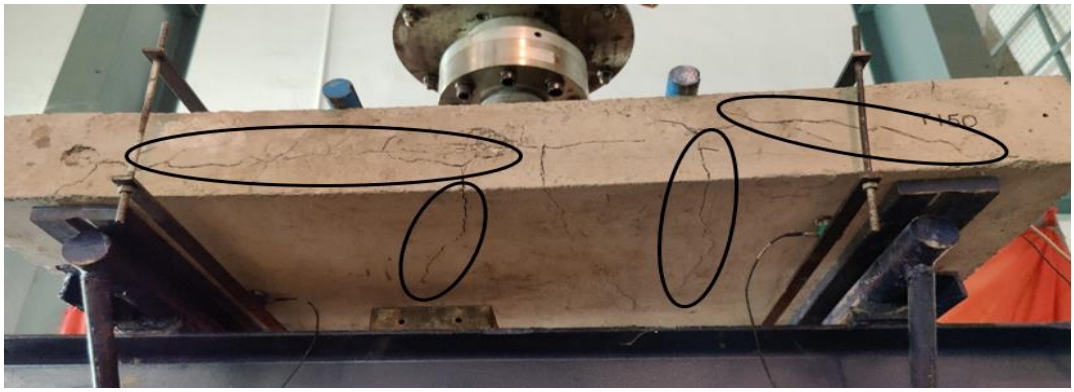

(c) EPS-H150

(d) EPS-H200

Figure 6.2 Visuals of flexural tested EPS panels exposed to elevated temperatures

Figure 6.3 Internal views of EPS-H150

6.3 FLEXURAL BEHAVIOUR OF EPS PANELS SUBJECVTED TO ELEVATED TEMPERATURES

This section analyzes the flexural behavior of EPS concrete panels subjected to elevated temperatures using the data obtained from four-point flexural loading tests. The key focus lies on interpreting the load-deflection curves for both control and heat-exposed specimens.

6.3.1 Load deflection response of control panel

The control EPS panel exhibited a characteristic load-deflection response during the flexural loading test. As illustrated in Figure 6.4, the initial portion of the curve represents the elastic phase. A distinct bend in the curve marks the formation of the first flexural crack at a load of 5.9 kN, appearing between the loading points on the bottom concrete wythe. Up to this point (19.5 kN and 0.7 mm deflection), the panel's behavior remained proportional, signifying a linear elastic response. Notably, no shear cracks were observed throughout the elastic phase. Beyond the elastic limit, the load-deflection curve exhibits a change in slope, indicating the transition to the plastic phase. This phase is characterized by increased load causing the formation of shear cracks near the supports and additional flexural cracks (Figure 6.4). The observed cracking can be attributed to the limitations of the welded shear connectors in effectively distributing the load across the concrete wythes. Ultimately, the panel experienced a sudden failure at a peak load of 35.95 kN and a corresponding deflection of 5.21 mm.

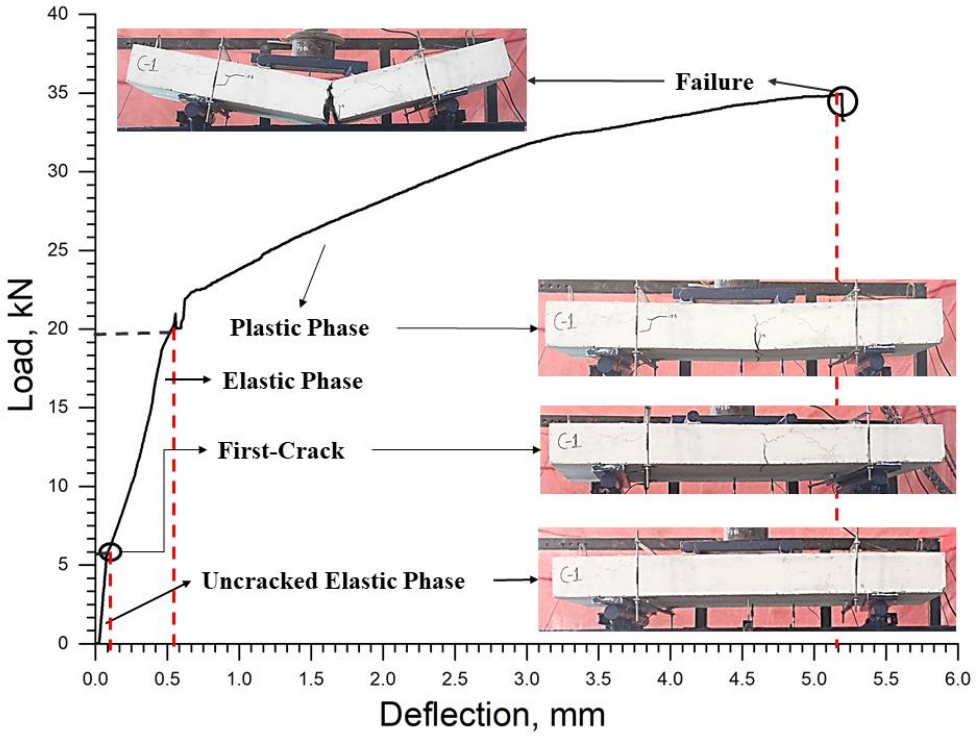

Figure 6.4 Load deflection curve of control EPS sandwiched concrete panels

6.3.2 Performance of Heat Exposed EPS Panels

Similar flexural loading tests were conducted on heat-exposed EPS panels (EPS-H50, EPS-H100, EPS-H150, and EPS-H200). Their load-deflection curves were then compared with the control specimen (Figure 6.5). Interestingly, the yield load of the EPS-H50 and EPS-H100 panels increased by 8.2% and 3.79%, respectively. The behavior can be attributed to the

removal of capillary water from the mortar, which leads to a denser microstructure (Tongaroonsri and Tangtermsirikul 2008). However, the ultimate load-bearing capacity of EPS-H50 only showed a marginal increase of 1.8%.

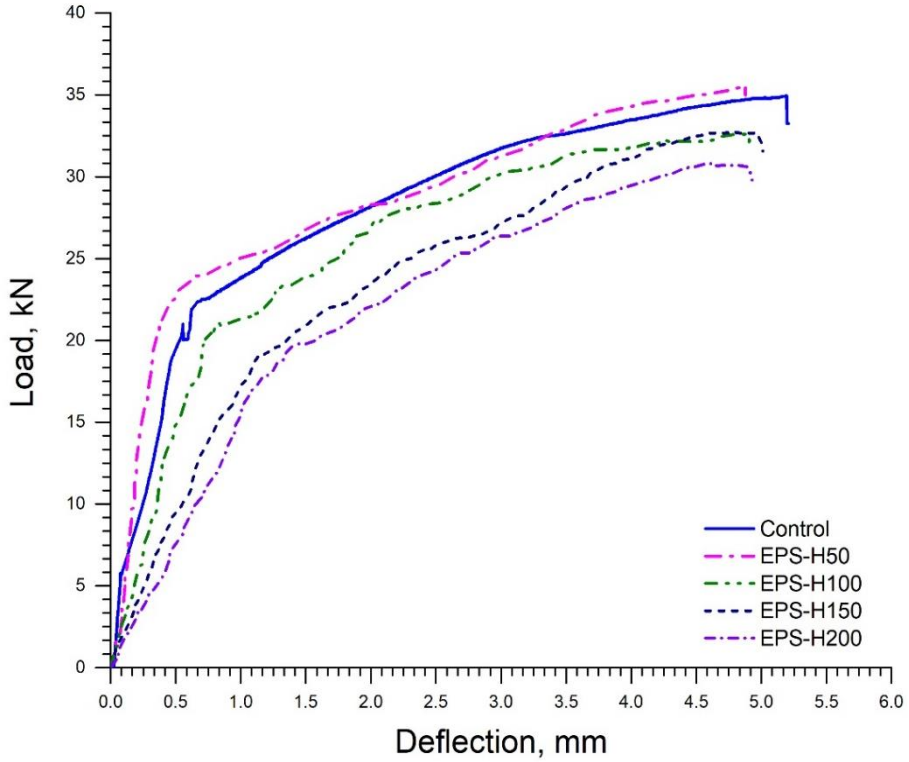

Figure 6.5 Load-deflection curve of control and temperature exposed EPS sandwiched concrete panels

A contrasting trend was observed for yield deflection. The yield deflection of EPS-H100, EPS-H150, and EPS-H200 panels increased by 10.14%, 61.71%, and 65.71%, respectively, compared to the control panel. Despite these increases, both the ultimate deflection and ultimate load capacity decreased for all heat-exposed panels except EPS-H50 (refer to Table 6.1). This decrease can be attributed to the decomposition of hydration products in the mortar exceeding 80°C, leading to micro-crack formation and a weakened bond with the wire mesh. Consequently, the ductility factor of EPS-H100, EPS-H150, and EPS-H200 panels decreased by 14.51%, 40.59%, and 46.10%, respectively.

In conclusion, the analysis of load-deflection curves reveals that exposure to temperatures up to 50°C does not significantly impact the performance of EPS panels. However, higher temperatures (up to 200°C) demonstrate a detrimental effect on their overall performance, particularly in terms of ductility, deflection capacity, and load-bearing capability.

Table 6.1 Various parameters under flexural loading

Panel Designation	**Yield Load, P_y (kN)**	**Ultimate Load, P_u (kN)**	**Yield Deflection, Δ_y (mm)**	**Ultimate Deflection, Δ_u (mm)**	**Ductility Factor, (DF = Δ_u/Δ_y)**	**Ultimate Energy E_u (kN.mm)**
Control	19.5	34.95	0.7	5.21	7.44	146.58
EPS-H50	21.11	35.58	0.5	4.88	9.76	138.5
EPS-H100	20.24	32.6	0.771	4.91	6.36	125.95
EPS-H150	18.97	32.78	1.132	5.01	4.42	117.43
EPS-H200	17.67	30.6	1.16	4.656	4.01	107.44

6.3.3 Stiffness and energy dissipation of heat exposed EPS panels

Table 6.2 presents the changes observed in yield stiffness, secant stiffness, and energy dissipation of EPS panels after exposure to elevated temperatures, while secant stiffness is determined by the peak load divided by the ultimate deflection (Bastin and Sharma 2017).

Table 6.2 Stiffness of the EPS panels and energy dissipation

Panel Designation	Yield Stiffness (kN/mm)	Secant Stiffness (kN/mm)	Energy Dissipation E_u (kN.mm)
Control	27.85	6.70	146.58
EPS-H50	42.22	7.29	138.5
EPS-H100	26.25	6.63	125.95
EPS-H150	16.75	6.54	117.43
EPS-H200	15.23	6.57	107.44

Compared to the control panel, EPS-H50 exhibited both higher yield stiffness and secant stiffness. Conversely, EPS-H150 and EPS-H200 displayed significant reductions in yield stiffness, reaching 39% and 45% declines, respectively. No substantial losses were observed in secant stiffness across the heat-exposed panels. The decrease in yield stiffness can be attributed to the reduced capacity for shear transfer. This reduction is likely caused by the differential melting of the sandwiched EPS insulation (Section 6.2.1). Furthermore, as discussed in Section 6.2.2, shrinkage of the EPS insulation above 100°C contributes to increased spacing between the wythes and insulation, further impacting yield stiffness. Energy dissipation, quantified by

the area under the load-deflection curve, reflects the material's plasticity. Heat-exposed EPS panels exhibited energy dissipation capacity losses of 5.51%, 14.07%, 19.88%, and 26% for EPS-H50, EPS-H100, EPS-H150, and EPS-H200, respectively, compared to the control panel. This reduction underscores the decreased ability of the panels to absorb energy and indicates compromised structural integrity post-exposure to elevated temperatures

In summary, the stiffness properties and energy dissipation of EPS panels are significantly affected by exposure to elevated temperatures, particularly above 150°C. This exposure leads to increased micro-cracking, reduced load-bearing capacity, and altered material properties, which collectively undermine the structural robustness and performance of the panels under extreme thermal conditions. These findings highlight the critical need for incorporating tools to detect early damage due to thermal exposure. Ensuring that these panels remain structurally fit without significant degradation for safety, and long-term performance in various construction and engineering applications.

6.4 DEGREE OF COMPOSITE ACTION

This section explores the concept of composite action in EPS concrete sandwich panels and its impact on their structural performance. It analyzes how exposure to elevated temperatures affects the degree of composite action within these panels.

Sandwich panels, such as those utilizing EPS insulation, exhibit unique behavior due to the varying materials employed throughout their thickness. These panels typically comprise two outer concrete wythes (layers) with EPS insulation sandwiched between them. The transfer of loads across the panel occurs through a combination of the EPS core and truss-shaped shear connectors embedded within the concrete. The degree of composite action serves as a metric to categorize these panels based on their load transfer capabilities. Fully composite panels behave essentially as a single structural unit, achieving complete lateral shear transfer. Conversely, non-composite panels exhibit separate bending profiles and limited load sharing under flexural loading.

6.4.1 Evaluation of composite action

. The composite action of the EPS concrete panels in this study was assessed using Equation 6.1, developed by (Pessiki and Mlynarczyk 2003). This equation leverages the measured deflection (δ) observed during the elastic behavior of the panels to determine their experimental moment of inertia (Iexp). This value is then compared to the theoretical moment

of inertia for both fully composite (Ic) and non-composite (Inc) scenarios, as presented in Table 6.3. The flexural rigidity (EIexp) for the four-point flexural loading tests was calculated using Equation 6.2. Table 6.4 summarizes the composite action of both the control and heat-exposed EPS panels. The analysis revealed that all panels exhibited partially composite behavior. While EPS-H50 showed a slight increase in composite action compared to the control panel, EPS-H150 and EPS-H200 displayed significant reductions of 47.55% and 54.04%, respectively. This indicates that exposure to elevated temperatures has a detrimental effect on the composite action of EPS concrete panels.

$$k\% = \frac{I_{exp} - I_{nc}}{I_c - I_{nc}} \quad \text{.....6.1}$$

$$EI_{exp} = \frac{23\,PL^3}{648\,\delta} \quad \text{.....6.2}$$

Table 6.3 Moment of Inertia calculation for composite and non-composite EPS panels

Non-Composite Panel		**Fully composite panel**	
M.O.I Top Wythe, I_{nc1}	3200000 mm^4	Area of composite panel, A	48000 mm^2
M.O.I Bottom Wythe, I_{nc2}	3200000 mm^4		
M.O.I of non-composite panel, $I_{nc} = I_{nc1} + I_{nc2}$	6.4×10^6 mm^4	M.O.I of composite Panel, I_c	10.36×10^7 mm^4

Table 6.4 Composite action of EPS panels

Panel Designation	**Flexural Rigidity, EI_{exp} (Nmm^2)**	**Experimental Moment of Inertia, I_{exp} (mm^4)**	**Degree of composite action, k_1 (%)**
Control	9.88	3.95	34.11
EPS-H50	10.49	5.99	55.08
EPS-H100	9.31	3.72	31.76
EPS-H150	5.94	2.37	17.89
EPS-H200	5.41	2.16	15.67

The observed reduction in composite action for heat-exposed panels can be attributed to several factors: As discussed in Section 6.2, EPS insulation experiences shrinkage at elevated

temperatures. This shrinkage can disrupt the effective bonding between the EPS core and the concrete wythes, hindering load transfer. High temperatures can induce micro-cracking within the concrete wythes. These cracks compromise the structural integrity of the concrete and its ability to act compositely with the EPS core. The elevated temperatures can also weaken or damage the shear connectors embedded within the concrete. This deterioration reduces their effectiveness in transferring shear forces between the wythes, thereby diminishing the composite action of the panel.

In conclusion, the degree of composite action plays a crucial role in the structural performance of EPS concrete panels. This study demonstrates that exposure to elevated temperatures can significantly reduce the composite action of these panels, potentially leading to performance degradation under flexural loads.

6.5 PASSIVE ACOUSTIC EMISSION MONITORING FOR DAMAGE DETECTION

This section explores the utilization of Passive Acoustic Emission (AE) monitoring as a tool for detecting damage in EPS concrete panels subjected to elevated temperatures. Here, we investigate the effectiveness of specific AE parameters in identifying damage progression within the panels.

Passive AE monitoring has emerged as a valuable technique for detecting damage initiation and progression within composite structures like EPS concrete panels. This technique relies on analysing stress waves emitted by the material during various damage mechanisms, such as micro-cracking and crack propagation. Several key AE parameters provide valuable insights into the health of the material: Cumulative AE hits quantify the total number of AE events recorded during the test. An increase in cumulative hits typically signifies intensifying damage activity within the material. Cumulative signal strength represents the total energy released during the AE events. Increasing cumulative signal strength suggests a more significant damage process similar to cumulative hits. The amplitude of each AE event reflects the intensity of the released energy. Higher amplitude values generally indicate more severe damage events, such as larger cracks. The rise angle measures the steepness of the initial rise in the AE waveform, potentially providing insights into the emission source. The frequency content of the AE signal can offer clues about the type of damage mechanism occurring within the material.

Figure 6.6 is worked to consolidate the AE hits line graph and amplitudes scatter plots with refence to time. In the control EPS panel (not exposed to elevated temperatures), the cumulative AE hits increased proportionally with the applied load. This behavior mirrored the changes observed in the load-deflection curve, suggesting a consistent correlation between the level of stress and the number of AE events. Additionally, scatter plots were generated to depict the relationship between AE amplitude and time. These plots revealed a gradual increase in amplitude with increasing load, potentially indicating a corresponding rise in crack intensity within the panel.

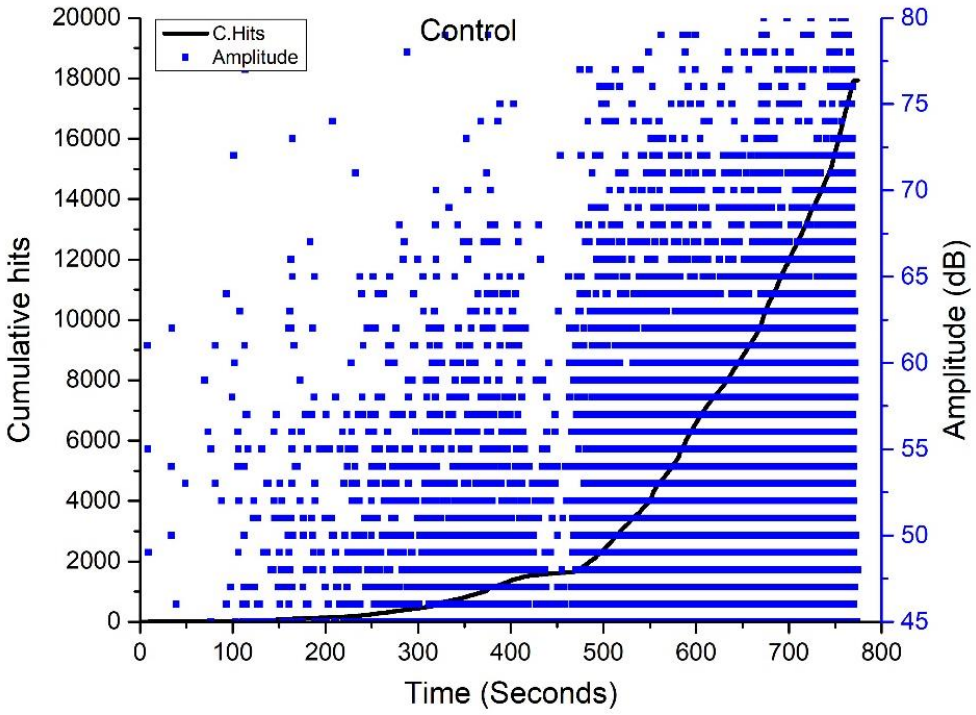

Figure 6.6 Cumulative hits-amplitude vs time plots of control panel

6.5.1 Impact of heat exposure on AE signature

Comparative analysis of AE data from heat-exposed EPS panels with the control panel utilized similar graphical representations. The plots for the EPS-H50 panel (exposed to 50°C) exhibited no significant deviations from the control panel (Figure 6.7a), suggesting minimal damage at this moderate temperature. However, panels exposed to higher temperatures (100°C and above) displayed distinct changes in their AE signatures (Figures 6.7b and 6.7 c & d).

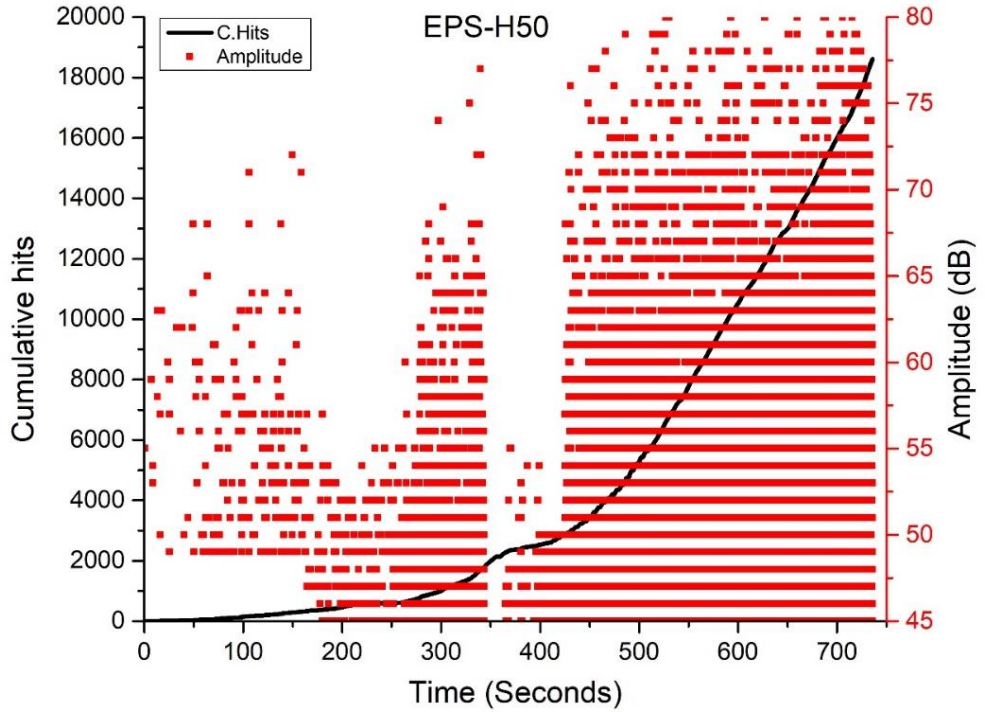

(a) EPS-H50

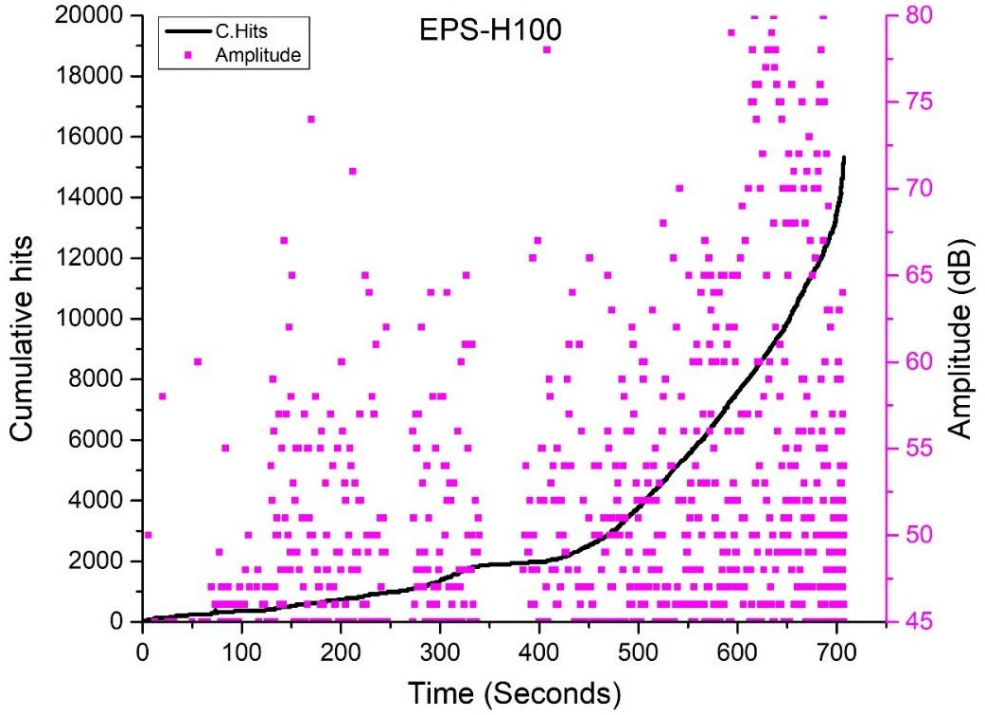

(b) EPS-H100

Figure 7 Cumulative hits-amplitude vs time plots heat exposed EPS panels (Cont.)

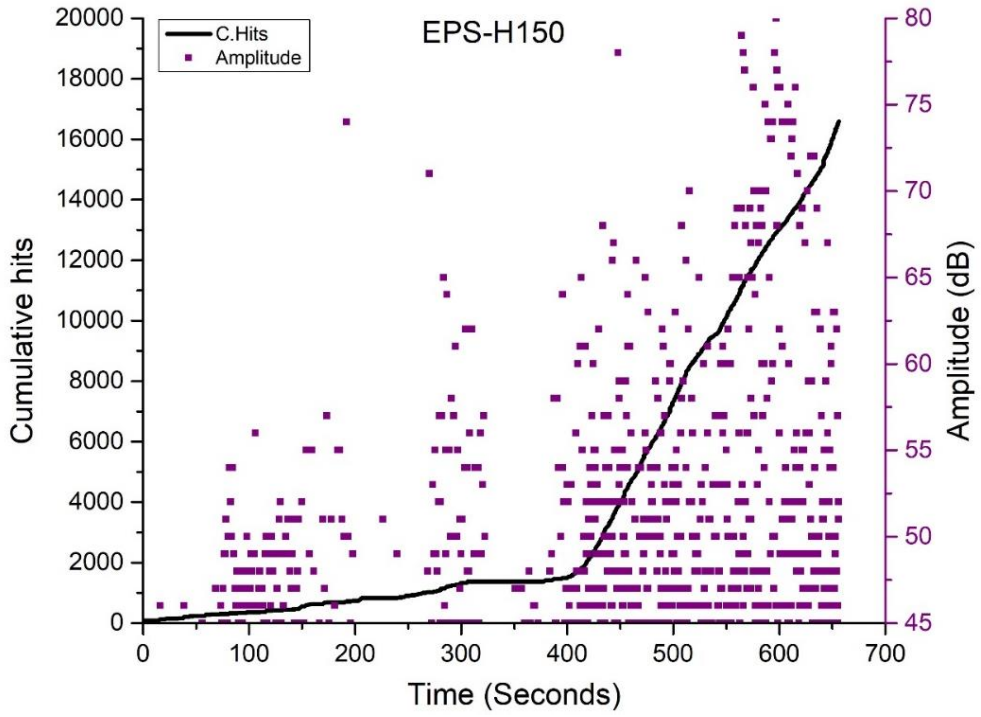

(c) EPS-H150

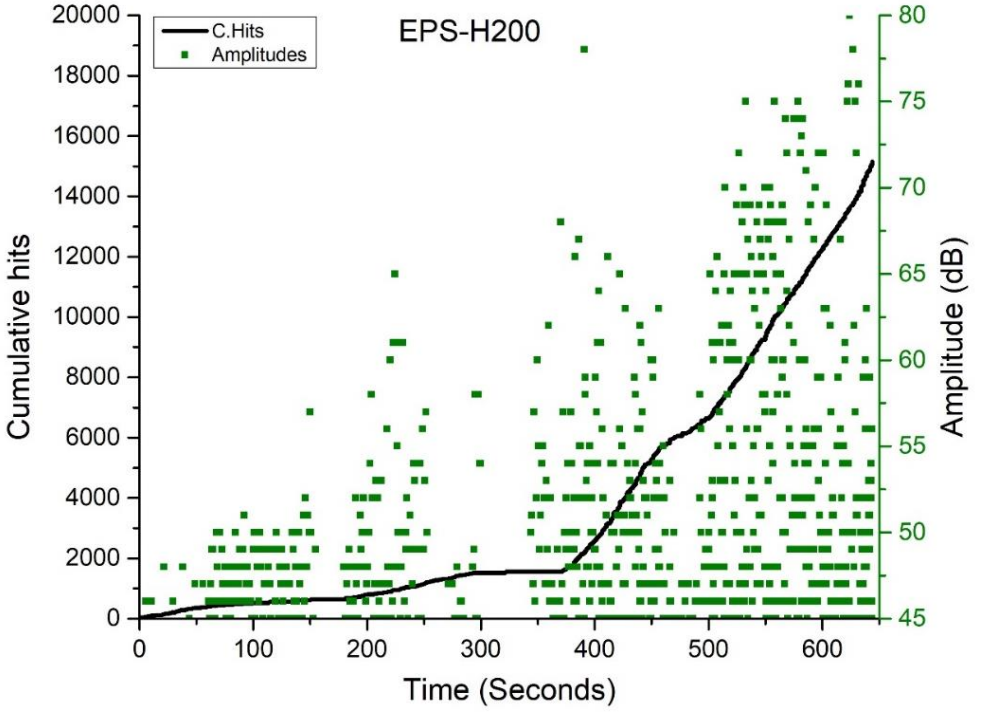

(d) EPS-H200

Figure 6.7 Cumulative hits-amplitude vs time plots heat exposed EPS panels

These changes manifested as a rise in cumulative AE hits, potentially signifying the formation of micro-cracks within the panels due to thermal expansion and contraction cycles. These panels' AE amplitudes were generally lower than the control panel. This phenomenon could be attributed to the smaller size and distributed nature of the micro-cracks as opposed to

larger, single cracks typically associated with higher amplitude emissions. The findings from this study demonstrate the effectiveness of AE monitoring for detecting damage in heat-exposed EPS concrete panels. By comparing the AE data plots from heat-exposed panels with those from the control panel, a qualitative assessment of the extent of thermal damage becomes possible. This comparative approach allows for a better understanding of how elevated temperatures influence the panels' material properties and structural integrity.

The ability of AE monitoring to detect and evaluate micro-damage within the material provides a valuable tool for predicting the long-term performance and safety of EPS panels in real-world applications. Early identification of potential issues through AE monitoring enables timely interventions and maintenance, ultimately preventing catastrophic failures. This approach promotes proactive strategies for ensuring EPS concrete panels' structural integrity and service life.

6.6 RISE ANGLE VS AVERAGE FREQUENCY FOR CRACK CLASSIFICATION

This section explores the utility of two key Acoustic Emission (AE) parameters, Rise Angle (RA) and Average Frequency (AF), in differentiating between crack modes within EPS concrete panels. By analyzing these parameters, we can gain valuable insights into the mechanisms of crack formation and propagation under various thermal conditions.

6.6.1 Understanding RA and AF for crack classification

A critical aspect of AE monitoring lies in distinguishing between different types of cracks, such as tensile and shear, as they indicate distinct damage mechanisms within the material. Here, we delve into the role of RA and AF in achieving this distinction. Rise Angle (RA) is the ratio of rise time to peak amplitude (measured in ms/V), and RA provides information about the crack growth speed. Generally, higher RA values indicate slower crack propagation, often associated with shear cracks. Conversely, lower RA values suggest faster crack propagation, characteristic of tensile cracks. Average Frequency (AF) represents the ratio of the total number of counts within an AE event to its duration. High AF values are typically linked to tensile cracks, whereas lower AF values are more commonly observed with shear cracks.

Scatter plots visualize the relationship between RA and AF (Figure 6.8). A dotted line serves as a demarcation between the two crack modes. Cracks falling above the line indicate tensile cracks, those below the line suggest shear cracks, and data points near the line may

represent mixed-mode cracks. Tensile cracks typically arise due to splitting within the material and are characterized by high AF and low RA values. Their formation involves a rapid release of energy as the crack propagates quickly. In contrast, shear cracks result from the sliding of pre-existing cracks within the material. They exhibit high RA values and low AF values, signifying slower crack growth and a more gradual release of energy. A higher prevalence of shear cracks can indicate the presence of pre-existing weaknesses within the material.

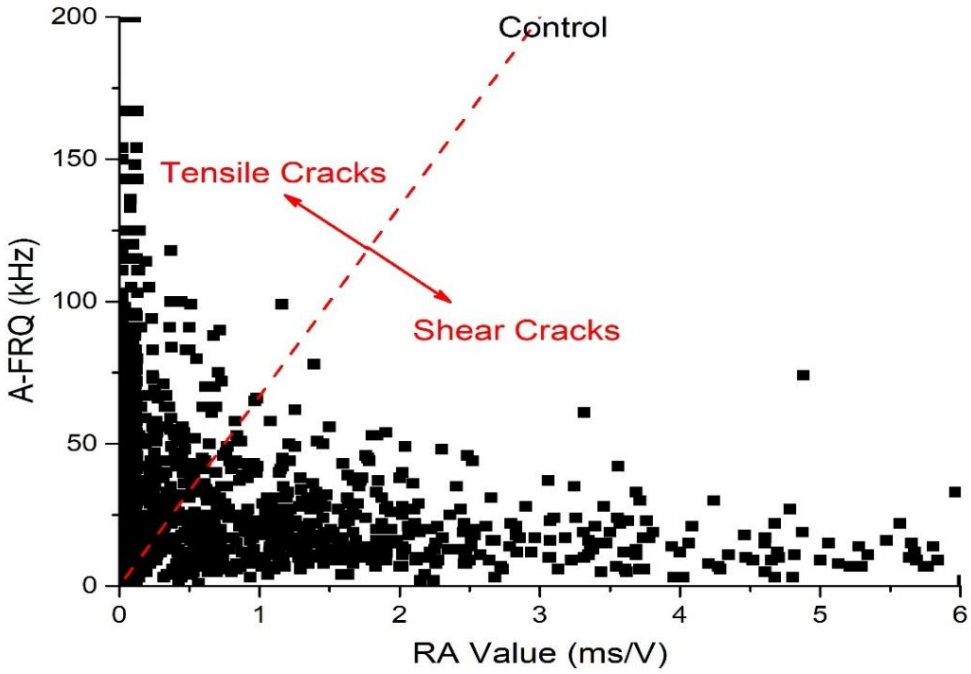

Figure 6.8 Rise angle vs average frequency plots of control panel

6.6.2 Impact of heat exposure on crack modes

The AE data from heat-exposed EPS panels were compared with the control panel using RA vs. AF plots (Figure 6.9). The control panel exhibited a balanced distribution of tensile and shear cracks, reflecting the expected behavior under normal conditions.

Panels subjected to flexural loading were analyzed for RA and AF values using a moving average of 100 AE events (Sharma et al. 2021). A distinct trend emerged: panels exposed to temperatures of 100°C and above displayed a significant increase in the prevalence of shear cracks compared to the control panel. This shift in the crack mode distribution suggests that thermal stress substantially influences the cracking behavior of the panels, potentially leading to more shear-type failures. The density of data points within the plots correlates with the number of AE hits recorded for each specimen (refer to Section 6.4.1). This density provides a quantitative measure of crack activity within the panels. Furthermore, the ratio of shear

cracks to tensile cracks indicates the severity of thermal damage, with a higher ratio suggesting more extensive damage.

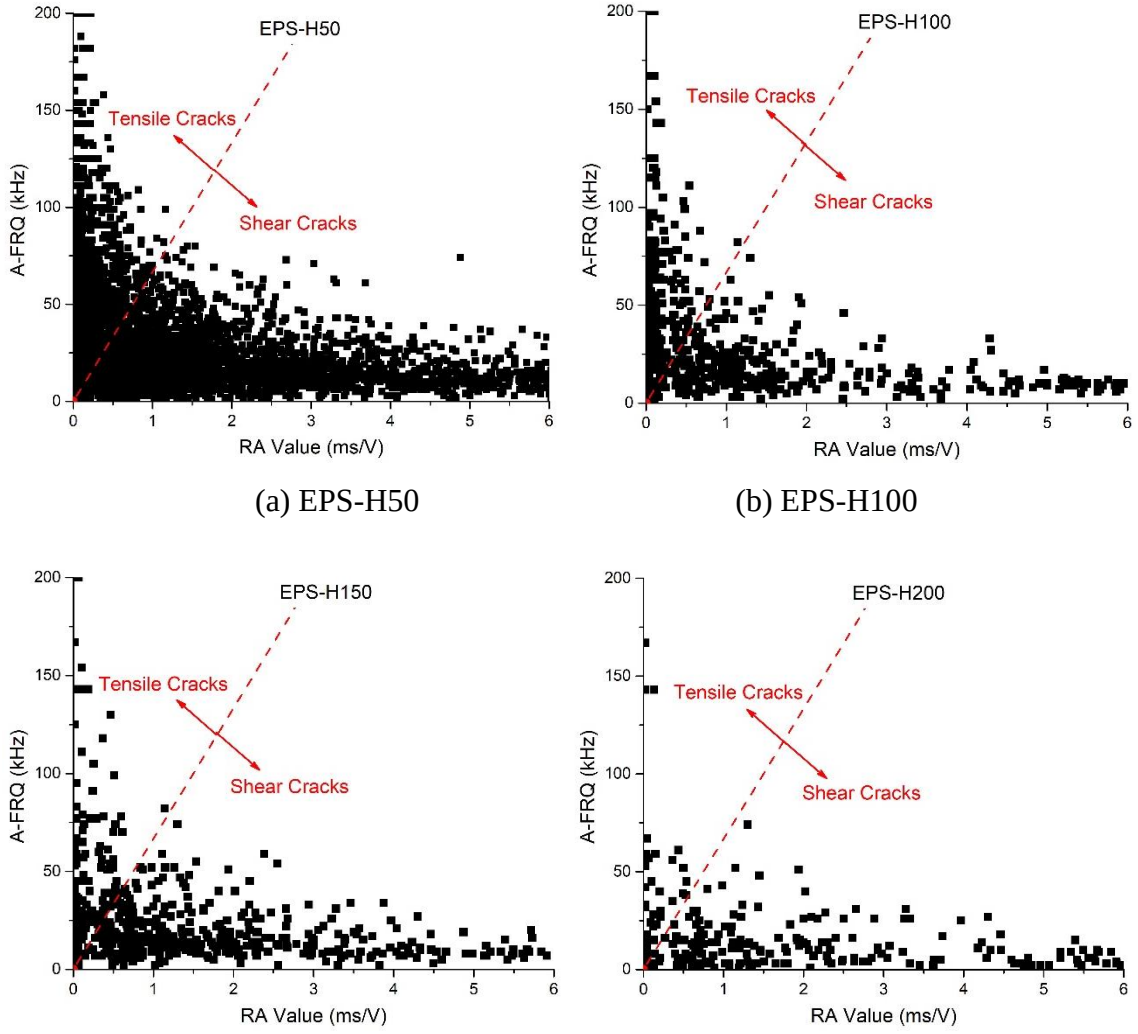

(a) EPS-H50 (b) EPS-H100

(c) EPS-H150 (d) EPS-H200

Figure 6.9 Rise angle vs average frequency plots of heat exposed EPS panels

The combined analysis of RA and AF effectively differentiates and classifies crack types within EPS concrete panels. Early identification of a higher concentration of shear cracks can serve as a valuable warning sign of potential deterioration within the panels. Notably, EPS-H200 (exposed to the highest temperature) exhibited the most shear cracks, validating the effectiveness of AE monitoring for early damage detection in EPS panels. This analysis underscores the importance of AE monitoring for discerning crack types by analyzing RA and AF, engineers can gain insights into the dominant crack modes within the panels, providing a more comprehensive understanding of the damage mechanisms. Assessing structural integrity

the ability to differentiate between crack types allows for a more informed evaluation of the structural integrity of the panels under varying thermal conditions.

By monitoring and analyzing AE data, engineers can proactively address potential issues and implement preventative maintenance strategies, ultimately ensuring the longevity and performance of EPS panels in diverse applications. This approach safeguards the structural health of EPS panels exposed to elevated temperatures.

6.7 CUMULATIVE AE SIGNAL STRENGTH FOR DAMAGE ASSESSMENT

This section explores the application of Cumulative Acoustic Emission (AE) Signal Strength as a valuable tool for evaluating damage progression in EPS concrete panels subjected to elevated temperatures. By analyzing the total energy released during AE events, we gain insights into the health of the material and identify the initiation and propagation of cracks.

6.7.1 Quantifying damage using AE signal strength

AE signal strength is a critical parameter measured during AE monitoring. It represents the integral of the rectified voltage signal throughout an entire AE waveform. In simpler terms, it quantifies the total energy released during a single crack event within the material. This measurement provides a comprehensive understanding of the material's structural health and the onset of damage. Figure 6.10 depicts a plot that combines cumulative AE signal strength, load, and time. This visualization allows us to correlate changes in load with variations in the total energy released through AE events. Sharp increases in signal strength indicate sudden bursts of energy, often associated with crack formation or structural faults within the panel. These spikes in the signal strength plot coincide with corresponding changes in the load-time curve, offering real-time insights into the structural behavior of the panel during testing. In the context of EPS panels, cumulative signal strength (CSS) serves as a predictive tool for early detection of crack initiation by monitoring the CSS plot, we can identify early signs of cracking within the panel through the detection of increased energy release. Assessment of panel integrity the overall trend of the CSS plot can indicate the integrity of the panel. A gradual increase in CSS alongside increasing load suggests that the panel is maintaining its structural integrity. Conversely, sudden spikes or a significant deviation from the expected pattern may signal potential damage.

6.7.2 AE signal strength analysis of EPS panels

The control panel (Figure 6.10) exhibits a steady increase in load over time, reaching a peak of approximately 35 kN at around 800 seconds. The corresponding CSS plot (in red) shows a gradual rise, indicating the accumulation of minor cracking events (micro-events) as the load on the panel increases. The CSS reaches a value of around 4.5 x 10^9 µV/s at the peak load, suggesting a correlation between the applied load and the AE activity within the panel. This steady rise implies that the control panel maintains its structural integrity up to the peak load without experiencing significant damage before failure.

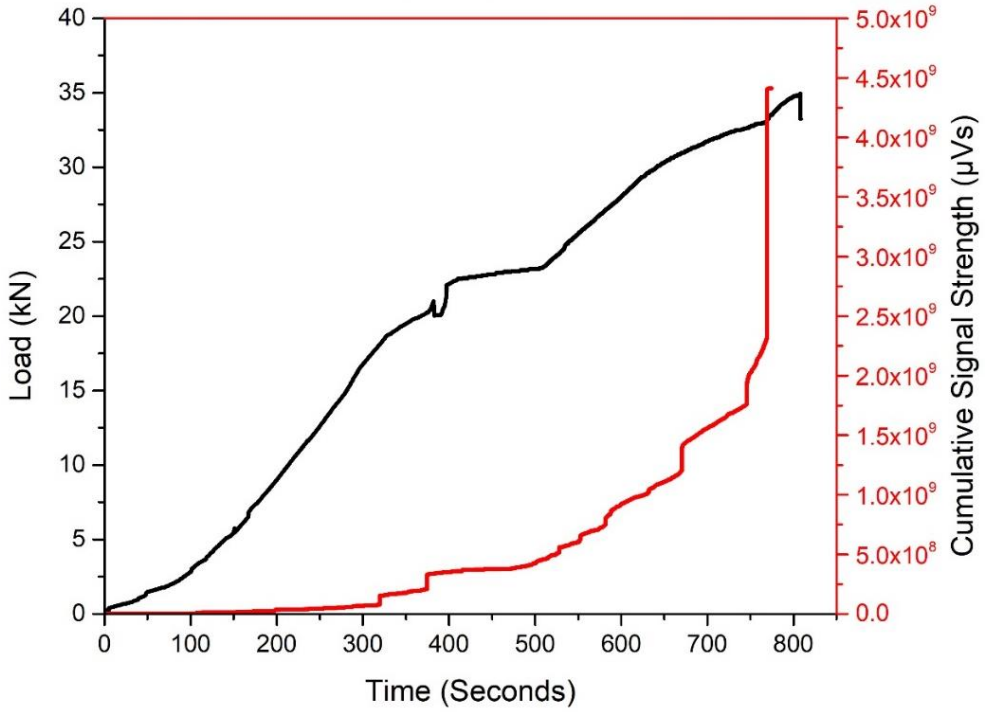

Figure 6.10 CSS-Load vs time plot of control panel

The load-time curve for the EPS-H50 panel (Figure 6.11a) resembles the control panel, with a gradual increase in load up to around 35 kN at approximately 780 seconds. However, the CSS plot reveals a notable difference. While the initial CSS values are like the control panel, a more rapid rise in CSS is observed beyond 400 seconds, reaching a similar peak value of 4.5 x 10^9 µV/s earlier than the control panel. This accelerated increase in AE activity suggests that the EPS-H50 panel, while achieving a comparable peak load, experiences earlier micro-crack formation. The exposure to 50°C likely induces initial micro-cracks, which propagate as the load increases, leading to a higher rate of AE events.

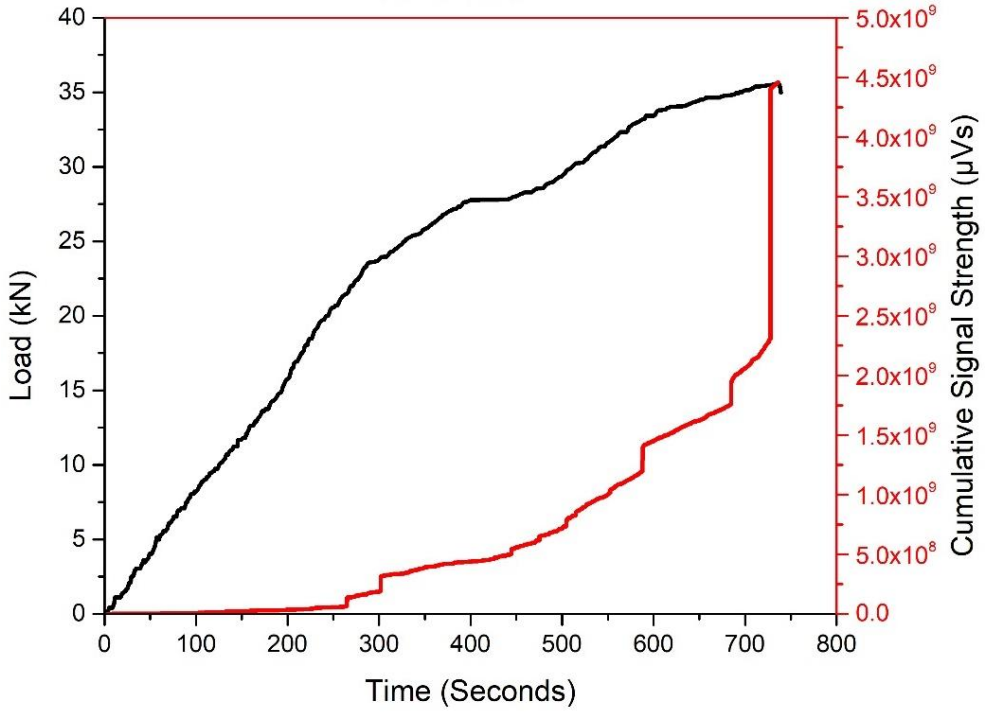

(a) EPS-H50

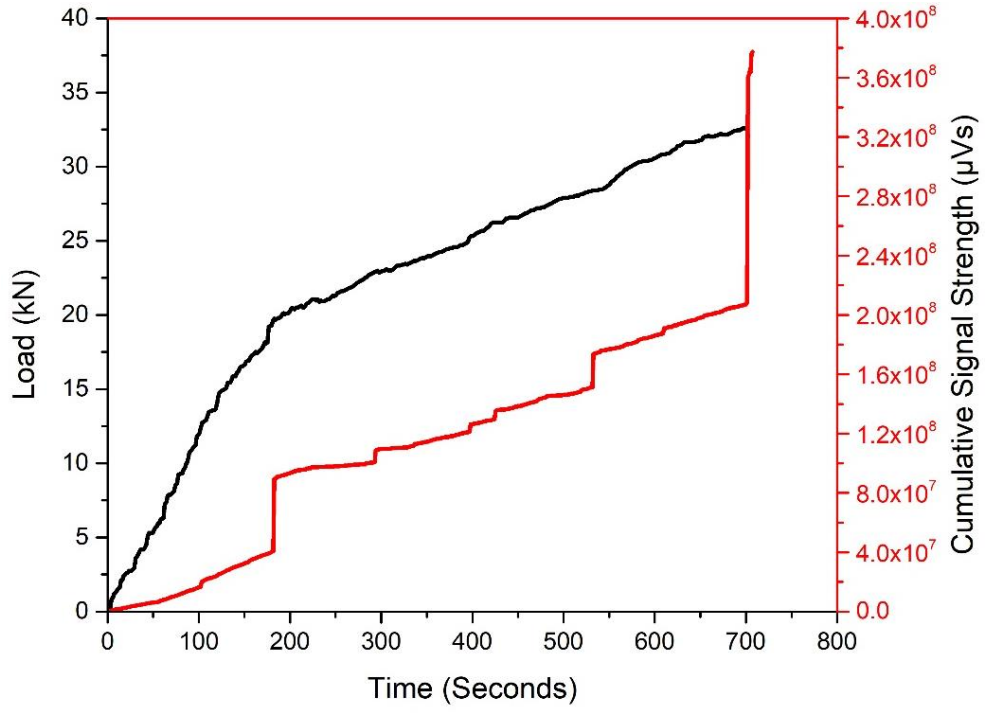

(b) EPS-H100

Figure 6.11 CSS-Load vs time plot of heat exposed panels (Cont.)

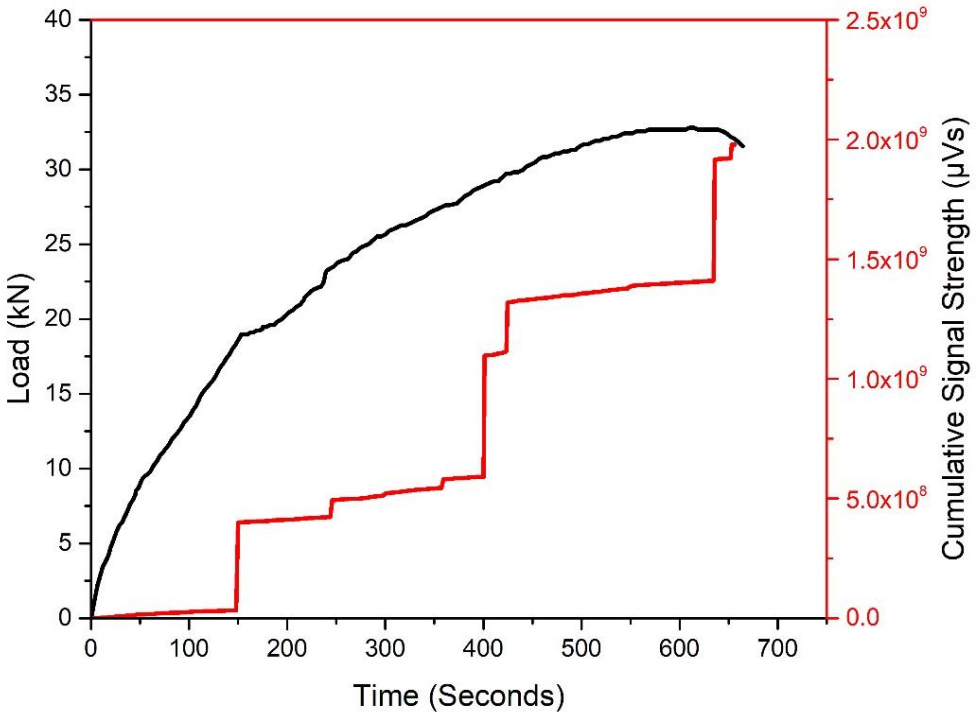

(c) EPS-H150

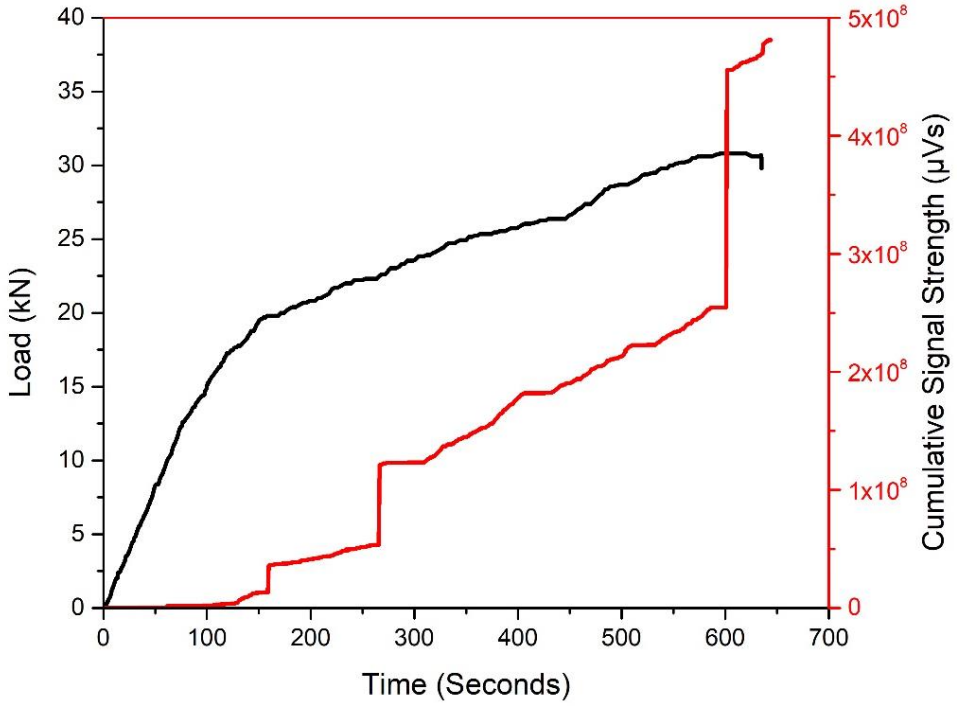

(d) EPS-H200

Figure 6.11 CSS-Load vs time plot of heat exposed panels EPS-H150 & EPS-H200

EPS-H100 Panel (100°C): The EPS-H100 panel (Figure 6.11b) displays a considerably different response than the control and EPS-H50 panels. The load-time curve for EPS-H100

reaches a lower peak load of around 32.6 kN compared to the other panels. This reduction in peak load signifies a decline in the panel's structural integrity due to thermal exposure. The corresponding CSS plot for EPS-H100 exhibits a significantly lower maximum value of 3.8 x 10^8 μV/s, indicating reduced AE activity. This lower CSS value reflects a higher concentration of micro-cracks within the panel. Higher temperatures exacerbate the formation of micro-cracks, leading to diminished structural performance and overall integrity.

The EPS-H150 panel (Figure 6.11c) exhibits behavior similar to the EPS-H100 panel. It sustains a peak load of around 32.78 kN, comparable to EPS-H100. However, the CSS plot for EPS-H150 shows a significantly lower maximum value of approximately 2.0 x 10^9 μV/s, indicating reduced AE activity compared to the control panel. Interestingly, it shows a larger release of CSS at lower loads of 13 kN. The exposure to higher temperatures (150°C) may have caused more significant initial damage, reduced the panel's overall load-bearing capacity and led to fewer AE events as the material's integrity is compromised.

The EPS-H200 panel (Figure 6.11d) exhibits a distinctly different behavior. The load-time curve reaches a peak load of around 30.6 kN, lowest of all considered EPS panels. The CSS plot for EPS-H200 shows a significantly lower maximum value of approximately 5.0 × 10^8 μV/s, indicating reduced AE activity compared to the other panels. This lower CSS suggests that serious micro-cracking occurred inside the EPS panel when it was exposed to 200^0C temperature. The exposure to higher temperatures may result in catastrophic failures in the structures.

In conclusion, the comparative analysis of the load and CSS plots reveals critical insights into the damage mechanisms of EPS panels under varying thermal conditions. The control panel maintains structural integrity up to high loads with gradual AE activity. The EPS-H50 panel shows earlier micro-damage onset, while the EPS-H100, EPS-H150, and EPS-H200 panel experiences more severe initial damage, resulting in reduced load capacity and lower AE activity. The analysis of CSS-time plots provides a quantitative means to assess damage severity and structural interventions' effectiveness. The decline in signal strength directly indicates structural weakening, guiding decisions for remedial measures to ensure the continued safety and reliability of EPS panel structures. These findings highlight the importance of thermal effects on EPS panel performance and the utility of AE monitoring in assessing damage progression.

6.8 CLOSING REMARKS

This chapter has provided a comprehensive experimental investigation into the flexural performance of EPS sandwich concrete panels exposed to elevated temperatures. The detailed analysis of various parameters, such as yield load, ultimate load, yield deflection, ultimate deflection, ductility factor, stiffness, and composite action under four-point flexural loading, has highlighted the significant impacts of heat exposure on the structural integrity of these panels.

The visual and mechanical testing, supported by load-deflection curves and stiffness measurements, underscores the vulnerability of EPS panels to high-temperature conditions, particularly beyond 100°C. Furthermore, the study has demonstrated the efficacy of acoustic emission (AE) monitoring as a non-destructive tool for assessing and predicting damage in heat-exposed EPS panels. The analysis of AE parameters, including cumulative AE hits, amplitude, rise angle, average frequency, and cumulative signal strength, provides valuable insights into crack initiation and progression within the panels. The comparative evaluation of AE data across different thermal exposures highlights the potential of AE monitoring in detecting early signs of structural deterioration, thereby facilitating timely maintenance and ensuring structural safety.

CHAPTER 7

CONCLUSIONS

7.1 GENERAL

This chapter summarizes the key findings after investigating 51 EPS sandwiched concrete panels subjected to various environmental exposures. The following sections detail the observed effects of corrosion, acid and sulfate attacks, and elevated temperatures on these panels' flexural performance and structural integrity. Additionally, the effectiveness of Acoustic Emission (AE) monitoring as a non-destructive testing method is explored.

7.2 EVALUATION OF CORROSION EFFECTS ON FLEXURAL PERFORMANCE OF EPS PANELS

The following conclusions are drawn after evaluating the performance of the EPS sandwiched concrete panels subjected to accelerated corrosion:

1. The rust oozing out between the concrete wythes and the EPS insulation indicates that chloride-laden water can penetrate the interface despite the adhesive bond between the EPS and concrete.

2. Initial stages of corrosion may not be visible on the surface and can remain hidden within the panel. Corrosion was observed to be concealed around the EPS beads, delaying surface visibility until the corrosion became more severe.

3. Shear connectors are particularly susceptible to corrosion due to the cavities formed around them as they pierce the EPS insulation, creating a favorable environment for corrosion in the presence of moisture.

4. Load-deflection plots of control and corroded EPS panels revealed that failure occurred along fissures generated by corrosion. EPS panels with increasing corrosion levels exhibited brittle behavior under flexural loading. Panels EPS-C05, EPS-C10, EPS-C15, and EPS-C20 exhibited a decrease in ultimate flexural load-carrying capacity of 6.98%, 13.93%, 20.62%, and 60.45%, respectively, compared to the control panel. Therefore, progressive corrosion leads to a decrease in the overall load-bearing capacity of the panels.

5. The observed reduction in the Ductility Factor (DF) underscores the detrimental impact of corrosion on EPS panels' structural integrity and flexibility. The significant damage to shear connectors due to corrosion and the corrosion of the wire mesh reinforcement in the wythes contribute to the decrease in ductility of corroded panels.

6. AE monitoring of corroded EPS panels during flexural testing proved to be effective. AE hits, and their amplitudes accurately estimate the initiation and progression of internal damage in the form of micro and macro-cracks within the panels.

7. The correlation of cumulative AE hits with damage progression during loading can be a valuable tool for non-destructive testing of EPS sandwich concrete panels. Cumulative AE hits and their amplitudes successfully indicate damage progression and intensity in various corroded EPS panels. Damage initiation in Stage I, indicated by a slow rise in AE hits with average amplitudes of 50–60 dB, is followed by Stage II, a calm phase with fewer AE hits of lower amplitudes. Stage III involves macro-cracking with many AE hits and average amplitudes of 65–80 dB.

8. AE X-Y event plots effectively pinpoint the location of faults before they become visible on the surface. A close match was observed between the X-Y event plots and visual images of the EPS sandwich concrete panels.

7.3 EVALUATING THE EFFECTS OF AGGRESSIVE ACIDIC AND SULPHATE ENVIRONMENTS ON EPS PANELS

The following conclusions are drawn after evaluating the performance of the EPS sandwiched concrete panels exposed to acid and sulphate attack.

1. The initial stages of acid and sulfate attacks on EPS panels are not immediately noticeable. Significant degradation becomes apparent only after prolonged exposure. For instance, exposure to acid for 14 and 21 days resulted in a 20% and 25% loss in flexural strength, respectively. After 28 days, the loss of strength increased dramatically to 62.74%. The strength degradation is exponential after the initial 21-day exposure period.

2. AE monitoring successfully detected damage initiation and progression even during the early stages of exposure. Cumulative AE hits were drastically reduced with increased exposure to the acidic environment. The amplitudes of AE signals also

indicated the loss of strength, averaging below 50 dB for the extensively exposed EPS-A28 panel. This correlation between cumulative AE hits and damage progression highlights the potential of AE as a non-destructive testing method for EPS sandwich concrete panels.

3. A significant Ductility Factor (DF) loss was observed for acid-exposed EPS panels. Panels EPS-A14, EPS-A21, and EPS-A28 exhibited reductions in DF by 55.11%, 53.63%, and 56.05%, respectively.

4. EPS panels exposed to sulfate for up to 180 days retain ultimate strength comparable to the control panel. However, beyond 180 days, strength degradation is observed, with EPS-S360 failing at a flexural load 42.71% lower than the control. Initial sulfate exposure leads to a loss of initial stiffness in the EPS panels after 90 days.

5. AE monitoring of sulfate-exposed panels shows a slight increase in cumulative AE hits after 180 days. This is correlated with internal voids filled by gypsum produced from sulfate exposure, as indicated by an increase in the mass of simultaneously exposed mortar cubes.

6. AE effectively classifies crack types in EPS panels exposed to acid and sulfate environments. Acid-exposed panels show shear cracks during Stage I after 21 days of exposure. Sulfate-exposed panels exhibit increased shear cracks with prolonged exposure, with EPS-S360 showing predominant shear cracks in Stage I.

7.4 PERFORMANCE OF EPS PANELS UNDER ELEVATED TEMPERATURES

The experimental investigation conducted in this chapter offers several key conclusions regarding the flexural performance of EPS sandwich concrete panels when exposed to elevated temperatures:

1. EPS sandwich concrete panels exhibit significant degradation in structural integrity when exposed to elevated temperatures. The primary causes of this degradation are the thermal decomposition of hydration products in the concrete matrix and the shrinkage and weakening of EPS insulation.

2. The flexural performance of EPS panels is considerably affected by heat exposure. While the panels maintain structural integrity up to 50°C, exposure to temperatures

beyond 100°C results in decreased load-bearing capacity, increased yield deflection and reduced ductility. Panels exposed to temperatures up to 200°C showed a marked decrease in ultimate load capacity and structural stiffness.

3. Heat exposure leads to a substantial decline in the stiffness properties of EPS panels. The yield and secant stiffness were notably reduced in panels exposed to higher temperatures. Additionally, the energy dissipation capacity of these panels decreased significantly, indicating a compromised ability to absorb and dissipate energy under flexural loads.

4. The degree of composite action in EPS sandwich concrete panels deteriorates with increased thermal exposure. Panels exposed to higher temperatures showed a reduction in composite action, attributed to the shrinkage of EPS insulation and micro-cracking of the concrete. This reduction in composite action impacts the load transfer efficiency and overall structural performance of the panels.

5. AE monitoring proved an effective non-destructive tool for detecting and assessing damage in EPS panels exposed to elevated temperatures. Variations in AE hits align closely with the residual flexural strengths of heat-exposed EPS panels. Enhanced initial stiffness in EPS-H50 is discernible from early AE hits in AE vs. time plots. RA vs. AF plots effectively identify crack types in EPS panels, distinguishing between shear and tensile cracks. Early detection of shear cracks is crucial for damage assessment. CSS is an immediate indicator of internal cracks in EPS panels, detecting cracks not visible to the naked eye, with only 10% of total signal strength released up to the yield load. Cumulative strength decreases in temperature-exposed EPS panels.

The findings highlight the importance of implementing predictive maintenance strategies for EPS sandwich concrete panels exposed to high temperatures. Utilizing AE monitoring and understanding the degradation mechanisms can help develop preventive measures to enhance the resilience and longevity of these panels.

7.5 LIMITATIONS OF THE STUDY

The study provides valuable insights into the performance of EPS sandwiched concrete panels under various environmental conditions, but it is important to recognize certain limitations. The investigation was limited to 51 panels, which may not fully capture the wide

variability in panel behaviour under different real-world scenarios. Additionally, the thesis evaluates chloride, acid, sulphate exposure, and elevated temperatures independently. In practical conditions, however, multiple environmental factors often occur simultaneously, such as high temperatures coupled with chloride exposure in coastal regions. The absence of combined environmental stressors could limit the applicability of the findings to real-world situations. Moreover, the accelerated testing conditions used (such as corrosion and temperature exposure) may not perfectly simulate long-term, natural degradation processes. While AE monitoring proved effective as a non-destructive evaluation technique, its reliance on subjective interpretation and the lack of standardized criteria for AE data analysis present challenges for consistent and reliable damage detection. Future studies should address these limitations by expanding the sample size, refining AE data evaluation methods, and investigating prolonged exposure durations to better simulate natural degradation and combined environmental factors.

7.6 CLOSING REMARKS

In conclusion, this thesis has comprehensively evaluated the performance of EPS sandwiched concrete panels under various aggressive environmental conditions, including corrosion, acid attack, sulphate attack, and elevated temperatures. EPS panels are increasingly adopted for their lightweight nature, superior insulation properties, and cost-effectiveness, especially in residential buildings. The study reveals that aggressive environmental degradations are difficult to notice in the initial phase. To detect the initial degradation of the EPS panels AE technique of non-destructive evaluation of the structural health proves to be efficient. This study has addressed the critical gap in understanding EPS panels performance under severe environmental conditions and their detection using AE technique.

7.7 PRACTICAL APPLICATION

The outcomes of the study are crucial for the use in the emerging construction materials. It can be used as a continuously AE monitoring system for EPS panels which can indicate the occurrence of faults well before catastrophic failure. The study can help in establishing the thresholds and indicators of damage for practical use in AE live monitoring.

7.8 FUTURE SCOPE OF WORK

This research paves the way for the future incorporation of Acoustic Emission (AE) techniques and evaluation of other NDT to identify the degradation of EPS panels in the field,

particularly in environments where aggressive conditions are prevalent. Future studies should focus on the following areas:

1. The technique can be readily used for evaluation of existing EPS panel structures. The field implementation of AE monitoring needs to be extensively explored for development of robust AE monitoring systems for real-time detection of degradation in EPS panels.

2. The degradation of EPS panels under long-term environmental conditions, including cyclic temperature variations, alternate wetting and drying conditions and cyclic loading needs to be explored.

3. The EPS panels can be tried to be evaluated using other NDT technologies like Infrared Thermography (IRT), Digital Image Correlation (DIC) and other emerging technologies.

4. The EPS panels with different corrosion resisting coatings on shear connectors can be studied to evaluate the durability. The shear connectors are crucial for composite action and are susceptible for early corrosion.

REFERENCES

1. Abolhasani, A., Shakouri, M., Dehestani, M., Samali, B., and Banihashemi, S. 2022. A comprehensive evaluation of fracture toughness, fracture energy, flexural strength and microstructure of calcium aluminate cement concrete exposed to high temperatures. Engineering Fracture Mechanics, **261**. Elsevier Ltd. doi:10.1016/j.engfracmech.2021.108221.

2. Ahmad, A., and Singh, Y. 2021a. In-plane behaviour of expanded polystyrene core reinforced concrete sandwich panels. Construction and Building Materials, **269**: 121804. Elsevier. doi:10.1016/J.CONBUILDMAT.2020.121804.

3. Ahmad, A., and Singh, Y. 2021b. Flexural behavior of Expanded Polystyrene core Reinforced Concrete Sandwich Panels with different construction methods and end conditions. Structures, **34**: 2900–2911. Elsevier. doi:10.1016/J.ISTRUC.2021.09.051.

4. Ahmad, S. 2003. Reinforcement corrosion in concrete structures, its monitoring and service life prediction—a review. Cement and Concrete Composites, **25**(4–5): 459–471. Elsevier. doi:10.1016/S0958-9465(02)00086-0.

5. Ahmad, S., Al-Huri, M.A., Al-Osta, M.A., Maslehuddin, M., and Al-Gadhib, A.H. 2022. An Experimental Approach to Evaluate the Effect of Reinforcement Corrosion on Flexural Performance of RC Beams. Buildings, **12**(12): 2222. Multidisciplinary Digital Publishing Institute. doi:10.3390/BUILDINGS12122222.

6. Ahmed, O., Ahmad, S., and Adekunle, S.K. 2024. Carbon dioxide sequestration in cementitious materials: A review of techniques, material performance, and environmental impact. Journal of CO2 Utilization, **83**: 102812. Elsevier. doi:10.1016/J.JCOU.2024.102812.

7. Alexander, M., Bertron, A., and Belie, N. De. 2013. Performance of cement-based materials in aggressive aqueous environments.

8. Alharthi, F.M., Al-Osta, M.A., Rahman, M.K., Bahraq, A.A., Ahmad, S., Al-Zahrani, M.M., and Elamary, A.S. 2024. Flexural Behavior of Concrete Hollow-Core Beams Reinforced with GFRP Bars: Experimental and Analytical Investigation. Arabian Journal for Science and Engineering, **49**(4): 5267–5286. Springer Nature. doi:10.1007/S13369-023-08372-W/TABLES/5.

9. Ali, S.M., Hui, K.H., Hee, L.M., Leong, M.S., Abdelrhman, A.M., and Al-Obaidi, M.A. 2019. Observations of changes in acoustic emission parameters for varying corrosion defect in reciprocating compressor valves. Ain Shams Engineering Journal, **10**(2): 253–265. Elsevier. doi:10.1016/J.ASEJ.2019.01.003.

10. Alyamaç, K.E., Ulaş, M.A., Taş, Y., and Ghafari, E. 2018. Feasibility Analysis of NDT Methods Using to Estimate the Concrete Strength as Part of Urban Regeneration. Turkish Journal of Science and Technology, **13**(1): 9–17. Fırat University.

11. Amran, M.Y.H., Rashid, R.S.M., Hejazi, F., Ali, A.A.A., Safiee, A., and Bida, M.S. 2018. Structural Performance of Precast Foamed Concrete Sandwich Panel Subjected to Axial Load. KSCE Journal of Civil Engineering, **22**(4): 1179–1192. doi:10.1007/s12205-017-1711-6.

12. Amran, Y.H.M., Rashid, R.S.M., Hejazi, F., Safiee, N.A., and Ali, A.A.A. 2016. Response of precast foamed concrete sandwich panels to flexural loading. Journal of Building Engineering, **7**: 143–158. doi:10.1016/j.jobe.2016.06.006.

13. Andrade, C., Martínez-Serrano, A., Sanjuán, M.Á., and Tenorio, J.A. 2023. Strength and Resistance to Sulfates, Carbonation and Chlorides Ingress by Substitution of Binder by Hydrotalcite in Several Cement Types. Construction Materials, **3**(3): 305–319. MDPI AG. doi:10.3390/CONSTRMATER3030020.

14. Andrade, C., Serrano, A.M., Sanjuán, M.Á., and Ríos, J.A.T. 2021. Reduced Carbonation, Sulfate and Chloride Ingress Due to the Substitution of Cement by 10% Non-Precalcined Bentonite. Materials, **14**(5). doi:https://doi.org/10.3390/ma14051300.

15. Andrade Perdrix, C., Saucedo-Mora, L., López Hombrados, C., Barroso, J., and Zamora Bragado, A. 2016. Experimental evaluation of the structural integrity of reinforced concrete beams through Digital Image Correlation (DIC): energy released by the material and modes of failure. Congreso Nacional PRE-CONPAT 16 España,.

16. ASTM A1064 / A1064M-18a. 2018. Standard Specification for Carbon-Steel Wire and Welded Wire Reinforcement, Plain and Deformed, for Concrete. West Conshohocken, PA.

17. ASTM C 578–04. 2004. Standard Specification for Rigid, Cellular Polystyrene Thermal Insulation. West Conshohocken, PA.

18. ASTM G31-72. 2004. Standard Practice for Laboratory Immersion Corrosion Testing of Metals.

19. Bahekar, P. V., and Gadve, S.S. 2017. Impressed current cathodic protection of rebar in concrete using Carbon FRP laminate. Construction and Building Materials, **156**: 242–251. Elsevier. doi:https://doi.org/10.1016/j.conbuildmat.2017.08.145.

20. Bahekar, P. V., and Gadve, S.S. 2019. Effects of Impressed Current Cathodic Protection on Carbon Fiber-Reinforced Polymer Strengthened Flexural Reinforced Concrete Members. Corrosion, **75**(6): 693–703. Allen Press. doi:https://doi.org/10.5006/2916.

21. Barbhuiya, S., and Kumala, D. 2017. Behaviour of a sustainable concrete in acidic environment. Sustainability (Switzerland), **9**(9). MDPI. doi:10.3390/su9091556.

22. Bassuoni, M.T., and Nehdi, M.L. 2007. Resistance of self-consolidating concrete to sulfuric acid attack with consecutive pH reduction. Cement and Concrete Research, **37**(7): 1070–1084. doi:10.1016/J.CEMCONRES.2007.04.014.

23. Bastin, D.R.A., and Sharma, U.K. 2017. A study on different techniques of restoration of fire damaged reinforced concrete flexural members. Journal of Structural Fire Engineering, **8**(2): 131–148. Emerald Group Holdings Ltd. doi:10.1108/JSFE-03-2017-0026.

24. Bellamy, L.A. 2014. Variable density concrete walls engineered for energy performance. *In* International Conference on Building Envelope Systems and Technologies . *Edited by* H. Gerhardt. Aachen, Germany.

25. Benayoune, A., Samad, A.A.A., Abang Ali, A.A., and Trikha, D.N. 2007. Response of pre-cast reinforced composite sandwich panels to axial loading. Construction and Building Materials, **21**(3): 677–685. Elsevier. doi:10.1016/J.CONBUILDMAT.2005.12.011.

26. Benayoune, A., Samad, A.A.A., Trikha, D.N., Ali, A.A.A., and Ellinna, S.H.M. 2008. Flexural behaviour of pre-cast concrete sandwich composite panel - Experimental and theoretical investigations. Construction and Building Materials,. doi:10.1016/j.conbuildmat.2006.11.023.

27. Bishnoi, U., Danie Roy, A.B., and Kwatra, N. 2021. Out of plane performance of novel concrete sandwich panel using different geosynthetics. Construction and

Building Materials, **300**: 124186. Elsevier. doi:10.1016/J.CONBUILDMAT.2021.124186.

28. Bishnoi, U., Roy, A.B.D., and Kwatra, N. 2024. In-plane shear behaviour of concrete sandwich panels reinforced with various geogrids. European Journal of Environmental and Civil Engineering, **28**(8): 1813–1829. Taylor & Francis. doi:10.1080/19648189.2023.2276141.

29. Borodinecs, A., and Jacnevs, V. 2023. Theoretical Evaluation of Structural Insulated Panel Walls in Baltic Climatic Conditions. Journal of Sustainable Architecture and Civil Engineering, **32**(1): 186–195. Exeley Inc.

30. Breit, W. 2004. Acid resistance of concrete. *In* Internation RILEM Symposium on Concrete Science and Engineering.

31. Bureau of Indian Standards. 2004. IS 4671: 1984 Specifications for expanded polystyrene for thermal insulation purposes. New Delhi.

32. Burud, N.B., and Chandra Kishen, J.M. 2023. Investigation of long memory in concrete fracture through acoustic emission time series analysis under monotonic and fatigue loading. Engineering Fracture Mechanics, **277**: 108975. Pergamon. doi:10.1016/J.ENGFRACMECH.2022.108975.

33. Bush, T.D., and Stine, G.L. 1994. Flexural behavior of composite precast concrete sandwich panels with continuous truss connectors. PCI Journal, **2**(39): 112–121.

34. Carbonari, G., Cavalaro, S.H.P., Cansario, M.M., and Aguado, A. 2012. Flexural behaviour of light-weight sandwich panels composed by concrete and EPS. Construction and Building Materials, **35**: 792–799. Elsevier. doi:10.1016/J.CONBUILDMAT.2012.04.080.

35. CBRI. 2017. Manual for Expanded Polystyrene (EPS) Core Panel System and its field Application. Roorkee.

36. Chakraborty, S., Reddy, S., and Subramaniam, K.V.L. 2021. Experimental evaluation and analysis of flexural response of sandwich beam panels with an expanded polystyrene core. Structures, **33**: 3798–3809. Elsevier. doi:10.1016/J.ISTRUC.2021.06.088.

37. Chang, Z.T., Song, X.J., Munn, R., and Marosszeky, M. 2005. Using limestone aggregates and different cements for enhancing resistance of concrete to sulphuric acid attack. Cement and Concrete Research, **35**(8): 1486–1494. doi:10.1016/J.CEMCONRES.2005.03.006.

38. Chen, A., Yossef, M., and Hopkins, P. 2020. A comparative study of different methods to calculate degrees of composite action for insulated concrete sandwich panels. Engineering Structures, **212**: 110423. Elsevier. doi:10.1016/J.ENGSTRUCT.2020.110423.

39. Chen, W., Hao, H., Hughes, D., Shi, Y., Cui, J., and Li, Z.X. 2015. Static and dynamic mechanical properties of expanded polystyrene. Materials & Design, **69**: 170–180. Elsevier. doi:10.1016/J.MATDES.2014.12.024.

40. Choi, I., Kim, J.H., and Kim, H.R. 2015. Composite Behavior of Insulated Concrete Sandwich Wall Panels Subjected to Wind Pressure and Suction. Materials, **8**(3): 1264–1282. Multidisciplinary Digital Publishing Institute. doi:10.3390/MA8031264.

41. Choi, W., Jang, S.J., and Yun, H. Do. 2019a. Design properties of insulated precast concrete sandwich panels with composite shear connectors. Composites Part B: Engineering, **157**: 36–42. Elsevier. doi:10.1016/J.COMPOSITESB.2018.08.081.

42. Choi, W., Jang, S.J., and Yun, H. Do. 2019b. Design properties of insulated precast concrete sandwich panels with composite shear connectors. Composites Part B: Engineering, **157**: 36–42. Elsevier. doi:10.1016/J.COMPOSITESB.2018.08.081.

43. Choi, W., Jang, S.-J., and Yun, H.-D. 2019c. Design properties of insulated precast concrete sandwich panels with composite shear connectors. Composites Part B: Engineering, **157**: 36–42. doi:10.1016/j.compositesb.2018.08.081.

44. Classen, M., Herbrand, M., Adam, V., Kueres, D., and Sarac, M. 2018. Puzzle-shaped rib shear connectors subjected to combined shear and tension. Journal of Constructional Steel Research, **145**: 232–243. Elsevier. doi:10.1016/J.JCSR.2018.02.036.

45. COMFORTECH BUILDING PERFORMANCE SOLUTIONS. (n.d.). Fire Resistance Rating. Available from https://www.comfortech.co.nz/passive-fire-protection/fire-resistance-rating/. [accessed 4 June 2024].

46. D. Bush, T., and Wu, Z. 1998. Flexural Analysis of Prestressed Concrete Sandwich Panels with Truss Connectors. PCI Journal,.

47. Daniel Ronald Joseph, J., Prabakar, J., and Alagusundaramoorthy, P. 2018. Flexural behavior of precast concrete sandwich panels under different loading conditions such as punching and bending. Alexandria Engineering Journal, **57**(1): 309–320. Elsevier B.V. doi:10.1016/J.AEJ.2016.11.016.

48. Daniel Ronald Joseph, J., Prabakar, J., and Alagusundaramoorthy, P. 2019a. Experimental studies on through-thickness shear behavior of EPS based precast concrete sandwich panels with truss shear connectors. Composites Part B: Engineering, **166**: 446–456. doi:10.1016/j.compositesb.2019.02.030.

49. Daniel Ronald Joseph, J., Prabakar, J., and Alagusundaramoorthy, P. 2019b. Experimental study on the flexural behavior of insulated concrete sandwich panels with wires as shear connectors. Alexandria Engineering Journal, **58**(3): 901–908. doi:10.1016/j.aej.2019.08.005.

50. Daniyal, M., and Akhtar, S. 2020. Corrosion assessment and control techniques for reinforced concrete structures: a review. Journal of Building Pathology and Rehabilitation, **5**(1): 1. doi:10.1007/s41024-019-0067-3.

51. David Salmon, B.C., and Einea, A. 1995. Partially composite sandwich panel deflections. Journal of structural engineering, **121**(4): 778–783.

52. Davies, G.A.O., Hitchings, D., Besant, T., Clarke, A., and Morgan, C. 2004. Compression after impact strength of composite sandwich panels. Composite Structures, **63**(1): 1–9. Elsevier. doi:10.1016/S0263-8223(03)00119-3.

53. Ede, A.N., and Ogundiran, A. 2014. Thermal Behaviour and Admissible Compressive Strength of Expanded Polystyrene Wall Panels of Varying Thickness. Current Trends in Technology and Science, **3**(2): 110–117.

54. Egbon, B., and Tomlinson, D. 2021. Experimental investigation of longitudinal shear transfer in insulated concrete wall panels with notched insulation. Journal of Building Engineering, **43**. Elsevier Ltd. doi:10.1016/J.JOBE.2021.103173.

55. Einea, P.E.A., Salmon, D.C., Fogarasi, G.J., Culp, T.D., and Tadros, M.K. 1991. State-of-the-art of precast concrete sandwich panels. PCI journal, **6**(36): 78–98.

56. Farnam, Y., Geiker, M.R., Bentz, D., and Weiss, J. 2015. Acoustic emission waveform characterization of crack origin and mode in fractured and ASR damaged concrete. Cement and Concrete Composites, **60**: 135–145. Elsevier. doi:10.1016/J.CEMCONCOMP.2015.04.008.

57. Gara, F., Ragni, L., Roia, D., and Dezi, L. 2012. Experimental tests and numerical modelling of wall sandwich panels. Engineering Structures, **37**: 193–204. Elsevier. doi:10.1016/J.ENGSTRUCT.2011.12.027.

58. Garhwal, A., Sharma, S., and Roy A B, D. 2022. Performance of Expanded Polystyrene (EPS) sandwiched concrete panels subjected to accelerated corrosion. Structures, **43**: 1057–1072. Elsevier. doi:10.1016/J.ISTRUC.2022.07.020.

59. Garhwal, S., Sharma, S., and Sharma, S.K. 2021a. Monitoring the flexural performance of GFRP repaired corroded reinforced concrete beams using passive acoustic emission technique. Structural Concrete, **22**(1): 198–214. doi:10.1002/suco.202000247.

60. Garhwal, S., Sharma, S., and Sharma, S.K. 2021b. Acoustic Emission Monitoring of RC Beams Corroded to Different Levels Under Flexural Loading. Arabian Journal for Science and Engineering, **46**(5): 4319–4335. doi:10.1007/s13369-020-04930-8.

61. Gaur, H., Moka, V.T.K., Chidambaram, S.R., and Kwatra, N. 2022. Hysteretic Performance of Precast Beam-Column Joint with Improved Energy Dissipation Capacity. *In* Advances in Structural Mechanics and Applications. *Edited by* J.A.F. de O. Correia, S. Choudhury, and S. Dutta. Springer, Cham. pp. 336–349.

62. Giriraju, R., Sengupta, A.K., and Pillai, R.G. 2022. Tensile Behaviour of Corroded Strands in Prestressed Concrete Systems. Journal of The Institution of Engineers (India): Series A, **103**(3): 867–879. Springer. doi:10.1007/S40030-022-00656-Y/FIGURES/12.

63. Glasser, F.P., Marchand, J., and Samson, E. 2008. Durability of concrete — Degradation phenomena involving detrimental chemical reactions. Cement and Concrete Research, **38**(2): 226–246. Pergamon. doi:10.1016/J.CEMCONRES.2007.09.015.

64. Goyal, A., Pouya, H.S., and Ganjian, E. 2023. Electrochemical Performance of Concrete Conductive Anode Paint Used as an Impressed Current Anode Material. Journal of Materials in Civil Engineering, **35**(7). American Society of Civil Engineers (ASCE). doi:https://doi.org/10.1061/JMCEE7.MTENG-15550.

65. Grosse, C.U., and Ohtsu, M. 2008. Acoustic emission testing: Basics for Research-Applications in Civil Engineering. Acoustic Emission Testing: Basics for Research-Applications in Civil Engineering,: 1–404. Springer Berlin Heidelberg. doi:10.1007/978-3-540-69972-9/COVER.

66. Gu, Y., Omikrine Metalssi, O., Martin, R.P., Fen-Chong, T., and Dangla, P. 2020. Locating ettringite due to DEF at the pore scale of cement paste by heat-based dissolution tests. Construction and Building Materials, **258**: 120000. Elsevier. doi:10.1016/J.CONBUILDMAT.2020.120000.

67. Gutberlet, T., Hilbig, H., and Beddoe, R.E. 2015. Acid attack on hydrated cement — Effect of mineral acids on the degradation process. Cement and Concrete Research, **74**: 35–43. Pergamon. doi:10.1016/J.CEMCONRES.2015.03.011.

68. Hamed, E. 2018. Creep in Precast-Concrete Sandwich Panels Made with Diagonal-Bar Shear Connectors. Journal of Engineering Mechanics, **144**(11): 04018102. American Society of Civil Engineers (ASCE). doi:10.1061/(ASCE)EM.1943-7889.0001529/ASSET/505ADA53-4FB3-4578-8D40-D04C459CCC07/ASSETS/IMAGES/LARGE/FIGURE11.JPG.

69. Hasanzadeh, R., Azdast, T., Lee, P.C., and Park, C.B. 2023. A review of the state-of-the-art on thermal insulation performance of polymeric foams. Thermal Science and Engineering Progress, **41**: 101808. Elsevier. doi:10.1016/J.TSEP.2023.101808.

70. Hassan, T.K., and Rizkalla, S.H. 2010. Analysis and design guidelines of precast, prestressed concrete, composite load-bearing sandwich wall panels reinforced with CFRP grid. PCI Journal, **55**(2): 147–162. Precast/Prestressed Concrete Institute. doi:10.15554/PCIJ.03012010.147.162.

71. Hou, H., Ji, K., Wang, W., Qu, B., Fang, M., and Qiu, C. 2019. Flexural behavior of precast insulated sandwich wall panels: Full-scale tests and design implications. Engineering Structures, **180**: 750–761. Elsevier. doi:10.1016/J.ENGSTRUCT.2018.11.068.

72. Hou, H., Wang, W., Qu, B., and Dai, C. 2020. Testing of insulated sandwich panels with GFRP shear connectors. Engineering Structures, **209**: 109954. Elsevier. doi:10.1016/J.ENGSTRUCT.2019.109954.

73. Huang, J.Q., and Dai, J.G. 2019. Direct shear tests of glass fiber reinforced polymer connectors for use in precast concrete sandwich panels. Composite Structures, **207**: 136–147. Elsevier. doi:10.1016/J.COMPSTRUCT.2018.09.017.

74. Huang, J.Q., Xu, Y.Y., Huang, H., and Dai, J.G. 2022. Structural behavior of FRP connector enabled precast geopolymer concrete sandwich panels subjected to one-side fire exposure. Fire Safety Journal, **128**: 103524. Elsevier. doi:10.1016/J.FIRESAF.2022.103524.

75. Huang, Y., Yang, C., Ji, X., Lu, D., and Song, Q. 2024. Seismic response of expanded polystyrene (EPS) sandwiched concrete panels system in buildings: Damage distribution and correlation analysis of parameters. Journal of Building Engineering, **91**: 109608. Elsevier. doi:10.1016/J.JOBE.2024.109608.

76. Idrissi, H., and Limam, A. 2003. Study and characterization by acoustic emission and electrochemical measurements of concrete deterioration caused by reinforcement steel corrosion. NDT & E International, **36**: 563–569. doi:10.1016/S0963-8695(03)00064-1.

77. Irico, S., Meyst, L. De, Qvaeschning, D., Alonso, M.C., Villar, K., and Belie, N. De. 2020. Severe Sulfuric Acid Attack on Self-Compacting Concrete with Granulometrically Optimized Blast-Furnace Slag-Comparison of Different Test Methods. Materials, **13**(6). Multidisciplinary Digital Publishing Institute (MDPI). doi:10.3390/MA13061431.

78. Jajodia, R., and Gadve, S. 2023. Shear strength of plain concrete. Strain, **59**(3): 12436. John Wiley & Sons, Ltd. doi:https://doi.org/10.1111/str.12436.

79. Janfeshan Araghi, H., Nikbin, I.M., Rahimi Reskati, S., Rahmani, E., and Allahyari, H. 2015. An experimental investigation on the erosion resistance of concrete containing various PET particles percentages against sulfuric acid attack. Construction and Building Materials, **77**: 461–471. Elsevier Ltd. doi:10.1016/J.CONBUILDMAT.2014.12.037.

80. Ji, Y., Kim, Y.J., and Jia, Y. 2021. Performance characterization of plain and CFRP-bonded concrete subjected to sulfuric acid. Materials and Design, **197**. Elsevier Ltd. doi:10.1016/J.MATDES.2020.109176.

81. Jithin, P.U., and Joseph, A. 2023. Thermal and Structural Behavior of Precast Concrete Sandwich Panels. Lecture Notes in Civil Engineering, **284**: 511–522. Springer Science and Business Media Deutschland GmbH. doi:10.1007/978-3-031-12011-4_40/COVER.

82. Jyoti Basu, D., Acharjee, D., and Bandyopadhyay, D. 2022. Numerical study on fire resistance behavior of EPS sandwich panels. Materials Today: Proceedings, **60**: 459–465. Elsevier. doi:10.1016/J.MATPR.2022.01.319.

83. Kawasaki, Y., Wakuda, T., Kobarai, T., and Ohtsu, M. 2013a. Corrosion mechanisms in reinforced concrete by acoustic emission. Construction and Building Materials, **48**: 1240–1247. Elsevier. doi:10.1016/J.CONBUILDMAT.2013.02.020.

84. Kawasaki, Y., Wakuda, T., Kobarai, T., and Ohtsu, M. 2013b. Corrosion mechanisms in reinforced concrete by acoustic emission. Construction and Building Materials, **48**: 1240–1247. Elsevier. doi:10.1016/J.CONBUILDMAT.2013.02.020.

85. Kazem, H., Bunn, W.G., Seliem, H.M., Rizkalla, S.H., and Gleich, H. 2015. Durability and long term behavior of FRP/foam shear transfer mechanism for concrete sandwich panels. Construction and Building Materials, **98**: 722–734. Elsevier Ltd. doi:10.1016/J.CONBUILDMAT.2015.08.105.

86. Kim, J.H., and You, Y.C. 2015. Composite behavior of a novel insulated concrete sandwich wall panel reinforced with GFRP shear grids: Effects of insulation types. Materials, **8**(3): 899–913. MDPI AG. doi:10.3390/ma8030899.

87. Kinnane, O., West, R., and Hegarty, R.O. 2020. Structural shear performance of insulated precast concrete sandwich panels with steel plate connectors. Engineering Structures, **215**: 110691. Elsevier. doi:10.1016/J.ENGSTRUCT.2020.110691.

88. Klak, F., Jomaa'h, M., and Ahmad, S. 2022. Behavior of Reinforced Concrete Members Exposed to Fire. Tikrit Journal of Engineering Sciences, **29**(4): 56–68. doi:https://doi.org/10.25130/tjes.29.4.7.

89. Lameiras, R., Barros, J., Azenha, M., and Valente, I.B. 2013a. Development of sandwich panels combining fibre reinforced concrete layers and fibre reinforced

polymer connectors. Part II: Evaluation of mechanical behaviour. Composite Structures, **105**: 460–470. Elsevier. doi:10.1016/J.COMPSTRUCT.2013.06.015.

90. Lameiras, R., Barros, J., Valente, I.B., and Azenha, M. 2013b. Development of sandwich panels combining fibre reinforced concrete layers and fibre reinforced polymer connectors. Part I: Conception and pull-out tests. Composite Structures, **105**: 446–459. Elsevier. doi:10.1016/J.COMPSTRUCT.2013.06.022.

91. Li, K., Li, Y., Zou, Y., Yuan, B., Walsh, A., and Carradine, D. 2023. Improving the Fire Performance of Structural Insulated Panel Core Materials with Intumescent Flame-Retardant Epoxy Resin Adhesive. Fire Technology, **59**(1): 29–51. Springer. doi:10.1007/S10694-021-01203-0/FIGURES/13.

92. Malik, M., Bhattacharyya, S.K., and Barai, S. V. 2021. Thermal and mechanical properties of concrete and its constituents at elevated temperatures: A review. Construction and Building Materials, **270**: 121398. Elsevier. doi:10.1016/J.CONBUILDMAT.2020.121398.

93. Mazzuca, P., Firmo, J.P., Correia, J.R., and Castilho, E. 2021. Mechanical behaviour in shear and compression at elevated temperature of polyethylene terephthalate (PET) foam. Journal of Building Engineering, **42**: 102526. Elsevier. doi:10.1016/J.JOBE.2021.102526.

94. Miller, T., Hauser, C.J., and Kundu, T. 2002. Nondestructive Inspection of Corrosion and Delamination at the Concrete-Steel Reinforcement Interface. *In* Nondestructive Evaluation. ASMEDC. pp. 121–128.

95. Mohajan, H., and Mohajan, H.K. 2018. Acid Rain is a Local Environment Pollution but Global Concern. Open Science Journal of Analytical Chemistry, **3**(5): 47–55.

96. Moka, V.T.K., and Siva Chidambaram, R. 2023. Experimental Investigation on Flexural Behavior of Precast Beam–Beam Connections Using Mechanical Connectors. *In* Lecture Notes in Civil Engineering. *Edited by* M. Shrikhande, P. Agarwal, and P.C.A. Kumar. Springer, Singapore. pp. 627–637.

97. Naito, C., Hoemann, J., Beacraft, M., and Bewick, B. 2011. Performance and Characterization of Shear Ties for Use in Insulated Precast Concrete Sandwich Wall

Panels. Journal of Structural Engineering, **138**(1): 52–61. American Society of Civil Engineers. doi:10.1061/(ASCE)ST.1943-541X.0000430.

98. Najjar, M.F., Nehdi, M.L., Soliman, A.M., and Azabi, T.M. 2017. Damage mechanisms of two-stage concrete exposed to chemical and physical sulfate attack. Construction and Building Materials, **137**: 141–152. Elsevier. doi:10.1016/J.CONBUILDMAT.2017.01.112.

99. O'Hegarty, R., Amedeo, G., and Kinnane, O. 2024. The impact of compromised insulation on building energy performance. Energy and Buildings, **316**: 114337. Elsevier. doi:10.1016/J.ENBUILD.2024.114337.

100. O'Hegarty, R., and Kinnane, O. 2020. Review of precast concrete sandwich panels and their innovations.

101. O'Hegarty, R., Kinnane, O., Grimes, M., Newell, J., Clifford, M., and West, R. 2021. Development of thin precast concrete sandwich panels: Challenges and outcomes. Construction and Building Materials, **267**: 120981. Elsevier. doi:10.1016/J.CONBUILDMAT.2020.120981.

102. O'Hegarty, R., Reilly, A., West, R., and Kinnane, O. 2020. Thermal investigation of thin precast concrete sandwich panels. Journal of Building Engineering, **27**: 100937. Elsevier. doi:10.1016/J.JOBE.2019.100937.

103. O′Hegarty, R., West, R., Reilly, A., and Kinnane, O. 2019. Composite behaviour of fibre-reinforced concrete sandwich panels with FRP shear connectors. Engineering Structures, **198**: 109475. Elsevier. doi:10.1016/J.ENGSTRUCT.2019.109475.

104. Ohtsu, M., and Ono, K. 1986. The generalized theory and source representations of acoustic emission. Journal of Acoustic Emission, **5**.

105. Ohtsu, M., and Tomoda, Y. 2007. Corrosion Process in Reinforced Concrete Identified by Acoustic Emission. MATERIALS TRANSACTIONS, **48**(6): 1184–1189. The Japan Institute of Metals and Materials. doi:10.2320/MATERTRANS.I-MRA2007844.

106. Pan, P., He, Z.Z., Wang, H., and Kang, Y. 2022. Experimental investigation of C-shaped glass-fiber-reinforced polymer connectors for sandwich insulation wall

panels. Engineering Structures, **250**: 113462. Elsevier. doi:10.1016/J.ENGSTRUCT.2021.113462.

107. Pessiki, S., and Mlynarczyk, A. 2003. Experimental evaluation of the composite behavior of precast concrete sandwich wall panels. PCI Journal, **48**(2): 54–71. Precast/Prestressed Concrete Institute. doi:10.15554/PCIJ.03012003.54.71.

108. Pillai, R.G., Manickam, K., Joseline, D., and Srinivasan, S. 2024. Corrosion and Its Control in Prestressed Concrete Structures. *In* Smart & Sustainable Infrastructure: Building a Greener Tomorrow. *Edited by* N. Banthia, S. Soleimani-Dashtaki, and S. Mindess. Springer, Cham, Vancouver, Canada. pp. 889–895.

109. Plastics NZ. 2024. Recycled polystyrene on the rise as quick cost-effective option for aiding construction. Available from https://www.plastics.org.nz/. [accessed 3 June 2024].

110. Poon, C.S., Azhar, S., Anson, M., and Wong, Y.L. 2003. Performance of metakaolin concrete at elevated temperatures. Cement and Concrete Composites, **25**(1): 83–89. Elsevier. doi:10.1016/S0958-9465(01)00061-0.

111. Prem, P.R., Verma, M., and P.S.Ambily. 2021. Damage characterization of reinforced concrete beams under different failure modes using acoustic emission. Structures, **30**: 174–187. Elsevier. doi:10.1016/J.ISTRUC.2021.01.007.

112. Pulkit, U., and Adhikary, S. Das. 2022. Effect of micro-structural changes on concrete properties at elevated temperature: Current knowledge and outlook. Structural Concrete, **23**(4): 1995–2014. John Wiley & Sons, Ltd. doi:10.1002/SUCO.202000365.

113. Radhika, V., and Chandra Kishen, J.M. 2024a. Bayesian analysis of acoustic emission data for prediction of fatigue crack growth in concrete. Theoretical and Applied Fracture Mechanics, **131**: 104385. Elsevier. doi:https://doi.org/10.1016/j.tafmec.2024.104385.

114. Radhika, V., and Chandra Kishen, J.M. 2024b. A comparative study of crack growth mechanisms in concrete through acoustic emission analysis: Monotonic versus fatigue loading. Construction and Building Materials, **432**: 136568. Elsevier. doi:10.1016/J.CONBUILDMAT.2024.136568.

115. Rajeshwaran, R., and Logeshwari, J. 2023. Experimental investigation on performance of sandwich wall infill in framed structure. Materials Today: Proceedings,. Elsevier. doi:10.1016/J.MATPR.2023.04.477.

116. Raju, P., Rao Gangolu, A., Poluraju, P., and Appa Rao, G. 2014. Behaviour of 3D-Panels for Structural Applications under General Loading: A State-of-the-Art. International Journal of Research in Engineering and Technology, **03**(16): 2321–7308.

117. Ramli Sulong, N.H., Mustapa, S.A.S., and Abdul Rashid, M.K. 2019. Application of expanded polystyrene (EPS) in buildings and constructions: A review. Journal of Applied Polymer Science, **136**(20): 47529. John Wiley & Sons, Ltd. doi:10.1002/APP.47529.

118. Rao, G.A., and Poluraju, P. 2020. Cyclic behaviour of precast reinforced concrete sandwich slender walls. Structures, **28**: 80–92. Elsevier. doi:10.1016/J.ISTRUC.2020.08.046.

119. Reis, H., Ervin, B.L., Kuchma, D.A., and Bernhard, J.T. 2005. Estimation of Corrosion Damage in Steel Reinforced Mortar Using Guided Waves. Journal of Pressure Vessel Technology, **127**(3): 255–261. doi:10.1115/1.1989352.

120. Sadeghi-Pouya, H., Goyal, A., and Ganjian, E. 2021. Performance assessment of cathodically protected reinforced concrete structure based on alternative performance criterion: a case study. Journal of Building Pathology and Rehabilitation, **6**(1): 1–9. Springer Science and Business Media B.V. doi:10.1007/S41024-021-00108-3/METRICS.

121. Sakthivel, T., Gettu, R., and Pillai, R.G. 2021. Drying shrinkage of concrete with blended cementitious binders: Experimental study and application of models. The Indian Concrete Journal, **95**: 34–50.

122. Salmon, D.C., Einea, A., Tadros, M.K., and Culp, T.D. 1997. Full Scale Testing of Precast Concrete Sandwich Panels. Structural Journal, **94**(4): 354–362. doi:10.14359/486.

123. Sanchez, J., Fullea, J., and Andrade, C. 2017. Corrosion-induced brittle failure in reinforcing steel. Theoretical and Applied Fracture Mechanics, **92**: 229–232. Elsevier B.V. doi:10.1016/J.TAFMEC.2017.08.006.

124. Shahidan, S., Pulin, R., Muhamad Bunnori, N., and Holford, K.M. 2013. Damage classification in reinforced concrete beam by acoustic emission signal analysis. Construction and Building Materials,. doi:10.1016/j.conbuildmat.2013.03.095.

125. Shams, A., Stark, A., Hoogen, F., Hegger, J., and Schneider, H. 2015. Innovative sandwich structures made of high performance concrete and foamed polyurethane. Composite Structures, **121**: 271–279. Elsevier. doi:10.1016/J.COMPSTRUCT.2014.11.026.

126. Sharma, A., Sharma, S., Sharma, S., and Mukherjee, A. 2018. Investigation of deterioration in corroding reinforced concrete beams using active and passive techniques. Construction and Building Materials, **161**: 555–569. doi:10.1016/j.conbuildmat.2017.11.165.

127. Sharma, G., Sharma, S., and Sharma, S.K. 2021. Fracture monitoring of steel and GFRP reinforced concrete beams using acoustic emission and digital image correlation techniques. Structural Concrete, **22**(4): 1962–1976. doi:10.1002/suco.202000650.

128. Sharma, G., Sharma, S., and Sharma, S.Kr. 2020. Monitoring structural behaviour of concrete beams reinforced with steel and GFRP bars using acoustic emission and digital image correlation techniques. Structure and Infrastructure Engineering,: 1–16. doi:10.1080/15732479.2020.1836661.

129. Sharma, S., and Mukherjee, A. 2011. Monitoring Corrosion in Oxide and Chloride Environments Using Ultrasonic Guided Waves. Journal of Materials in Civil Engineering, **23**(2): 207–211. doi:10.1061/(ASCE)MT.1943-5533.0000144.

130. Shea, J.J. 2011. Identifying causes for certain types of electrically initiated fires in residential circuits. Fire and Materials, **35**(1): 19–42. John Wiley & Sons, Ltd. doi:10.1002/FAM.1033.

131. Shewale, M., Murthi, P., and Chidambaram, S. 2023. Functional performance of textile reinforced mortar in strengthening structural members: A critical review. *In* AIP Conference Proceedings. American Institute of Physics Inc.

132. Shmulsky, R., Senalik, C.A., Khademibami, L., Mohammadabadi, M., Seale, R.D., Williamson, T., and Ross, R.J. 2023. Investigation of the Role of Shear Deflection

in the Flexural Performance of Structural Insulated Panels. Forest Products Journal, **73**(4): 378–383. Allen Press. doi:10.13073/FPJ-D-23-00032.

133. Singh, P., Yogesh, R., Bhowmik, S., and Kishen, J.M.C. 2023. Insights into the fracturing process of plain concrete under crack opening. International Journal of Fracture, **241**(2): 153–170. Springer Science and Business Media B.V. doi:10.1007/S10704-023-00692-0/FIGURES/21.

134. Singh, S., Sharma, S., and Kwatra, N. 2022. A novel damage index for reinforced concrete beam-column joint using acoustic emission technique. European Journal of Environmental and Civil Engineering, **26**(16): 8321–8345. Taylor & Francis. doi:10.1080/19648189.2021.2023653.

135. Smakosz, Ł., and Tejchman, J. 2014. Evaluation of strength, deformability and failure mode of composite structural insulated panels. Materials & Design (1980-2015), **54**: 1068–1082. Elsevier. doi:10.1016/J.MATDES.2013.09.032.

136. Soive, A., and Tran, V.Q. 2017. External sulfate attack of cementitious materials: New insights gained through numerical modeling including dissolution/precipitation kinetics and surface complexation. Cement and Concrete Composites, **83**: 263–272. Elsevier Ltd. doi:10.1016/J.CEMCONCOMP.2017.07.024.

137. Solomon, A.A., and Hemalatha, G. 2017. Inspection of properties of Expanded Polystyrene (EPS), Compressive behaviour, bond and analytical examination of Insulated Concrete Form (ICF) blocks using different densities of EPS. International Journal of Civil Engineering and Technology, **81**(8): 209–221.

138. Sun, D., Wu, K., Shi, H., Miramini, S., and Zhang, L. 2019. Deformation behaviour of concrete materials under the sulfate attack. Construction and Building Materials, **210**: 232–241. Elsevier. doi:10.1016/J.CONBUILDMAT.2019.03.050.

139. Sylaj, V., Fam, A., Hachborn, M., Journal, R.B.-P., and 2020, undefined. 2020. Flexural response of double-wythe insulated ultra-high-performance concrete panels with low to moderate composite action. pci.orgV Sylaj, A Fam, M Hachborn, R BurakPCI Journal, 2020•pci.org,.

140. Tahir, M.N., and Hamed, E. 2021. Effects of temperature and thermal cycles on the mechanical properties of expanded polystyrene foam. Journal of Sandwich

Structures & Materials, **24**(3): 1535–1555. SAGE PublicationsSage UK: London, England. doi:10.1177/10996362211063152.

141. The BPF Expanded Polystyrene Group | Sustainability. (n.d.). Available from https://www.eps.co.uk/sustainability/index.html. [accessed 3 June 2024].

142. Tomlinson, D., and Fam, A. 2016a. Combined Loading Behavior of Basalt FRP–Reinforced Precast Concrete Insulated Partially-Composite Walls. Journal of Composites for Construction, **20**(3): 04015060. American Society of Civil Engineers (ASCE). doi:10.1061/(asce)cc.1943-5614.0000611.

143. Tomlinson, D., and Fam, A. 2016b. Analytical approach to flexural response of partially composite insulated concrete sandwich walls used for cladding. Engineering Structures, **122**: 251–266. Elsevier Ltd. doi:10.1016/J.ENGSTRUCT.2016.04.059.

144. Tomlinson, D., Fam, A., and Asce, M. 2016a. Analysis and Parametric Study of Partially Composite Precast Concrete Sandwich Panels under Axial Loads. Journal of Structural Engineering, **142**(10): 04016086. doi:10.1061/(ASCE)ST.

145. Tomlinson, D., Fam, A., and Asce, M. 2016b. Analysis and Parametric Study of Partially Composite Precast Concrete Sandwich Panels under Axial Loads. Journal of Structural Engineering, **142**(10): 04016086. American Society of Civil Engineers. doi:10.1061/(ASCE)ST.1943-541X.0001560.

146. Tongaroonsri, S., and Tangtermsirikul, S. 2008. Influence of mixture condition and moisture on tensile strain capacity of concrete. Science Asia, **34**: 59–68. doi:10.2306/scienceasia1513-1874.2008.34.059.

147. Uzal, A., Sonmez, F.O., Oz, F.E., Cinar, K., and Ersoy, N. 2018. A composite sandwich plate with a novel core design. Composite Structures, **193**: 198–211. doi:https://doi.org/10.1016/j.compstruct.2018.03.047.

148. Vishnu, B., Chauhan, A., Roy, D., and Sharma, U.K. 2017. Influence of various exposure conditions on the structural performance of sandwich wall panels. Indian Concrete Journal, **91**(11): 21–31.

149. Waseem Shah, M., and Waseem Shah, S.S. 2023. SIP construction with EPS and galvanised electro-welded mesh. Technium: Romanian Journal of Applied Sciences and Technology, **13**: 42–52. PLUS COMMUNICATION CONSULTING SRL. doi:10.47577/TECHNIUM.V13I.9573.

150. Woltman, G., Tomlinson, D., and Fam, A. 2013. Investigation of Various GFRP Shear Connectors for Insulated Precast Concrete Sandwich Wall Panels. Journal of Composites for Construction, **17**(5): 711–721. American Society of Civil Engineers. doi:10.1061/(ASCE)CC.1943-5614.0000373.

151. Xiao, J., and König, G. 2004. Study on concrete at high temperature in China—an overview. Fire Safety Journal, **39**(1): 89–103. Elsevier. doi:10.1016/S0379-7112(03)00093-6.

152. Xie, F., Li, J., Zhao, G., Zhou, P., and Zheng, H. 2020. Experimental study on performance of cast-in-situ recycled aggregate concrete under different sulfate attack exposures. Construction and Building Materials, **253**. Elsevier Ltd. doi:10.1016/J.CONBUILDMAT.2020.119144.

153. Xiong, L., Bruck, D., and Ball, M. 2017. Preventing accidental residential fires: the role of human involvement in non-injury house fires. Fire and Materials, **41**(1): 3–16. John Wiley & Sons, Ltd. doi:10.1002/FAM.2356.

154. Xue, W., Li, Y., Fu, K., Hu, X., and Li, Y. 2020. Accelerated ageing test and durability prediction model for mechanical properties of GFRP connectors in precast concrete sandwich panels. Construction and Building Materials, **237**. Elsevier Ltd. doi:10.1016/J.CONBUILDMAT.2019.117632.

155. Yanjie, B., Hui, S., Bai, Y., and Cai, Y. 2022. Mechanical properties and damage mechanisms of concrete under four temperature gradients combined with acoustic emission method. Journal of Building Engineering, **57**: 104906. Elsevier. doi:10.1016/J.JOBE.2022.104906.

156. Yu, A.P., Naqvi, M.W., Hu, L.B., and Zhao, Y.L. 2020. An experimental study of corrosion damage distribution of steel bars in reinforced concrete using acoustic emission technique. Construction and Building Materials, **254**: 119256. Elsevier. doi:10.1016/J.CONBUILDMAT.2020.119256.

157. Yu, C., Sun, W., and Scrivener, K. 2013. Mechanism of expansion of mortars immersed in sodium sulfate solutions. Cement and Concrete Research, **43**(1): 105–111. Pergamon. doi:10.1016/J.CEMCONRES.2012.10.001.

158. Zaki, A., Chai, H.K., Aggelis, D.G., and Alver, N. 2015. Non-Destructive Evaluation for Corrosion Monitoring in Concrete: A Review and Capability of

Acoustic Emission Technique. Sensors, **15**(8): 19069–19101. Multidisciplinary Digital Publishing Institute. doi:10.3390/S150819069.

159. Zhao, C., Li, Z., Deng, K., and Wang, W. 2018. Experimental investigation on the bearing mechanism of Perfobond rib shear connectors. Engineering Structures, **159**: 172–184. Elsevier. doi:10.1016/J.ENGSTRUCT.2017.12.047.

160. Zivica, V., and Bajza, A. 2001. Acidic attack of cement based materials — a review.: Part 1. Principle of acidic attack. Construction and Building Materials, **15**(8): 331–340. Elsevier. doi:10.1016/S0950-0618(01)00012-5.